UNIVERSITÀ DI PARMA

Dottorato di Ricerca in

SCIENZA E TECNOLOGIA DEI MATERIALI

Ciclo XXX

NEW MATERIALS FOR SAMPLE TREATMENT, MS-BASED METHODS AND CLINICAL APPLICATIONS

Coordinatore:

Chiar.mo Prof. Enrico Dalcanale

Tutore:

Chiar.ma Prof. Federica Bianchi

Dottorando: Nicolò Riboni

Anni 2014-2017

Riboni Nicolò, Parma, 2017

"Theory is when you know everything but nothing works.
Practice is when everything works but no one knows why.
In our lab, theory and practice are combined:
nothing works and no one knows why."
"It could be worse… it could be raining"
A. Einstein and M. Feldman

Contents

Abstract

The development and application of new materials for analytical purposes is a very promising and attractive research area.

The synergy between material science and analytical chemistry has allowed to develop new materials able to boost the detection of the investigated compounds. In analytical chemistry the progresses achieved in this field allowed to develop both new detection and extraction techniques characterized by enhanced performances in terms of selectivity and sensitivity. In fact, the use of new sorbents for both the extraction and the enrichment of the analytes from complex matrices such as polluted water, biological fluids, soil has allowed to fasten the analysis times as well as to increase method sensitivities. In this context, great attention is focused also on the development of new devices able to perform in-situ and real-time analyses through remote control (smartphone interfaces, clouds systems, LAN networks...).

Mass spectrometry is one of the most powerful technique for the detection and identification of organic and inorganic compounds. Being able to provide both molecular weight and structural information, it is widely used in analytical laboratories for academic research, industrial product development, regulatory compliance as well as for proteomic or metabolomic studies, DNA characterization, drug discovery, environmental monitoring, food analysis, forensic and homeland security. The advent of ambient MS technology paved the way for the development of a great variety of applications and innovations characterized by high-throughput: the challenge of analyzing samples in their native state without sample treatment encouraged the development of new techniques among which the spray-based ionization ones including desorption electrospray ionization (DESI), paper spray ionization (PSI), laser ablation electrospray ionization (LAESI)and so on. Novel materials and new instrumental configurations are under study to enhance the performance of the different ion sources.

Finally, in the last decade, the use of nanomaterials opened a new era in chemistry: different nanosystems have been proposed for catalysis, analytes extractions and biomedical purposes.

This PhD thesis has the aim of developing new materials for MS-based methods, sample pretreatment and clinical applications. Two main different analytical fields are involved: environmental monitoring and bioanalysis.

Environmental monitoring is a very active field of research: industrialization and anthropogenic activities led to a dramatic increase in pollution, thus requiring the development of new methods and devices able to detect pollutants in air, water and solid at trace levels. Pre-concentration is a common approach used to increase the performances of the analytical methods in terms of sensitivity and selectivity. The design and synthesis of novel materials characterized by both enhanced selectivity toward specific classes of pollutants and high enrichment factors, paved the way to develop new methods and devices able to perform real-time and in-situ analyses of hazardous compounds at sub-$\mu g/m^3$ levels. In addition, when untargeted analyses have to be performed, materials characterized by high absorption capabilities toward the widest possible range of pollutants are required.

In the present thesis, **Chapter 1** and **2** are devoted to the development of new sorbent materials for environmental analysis with particular attention to air monitoring.

More precisely, in **Chapter 1**, a comprehensive study including the design, synthesis and characterization of new supramolecular receptors to be used as coatings for solid-phase microextraction (SPME) for the selective monitoring of airborne pollutants, namely benzene, toluene, ethylbenzene and xylenes (BTEX) is reported. The receptors were rational designed in order to be selective toward BTEX and characterized by enhanced extraction capabilities toward benzene, a well-recognized carcinogenic compound. The SPME fibers were characterized in terms of film thickness, morphology and thermal stability showing extraction capabilities higher than those achieved by using commercially available materials. All the developed methods were fully validated and used for real sample analyses. Finally, the development of a simple, stand-alone, and unsupervised sensing device using the synthetized receptors as preconcentrating unit is reported.

In **Chapter 2**, the capabilities of new multipurpose absorbent tubes, using non granular active carbon were tested for the untargeted analysis of semi-volatile pollutants. Since these compounds are characterized by different properties in terms of molecular weight and polarity, their detection is very challenging. Nowadays, the use of multi-sorbent tubes is affected by a major drawback:

environmental humidity causes a dramatic decrease in the extraction capabilities of the adsorptive materials. By contrast, the material proposed in this study was not influenced by the presence of moisture, thus allowing to develop and validate a thermal desorption GC-MS method for the determination of chlorobenzenes and polycyclic aromatic hydrocarbons in air. No clogging of the adsorbent material was observed even when analyses were performed under high relative humidity conditions.

Bioanalysis is another important field of research: new materials and methods devoted to the analysis of biomolecules coupled with the use of statistical tools in order to identify disease biomarkers have been successfully developed.

Sample pretreatment is a key parameter also in bioanalysis: the development of new extraction techniques allows both to remove possible interfering compounds from complex matrices like body fluids (urine, blood and saliva) and to perform clean-up and preconcentration of the analytes even when low sample volumes (tens of microliters) are available.

In **Chapter 3**, the performances of *microextraction by packed sorbent* (MEPS) technique were tested in order to develop a MEPS-LC-MS method for the determination of dexamethasone and dexamethasone disodium phosphate in human aqueous humor. Experimental design and the multicriteria method of the desirability functions were applied to optimized the extraction conditions. Finally, the method was validated following the guidelines for bioanalytical methods.

Another part of the research activity was devoted to the development of novel materials for MS-based methods with applications in the both environmental and bioanalytical field. Advances in interfacing *liquid chromatography and electron ionization (EI) mass spectrometry* are presented in **Chapter 4**. The improvement of a new prototype for Direct-EI LC-MS analyses based on the development of new ion source coatings is discussed. In fact, the vaporization surface of the ion source is a key issue for the detection and characterization of targeted and untargeted compounds, especially for analytes characterized by high-molecular weight which require high-source temperatures to be detected properly. Three inorganic coatings, based on silica, titania and zirconia synthesized by sol-gel technology were developed in order to increase the chemical inertness of the commercial stainless steel ion sources. The materials were characterized in terms of film thickness, morphology and

thermal stability. Finally, they were tested for the Direct-EI LC-MS determination of environmental pollutants, i.e. polycyclic aromatic hydrocarbons and hormones: the results achieved proved that silica coating allowed to obtain better performances compared to the uncoated ion sources.

Mass spectrometry and in particular novel analytical techniques like *Desorption Electrospray Ionization High Resolution Mass Spectrometry* (DESI-HRMS) are crucial when fast, selective and sensitive methods for high throughput analyses are required.

In **Chapter 5,** new materials for the DESI-HRMS analysis of new psychoactive substances (NPS) are presented. NPS are a very large group of drugs of abuse not controlled by international conventions, thus being considered as a major threat to public health. In order to take preventive actions so as to be able to reduce driving under the influence of drugs of abuse, a MEPS-DESI-HRMS screening method for the detection of NPS at low concentration in oral fluids was developed.

Unmodified and functionalized polylactide films were used as DESI supporting materials and their performances were compared with those of commercially available polytetrafluoroethylene slides. Both surface hydrophobicity and morphology proved to be able to affect the ionization efficiency of the investigated analytes.

Finally, the MEPS-DESI-HRMS method was optimized and validated following the guidelines for bioanalytical methods, thus obtaining detection and quantitation limits at μg/l level.

The progresses in material chemistry made also possible to develop new drugs characterized by nm-size, high pharmaceutical activity and low side effects.

In **Chapter 6**, a new hybrid system characterized by a superparamagnetic iron oxide core and functionalized by odorant binding proteins (OBPs) acting as *quorum quenching agents*, was developed in order to bind different inducers and metabolites (like pyocyanin) produced by antibiotic resistant bacteria. The iron oxide nanoparticle cores were functionalized by a long-chain phosphonic acid and then conjugated with the OBPs. Nanoparticles were characterized in terms of magnetization, composition and dimensions. Finally, the amount of conjugated protein was assessed by using the BCA protein assay kit. The major advantage of the proposed approach relies on the possibility of using an external magnetic field to drive the nanodrugs to a

specific inflamed area of the lungs, thus both increasing the local concentration of the active principle and reducing the side-effects.

Chapter 1

Supramolecular Receptors for BTEX in Air

The research study presented in this chapter has been published in the following research articles:

N. Riboni, J.W. Trzcinski, F. Bianchi, C. Massera, R. Pinalli, L. Sidisky, E. Dalcanale, M. Careri, *Conformationally blocked quinoxaline cavitand as solid-phase microextraction coating for the selective detection of BTEX in air*, Anal. Chim. Acta 905 (2016) 79-84.

F. Bertani, N. Riboni, F. Bianchi, G. Brancatelli, E.S. Sterner, R. Pinalli, S. Geremia, T.M. Swager, E. Dalcanale, *Triptycene-Roofed Quinoxaline Cavitands for the Supramolecular Detection of BTEX in Air*, Chem-Eur J, 22 (2016) 3312–3319.

J.W. Trzcinski, R. Pinalli, N. Riboni, A. Pedrini, F. Bianchi, S. Zampolli, I. Elmi, C. Massera, F. Ugozzoli, E. Dalcanale, *In Search of the Ultimate Benzene Sensor: The EtQxBox Solution, ACS Sens.*, 2 (2017) 590−598.

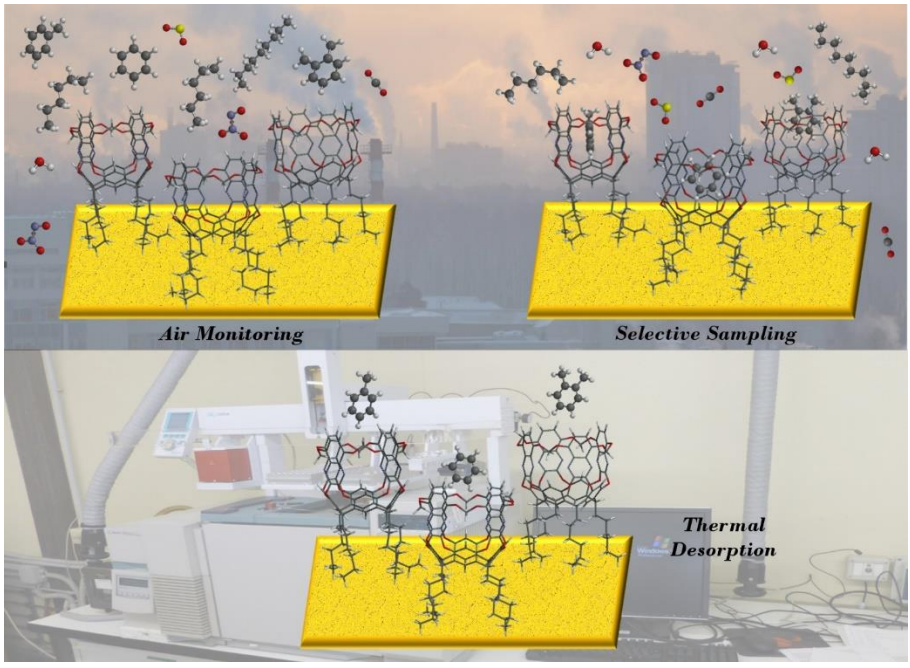

1.1 Introduction

1.1.1 *Air monitoring*

The increase of air pollution related to the anthropogenic activity and the high industrialization level required the design of new air quality control systems capable of fast detection of dangerous pollutants at trace levels.

Selective monitoring and high-precision measurement of aromatic volatile organic compounds, namely, BTEX (benzene, toluene, ethylbenzene and xylenes) is one of the most longstanding and challenging problems, due to the need of determining low concentration levels of the targeted analytes in the presence of overwhelming amounts of water, aliphatic hydrocarbons and other possible interferences [1]. In particular, owing to its carcinogenicity [2], highly selective and sensitive benzene detection is of paramount importance, being only 5 $\mu g/m^3$ the EU threshold limit value for average exposure [3].

Pollutants pre-concentration allows BTEX enrichment from both urban and indoor air [4], therefore active and passive samplers have been developed.

In passive devices, the trapping material is exposed to the urban air and the compounds are sampled by simple diffusion. These samplers are made of different geometry and contain highly absorbing materials (**Figure 1.1**). Depending on the analytes and the nature of the sampler, the sampling time can vary from 24 h up to a week of exposure. The detection of the analytes is off-line: the samplers are collected and sent to a laboratory for the analytical evaluations. BTEX monitoring is usually performed by passive samplers, resulting in data regarding averaged exposure levels [5].

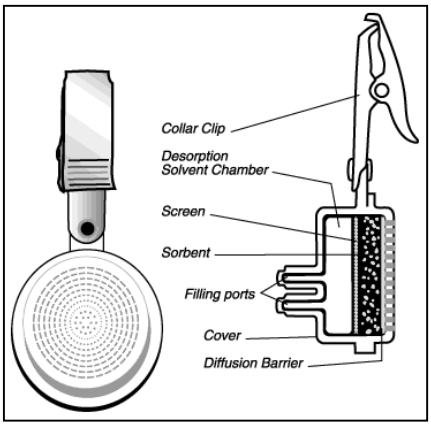

Figure 1.1 Scheme of a SKC passive sampler

The advantages of passive sampling rely on the low costs, no need of maintenance and the simplicity of the sampling, thus not requiring trained operators. The major drawback is the off-line analysis, carried out in lab, often by using dangerous solvents for the desorption of the analytes from the cartridge. In fact, the extraction of the trapped compounds is usually performed by using CS_2, thus leading to issues related to disposal, safety and of environmental concern.

Active samplers are characterized by the presence of a pump inside the system, thus allowing sample enrichment. In the active sampling, a preconcentrator (PC) is located just after the inlet (**Figure 1.2**). The trapping material can be desorbed both by using organic solvents or a thermal desorption unit, leading to a preconcentration and a focalization of the compounds at the beginning of the gas-chromatographic column.

Active samplers have the great advantage of being able to perform both in-situ and on-line real-time analyses, thus allowing the monitoring of the concentration of the investigated compounds in air at a specific time.

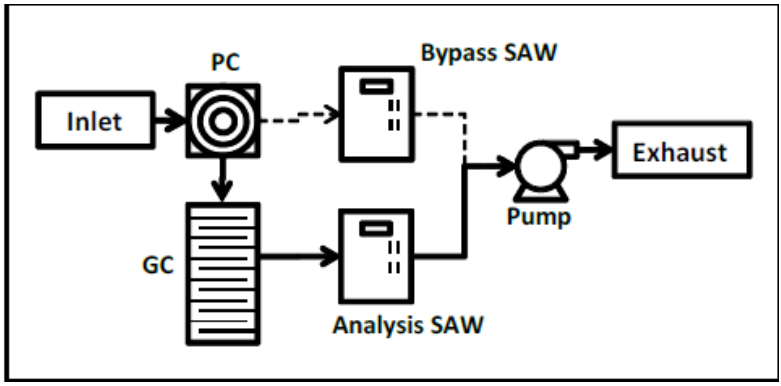

Figure 1.2 Scheme of an active sampler

Present real-time benzene monitoring systems for in-field environmental applications are bulky and/or expensive, being miniaturized systems derived from laboratory instrumentation [6-8]; in addition, trained users are usually required. Simple and low-cost systems have been proposed [9], such as metal oxide sensors, quartz microbalances, surface acoustic waveguides and polymeric sensors [10].

Regardless of the active or passive nature of the system, the key point for BTEX detection is the preconcentration step: the major drawbacks of the

nowadays-used materials are related to both lack of selectivity and the use of time-consuming procedures. Even though proposed for the analyses of BTEX these sorbents, mainly graphitized carbon and polymers based on divinylbenzene, are characterized by high enrichment capabilities towards a plethora of similar compounds, i.e. PAHs and aliphatic hydrocarbons. The adsorption is in fact based on non-covalent interaction, such as π-π and CH-π interactions, ideals for the BTEX enrichment, but usually the material lacks a discriminating functionalization, able to limit the adsorption of other compounds. Therefore, the presence of high concentration levels of interfering analytes, such as aliphatic hydrocarbons, could lead to decrease the analytical sensitivity.

A material suitable for the BTEX monitoring has to be characterized by:

1. Selectivity toward the target molecules by specific interaction (such as hydrogen bond, π-π and CH-π interactions), thus limiting the adsorption of interfering compounds that can give rise to the possibility of signal suppression, enhancement or non-linearity. In addition, selective adsorption allows to by-pass long and complex sample treatments or chromatographic separations.
2. Highly sensitivity: the material has to be characterized by high enrichment capabilities toward the targeted molecules, thus allowing their detection at trace levels.
3. Easy desorption: the material has to be desorbed completely in one step, not being affected by memory effect. Thermal desorption is suggested since it allows the development of remote and independent systems characterized by the need of low maintenance, thus avoiding the use of organic and/or dangerous solvents.

1.1.2 Solid Phase Microextraction

Sampling and sample preparation are essential steps in analysis, greatly influencing the reliability and accuracy of results, and both the time and costs of analysis. Solid Phase Microextraction (SPME) is a fast, solventless, low cost and automatable alternative to conventional sample extraction devices, proposed by Pawliszyn in 1989 [11,12]. SPME has been widely used in different fields of analytical chemistry and is ideally suited for coupling with mass spectrometry (MS).

The core of this technique is a silica or metal needle coated by an appropriate stationary phase, mounted on a designed syringe (**Figure 1.3**). The analytes are extracted from the sample and concentrated onto the fiber coating by absorption/adsorption processes.

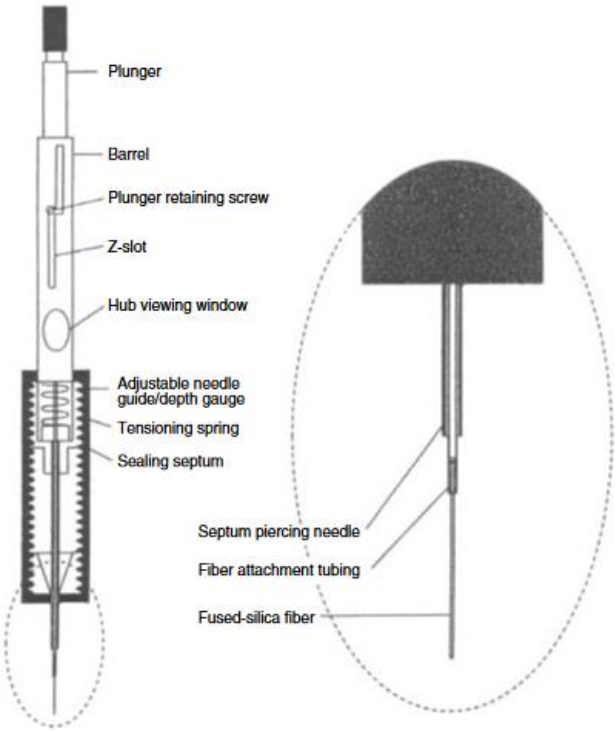

Figure 1.3 SPME scheme

Extraction is based on gas – liquid, gas-solid or liquid – liquid partitioning, depending on both the fiber coating and the matrix. Kinetics of the SPME extraction process depend on several parameters (i.e. film thickness, type of coating and porosity) and sampling times are usually in the order of few minutes.

After sampling, the analytes absorbed on the fiber are desorbed directly into the inlet of the chromatograph. Gas chromatography (GC) is one of the preferentially used techniques. In this case, thermal desorption takes place in the hot GC injector. SPME extraction can be also coupled with liquid chromatography (HPLC): the needle is exposed into a modified valve, and the analytes are eluted by the mobile phase.

There are two typical SPME applications: headspace (HS) sampling or direct immersion (DI) (**Figure 1.4**). HS extraction followed by GC-MS analysis is the most commonly applied method for the extraction of volatile compounds, whereas DI followed by GC or HPLC analysis, is used for detecting polar and non-volatile compounds.

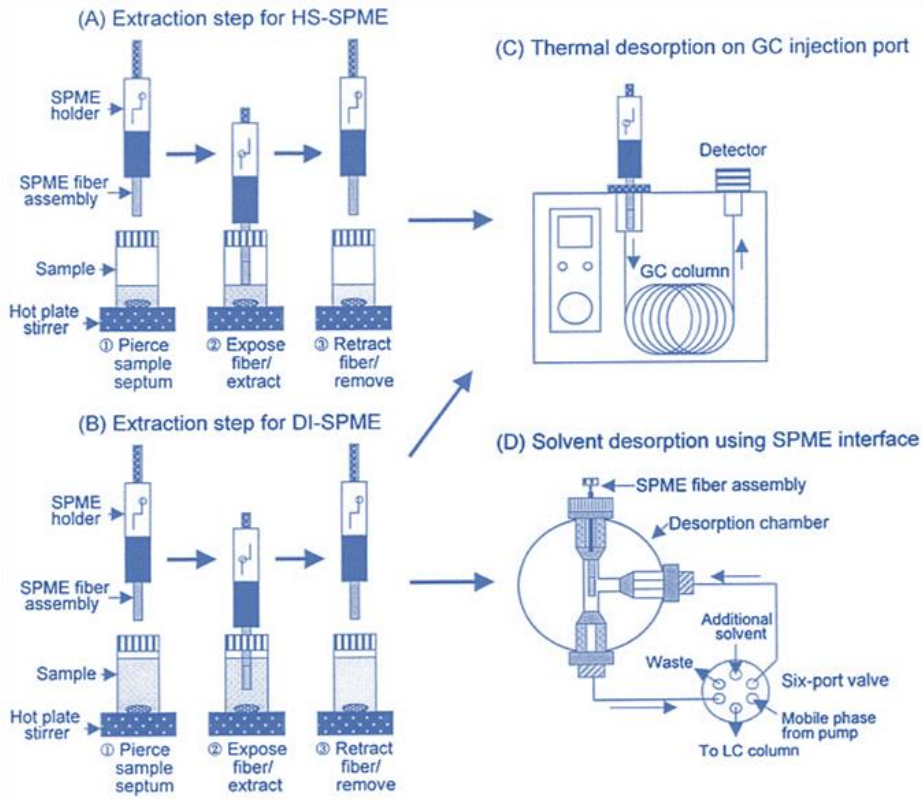

Figure 1.4 SPME analysis scheme

Commercially available stationary phases, summarized in **Table 1**, can be classified as non-bonded, bonded and cross-linked, depending on the immobilized coating. Non-bonded phases are stable in water-miscible organic solvents (up to 20% organic content), but slight swelling may occur in non-polar solvents. Bonded phases are compatible with the majority of organic solvents except for some non-polar solvents, like hexane and dichloromethane. Cross-linked phases are stable in most solvents (**Table 1.1**).

Table 1.1: Summary of commercially available SPME fibers

Fiber coating	Film thickness (μm)	Polarity	Coating method	Operating temperature (°C)
PDMS	100, 30	Non-polar	Non-bonded	280
PDMS	7	Non-polar	Bonded	340
PDMS - DVB	60, 65	Bipolar	Cross-linked	270
PA	85	Polar	Cross-linked	320
CAR - PDMS	75, 85	Bipolar	Cross-linked	320
DVB - Carbowax	65, 70	Polar	Cross-linked	265
DVB – CAR - PDMS	50/30	Bipolar	Cross-linked	270

PDMS: Polydimethylsiloxane
DVB: divinylbenzene
PA: poliacrylate
CAR: Carboxen

PDMS-DVB, CAR-PDMS and DVB-CAR-PDMS coatings have been proposed for BTEX sampling both in air and in water [13-15]. The main drawback of the commercial fibers is related to the lack of selectivity towards BTEX: these coatings are in fact aspecific polymers and can absorb all the VOCs present in the sample, resulting in the decrease of both limit of detection and enrichment capabilities.

In order to overcome the selectivity problem, new coatings were properly designed and synthetized: carbon nanotubes [16], graphene nanosheets [17], cobalt [18] and zinc oxide nanoparticles [19], vinyl-functionalized mesoporous organosilica [20], molecular imprinted polymers (MIP) [21] and different ionic liquids-based materials [22-24] have been proposed for BTEX enrichment from both water and air samples.

The research efforts are still devoted to the development of materials characterized by robustness and high selectivity, enhanced enrichment factors and low limits of detection.

Rational design of supramolecular receptors as sensing materials can be particularly attractive to address the selectivity issue, by designing a host capable of complexing targeted guests by exploiting specific interactions and/or creating key-lock structures, characterized by optimized space fitting.

1.1.3 *Tetraquinoxaline cavitand*

The resorcinarene unit is a versatile scaffold for the development of supramolecular receptors, obtained by bridging the phenolic oxydryl groups with proper synthons.

Tetraquinoxaline cavitands (**QxCav**) are formed by nucleophilic aromatic substitutions with dichloroquinoxaline moieties [25-27]. This functionalization allows to obtain a deep, hydrophobic and electron rich cavity, given by the electron-rich quinoxaline walls (**Figure 1.5**).

Figure 1.5 Structure of **QxCav**

The quinoxaline units can present at either axial or equatorial positions: the receptor is able to perform reversible switching between a closed *vase* conformation, characterized by a deep cavity (7 Å wide and 8 Å deep), suitable for guest hosting, and an open *kite* conformation, with a flat extended surface (**Figure 1.6**). In the latter case, dimerization of the system is possible [28].

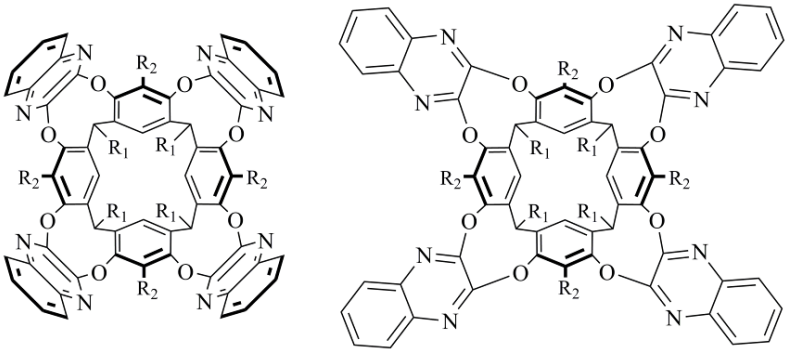

Figure 1.6 Structure of QxCav in vase (left) and kite (right) conformation.

In solution the *vase* ↔ *kite* equilibrium is controlled by solvation (**Figure 1.7**): at low temperatures, solvation of the larger surface favors the kite conformer, whereas, at higher temperature, the entropy becomes unfavorable and the vase conformation predominates. Moreover, at low pH the quinoxaline nitrogens become protonated leading to repulsive interactions between the walls, thus promoting the cavity opening to the kite conformation.

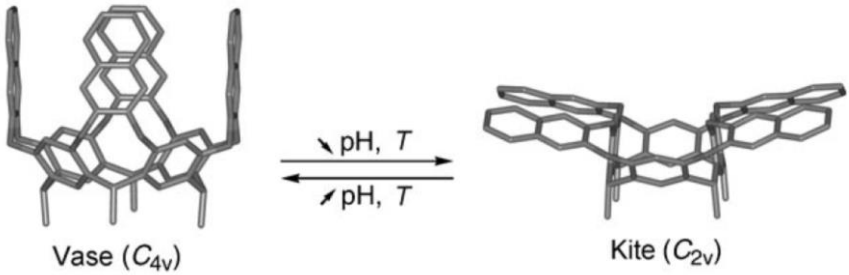

Figure 1.7 Vase to kite conformational equilibrium of QxCav in the solution.

In the solid state, the equilibrium is strongly moved toward the vase form and conformational changes are both limited and temperature dependent.

Vibrational measurements, coupled with theoretical calculations [29], indicate that the QxCav cavity is *breathing* in the solid state (**Figure 1.8**). It is reasonable to assume that the *breathing* is amplified by increasing the temperature. The vase opening reduces the interaction between the cavity walls and the guests making the receptor less sensitive and selective.

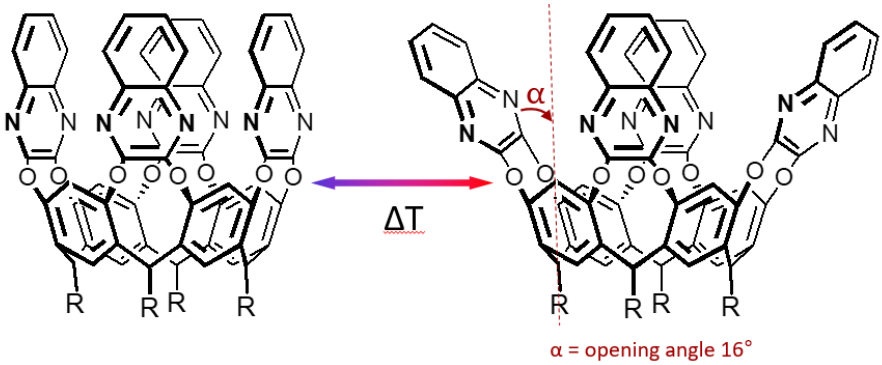

Figure 1.8 QxCav *breathing* in solid state.

In solid-state hundreds of possible conformations exist and interconvert at ambient temperature: a simulation depicting more than 1000 overlaid structures of the QxCav is shown in **Figure 1.9** [30].

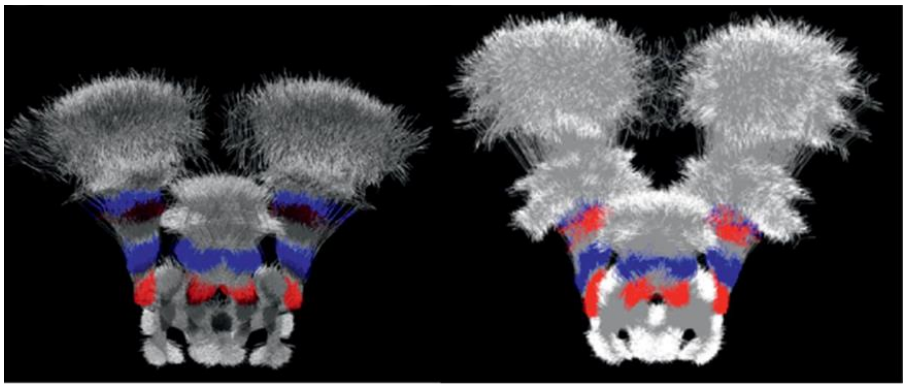

Figure. 1.9. Overlay of 1000 structures of the QxCav vase forms sampled from molecular dynamics simulations [30]

QxCav was already proposed by our research group both as adsorbent material for dynamic headspace [31] and as SPME coating for the selective sampling of BTEX from water samples [32]. QxCav in the vase conformation presents a strong affinity toward aromatic guests both in solution and in gas phase [33-36]. The complexes are stabilized by: i) non-covalent interactions between the π electrons of the quinoxaline walls and the π electrons and C-H groups of the guests; ii) two near-hydrogen bonds between two guest hydrogens aligned along the π orbital of resorcinarene atoms (**Figure 1.10**).

The calculated complexation energy for benzene (- 6.85 kJ/mol) and toluene (- 6.88 kJ/mol) are very close, therefore guests' discrimination is impossible by using QxCav. The theoretical calculation related to the binding energies were also confirmed by experimental data.

These findings can be ascribed to the changes of the cavity size related to the free flapping of the quinoxaline walls between vase and kite conformation at ambient temperatures.

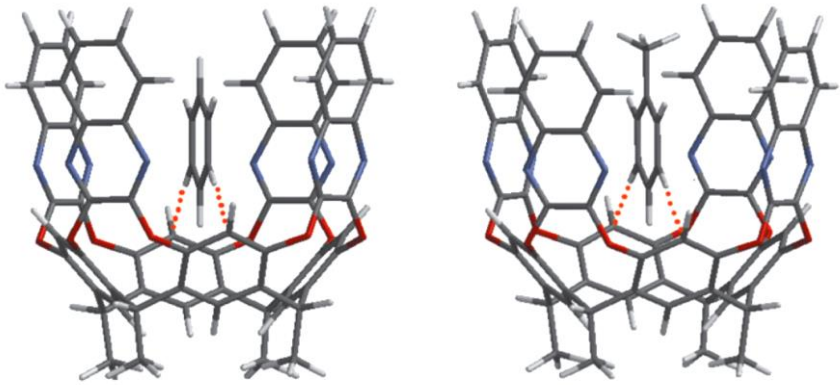

Figure 1.10. Model of the **QxCav@benzene** and **QxCav@toluene** complexes.

The main advantages of the use of tetraquinoxaline cavitands over the commercial available materials towards BTEX detection are i) increased of the enhancement factors; ii) lower detection limits; iii) increase of selectivity towards the aromatic targets: water and aliphatic compounds are not retained by the proposed material, being only physisorbed outside the receptor, thus allowing an easy removal of the interferences before the GC-MS analysis.

In 2007, a research study proposed the development of miniaturized system composed by a QxCav-based preconcentration unit, a Si-micromachined GC column and a Si-integrated MOS sensor (**Figure 1.11**) [37].

This device has been successfully field-tested. Despite its good performances, this system is rather complex and it is not suited for low-cost distributed sensing, because of the need of a GC separation between benzene and the other targeted compounds.

Figure 1.11 Photograph of the developed monitoring system [37]

In order to increase the selective capabilities of the receptor, QxCav can be considered as an excellent starting point for the design and the synthesis of new receptors, based on the functionalization of the quinoxaline walls at the upper rim.

In a published study, a modified version of the QxCav, functionalized at the upper rim with a carboxylic group (QxCavCOOH), was used to develop a selective SPME coating for the determination of nitroaromatic explosives and taggants at trace levels in air and soil [38].

The aim of the present research activity was the design and synthesis of new cavitands characterized by increased performances towards BTEX trapping with particular attention to the capability of discriminating benzene from the other aromatic hydrocarbons. The receptors have been tested by developing SPME fibers. Finally, the performances of the materials were assessed by developing and validating proper analytical methods suitable for BTEX detection in urban air.

1.2 Material and Methods

1.2.1 *Chemicals and materials*

Benzene and ethylbenzene (99.8 and 99.5% purity, respectively) were from Carlo Erba (Milano, Italy). Benzene-d_6 (internal standard, 99.96 atom % D), n-pentane (> 99% purity), n-nonane (> 99% purity), toluene (> 99.9% purity), n-hexane (> 97% purity), n-octane (> 98% purity) and chloroform (anhydrous > 99%), from Merk S.p.A. (Milan, Italy). n-heptane (> 95% purity) was provided by Lab-Scan (Dublin, Ireland), whereas *m*-xylene, *p*- and *o*-xylene (> 98% purity) were from Fluka (Milan, Italy).

1 cm SPME bare fused-silica fibers and 1 cm commercial fibers DVB-CAR-PDMS were purchased from Supelco (Bellefonte, PA, USA). Duralco 4460 epoxy glue was provided by Cotronics Corp. (Brooklyn, NY, USA). 1L Tedlar® Gas Sampling Bags w/PLV and Thermogreen® LB-2 Septa were from Sigma Aldrich.

1.2.2 *Structural determination and fiber characterization*

Intensity data and cell parameters for host@guest were recorded at 190 K on a Bruker APEX II equipped with a CCD area detector and a graphite monochromator (Mo K_α radiation λ=0.71073 Å). The structure was solved by direct methods using the SIR97 program [39] and refined on F_0^2 by full-matrix least squares procedures using the SHELXL-97 program [40,41]. Both programs were used in the WinGX suite [42]. Data reductions were performed using the SAINT [43] and SADABS [44,45] programs. The PLATON SQUEEZE procedure [46] was used to treat regions of diffuse solvent which could not be sensibly modeled in terms of atomic sites. Their contribution to the diffraction pattern was removed and modified F_o^2 written to a new HKL file and the number of electrons located were included in the formula, formula weight, calculated density, m and F(000). All the non-hydrogen atoms were refined with anisotropic atomic displacements, with the exclusion of some atoms of a disordered alkyl chains at the lower rim. The hydrogen atoms were included in the refinement at idealized geometries (C-H 0.95 Å) and refined "riding" on the corresponding parent atoms.

The weighting scheme used in the last cycle of refinement was $w=1/[\sigma^2F_o^2+(0.0911\ P)^2]$ where $P=(F_o^2+2F_C^2)$. Geometric calculations were performed with the PARST97 program [47].

Thermogravimetric analysis (TGA) was performed using a TGA 7 instrument (PerkinElmer, Waltham, MA) over the temperature range 40-400 °C (heating rate: 10 °C min^{-1}) under inert (N_2) atmosphere.

Coating thickness and surface morphology were investigated by using environmental scanning electron microscopy (ESEM) with a Leica 430i instrument (Leica, Solms, Germany).

Fiber bleeding was investigated by desorbing the fibers in the GC injection port for 2 min at 250 °C. Fiber-to-fiber and batch-to-batch repeatability (by preparing 3 different batches) were evaluated for headspace analysis by using four fibers in each case. Three replicated measurements for each fiber were always performed.

1.2.3 SPME analysis

Prior to use, all the fibers were conditioned in the GC injection port at 275 °C for 1 h under a helium flow. Air sampling of BTEX was performed by manually exposing the SPME fibers in an air atmosphere containing a mixture of the aromatic compounds and linear hydrocarbons (from C_6 to C_9). More precisely, the air atmosphere was generated by using a gas distribution system in which certified cylinders were connected to mass flow controllers able to provide a calibrated mixture of both BTEX and linear hydrocarbons at different concentrations in synthetic air [47]. A volume of 1 L was sampled. Extraction was carried out at room temperature for 15 min. BTEX desorption was carried out by exposing the fiber in the GC injector for 2 min at 250 °C. The same procedure was applied using the commercial fibers 2 cm-50/30 µm DVB-CAR-PDMS (Supelco).

1.2.4 GC-MS analysis

A HP 6890 Series Plus gas chromatograph (Agilent Technologies, Palo Alto, CA) equipped with a MSD 5973 mass spectrometer (Agilent Technologies) was used. Helium was used as the carrier gas at a constant flow rate of 1 mL/min; the gas chromatograph was operated in splitless mode for 1 min with the PTV injector (Agilent Technologies) maintained at the temperature

of 250 °C and equipped with a 1.5 mm i.d. multibaffled liner (Agilent Technologies).

Chromatographic separation was performed on a 30 m x 0.25 mm, df 0.25 µm HP-5 ms capillary column (Agilent Technologies), using the following temperature programme: 40 °C for 8 min, then 20 °C/min up to 200 °C.

The transfer line and source were maintained at the temperatures of 220 and 150 °C, respectively. Preliminarily, full scan EI data were acquired to determine appropriate masses for selected-ion monitoring mode (SIM) used for BTEX quantitation (*m/z* 78 and 84 for benzene and d_6-benzene; *m/z* 91 for toluene; *m/z* 91 and 106 *m/z* for ethylbenzene and xylenes; *m/z* 43, 57, 72 and 86 for hexane; *m/z* 43, 57, 71 and 100 for heptane; *m/z* 43, 57, 85 and 114 for octane; *m/z* 43, 57, 85 and 128 for nonane) under the following conditions: ionization energy: 70 eV; mass range: 35-250 amu; scan time: 3 scan s^{-1}; electron multiplier voltage: 2200 V. Signal acquisition and data handling were performed using the HP Chemstation (Agilent Technologies).

1.2.5 *Method Validation*

Method validation was performed according to EURACHEM guidelines [48] using not contaminated air as blank matrix and following the same procedure reported in previous studies [49].

Detection (y_D) and quantitation (y_Q) responses were expressed as signals based on the mean blank (x_b) and the standard deviation of blank responses (s_b) as follows:

$$y_D = x_b + 2t\, s_b$$

$$y_Q = x_b + 10t\, s_b$$

where t is the constant of the t-student one-tailed distribution at 95% confidence level. The value x_b and s_b were calculated performing ten measurements of not contaminated air.

The respective LODs and LOQs were obtained as a projection of the corresponding signals y_D and y_Q through the calibration plot of the corresponding analytes.

Calibration curves (six concentration levels, three replicated measurements for each level) were evaluated by analyzing blank air samples spiked with the proper amount of the investigated analytes. Linearity was evaluated on six

concentration levels in the LOQ-3500 ng/m^3 for benzene, LOQ-4100 ng/m^3 for toluene, LOQ-4700 ng/m^3 for ethylbenzene, *m*-, *p*-, and *o*-xylenes.

Homoschedasticity was verified by applying the Bartlett test. Mandel's fitting test was also performed to check the goodness of fit and linearity. The significance of the intercept (significance level 5%) was established by running a Student's t-test.

Intra-day repeatability and intermediate precision were calculated in terms of RSD % on two concentration levels i.e. 35 and 350 ng/m^3 for benzene, 40-400 ng/m^3 for toluene, 47-470 ng/m^3 for ethylbenzene, *m*-, *p*- and *o*-xylenes by performing six replicated measurements for each level. Intermediate precision was estimated over three days verifying homoscedasticity of the data and performing the analysis of variance (ANOVA) at the confidence level of 95%.

Trueness was calculated in terms of relative recovery rate (RR%) as follows:

$R.R.\% = c_1/c_2\ 100$

where c_1 is the measured concentration and c_2 is the concentration calculated from the quantity spiked into the sample. Two concentration levels i.e. 24 and 240 ng/m^3 for each analyte with 10 replicated measurements were analyzed in the case of QxBox cavitands. DiTriptyQxCav trueness was assessed at the LOQs and the highest calibration level for all the analytes (n=10).

1.2.6 Real Samples

Three air samples were collected, at different times (9:00, 12:00 and 16:00), by using 1L Tedlar® Gas Sampling Bag w/PLV and Thermogreen® LB-2 Septa (Sigma Aldrich) in a traffic busy street in Parma, Italy. The values of relative humidity obtained from the meteorological station were 66 and 75%, respectively. The bags were immediately sent to the laboratory and submitted to SPME analysis (15 min at room temperature).

1.2.7 Prototype testing

Due to the linearity of the PID response to benzene and toluene, the responses of the EtQxBox/PID system at the two de-sorption temperatures (T1 = 150°C and T2 = 220°C) are a linear combination of the amounts of benzene and toluene released at each temperature:

AP1 = SP1(B) * [B] + SP1(T) * [T] (1a)

$AP2 = SP2(B) * [B] + SP2(T) * [T]$ (1b)

where AP1 and AP2 are the areas of the peaks at T1 and T2 respectively, [B] and [T] are the concentrations of benzene and toluene, and SP1(B) is the sensitivity towards benzene of the first peak, SP1(T) is the sensitivity towards toluene of the first peak, and so forth for the second peak.

The system is calibrated by performing two measurements, one of benzene only and one of toluene only, and using the areas of the peaks AP1 and AP2 to calculate the four sensitivities:

when $[T] = 0$: $SP1(B) = AP1 / [B]$ and $SP2(B) = AP2 / [B]$ (2a)

when $[B] = 0$: $SP1(T) = AP1 / [T]$ and $SP2(T) = AP2 / [T]$ (2b)

With the four sensitivities determined using (2a) and (2b), the equations (1a) and (1b) can be solved for [B] and [T], and each measurement yielding two areas AP1 and AP2 can be used to predict the concentration of benzene and toluene.

1.3 Result and Discussion

1.3.1 *Rational design*

The design of new molecular receptors has to consider the requirement of both electronic and shape complementary toward the target molecules, with the aim of improving the recognition between host and guest, by tuning the molecular interactions and creating a proper steric engulfment.

In order to improve the selectivity of QxCav towards BTEX two different approaches were followed:

1. QxCav cavity blocking by using methylenoxy and ethylenoxy bridges;
2. Introduction at the upper rim of the receptor of triptycene units, having high steric hindrance.

1. QxBox Cavitands

The first approach was associated to the blocking of the QxCav cavity in the *vase* form, thus producing a freezing of the receptor and allowing a noticeable decrease in the number of the guests able to fit the reduced dimension of the cavity. In addition, this should increase the complexation forces, strengthening the complexation of aromatic guests, with a resulting gaining in sensitivity.

The functionalization of the quinoxalines at the upper rim is the key point in order to achieve the cavity freezing: the idea was to bridge the quinoxaline walls via ether bridges between 5 and the 8 positions (**Figure 1.12**), thus obtaining a new class of receptors, the QxBox cavitands.

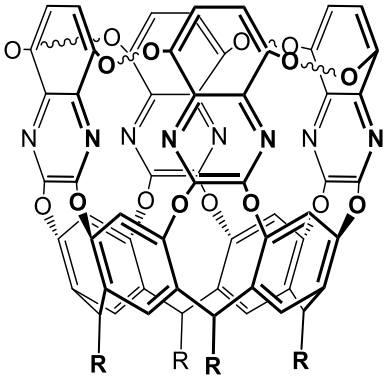

Figure 1.12 Scheme of a QxBox

The QxBox cavitands are characterized by three different rims of electron-rich aromatics rings capable of complexing the aromatic guests, by intermolecular attractive interactions. The QxBox structure is depicted in **Figure 1.13** and can be summarized as follows:

1. at the lower rim, the π electrons of the aromatic rings of the resorcinarene scaffold interact with two "bottom" C−H groups of the analytes *via* C−H···π interactions;
2. at the medium rim, the nitrogen atoms of the quinoxaline rings can act as hydrogen bond acceptors toward the *equatorial* C−H groups of benzene, toluene, or xylenes;
3. the aromatic rings of the quinoxaline at upper rim of the cavitand are able to interact *via* C−H···π interactions.

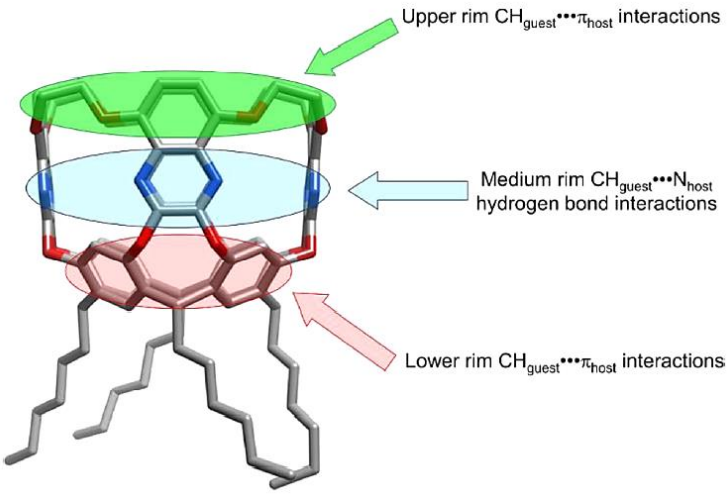

Figure 1.13 QxBox cavitand with lower, medium, and upper rim interaction sites highlighted

Regarding the host-guest interactions, it has to be pointed out that benzene recognition is driven mainly by size complementarity and CH–π and π –π interactions with electron rich cavity. A similar behavior is present in the other TEX, characterized by additional CH–π interaction between the quinoxaline walls and the methyl substituent. However, it has to be taken into account that a different steric hindrance is present among the BTEX: in order to increase the recognition capabilities, the host has to be characterized by a very small cavity, fitting preferentially benzene over the TEX, even in the case of the toluene, the guest with the closest steric engulfment.

To this purpose, we designed the MeQxBox and the EtQxBox, characterized by methylenoxy and ethylenoxy bridges respectively (**Figure 1.14**), connecting the quinoxaline walls.

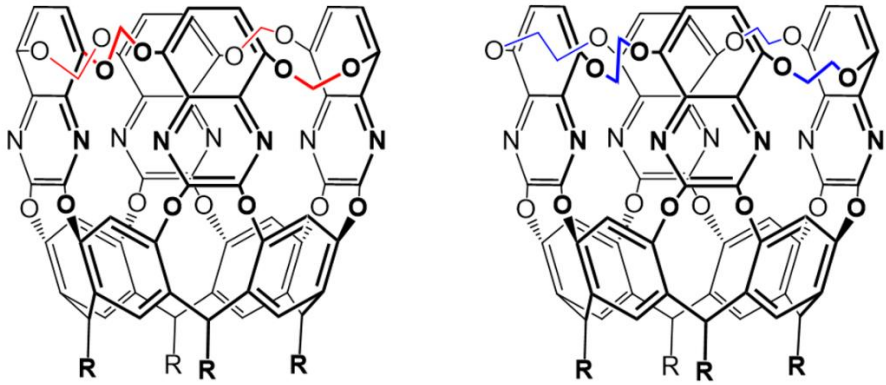

Figure 1.14 Scheme of the MeQxBox (left) and EtQxBox (right)

2. TriptyQxCav cavitands

The freezing of the system proposed by bridging the quinoxaline walls is not the only possible approach in order to block the QxCav *breathing*.

As reported by Diederich and co-workers [50, 51], by functionalizing the upper rim of quinone-based cavitands with trypticene units, a complete steric encapsulation of the guests in a closed *vase* conformation occurs. This phenomenon increases the association constants and reduce the guest exchange rates, owing to steric congestion [52].

The main drawback is that by using quinolone cavitands, the *vase* conformation is only present in the reduced hydroquinone state: upon exposure to air, the system oxidizes to quinones, thus promoting the switching to the open *kite* conformation, which is not suitable for guest complexation [53].

Since benzene recognition over TEX occurs only by exploiting their different steric hindrance, by introducing bulky elements on the host structure, such as triptycene units, an enhanced discrimination in the recognition process could be achieved. This functionalization at the upper rim of the cavitands could modify the shape complementarity between the host and the guest and affect the stability of the obtained complex.

To this end, we designed a new class of triptycene tetraquinoxaline *roofed* cavitands: MonoTriptyQxCav (**Figure 1.15 a**) and DitriptyQxCav (**Figure 1.15 b**), characterized by one or two triptycene molecules at the upper rim respectively. The functionalization can lead to a tighter cavity opening, with the aim to improve benzene over TEX affinity in either the adsorption or desorption step.

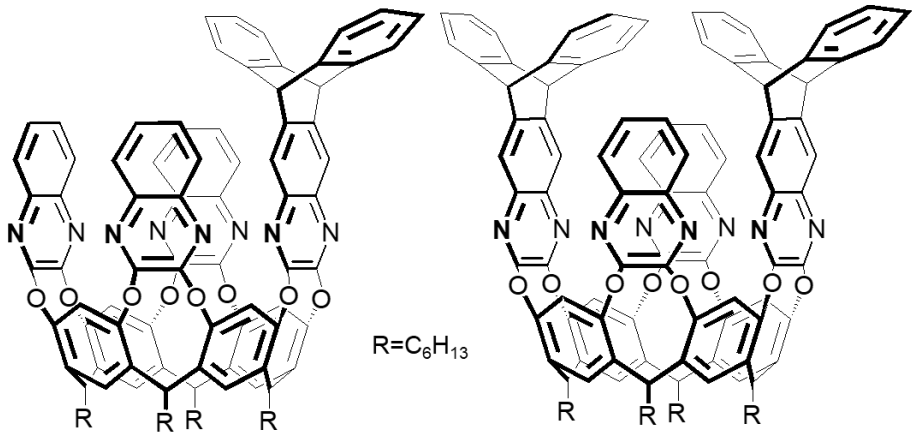

Figure 1.15 Scheme of the MonotriptyQxCav (left) and DitriptyQxCav (right)

1.3.2 Synthesis of the functionalized cavitands

The syntheses and the NMR characterizations of the QxBox cavitands discussed in this thesis are briefly reported. A detailed explanation is presented in the published articles [54,55].

The synthesis of the QxBox cavitands is presented in Schemes **1.1-1.3**, and can be summarized as follows:

1. Synthesis of the resorcinarene scaffold characterized by hexyl feet (**Scheme 1.1)**: the length of the alkyl chains is a good compromise between solubility and ease of crystallization, in order to facilitate the purification of both intermediates and final products.

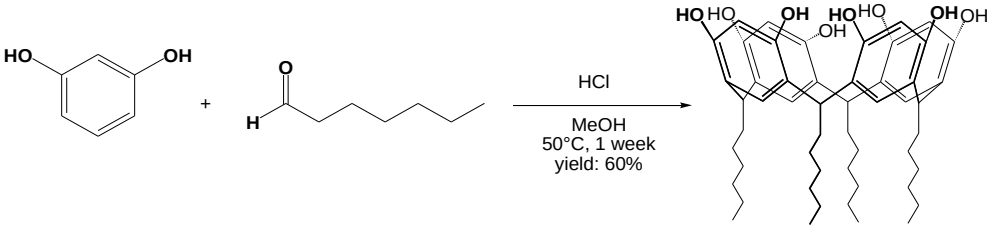

Scheme 1.1

2. Synthesis of the 2,3-dichloro-5,8-dimethoxy quinoxaline bridging unit (**Scheme 1.2)**.

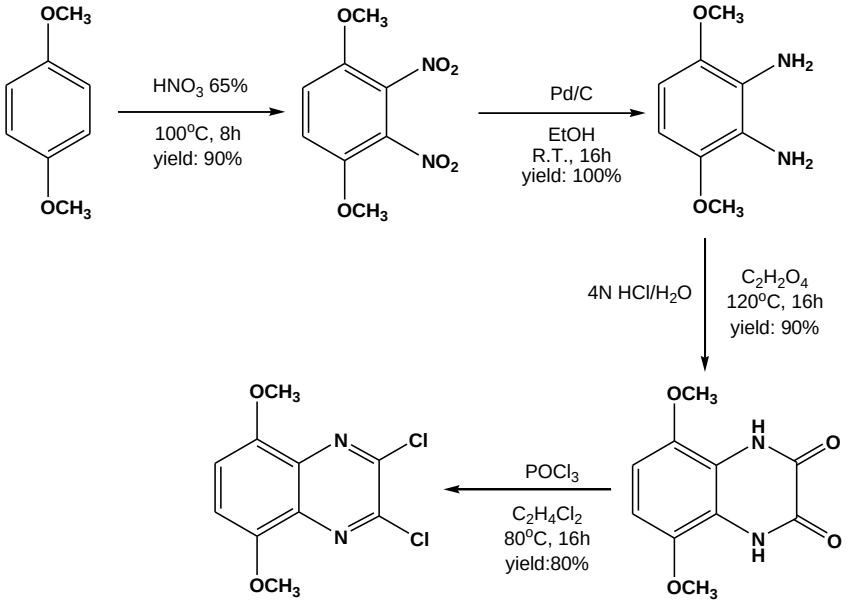

Scheme 1.2

3. Synthesis of the QxBox cavitands (**Scheme 1.3**). It involved the fourfold bridging reaction of the resorcinarene scaffold with 2,3-dichloro-5,8-dimethoxy quinoxaline under basic conditions to obtain the octamethoxyquinoxaline cavitand. Subsequently, the cleavage of the methoxy groups at the upper rim, *via* $AlCl_3$ in dry toluene was performed, leading to the octahydroxyquinoxaline cavitand. The reagents in last synthetic step differentiate the synthesis of the MeQxBox and the EtQxBox, whereas the reaction conditions were the same. The yield of the MeQxBox was only 5%, whereas a good yield (44%) was associated to the synthesis of the EtQxBox: this behavior

can be explained taking into account that the use of the methoxy bridges produce a very tight and strained cavity, thermodynamically unfavorable.

Although several reaction conditions were tested (solvent, temperature, reaction times and pressure), no significant improvements in the yield of the final step were obtained, thus proposing the synthesis based on the use of an excess of chlorobromomethane under basic conditions was proposed.

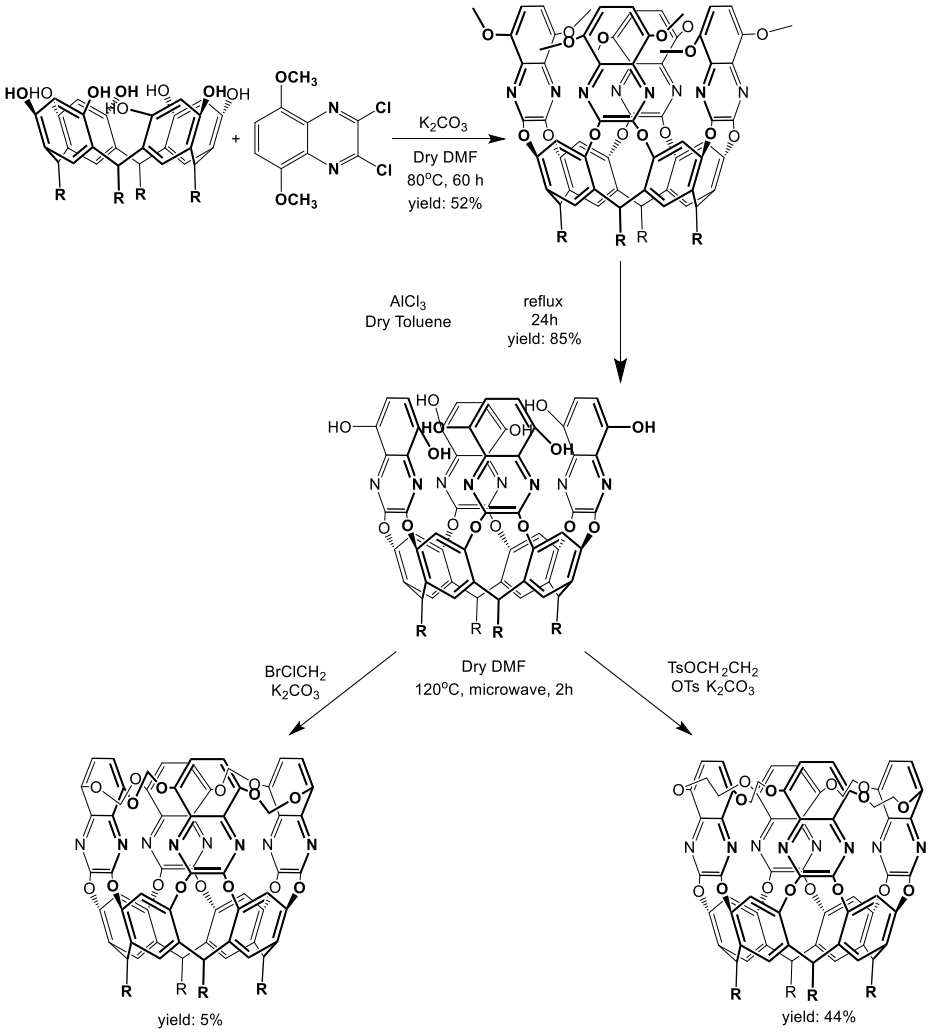

Scheme 1.3

The synthesis of the triptycene-functionalized cavitands is presented in Schemes **1.4-1.6** and is exhaustively reported in the published article [56] and in F. Bertani's PhD thesis [57].

The resorcinarene skeleton is the same as that reported in the synthesis of the QxBox cavitands. The synthesis of the 2,3-dihydroxy-6,7-triptycenequinoxaline is depicted in **Scheme 1.4**.

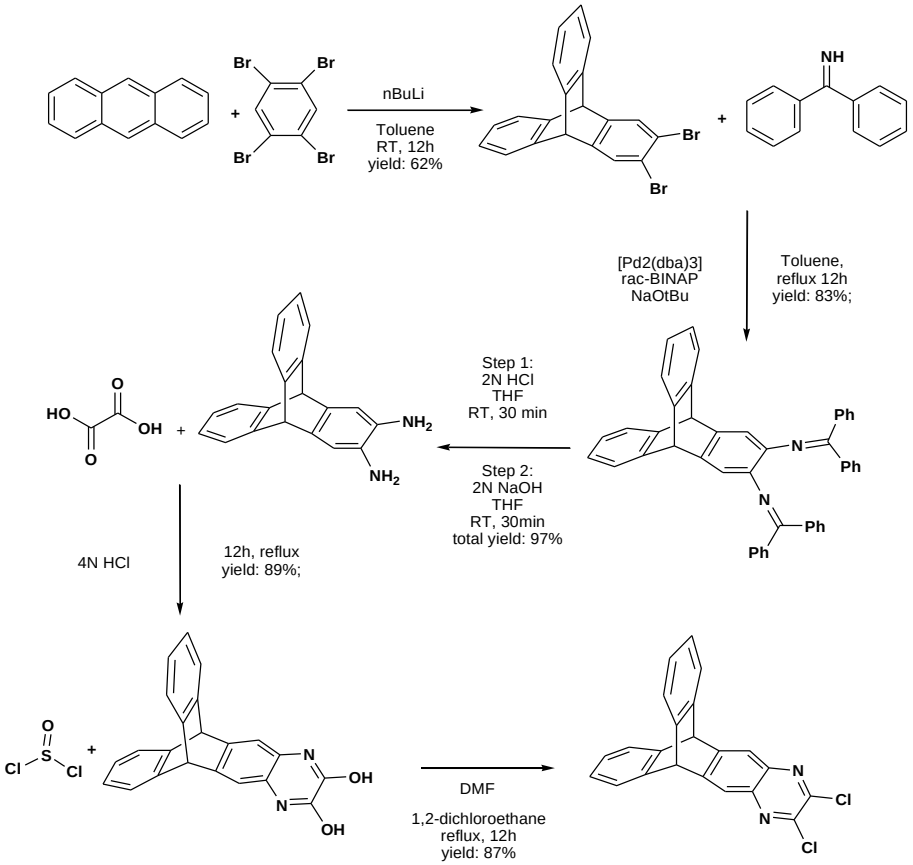

Scheme 1.4

The preparation of the monofunctionalized triptycene cavitand (MonotriptyQxCav) required the synthesis of a tetraquinoxaline cavitand (QxCav), followed by the selective removal of one quinoxaline unit, by using 1.1 equivalent of catechol, in presence of cesium fluoride as base, and the final bridging with one 2,3-dihydroxy-6,7-triptycenequinoxaline.

The ditriptycene cavitand (DiTriptyQxCav) was obtained from the QxCav, by removing two quinoxaline walls by using 3.3 equivalent of catechol. Subsequently, the bridging with two 2,3-dihydroxy-6,7-triptycenequinoxaline units allowed to obtain the purified final cavitand with 46% of yield.

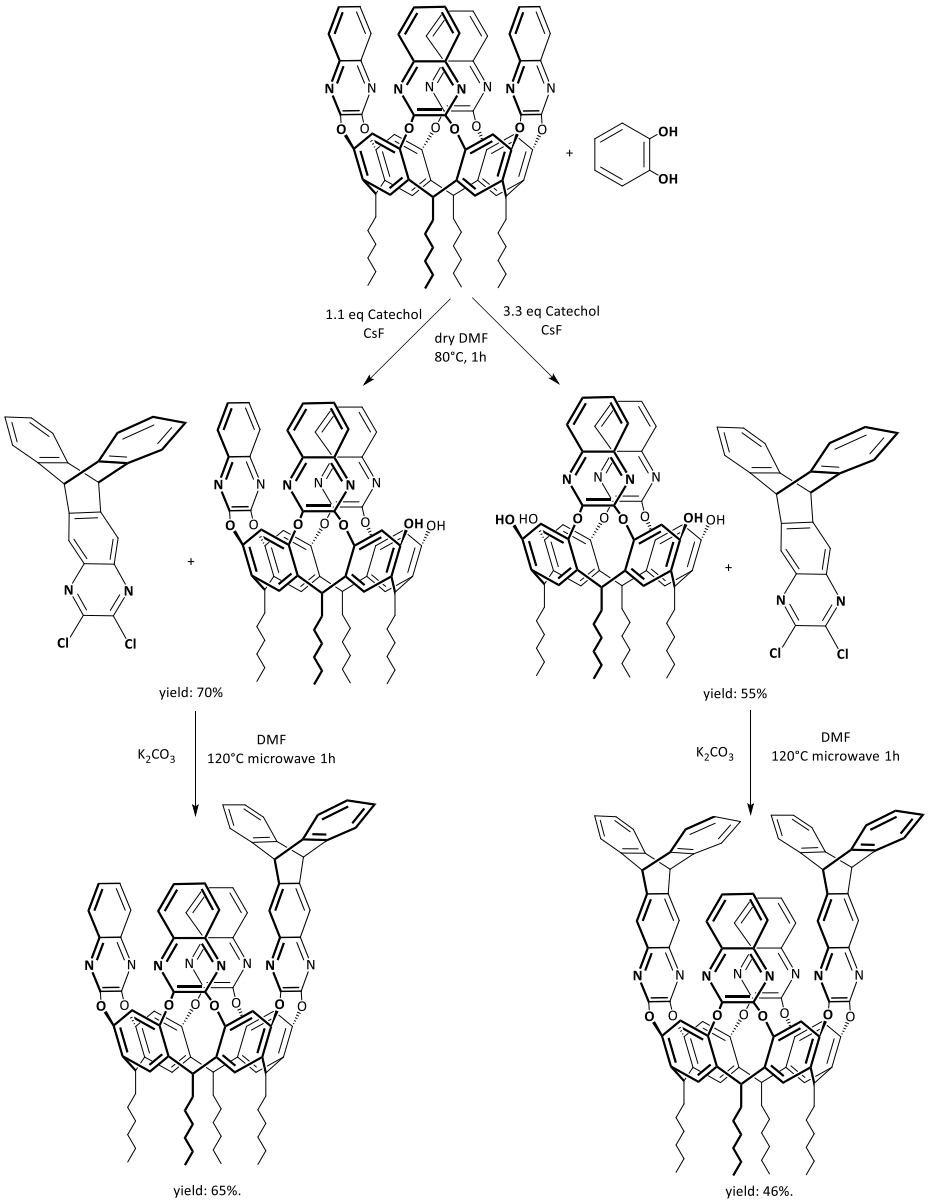

Scheme 1.5

1.3.3 XRD Analysis

The inclusion capabilities of the synthetized cavitands toward BTEX were studied by different crystallization experiments, performed in collaboration with Prof. C. Massera, from the University of Parma and Prof. S. Geremia, from the University of Trieste. The experiments were carried out by dissolving the receptors and the guests in a proper solvent and performing a low-evaporation crystallization.

The MeQxBox cavitand host-guest crystals were obtained only for the benzene complex by slowly evaporating a chloroform solution. The molecular structure of benzene@MeQxBox is shown in **Figure 1.16**.

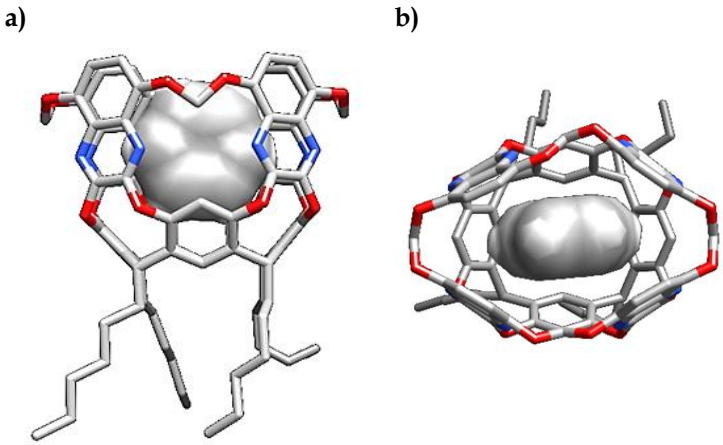

Figure 1.16 Molecular structure of benzene@MeQxBox complex crystallized from $CHCl_3$. The guest is shown in space filling mode a) side view, b) top view. The hydrogen atoms of the receptor and lattice solvent molecules have been omitted for clarity.

As expected, the presence of short methoxy bridging groups at the upper rim lead to obtain a highly strained structure, where the quinoxaline units are conformationally blocked: the space available for the guest complexation is reduced compared to the parent QxCav. The cavity is rhombohedral and can be perfectly fitted by benzene. The guest is stabilized by CH-π interactions between its hydrogen atoms and the quinoxaline walls. The inward facing hydrogen atoms of the methylendioxy bridges further stabilize the complex, *via* van der Waals interactions.

The EtQxBox cavitand crystal structures have been obtained for benzene, toluene and *o*-xylene from DMSO solutions (**Figure 1.17**). Benzene is deeply included within the cavity: two CH-π interactions with the lower aromatic rim of the cavitand and two bifurcated CH-N interactions with the nitrogen of adjacent quinoxalines are present.

The toluene@EtQxBox complex is characterized by the same interactions present in EtQxBox@benzene, but it is enforced by the different orientation of the guest: in order to maximize the binding energy, toluene is almost parallel to two quinoxaline walls of the cavitand, leading to an increase of the π-π interactions. The methyl substituent of the guest is present in two equivalent positions, forming adjunctive CH-π interactions with the blocked aromatic rings at the upper rim of the cavitand.

The behavior of the *o*-xylene is very similar to that of the toluene complex, leading to *o*-xylene@EtQxBox, characterized by a comparable geometry and additional CH-π interactions, increasing even more the complexation binding energy.

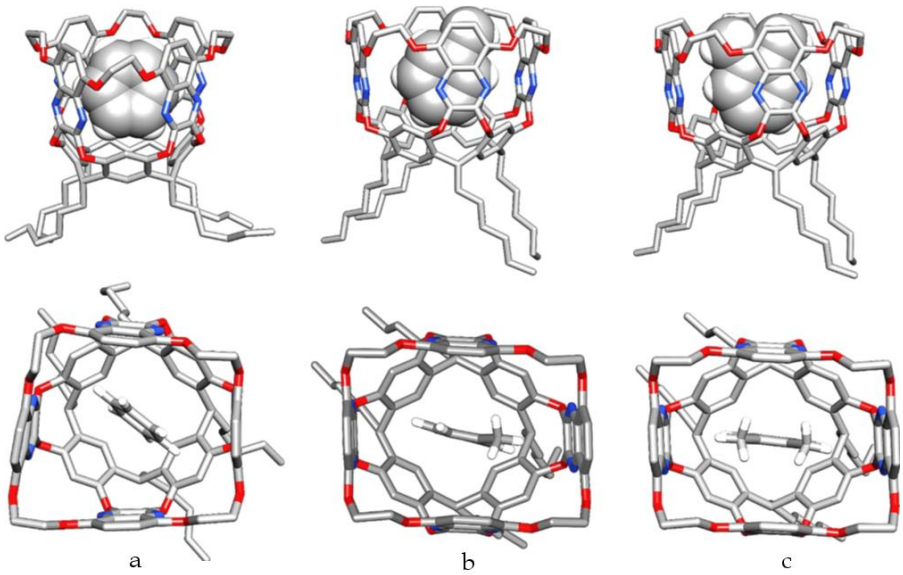

Figure 1.16 Side and top view of the molecular structures of benzene@EtQxBox (a), toluene@EtQxBox (b), and *o*-xylene@EtQxBox (c) host-guest complexes. Only the hydrogen atoms of the guest are shown.

The X-ray structure of the triptycene cavitands show that the vase form is present in the solid state. The MonoTriptyQxCav shows parallel quinoxaline walls, despite the presence of the bulky triptycene unit, whereas the difunctionalization leads to a structure distortion.

Crystals of both cavitands with benzene were obtained by slow evaporation of a chloroform solution. In the MonoTriptyQxCav@benzene complex (**Figure 1.17** a,c,e,g) benzene is localized in front of the pyrazine rings of the quinoxaline walls, forming a 45° angle. In DiTriptyQxCav@benzene complex (**Figure 1.17** b,d,f,h), the guest faces exactly the two inner quinoxalines, in a distorted structure. The triptycene units block the system, forming CH-π interactions with the guest, acting as a molecular roof.

As can be clearly seen in **Figure 1.17** g and h the functionalization strongly reduces the cavity opening, thus limiting the interaction with the environment and influencing the adsorption/desorption equilibria.

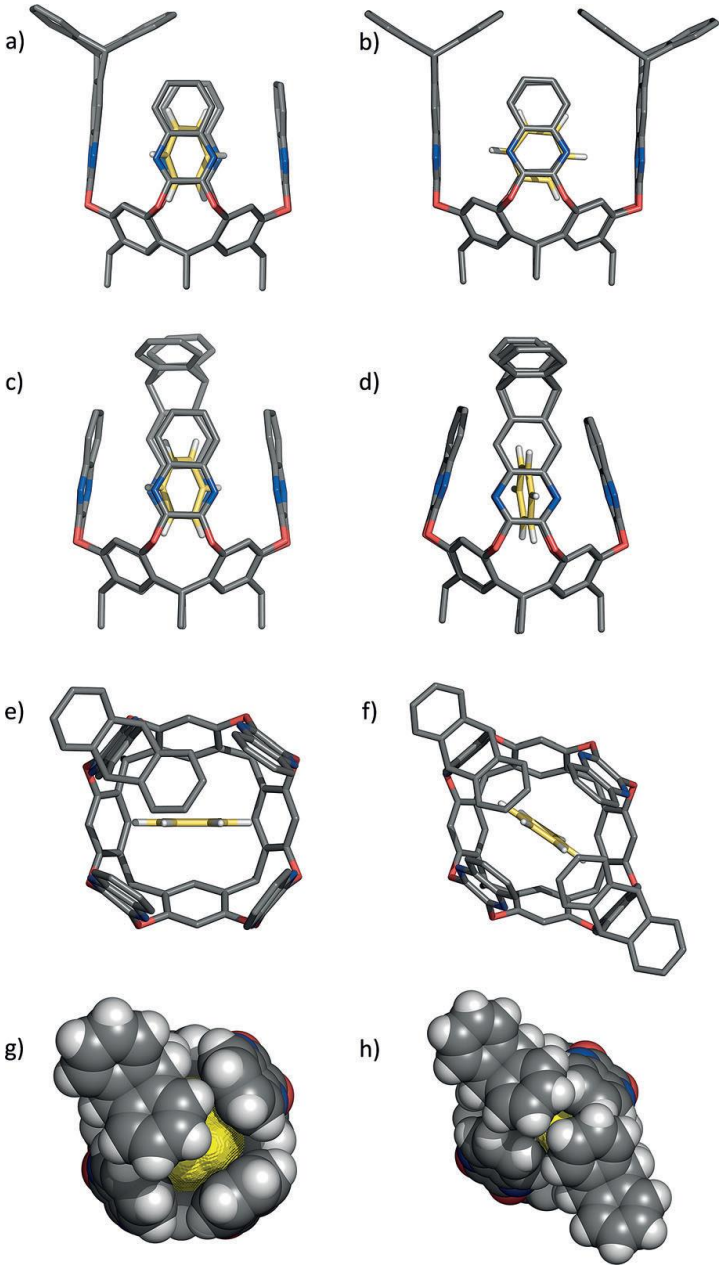

Figure 1.17 Side (a-d) and top (e-h) views of the crystal structures of complexes benzene@MonoTriptyQxCav (left) and benzene@DiTriptyQxCav (right). Solvent molecules, n-hexyl chains, and hydrogen atoms are omitted for clarity. The volume available inside the cavity is depicted in yellow.

1.3.4 *SPME fiber characterization*

In order to test the capabilities of the cavitands toward BTEX sampling, SPME coatings were developed and characterized.

The first step was to demonstrate the thermal behavior of cavitands by means of thermogravimetric analyses (TGA). Excellent stabilities were demonstrated for all the cavitands: with respect to the parent QxCav, the additional functionalization did not reduce the thermal stability of the modified receptors:

1. The TGA of MeQxBox showed a stability up to 350 °C (**Figure 1.16**)

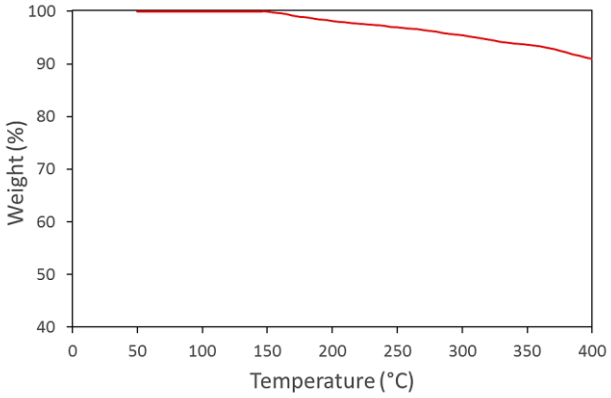

Figure 1.18 TGA of MeQxBox

2. EtQxBox was stable up to 300 °C (**Figure 1.17**)

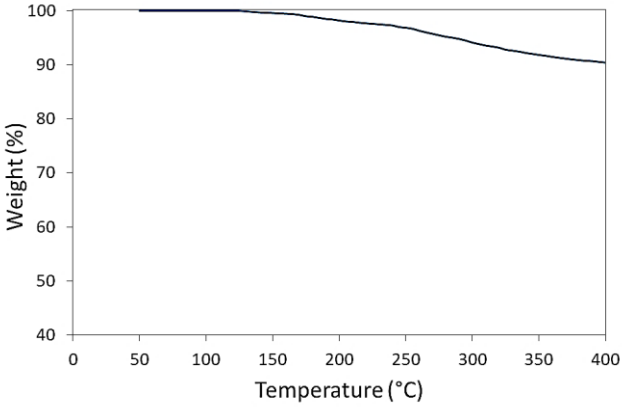

Figure 1.19 TGA of EtQxBox

3. The thermal stabilities of TriptyQxCav cavitands were also compared with that of the unsubstituted QxCav after complexation with benzene. The samples were completely solubilized in benzene and the solvent was removed by low pressure evaporation. The entrapped guests were desorbed at higher temperatures if compared to their boiling point. The release temperature is a good indicator of the forces involved in benzene complexation: the higher is the value, the stronger is the host-guest complex.

   The TGA traces shown in **Figure 1.18** are characterized by two different weight losses due to the desorption of the complexed benzene and the decomposition of the cavitands, respectively.

   The presence of the triptycene roof increased the temperature range for the release of benzene from the cavity if compared to QxCav, for both MonoTriptyQxCav and DiTriptyQxCav. This behavior can be ascribed to the steric effect of the triptycene roofs and the additional CH-π interactions. The triptycene cavitands were stable up to 450°C.

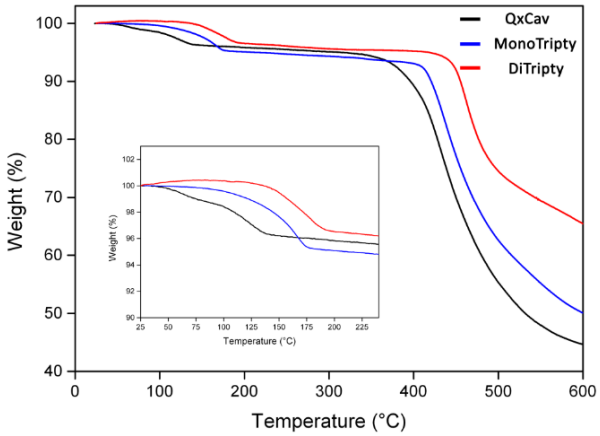

Figure 1.20 TGA analysis of QxCav, MonoTriptyQxCav and DiTriptyQxCav cavitands under nitrogen; benzene release is highlighted in the insert.

The coatings were applied by vertically dipping the bare silica support of the fibers (1 cm length) in Duralco 4460 epoxy glue and, after 2 min, in the respective cavitands powder for four times. In this way approximately 7.0 ± 0.5 mg of cavitand powder were loaded onto the fibers. At least four fibers were prepared and tested both for fiber-to-fiber and batch-to-batch repeatability.

The thermal stability of the coating was also evaluated by conditioning the obtained SPME fibers in the GC injector port at 250°C for 2 min: no significant bleeding was observed, thus confirming the thermal resistance of the materials.

The morphology of the coated fibers was investigated by environmental scanning electron microscopy (ESEM) under different magnifications. The analyses showed a homogeneous and uniform distribution of the cavitand all along the fiber. The average thickness of coating was measured for all the fibers: 35 ± 4 µm for MeQxBox, 40 ± 6 µm for EtQxBox, 30 ± 5 µm for MonoTriptyQxCav and 37± 7 µm for DiTriptyQxCav (analysis performed on 5 points for each image for 3 different fibers of the batch).

Examples of the obtained coatings are reported in **Figure 1.21**.

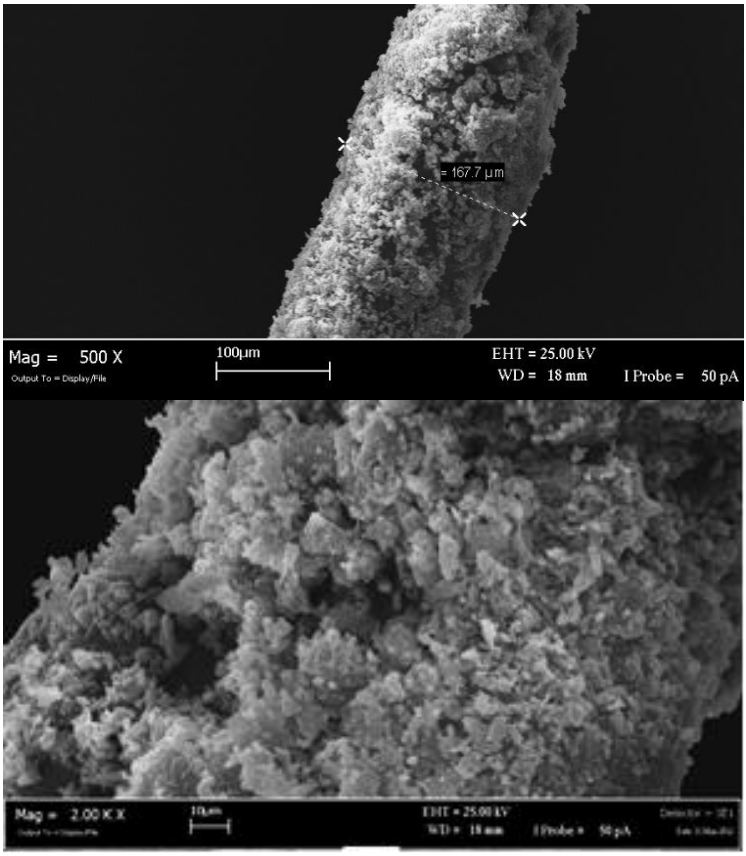

Figure 1.21 Scanning electron microscope image of the MeQxBox (top) and EtQxBox (down)

1.3.5 *SPME selectivity studies*

Preliminary experiments were performed in order to achieve the best extraction conditions in terms of extraction time. A 5-20 min range was investigated in order to achieve the better extracting performances: the extraction of the analytes occurs until an adsorption/desorption equilibrium is set, reaching a plateau in the GC-MS response. All the cavitands coating were characterized by the same behavior: a dramatic increase in signals was obtained up to 15 minutes, while no significant differences between the responses at 15 and 20 min were achieved. Thus, 15 min was selected for BTEX extraction.

Additional experiments were performed in order to assess the variability of the responses of the cavitand coatings by operating under different humidity levels (30% and 80%, BTEX concentrations 300 ng/m^3). Student *t*-test did not show significant differences ($p > 0.05$) for all the investigated analytes, thus proving the suitability of the coating for urban air monitoring.

The selectivity studies were performed by analyzing an air mixture containing an amount of aliphatic hydrocarbons (from C_6 to C_9) up to two orders of magnitude higher than BTEX (38−56 µg/m^3 *vs* 385−473 ng/m^3 range for the QxBox cavitands, 38–56 µg/m^3 vs 3.49–4.74 µg/m^3 for the triptycene cavitands). The concentration levels of the aliphatic compounds were controlled in order to reproduce the concentration levels of real urban air. Consecutive desorption of the SPME fibers were performed from 50 to 250°C (**Figures 1.20-1.22**) in order to prove the selective desorption of the BTEX over the aliphatic interferences. The desorption temperature is related to the strength of the interactions between the receptor and the adsorbed compounds: analytes retained by strong interactions and/or inclusion inside the receptor are desorbed at higher temperatures compared to those characterized by weak and van-der-Waals interactions.

The possibility to desorb only the aliphatic compounds and detect the BTEX by selective desorption allows to improve the analytical performances, in terms of LODs, LOQs and enrichment factor, and has fasten the gas chromatographic separation, without the risk of peak coelution, thus obtaining short analysis times.

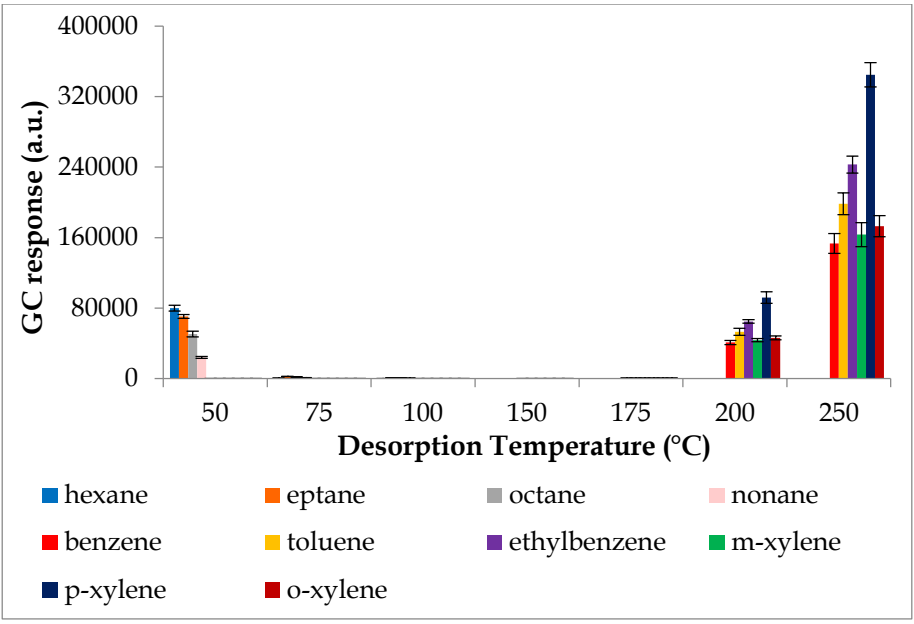

Figure 1.22 MeQxBox, HS-SPME-GC-MS conditions. Extraction time: 15 min, RT (n=3).

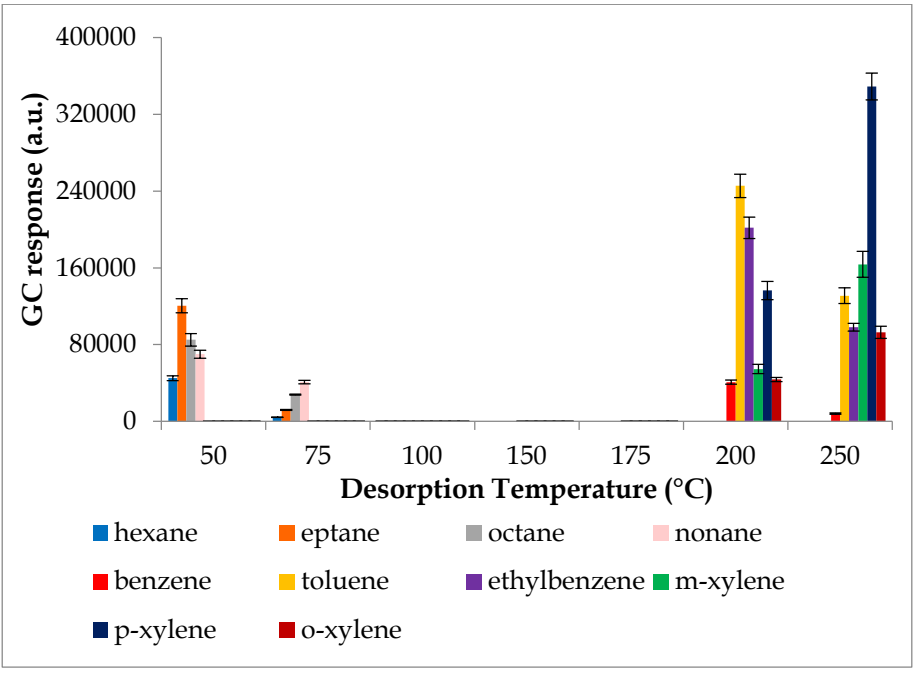

Figure 1.23 EtQxBox, HS-SPME-GC-MS conditions. Extraction time: 15 min, RT (n=3).

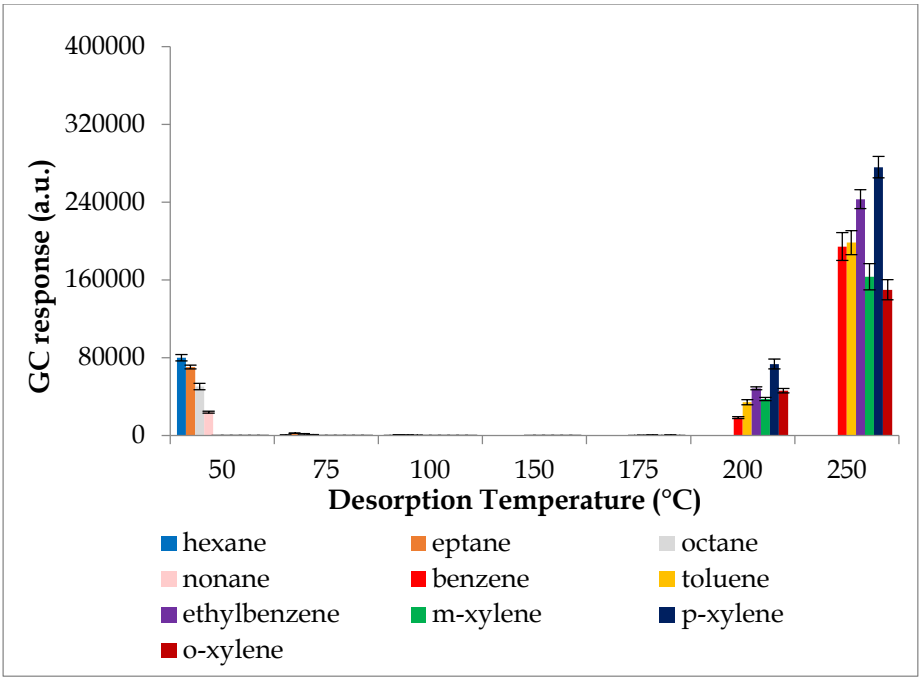

Figure 1.24 DiTriptyQxCav, HS-SPME-GC-MS conditions. Extraction time: 15 min, RT (n=3).

Consecutive desorption experiments at different temperatures showed that aliphatic hydrocarbons can be completely desorbed between 50 and 100 °C, whereas BTEX desorption begins at 200 °C and was exhaustive only at 250 °C. No carryover was observed after desorbing the analytes at this temperature.

The gap observed in desorption temperatures confirmed the hypothesis formulated during the cavitands design, as well as the data obtained by X-ray analysis and theoretical calculations. As expected, BTEX are complexed inside the cavity of the receptors, whereas aliphatic hydrocarbons are simply physisorbed by the organic coating. Low temperatures (up to 100°C) are able to remove the aliphatic hydrocarbons from the SPME coating, confirming that only weak van der Waals interaction are present.

By contrast, BTEX desorption begins at 200°C and is complete only at 250°C. This behavior reflects the affinity of the cavity for the aromatic guests, attributable to synergistic π–π and CH–π interactions. These findings are of pivotal importance: it is possible to remove the aliphatic interferences at low temperatures and detect the targeted analytes by using a high thermal

treatment. Unfortunately, in both QxBox and triptycene cavitands the SPME-GC-MS analysis did not allow the selective desorption of benzene over TEX.

1.3.6 *SPME enrichment factors*

The affinity of the synthetized cavitands toward BTEX was evaluated in terms of enrichment factors (EFs). EFs were calculated as the ratio of the concentration of the analyte in the fiber after the extraction to that of the analyte in the same gas standard mixture, i.e. by using the ratio of the chromatographic peak area of the analyte after SPME to that obtained by the direct injection of the same gas standard solution (n=3). This factor is also corrected considering the length and the thickness of the SPME fiber, thus allowing the comparison between all the synthetized fibers. Moreover, a comparison between the enrichment capabilities of the cavitand coating and commercially available adsorbent SPME fibers usually used for BTEX enrichment (namely 2 cm-50/30 µm DVB-CAR-PDMS) was performed (**Figure 1.21**).

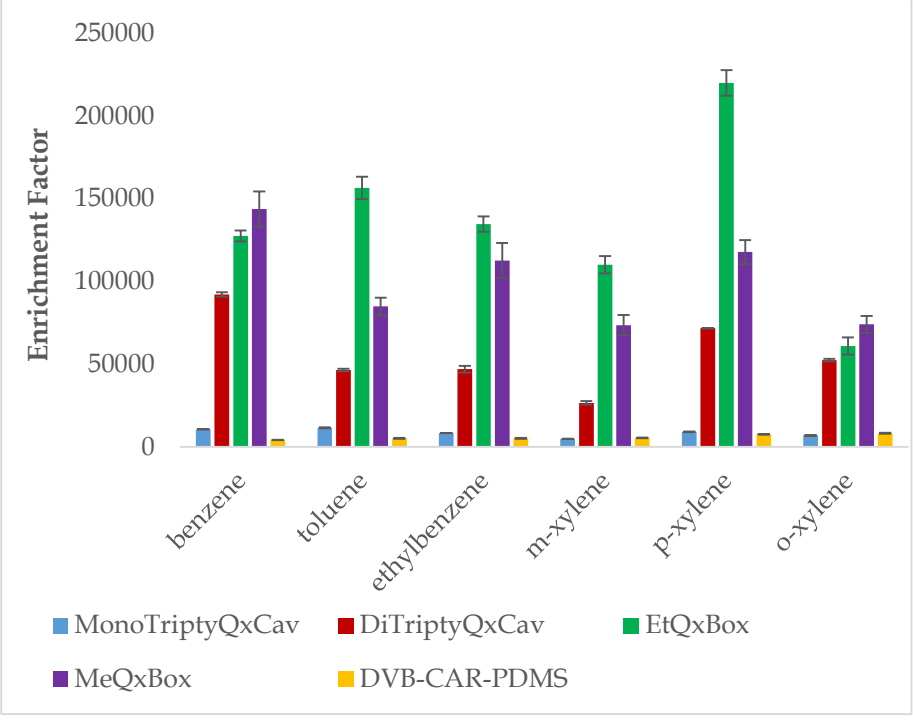

Figure 1.25 EFs comparison between the cavitand-based and the DVB–CAR–PDMS coatings for BTEX extraction. HS-SPME conditions: extraction time: 15 min, RT (n=3).

As shown in **Figure 1.25**, the enrichment capabilities of the developed cavitands were different

1. QxBox cavitands were characterized by excellent EFs, at least 30 times higher compared to those of the commercial fibers.
   MeQxBox and EtQxBox showed different selectivity towards BTEX: MeQxBox was characterized by an enhanced affinity towards benzene, being the analyte with the highest EF, thus proving that the presence of the methylendioxy bridges reduces the cavity opening, facilitating the entrance of benzene with respect to the other aromatic analytes. On the opposite, EtQxBox, due to the presence of ethoxy bridges, is characterized by a larger opening of the cavity, thus being suitable for the complexation of substituted aromatic hydrocarbons.
   As supposed, the steric hindrance has a pivotal importance in discriminating the analytes during the complexation: while benzene fit perfectly the cavity of the MeQxBox, the upper rim of the EtQxBox becomes too far to interact with benzene, becoming available for CH-π interactions with the methyl substituents of the TEX.
2. MonoTriptyQxCav did not show noticeable improvements compared to the commercially available fibers and the EFs are far lower compared to those achieved by the QxBox cavitands.
3. The enrichment capabilities of the DiTriptyQxCav were at least 5 times higher than those achieved using the DVB-CAR-PDMS fiber and 22 times higher for benzene complexation. The difunctionalized receptor has a benzene EF 9 times higher with respect to the monosubstituted one. Therefore, the presence of one triptycene unit is not sufficient in order to create a steric engulfment able to trap the analytes inside the cavity. On the contrary, the difunctionalization allowed to obtain enrichment capabilities comparable with those obtained by using the QxBox receptors. The two triptycene units act as a roof at the top of the cavity and trap the BTEX inside the cavity of the receptor. Moreover, additional interactions between the guest CH of the guest and the π electrons of the functionalizing units are present, thus enhancing the binding energy.

1.3.7 Method Validation

Finally, the method validation was performed following Eurachem guidelines [48], in order to prove the suitability of the developed coatings for the determination of BTEX in air at trace levels. LODs and LOQs were obtained using not contaminated air as blank matrix.

Excellent results in terms of LOD values were achieved, in the low ng/m^3 level for all the investigated compounds. **Table 1.2** shows the LODs of the synthetized cavitands compared to those of the DVB-CAR-PDMS fiber and the RADIELLO system, which is the most commonly used BTEX sampling device. Similarly, LOQs are reported in **Table 1.3**

Table 1.2: LOD values (ng/m^3) of the supramolecular coatings and of commercially available devices

	MeQxBox	**EtQxBox**	**DiTripty QxCav**	**QxCav**	**DVB-CAR-PDMS**	**RADIELLO**
Extraction Time (min)	15	15	15	15	15	1 440
benzene	0.4	0.7	1.7	5.2	17.1	1.6
toluene	0.6	0.4	3.1	7.2	2.1	1.5
ethylbenzene	0.5	0.4	1.3	5.7	4.8	1.2
m-xylene	1.2	0.8	2.0	10.0	6.1	1.3
p-xylene	0.6	0.3	1.3	9.0	6.1	1.7
o-xylene	1.0	0.5	2.2	12.5	14.3	2.0

Table 1.3: LOQ values (ng/m^3) of the developed coatings

	MeQxBox	**EtQxBox**	**DiTriptyQxCav**
benzene	1.3	2.0	5.5
toluene	1.1	0.9	10.0
ethylbenzene	1.4	1.0	4.3
m-xylene	2.9	2.1	6.6
p-xylene	1.4	0.8	4.5
o-xylene	2.5	1.3	7.3

As reported, the LODs of both the QxBox cavitands and DiTriptyQxCav coatings were very close, showing better performances in terms of sensitivity compared to the systems commonly used for air monitoring i.e. Radiello and DVB-CAR-PDMS commercial coatings. Additional advantages of the developed fibers rely on: i) use of shorter BTEX extraction times, thus speeding up BTEX monitoring, and ii) enhanced selectivity toward aromatic hydrocarbons.

By the analysis and the comparison of both the EFs and LODs obtained by MeQxCav and EtQxBox respectively, the role of the length of the bridging units can be clarified: the shorter methylendioxy chains reduce the cavity opening, thus allowing to obtain the lowest LOD and the highest EF for benzene. By contrast, in the EtQxBox, as discussed in **paragraph 1.2.5**, no selectivity among the BTEX was achieved. By comparing the LODs achieved by the functionalized receptors with those of the QxBox cavitand, a great improvement can be observed with a general decrease of the LOD values, approximately of one order of magnitude.

A good linearity was proven by applying Mandel's fitting test on three order of magnitude in the following concentration range: LOQ-3500 ng/m^3 for benzene, LOQ-4100 ng/m^3 for toluene, LOQ-4700 ng/m^3 for ethylbenzene, *m*-, *p*-, and *o*-xylenes.

As for precision, good results were obtained in terms of both intraday repeatability and intermediate precision, with RSD values always lower than 10%. In the case of intermediate precision, ANOVA showed that mean values were not significantly different among the 3 days giving p values >0.05 (n=5).

Extraction recoveries were calculated for all the analytes at two concentration levels, showing the excellent efficiency of the devised method. In particular, recoveries ranging from 99 ± 1% to 109 ± 1% were obtained by using MeQxBox, whereas values in the 96±1 - 108±1% and 97±1 - 107±1% were achieved by the EtQxBox and DitriptyQxCav coatings, respectively (n=10).

1.3.8 Real samples analysis

Finally, in order to prove the suitability of the method, both the MeQxBox and the DiTriptyQxCav coated fibers were used for the analysis of real environmental air samples taken near a traffic fixed-site air monitoring station, at three different times.

The BTEX concentration levels obtained were in agreement with those obtained by the on-line measurements performed by the fixed-site station, in which the automatic BTEX sampling is based on the following steps:

1. pre-concentration of the analytes using a Carbotrap B cartridge
2. thermal desorption
3. detection using a GC-PID integrated system

Since no significant differences were observed between the results achieved by the SPME-GC-MS analysis and the fixed site station data (**Table 1.4**), it can be stated that the developed method can be a reliable tool for the determination of BTEX in urban air.

Table 1.4: Comparison between the values ($\mu g/m^3$) obtained by using the SPME-GC-MS developed method and those obtained by the fixed-site station at three different sampling times

	MeQxBox	**Fixed Station**	**MeQxBox**	**Fixed Station**
	9:00		16:00	
benzene	2.7±0.3	2.9±0.1	2.1±0.1	1.8±0.2
toluene	7.7±0.5	7.1±0.3	6.0±0.5	6.7±0.4
ethylbenzene	1.5±0.2	1.0±0.4	0.9±0.1	0.7±0.1
xylenes	7.6±0.7	8.2±0.9	4.8±0.4	5.2±0.3

	DiTriptyQxCav	**Fixed Station**
	12:00	
benzene	1.8±0.2	1.6±0.1
toluene	5.4±0.4	6.1±0.5
ethylbenzene	1.1±0.1	0.9.±0.2
xylenes	5.2±0.3	5.5±0.4

1.3.9 *New prototype for fast BTEX monitoring*

A simple device for benzene monitoring having the developed cavitands as preconcentration material and a miniaturized photoionization detector (Mini-PID PPB by IonScience) was developed and tested under laboratory conditions (**Figure 1.26**) by the CNR of Bologna.

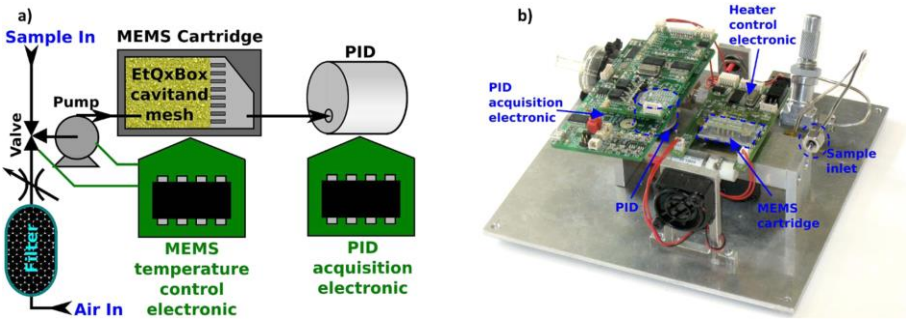

Figure 1.26 Schematic representation (a) and photograph (b) of the monitoring device

Compared to the mini-GC device already proposed [37] the system was designed in order to combine the BTEX preconcentration and separation into a single microelectromechanical sensor (MEMS) chip packed with 10 mg of a proper mesh of the cavitand.

By comparing the performances of the MeQxBox, EtQxBox and DiTriptyQxCav, the best results were achieved by using the EtQxBox cavitands. In fact, by applying a smart temperature program directly to the EtQxBox mesh, benzene is released at lower temperatures with respect to toluene and xylenes, whereas the other receptors were unable to perform this discrimination. Since the EtQxBox was able to desorb selectively benzene, a temperature desorption ramp can be used in order to replace the GC minicolumn.

The system, shown in **Figure 1.26**, is an active sampling device, consisting in a pump operating flow rates up to 120 mL/min. Obviously, the duration and flow rate of the sampling step can be adapted to specific applications. In order to produce an independent and portable system, scrabbled air is used as carrier gas: an activated carbon filter provides clean air directly into the MEMS, thus removing the need of inert gas.

The best results in terms of selectivity toward benzene were found by using a 30 mL/min flow. In **Figure 1.27** signals acquired by the PID detector during

the desorption temperature ramp are shown. The sampling of BTEX was performed by keeping the MEMS cartridge at room temperature and pumping the test mixture at 120 mL/min for a sampling time of 5 minutes. Then, the cartridge was heated by using an air flow of 30 mL/min by the heating programme reported below: after 2 minutes at room temperature, the temperature was increased to 90 °C for 40 s in order to obtain the complete removal of any nonspecifically adsorbed species. The subsequent temperature step at 150 °C is applied in order to release preferentially benzene. As can be seen from **Figure 1.27**, the scrabbled air resulted in a very small *blank* signal, thus confirming the suitability of the active carbon as filter of the ambient air. The red line represents the injection of 20 ppb_v of benzene: a relevant peak was present at 150°C, whereas only a slightly increase was shown when a mixture of 20 ppb_v benzene and 20 ppb_v toluene was injected (purple line). These first results demonstrated that only a very small amount of toluene was released at 150 °C, while it was completely desorbed by applying a subsequent heating step at 220°C. Benzene was totally released during the third desorption step, but in this case the signal of the toluene became predominant.

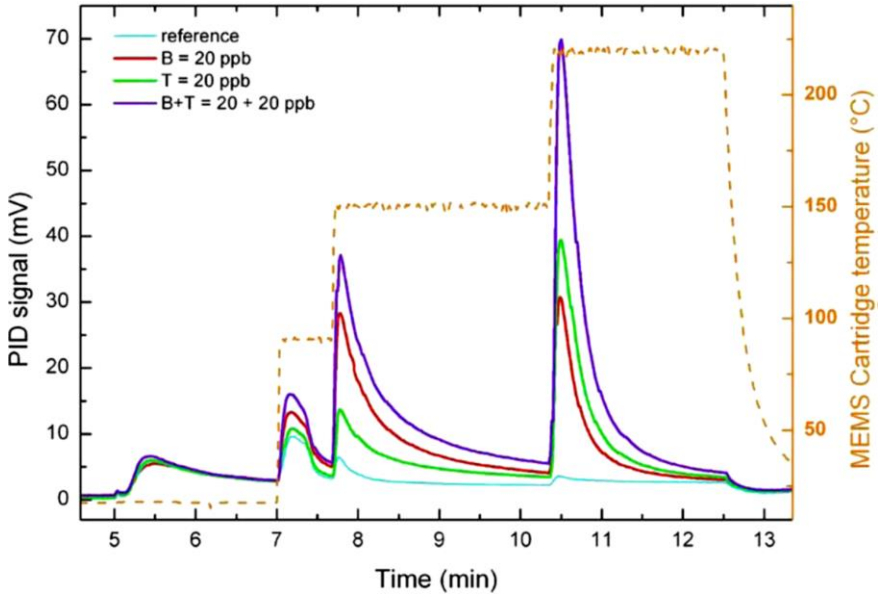

Figure 1.27 Responses of the PID detector to a proper temperature ramp for benzene (B, red), toluene (T, green), and a mixture of benzene and toluene (B+T, purple), compared to a "reference" sample of only air (cyan).

On the basis of these findings, it could be stated that the desorption step at 150°C was the most significant for benzene quantitation, since toluene interferes only slightly with the targeted analyte. Even if the obtained results were promising, the separation between benzene and toluene was not complete, due to the very short cartridge used in this work.

Nevertheless, by calibrating the system and using a simple linear combination of the responses at the two temperatures (150 and 220 °C), a deconvolution of the signal onto the two contributes was possible, and the small signal generated by toluene could be easily subtracted. The developed system was able to selectively quantify benzene in the 1.25-20 ppb_v range in presence of higher concentrations of toluene and xylenes. Future implementation will allow to obtain better performances.

The superior benzene complexation capabilities of EtQxBox over the simple QxCav are vital in order to obtain a system in which the chromatographic separation is avoided. The consequences of the stronger complexation capabilities and the freezing of the EtQxBox can be seen in **Figure 1.28,** where the effect of the temperature increase during the sampling step is compared for the two cavitands. QxCav rapidly decreases the complexation efficiency during the adsorption step at temperatures slightly higher than 20 °C, whereas EtQxBox maintains the preconcentration capabilities up to 60 °C; only at 100 °C the decrease of the complexation efficiency become evident. These findings further confirm that the presence of the bridging units among the quinoxaline walls leads to a conformationally blocked cavity, characterized by stronger host−guest interactions, thus increasing the selectivity and the enrichment capabilities of the receptor.

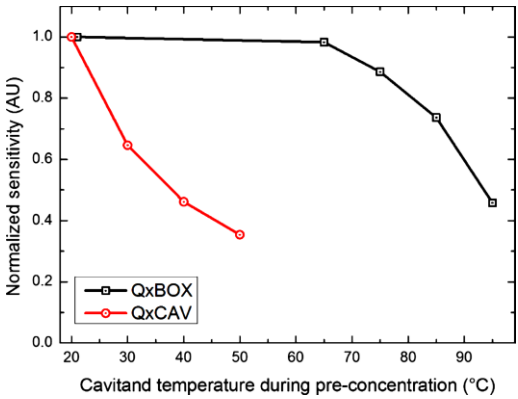

Figure 1.28 QxCav and EtQxBox normalized sensitivity (normalization at 20°C) toward benzene at increasing temperatures.

1.4 Conclusions

In this study we designed, synthetized and validated four new functionalized cavitands, to be used as SPME coatings for BTEX extraction in air. All the materials were selective toward BTEX, whereas aliphatic hydrocarbons were only physisorbed onto the fiber, thus allowing their desorption at low temperature. The SPME-GC-MS method was fully validated and the materials were used in real sample analysis.

DitriptyQxCav is characterized by two triptycene units at the upper rim of the cavitand. The functionalization produces a system distortion in the *vase* conformation and acts as a roof at the top of the cavity. This new receptor shows higher enrichment factors compared to the commercial SPME coatings.

QxBox cavitands are characterized by ether bridges between the quinoxaline walls, thus producing a freezing of the system and reducing the cavity opening. MeQxBox presents a very close and strained cavity, fitting perfectly benzene. Under these conditions, an absorbent characterized by the highest enrichment factor and lowest LOD for benzene among all the tested materials was obtained. The EtQxBox is characterized by a larger cavity. The benzene is complexed inside the cavitand but the quinoxaline walls are too far from the guest to obtain strong π–π and CH–π interactions. The presence of one (toluene) or two (xylene) methyl substituents increases the binding energy of the EtQxBox complexes through additional CH–π interactions. The different host@guest energies result in different benzene release temperatures compared to the other TEX when the cavitand is used as trapping material in the developed device. A novel sensor for ppb_v level detection of benzene in air was developed: it is based on a nano-PID detector equipped with MEMS cartridge, characterized by high electivity and sensitivity. In this stand-alone sensor, the cavitand receptor EtQxBox acts at the same time as selective preconcentrator and GC-like separation device. By applying a smart temperature pragramme, is possible to detect selectively benzene over the other TEX.

It is noteworthy that the ppb_v-level sensitivity was demonstrated with a simple, stand-alone, and unsupervised sensing device, autonomously sampling and analyzing test samples. In perspective, EtQxBox functionalized cavitand has enormous potentiality in order to develop both active samplers characterized by high selectivity and sensibility toward BTEX and stand-alone sensors for personal benzene exposure monitoring in industrial settings.

1.5 Acknowledgments

Thanks to all the researchers involved in the project: Prof. E. Dalcanale, Prof. M. Careri, Prof. C. Massera, Prof. R. Pianalli and Dr. F. Bertani from the department of SCVSA and Prof F. Ugozzoli from the department of Engeneering and Architecture of the University of Parma; Dr. J.W. Trzcinski from the University of Padova; Prof. S. Geremia and Dr. G. Brancatelli from the University of Trieste; Dr. S. Zampolli and Dr. I. Elmi from CNR-IMM Bologna; Prof. T.M. Swager and Dr. Elizabeth Sterner from Department of Chemistry, Massachusetts Institute of Technology, Cambridge (USA).

1.6 References

[1] F. Bianchi, R. Pinalli, F. Ugozzoli, S. Spera, M. Careri, E. Dalcanale, *Cavitands as superior sorbents for benzene detection at trace level*, New J. Chem., 27 (2003) 502– 509.

[2] IARC Monographs Volume 100F, http://monographs.iarc.fr/ENG/Monographs/vol100F/mono100F-24.pdf.

[3] Directive 2008/50/EC of the European Parliament and of the Council of 21 May 2008 on ambient air quality and cleaner air for Europe, http://ec.europa.eu/environment/air/quality/legislation/existing_leg.htm

[4] H. Lahlou, X. Vilanova, X. Correig, *Gas phase micro-preconcentrators for benzene monitoring: a review*, Sens. Actuators B, 176 (2013) 198-210.

[5] T. Gołecki, J. Namieśnik, *Passive sampling*, TrAC, 21 (2002) 276−291.

[6] E.H. Daughtrey, K.D. Oliver, J.R. Adams, K.G. Kronmiller, W.A. Lonneman, W.A.A. McClenny, *A comparison of sampling and analysis methodsfor low-ppbC levels of volatile organic compounds in ambient air*, J. Environ. Monit., 3 (2001) 166−174.

[7] Y. Ueno, T. Horiuchi, O. Niwa. *Air-Cooled Cold Trap Channel Integrated in a Microfluidic Device for Monitoring Airborne BTEX with an Improved Detection Limit*, Anal. Chem., 74 (2002) 1712−1717.

[8] M. Marc, M. Tobiszewski, B. Zabiegała, M. de La Guardia, J. Namiesnik, *Current air quality analytics and monitoring: A review*, Anal. Chim. Acta, 853 (2015) 116 –126.

[9] W. Bourgeois, A.C. Romain, J. Nicolas, R.M. Stuetz, *The use of sensor arrays for environmental monitoring: interests and limitations*. J. Environ. Monit., 5 (2003) 852−860.

[10] K. Arshak, E. Moore, G.M. Lyons, J. Harris, S.A. Clifford, *A review of gas sensors employed in electronic nose applications*, Sens. Rev., 24 (2004) 181−198.

[11] R.P. Belardi, J. Pawliszyn, *The application of chemically modified fused silica fibers in the extraction of organics from water matrix samples and their rapid transfer to capillary columns*, Water Pollution Res. J. Canada, 24 (1989) 179-191

[12] J. Pawliszyn, *Solid Phase-microextraction: Theory and Practice*, Wiley-VCH, New York, NY, USA, 1997.

[13] C.M. Almeida, L.V. Boas, *Analysis of BTEX and other substituted benzenes in water using headspace SPME-GC-FID: method validation*, J. Environ. Monit., 6 (2004) 80-88.

[14] L. Tuduri, V. Desauziers, J.L. Fanlo, *Potential of Solid-Phase Microextraction Fibers for the Analysis of Volatile Organic Compounds in Air*, J. Chromatogr. Sci. 39 (2001) 521-529.

[15] S. Tumbiolo, J-F. Gal, P-C. Maria, O. Zerbinati, *SPME sampling of BTEX before GC/MS analysis: examples of outdoor and indoor air quality measurements in public and private sites*, Ann. Chim., 95 (2005) 757–766.

[16] A. Sarafraz-Yazdi, A. Amiri, G. Rounaghi, H.E. Hosseini, *A novel solid-phase microextraction using coated fiber based sol-gel technique using poly(-ethylene glycol) grafted multi-walled carbon nanotubes for determination of benzene, toluene, ethylbenzene and o-xylene in water samples with gas chromatography-flame ionization detector*, J. Chromatogr. A, 1218 (2011) 5757-5764.

[17] M. Wu, L. Wang, B. Zeng, F. Zhao, *Fabrication of poly(3,4-ethylenedioxythiophene)-ionic liquid functionalized graphene nanosheets composite coating for headspace solid-phase microextraction of benzene derivatives*, J. Chromatogr. A, 1364 (2014) 45-52.

[18] M.B. Gholivand, M. Shamsipur, M. Shamizadeh, R. Moradian, B. Astinchap, *Cobalt oxide nanoparticles as a novel high-efficiency fiber coating for solidphase microextraction of benzene, toluene, ethylbezene and xylene from aqueous solutions*, Anal. Chim. Acta, 822 (2014) 30-36.

[19] D. Wang, Q. Wang, Z. Zhang, G. Chen, *ZnO nanorod array polydimethylsiloxane composite solid phase micro-extraction fiber coating: fabrication and extraction capability*, Analyst, 137 (2012) 476-480.

[20] F. Zhu, Y. Liang, L. Xia, M. Rong, C. Su, R. Lai, R. Li, G. Ouyang, *Preparation and characterization of vinyl-functionalized mesoporous organosilica-coated solid-phase microextraction fiber*, J. Chromatogr. A, 1247 (2012) 42-48.

[21] M. Azenha, E. Schillinger, E. Sanmartin, M.T. Regueiras, F. Silva, B. Sellergren, *Vapor phase testing of the memory-effect in benzene- and toluene*

imprinted polymers conditioned at elevated temperature, Anal. Chim. Acta, 802 (2013) 40-45.

[22] F. Zhao, M. Wang, Y. Ma, B. Zeng, *Electrochemical preparation of polyanilineionic liquid based solid phase microextraction fiber and its application in the determination of benzene derivatives*, J. Chromatogr. A, 1218 (2011) 389-391.

[23] X. Ma, M. Huang, Z. Li, J. Wu, *Hollow fiber supported liquid-phase microextraction using ionic liquid as extractant for preconcentration of benzene, toluene, ethylbenzene and xylenes from water sample with gas chromatography-hydrogen flame ionization detection*, J. Hazard. Mater., 194 (2011) 24-29.

[24] A. Sarafraz-Yazdi, H. Vatani, *A solid phase microextraction coating based on ionic liquid sol-gel technique for determination of benzene, toluene, ethylbenzene and o-xylene in water samples using gas chromatography flame ionization detector*, J. Chromatogr. A, 1300 (2013) 104-111.

[25] J. R. Moran, S. Karbach, D. J. Cram, *Cavitands: synthetic molecular vessels*, J. Am. Chem. Soc., 104 (1982) 5826-5828.

[26] J. A.Bryant, J. L. Ericson, D. J. Cram, *High preorganization of large lipophilic surfaces common to two complexing partners provides high binding free energies that vary dramatically with changes in organic solvent composition*, J. Am. Chem. Soc., 112 (1990) 1255-1256.

[27] D. J. Cram, H. J. Choi, J. A. Bryant, C. B. Knobler, *Host-guest complexation. 62. Solvophobic and entropic driving forces for forming velcraplexes, which are 4-fold, lock-key dimers in organic media*, J. Am. Chem. Soc., 114 (1992) 7748-7765.

[28] P. Roncucci, L. Pirondini, G. Paderni, C. Massera, E. Dalcanale, V. A. Azov, F. Diederich, *Conformational Behavior of Pyrazine-Bridged and Mixed-Bridged Cavitands: A General Model for Solvent Effects on Thermal "Vase–Kite" Switching*, Chem. Eur. J., 12 (2006) 4775-4784.

[29] I. Pochorovski, B. Breiten, W.B. Schweizer, F. Diederich, *FRET Studies on a Series of BODIPY-Dye-Labeled Switchable Resorcin[4]arene Cavitands*, F. Chem. Eur. J., 16 (2010) 12590-12602.

[30] L. Shirtcliff, H. Xu, F. Diederich, *Complexation and Dynamic Switching Properties of Fluorophore-Appended Resorcin[4]arene Cavitands*, Eur. J. Org. Chem., 2010 (2010) 846-855.

[31] F. Bianchi, R. Pinalli, F. Ugozzoli, S. Spera, M. Careri, E. Dalcanale, *Cavitands as superior sorbents for benzene detection at trace level*, New J. Chem., 27 (2003) 502-509.

[32] F. Bianchi, M. Mattarozzi, P. Betti, F. Bisceglie, M. Careri, A. Mangia, L. Sidisky, S. Ongarato, E. Dalcanale, *Innovative Cavitand-Based Sol-Gel Coatings for the Environmental Monitoring of Benzene and Chlorobenzenes via Solid-Phase Microextraction*, Anal. Chem., 80 (2008) 6423-6430.

[33] M. Vincenti, E. Dalcanale, P. Soncini, G. Guglielmetti, *Host-guest complexation in the gas phase by desorption chemical ionization mass spectrometry*, J. Am. Chem. Soc. 112 (1990) 445-447.

[34] M. Vincenti, E. Pelizzetti, E. Dalcanale, P. Soncini, *Molecular recognition in the gas phase*, Pure Appl. Chem., 65 (1993) 1507-1512.

[35] M. Vincenti, E. Dalcanale, *Host–guest complexation in the gas phase. Investigation of the mechanism of interaction between cavitands and neutral guest molecules*, J. Chem. Soc., Perkin Trans., 2 (1995) 1069-1076.

[36] M. Vincenti, A. Irico, E. Dalcanale, *Host-Guest Interactions in Mass Spectrometry*, in Advances in Mass Spectrometry (Eds.: E. J. Karijalainen, A. E. Hesso, J. E. Jalanen, U. P. Karijalainen), Elsevier Science, Amsterdam, Netherland, 1998.

[37] S. Zampolli, P. Betti, I. Elmi, E. Dalcanale, *A supramolecular approach to sub-ppb aromatic VOC detection in air*, Chem. Commun., 27 (2007) 2790−2792.

[38] F. Bianchi, A. Bedini, N. Riboni, R. Pinalli, A. Gregori, L. Sidisky, E. Dalcanale, M. Careri, *Cavitand-Based Solid-Phase Microextraction Coating for the Selective Detection of Nitroaromatic Explosives in Air and Soil*, Anal. Chem., 86 (2014) 10646−10652.

[39] A. Altomare, M.C. Burla, M. Camalli, G.L. Cascarano, C. Giacovazzo, A.A. Guagliardi, A.G.G. Moliterni, G. Polidori, R. Spagna, *Sir97: a new tool for crystal structure determination and refinement*, J. Appl. Crystallogr., 32 (1999) 115-119.

[40] G.M. Sheldrick, *SHELXL97. Program for Crystal Structure Refinement*, University of Gőttingen, Gőttingen, Germany, 1997.

[41] G.M. Sheldrick, *A short history of SHELX*, Acta Cryst. A, 64 (2008) 112-122.

[42] L.J. Farrugia, *WinGX suite for small-molecule single-crystal crystallography*, J. Appl. Crystallogr., 32 (1999) 837-838.

[43] SAINT, Software users guide, 6.0; bruker analytical X-ray systems, in: *Software Users Guide, Version 6.0*; Bruker Analytical X-ray Systems. Madison, WI, USA, 1999.

[44] G.M. Sheldrick, *SADABS Area-detector Absorption Correction*, 2.03, University of Gőttingen, Gőttingen, Germany, 1999.

[45] G.M. Sheldrick, *SADABS V. 2008/1. Program for the Empirical Absorption Correction of Area Detector Data*, University of Gőttingen, Gőttingen, Germany, 2008.
[46] P. van der Sluis, A.L. Spek, *BYPASS: an effective method for the refinement of crystal structures containing disordered solvent regions*, Acta Cryst. Sect. A, 46 (1990) 194-201.
[47] M. Nardelli, *Help for checking space-group symmetry*, J. Appl. Crystallogr., 29 (1996) 296-300.
[48] *The Fitness for Purpose of Analytical Methods: A Laboratory Guide to Method Validation and Related Topics*, EURACHEM Guide, 1st English ed., LGC Ltd., Teddington, U.K., 2014, http://www.eurachem.ul.pt.
[49] F. Bianchi, F. Bisceglie, M. Careri, S. Di Berardino, A. Mangia, M. Musci, *Innovative sol-gel coatings for solid-phase microextraction: development of fibers for the determination of polycyclic aromatic hydrocarbons at trace level in water*, J. Chromatogr. A, 1196-1197 (2008) 15-22.
[50] I. Pochorovski, C. Boudon, J.P. Gisselbrecht, M.O. Ebert, W.B. Schweizer, F. Diederich, *Quinone-Based, Redox-Active Resorcin[4]arene Cavitands*, Angew. Chem. Int. Ed., 51 (2012) 262 –266.
[51] I. Pochorovski, J. Milic´, D. Kolarski, C. Gropp, W.B. Schweizer, F. Diederich, *Evaluation of Hydrogen-Bond Acceptors for Redox-Switchable Resorcin[4]arene Cavitands*, J. Am. Chem. Soc., 136 (2014) 3852–3858.
[52] I. Pochorovski, F. Diederich, *Development of Redox-Switchable Resorcin[4]arene Cavitands*, Acc. Chem. Res., 47 (2014) 2096–2105.
[53] I. Pochorovski, M.O. Ebert, J.P. Gisselbrecht, C. Boudon, W.B. Schweizer, F. Diederich, *Redox-Switchable Resorcin[4]arene Cavitands: Molecular Grippers*, J. Am. Chem. Soc., 134 (2012) 14702–14705.
[54] N. Riboni, J.W. Trzcinski, F. Bianchi, C. Massera, R. Pinalli, L. Sidisky, E. Dalcanale, M. Careri, *Conformationally blocked quinoxaline cavitand as solid-phase microextraction coating for the selective detection of BTEX in air*, Anal. Chim. Acta 905 (2016) 79-84.
[55] J.W. Trzcinski, R. Pinalli, N. Riboni, A. Pedrini, F. Bianchi, S. Zampolli, I. Elmi, C. Massera, F. Ugozzoli, E. Dalcanale, In Search of the Ultimate Benzene Sensor: The EtQxBox Solution, ACS Sens. 2 (2017) 590−598.
[56] F. Bertani, N. Riboni, F. Bianchi, G. Brancatelli, E.S. Sterner, R. Pinalli, S. Geremia, T.M. Swager, E. Dalcanale, *Triptycene-Roofed Quinoxaline Cavitands*

for the Supramolecular Detection of BTEX in Air, Chem-Eur J, 22 (2016) 3312–3319.

[57] F. Bertani, *Multifunctional Nanomaterials: Theranostic Nanoparticles and SMM-decorated Surfaces*, Dottorato di ricerca in Scienza e Tecnologia dei Materiali Innovativi, XXVII ciclo.

Chapter 2

New Carbon Multipurpose Thermal Desorption Tubes for the Analysis of Semivolatile Compounds

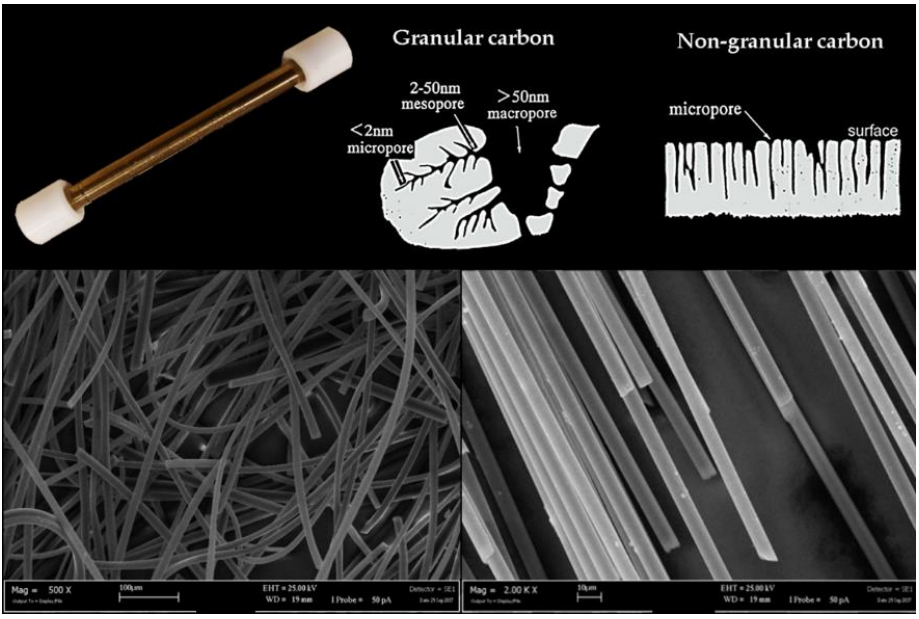

2.1 Introduction

2.1.1 Semivolatile Organic Compounds

Semivolatile organic compounds (SVOCs) are chemicals characterized by saturated vapor pressure in the range of 10^{-4} - 10^{-14} atm at 25°C [1]. The US EPA in 2007 listed more than one thousand SVOCs as high-production-volume chemicals. This means that these species are produced or imported in the USA in amounts larger than 1 million pounds per year.

The SVOCs class includes a wide number of chemicals, i.e. flame retardants (polybrominated diphenyl ethers); pesticides (chlorobenzene and chlorobenzene derivatives), plasticizers (phthalates), heat transfer fluids, (polychlorinated biphenyls), and combustion byproducts (polycyclic aromatic hydrocarbons, dioxins, and furans).

Several natural sources of SVOCs have been reported, mainly related to non-total combustion of organic matter.

SVOCs exposure can occur *via* inhalation, ingestion and dermal adsorption. Inhalation mainly depends on the airborne concentrations of SVOCs, both gaseous and adsorbed onto suspended particles. Dermal uptake may occur by direct transfer from the air to the skin, potentially mediated by clothing. Direct ingestion of SVOCs is another noteworthy health risk, since the presence of these compounds can be related to both food contamination and adsorption of polluted air.

Some SVOCs are known to be carcinogenic (such as benz(a)anthracene and benzo(a)pyrene), whereas others are characterized by chemical structures similar to human hormones. These compounds are able to either mimic or block endocrine activity (endocrine disruptors): previous studies suggested endocrine disrupting activities for several SVOCs, thus including polychlorinated biphenyls [2], brominated flame retardants [3], bisphenol A [4] and pesticides as hexachlorobenzene [5].

Although many SVOCs have been removed from the market because of their demonstrated or suspected health effects (such as polybrominated biphenyls), they are still considered compounds of environmental concern, due to their persistence and worldwide presence. SVOCs in environment are partitioned among several compartments, thus including gas phase, airborne particles,

water and different surfaces [6], depending on their physical properties [7], thus affecting both the fate and the pathways of human exposure [8].

One of the most important parameter in order to predict the partitioning between surface materials and air is the vapor pressure: as general rule, compounds characterized by lower vapor pressure are present at low concentration levels in air, being mainly deposited on both suspended particles, i.e. ultrafine nanoparticulate matter and dust, and large surfaces. This phenomenon is known as sink effect and it was reported in environmental chamber tests of SVOC emissions from materials [9]. Another key parameter associated to the partitioning between the gas phase and dust/particulate is the octanol-air partition coefficients (K_{oa}) [6].

Among the wide range of compounds classified as SVOCs, in this research study we focused on chlorobenzenes and PAHs.

2.1.2 *Chlorobenzene and Chlorobenzene Derivatives*

Since their introduction in 1929, chlorobenzene and chlorobenzene derivatives (chlorobenzenes or CBs) have been widely used in industrial and consumer applications such as pesticides, solvents, by-product materials of phenol-based manufacturing and heat transfer agents in electrical equipment [10]. Chlorobenzenes can be also formed during incomplete combustion processes and potentially discharged into the environment from waste incinerators.

Despite the restrictions on their use and manufacture from the 1970s [10], they are persistent and ubiquitous compounds, present in all environmental compartments: atmosphere (in the case of pesticides and repellents), soil (mainly for disposal or accidental releases of CBs from electrical installations, i.e. transformers and capacitors), and waterways (as degreasers, dyes intermediates and solvents) [11].

CBs are highly hazardous to health and have been ranked as priority pollutants by the US Environmental Protection Agency (EPA) [12]. A number of chlorobenzene derivatives are also included both in the Council Directive 76/464/EEC [13] regarding pollution of the aquatic environment, and in the Water Framework Directive 2000/60/EC [14].

A brief description of the use and effects of the most produced CBs is reported below:

1. **Chlorobenzene** is used primarily as: solvent for pesticide formulations, degreasing agent for automobile parts and chemical intermediate (i.e. in the synthesis of nitrochlorobenzene). Until '70s, its major role was in the DDT production [15]. Limited information is available on short-term effects: acute inhalation exposure of animals produces narcosis, restlessness, tremors, and muscle spasms [16]. Chronic exposures of humans affects the central nervous system: signals of neurotoxicity in humans include numbness, cyanosis, hyperesthesia, and muscle spasms [17]. No carcinogenic effects have been reported.
2. **1,2-dichlorobenzene** is largely manufactured in Europe, USA, Canada, Mexico and China. In 1999 its production in the Western World was 54,000 tons. This compound is an intermediate product in chemical syntheses and pharmaceutical preparations. The main industrial use of 1,2-dichlorobenzene is as a solvent, especially for the production of wool branding products.

   It is a toxic and persistent compound with a high potential for bioconcentration in the fatty tissue of biological species. Short-term exposure causes eye, skin and respiratory irritation. The acute effects of 1,2-dichlorobenzene by ingestion or inhalation are reported to be: headache, nausea, vomiting, vertigo, malaise and unconsciousness. Studies on animals have shown that 1,2-dichlorobenzene is capable of inducing acute hepatotoxic effects [18]. No carcinogenicity has been reported.
3. **1,3-dichlorobenzene** is a minor by-product occurring in chemical synthesis. The health risks are associated to respiratory inflammations and eye burns. Moreover, inhalation and skin adsorption can lead to headache, drowsiness, nausea, vomiting, diarrhea and abdominal cramps. Long-time exposures toward this compound could cause anemia, liver and kidneys damages and skin allergy. However, no evidence of carcinogenicity has been reported.
4. **1,4-Dichlorobenzene** is used to make mothballs, used in both restrooms and animal holding facilities, to control odors [19]. It is also present in fumigants, insecticides, lacquers, paints, and seed disinfection products [20]. Detectable concentrations of 1,4-dichlorobenzene were found in USA in drinking water, waste sites and food [20]. Moreover, Japanese studies [21] demonstrated the presence of this compound in adipose tissues,

blood samples and milk in humans. The main health risk of 1,4-dichlorobenzene is the possible occurrence of anemia, hepatotoxicity and nephropathy.

1,4-Dichlorobenzene is considered as possible human carcinogen based on evidence from studies in experimental animals: oral exposure to 1,4-dichlorobenzene caused tumors at several different tissue sites in mice and rats, such as benign and malignant liver tumors, kidney cancer and leukemia.

5. The main use of **1-2-3-trichlorobenzene** is as dyestuff and pigment intermediate, transformer oil and lubricant. The main way of exposure to humans occurs *via* inhalation, even if ingestion can also occur. Symptoms of poisoning *via* inhalation include cough and sore throat, whereas those associated to the oral route include abdominal pain, diarrhea, nausea and vomiting. No carcinogenicity has been shown.
6. **1,2,4-Trichlorobenzene** is used as dye carrier, solvent, herbicide intermediate, insecticide, heat-transfer medium, dielectric fluid in transformers, degreaser and lubricant [22].

   Acute inhalation exposure lead to local irritation of the lungs and dyspnea; chronic oral exposure has been observed to produce kidneys and liver diseases. EPA has classified 1,2,4-trichlorobenzene in the Group D, not classifiable as carcinogen to humans [23].
7. **1,2,4,5-Tetrachlorobenzene** is used as an intermediate in chemical industry to produce herbicides, insecticides and defoliants. The exposure occurs *via* inhalation, by eating contaminated food or absorption through skin. The main effects are related to eye, lung and skin irritations and liver or kidney lesions.
8. **Hexachlorobenzene** was used both as pesticide and in the production of rubber, aluminum, dyes and in wood preservation. Currently it is obtained as byproduct during the manufacture of other chemicals (mainly solvents) and pesticides [24].

   Hexachlorobenzene has been listed as a *pollutant of concern* by the EPA's Great Waters Program due to its persistence in the environment, potential to bioaccumulation, and toxicity to both humans and bio-organisms [25].

   Chronic oral exposure in humans results in liver diseases with associated skin lesions. Based on animal studies that have reported the occurrence of

different kind of cancer in liver, thyroid, and kidney, EPA has classified hexachlorobenzene as a probable human carcinogen (Group B2).

2.1.3 *Polycyclic aromatic hydrocarbons*

PAHs are hydrocarbons in which the carbon atoms are structurally arranged in a honeycomb-like system, with at least two fused rings.

Two classification of these compounds have been reported, depending on their structure (**Figure 2.1**):

- They can be classified as both alternant and non-alternant, depending on the presence of at least one four- or five-membered ring, among the most abundant 6-term aromatic rings.
- PAHs characterized by only one shared face are called ortho-fused (or cata-condensed), whereas peri-fused (or peri-condensed) compounds are characterized by multi-face condensation of the aromatic rings.

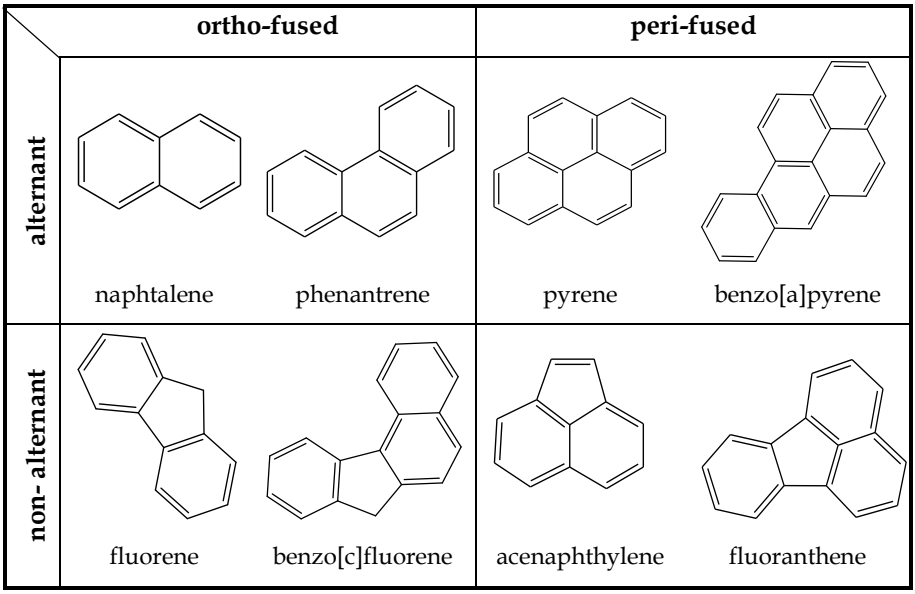

Figure 2.1 Examples of common PAHs structurally classified

Since PAHs is a wide class of compounds, different chemical, biological and physical properties are present, based on both the molecular weight and different ring arrangement.

PAHs are ubiquitous and persistent environmental contaminants, usually present as complex mixture in water, soil and air [26]. They are primarily originated from incomplete combustion of organic matter. Even if the synthetic mechanism has not been fully clarified, a simple process has been proposed: during high-temperature combustion in presence of low concentration of oxygen, the organic molecules are fragmented, mostly in free radicals (pyrolysis) and subsequently recombined to form the lightest PAHs in a pyrosynthesis process. These low-weight compounds can further undergo reaction cycles, thus generating more complex hydrocarbons [27].

Three are the primary PAHs sources, i.e. pyrogenic, biogenic and petrogenic [28]:

1. incomplete combustion or pyrolysis of organic matter: PAHs are emitted during industrial processes and other anthropogenic activities, such as power generation, waste incineration, fossil fuels and biomass combustions, cigarette smoking, and indoor domestic heating systems, thus including furnaces and wood stoves [27]. Natural sources are also present: wildfires, volcanic activity and crude oil vaporization lead to a minor release of PAHs in the atmosphere.
2. biosynthesis and degradation of biological materials in the environment by relatively rapid chemical or biological processes.
3. formation of fossil fuels by natural processes, such as anaerobic decomposition of buried dead organisms. This process occurs over geologic time (hundreds of millions of years)

The relative composition of the PAHs mixtures is strongly related to the primary source:

1. Petrogenic and pyrogenic PAHs mixtures are highly complex. The latter is the main source of PAHs release in environment: they can be formed by natural, domestic, and industrial processes that involve heating of organic matter at high temperatures (> 400°C). Incomplete combustion results in the formation of PAH-rich vapors, liquids, or particles that can enter the environment.
2. PAHs released from biogenic source, mainly consisting of single chemicals are not predominant over the total mass of PAHs in contaminated soils or sediments. Examples of biogenic PAHs include perylene and substituted compounds.

3. Petrogenic PAHs are formed from ancient organic matter converted under geologic temperatures (100–150°C) and pressures (hundreds of atm) over millions of years to form petroleum and coal. In this case, a dominance of alkylated PAHs over the parents is reported [29]. Petrogenic compounds can enter the environment through anthropogenic incidents (crude oil or fuel spills or discharges) or natural processes (erosion of coal beds or oil seeps).

Pyrogenic PAHs sources display a lower relative abundance of alkylated hydrocarbons in their profile than in petrogenics, along with a higher ratio of unsubstituted compounds having high molecular weights [29].

It has been suggested that the presence of both specific PAHs and diagnostic ratios between substituted/unsubstituted compounds could be used as marker in order to identify their major source, not only referring to the primary source, but also to their specific source, i.e. diesel, gasoline, wood… [30]. However, a limitation in the use of these approaches is related both to the heterogeneous degradation of hydrocarbons in atmosphere, water and soil, and to different gas phase/particle partitioning [31].

As for oral assimilation, high concentration levels of hydrocarbons are present in grilled, smoked or contaminated food [32]. Moreover, the deposition of particulate with adsorbed PAHs has been reported on cereals, vegetables and processed food, thus enhancing the ingestion of these compounds.

In ambient air, PAHs and congeners can be present in the gas-phase or adsorbed on particulate matter: their distribution depends on the specific vapor pressure, local temperature and K_{oa}. Hydrocarbons characterized by more than 5 condensed rings are almost entirely adsorbed on solid particles, whereas PAHs with 3 rings are present mostly in the gas phase [33].

Currently, benzo[a]pyrene is the only PAH classified as human carcinogen (Group 1) by IARC, whereas all the other hydrocarbons are set in Group 2A (probably carcinogenic to humans), 2B (possibly carcinogenic to humans), and 3 (not classifiable as carcinogenic to humans) [34].

Both the USA EPA and the UE have reported priority lists for PAHs monitoring in the environment: EPA suggests a careful monitoring of 16 PAHs, whereas in Europe 15+1 hydrocarbons are monitored for food safety purposes. Both lists include compounds characterized by high toxicity or

distribution. In **Table 2.1** are reported the PAHs present in at least one of the mentioned lists as-well-as in the IARC classification.

Table 2.1 PAHs present in EPA or UE lists and respective IARC classification

PAH	EPA 16 PAH	UE 15+1 PAH	IARC classification
Naphthalene	X		Group 2B
Acenaphtylene	X		-
Acenaphthene	X		Group 3
Fluorene	X		Group 3
Phenanthrene	X		Group 3
Anthracene	X		Group 3
Fluoranthene	X		Group 3
Pyrene	X		Group 3
Benzo[c]fluorene		X	Group 3
Benzo[a]anthracene	X	X	Group 2B
Chrysene	X	X	Group 2B
Cyclopenta[cd]pyrene		X	Group 2A
5-methylchrysene		X	Group 2B
Benzo[b]fluoranthene	X	X	Group 2B
Benzo[j]fluoranthene		X	Group 2B
Benzo[k]fluoranthene	X	X	Group 2B
Benzo[a]pyrene	X	X	Group 1
Dibenzo[a,h]anthracene	X	X	Group 2A
Indeno[1,2,3-cd]pyrene	X	X	Group 2B
Benzo[ghi]perylene	X	X	Group 3
Dibenzo[a,e]pyrene		X	Group 3
Dibenzo[a,h]pyrene		X	Group 2A
Dibenzo[a,i]pyrene		X	Group 2B
Dibenzo[a,l]pyrene		X	Group 2B

2.1.4 SVOCs Sampling

The increased interest on the detection of the SVOCs has to face the major problem related to the wide range of molecular weights and physiochemical properties of these compounds. International institutions and organizations (such as EPA and NIOSH) have proposed several analytical methods for the analysis of SVOCs in air [35,36].

The choice of a method to be used for SVOCs detection depends on both the physicochemical properties of the target analytes and the environmental matrix to be analyzed.

The sampling step is of pivotal importance when an analytical method is developed, strongly influencing the performances of the analysis. SVOCs are usually sampled by dynamic (or active) techniques, thus allowing the sampling of a fixed volume of air, forced to pass through a suitable trap, i.e. solid sorbents, absorbing solutions, reagents deposited on a carrier. Passive sampling has been also proposed for SVOCs monitoring, thus allowing the preconcentration of the analytes on very simple, stand-alone and cheap devices (**paragraph 1.1.1**).

In both active and passive approaches, the sampling method is based on trapping the analytes on a proper adsorbing material. In order to remove the particulates, one or more filters are usually placed before the sorbent trap.

In active sampling, high volume samplers (HVS) are commonly used when large sampling volumes are required: these devices can be mounted on pumps able to provide gas flow rates in the 100-500 l/min range [35]. Polyurethane foam and adsorbent resins (AR) are the most used materials: they are able to trap a wide range of SVOCs, thus including pesticides and PAHs. The major drawbacks are related to the laborious and time-consuming procedures required for both the clean-up of the materials and the desorption of the analytes. Both processes also require the use of large amount of organic solvents [37].

As for AR, their use is recommended for sampling nonpolar organic compounds such as PAHs and phosphorus pesticides; the most commonly used are XAD-2™, XAD-4™ and XAD-16™, hydrophobic cross-linked polystyrene and divinylbenzene polymers, presenting a macroporous structure [38]. All the mentioned materials can be combined each other or

with other common sorbents, such as Tenax-TA® and Chromosorb® 102 in order to concentrate a wide range of SVOCs [39].

SPE extraction columns packed with functionalized silica gel proved to be suitable for SVOCs enrichment in air [40]. The main advantage of this approach over classical sorption traps is that low volumes of organic solvents are required in the desorption step.

A noticeable alternative to both classical active and passive sampling is the combination of the active technique with denudation: respect to the classical approaches, based on the trapping of the analytes from both gas-phase and particulate matter, a denuder retains only analytes in the gas phase. In a denuder, a forced laminar flow of air causes the diffusion of the analytes through the walls of the denuder that are coated with a sorption medium (**Figure 2.2**). The compounds are transported by the air flow generated by a pump, and are adsorbed by the stationary phase of the denuder walls, whereas particulate is retained by the filter set at the beginning or at end of the system. The degree of enrichment of the target compounds depends on: i) intensity of the airflow, ii) geometry of the device and iii) kind of sorbent material.

The cylindrical denuder is the simplest and most commonly used device. Another kind of denuder is the annular device, that is characterized by the presence of several coaxial coated tubes, separated by an annular space through which the air flows.

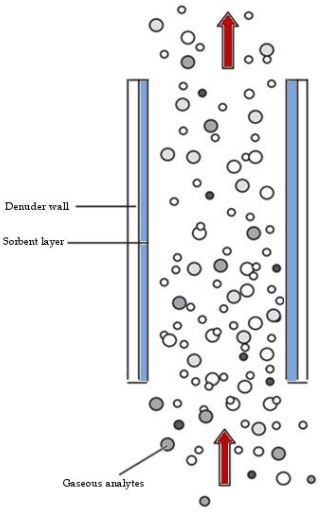

Figure 2.2 Denuder operating principle

Solid phase microextraction has also been proposed for SVOCs monitoring, for both chlorobenzenes [41] and PAHs [42].

Thermal desorption (TD) has proven to be an excellent desorption technique for the analysis of volatile organic compounds (VOCs); in addition, previous studies demonstrated that TD could be suitable also for the analysis of SVOCs, thus addressing the research toward the development of new materials for TD tubes.

2.1.5 *SVOCs Analysis*

Gas chromatography is the standard analytical technique used for the determination of chlorobenzenes in air, coupled with several detectors (i.e. electron capture detector (ECD) [43,44], flame ionization detector (FID) [45] and fluorescence). However, mass spectrometry is the preferred detection technique, being very sensitive and allowing qualitative analysis in order to identify univocally the analytes over possible interferences. Both tandem or high resolution mass spectrometry (GC-MS/MS and GCHRMS) have been proposed in order to improve the performances of this technique [46,47].

On-line process monitoring or low-cost sensors, such as metal oxide gas sensors [48], and colorimetric sensors [49], have been also proposed for the determination of chlorobenzene.

As for PAHs and congeners in environmental samples, they are usually analyzed by using GC-FID [50], GC-MS or GC-MS/MS [35,51], or high-performance liquid chromatography (HPLC) with UV-fluorescence detectors [52,53] or tandem mass spectrometry (LC-MS^n) [54,55].

In LC-MS, the atmospheric pressure photoionization (APPI) source is used for the analysis of PAHs, being suitable for the ionization of nonpolar compounds, whereas electrospray ionization (ESI) and atmospheric pressure chemical ionization (APCI) are characterized by low responses [56,57]. As a general comment it can be stated that tandem mass spectrometry is characterized by very low detection limits (sub-ng/l), thus allowing the identification of the analyte over possible interferences [58].

Finally, several sensors for the analysis of PAHs in water and soil have been proposed, i.e. enzyme-linked immunosorbent assays (ELISA) [59], fluorescence immunity analysis [60] and immuno-polymerase chain reaction sensor [61].

2.1.6 TD-GC-MS

As previously reported, GC-MS is the most used analytical technique for SVOCs analysis. Thermal desorption offers several advantages compared to solvent extraction: it is a rapid solvent-free technique, suitable for on-line coupling with gas chromatography, thus allowing a significant improvement in repeatability. A schematic representation of an on-line TD-GC-MS is depicted in **Figure 2.3.**

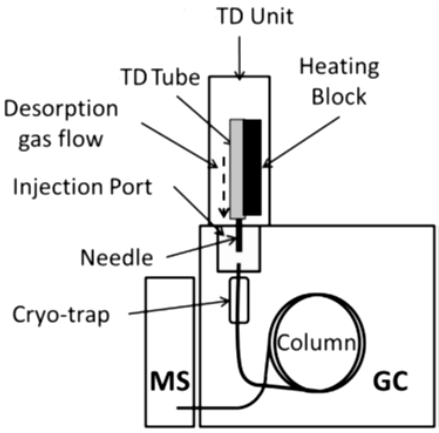

Figure 2.3 Schematic representation of a TD-GC-MS system

Due to their low vapor pressure, SVOCs can be strongly adsorbed onto the sorbent material, thus TD requires high temperatures and flows to desorb the analytes. The main drawbacks of this technique are related to both the incomplete desorption of the analytes from the TD-tube and the possibility of carryover effects [62].

A wide variety of commercial TD-tubes is present: these sorbents are characterized by different structures, chemical functionalization and porosity in order to obtain a selective entrapment of different classes of compounds. Some parameters of the adsorbent material, i.e. surface area, thermal stability, hydrophobicity and presence of functional groups can both affect the sampling capabilities and the breakthrough volumes.

In order to retain a wide range of SVOCs different types of adsorbents can be combined, thus obtaining multi-sorbent TD-tubes.

Nowadays, these multi-sorbent tubes are commonly used in various official methods to determine VOCs in outdoor and indoor air (such as in EPA TO-17 [63], 2549 NIOSH [64], and D-6196-97 ASTM methods [65]).

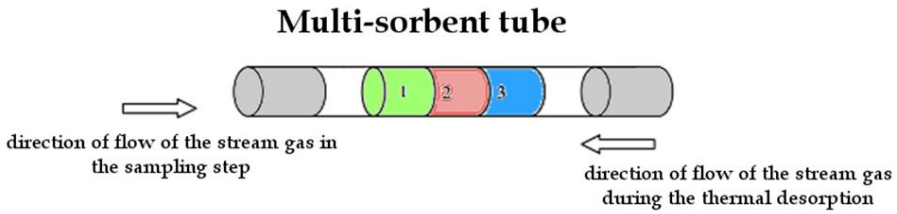

Figure 2.4 Multi-sorbent bed tube

Besides the complexity of the air sampled, the main disadvantages of the enrichment onto commercial multi-bed solid adsorbents are related to the presence of moisture. Major problems including tube clogging, leaches and scarce adsorption of the analytes arise in atmospheres characterized by medium-high humidity levels (40–90%) [66-68].

Depending on the type of adsorbents, water vapor can strongly reduce the adsorption capabilities of the tubes. Porous apolar polymers and graphitized carbons are less influenced by the presence of water with respect to materials based on carbon molecular sieves [69,70]. Besides the decrease of the sampling capability, ice accumulation in the cryogenic trap during the preconcentration step of the TD could occur.

Several approaches to remove moisture before the TD-step based both on the use of drying agents [67,71] and on the heating of the tube [72] were proposed.

Martins et al. [73] developed a TD-GC-MS method for 2- and 3-ring PAHs monitoring by using Tenax-TA® as sorbent material, whereas Li et al. [74] proposed the use of multi-sorbent tubes (Glass beads, Carbopack® C, and Carbopack® B) for the analysis of PAHs from 2- to 6-ring.

The aim of this study, carried out in collaboration with the ACES department of the Stockholm University, was to optimize and validate a TD-GC-MS method for the analysis of SVOCs (PAHs and CBs) by using new multipurpose thermal desorption tubes, based on the use of non-granular active carbon (NGAC).

2.2 Material and Methods

2.2.1 *Chemicals and Materials*

CBs (CBS mixture solution, 100 µg/ml in isooctane) and PAHs solutions (PAH-STK-A solution, 4 µg/ml in isooctane) were purchased from Wellington Laboratories, Ontario, Canada.

Carbotrap® 300 TD-tubes O.D. ¼ in. × I.D. 5 mm × L 7 in., stainless steel TD tube, preconditioned were purchased from Merk Spa, Darmstadt, Germany.

Homemade TD-tubes were assembled in-house using empty, precleaned stainless steel tubes (O.D. ¼ in. × I.D. 5 mm × L 7 in.) packed with two different NGAC materials.

2.2.2 *Material Characterization*

Thermogravimetric analysis was performed on a TGA 7 instrument (Perkin-Elmer, Waltham, MA, USA) over the temperature range 30-700 °C under inert atmosphere (N_2). Morphology was investigated by using scanning electron microscopy (SEM) with a Leica 430i instrument (Leica, Solms, Germany). Elemental analysis was performed on a CHNS-O EA1108 (Carlo Erba, Milan, Italy) elemental analyzer.

2.2.3 *Sampling Conditions*

PAHs and CBs solutions were spiked into an empty TD-tube, then the tube was heated at 150°C under nitrogen (flow 100 ml/min, controlled by an external flowmeter, Varian Digital optiflow 520) and connected to the primary trapping tube (Carbotrap® 300 or NGAC tube), maintained at room temperature. Finally, a third trap was connected to the primary tube, in order to evaluate the breakthrough volume. Sampling volumes of 1 and 10 liters were respectively tested.

2.2.4 *TD-GC-MS Analysis*

The TD-GC-MS system was composed by a Turbomatrix 650 thermal desorber, a Clarus 680 gas-chromatograph and a Clarus SQ8T mass spectrometer (Perkin Elmer SWE, Hägersten, Sweden).

The TD-tubes were purged for 1 min, then the desorption was performed at 400°C with a 50 ml/min helium flow for 20 min, by operating with the three-

way valve and the transfer line maintained at their maximum operating temperature, i.e. 265 and 270°C respectively. The analytes were preconcentred on a Tenax cryo-trap at -40°C and desorbed at 300°C with a 7.8 ml/min helium flow for 60 min. A split of 77% was applied, thus a 1.8 ml/min flow was injected in the GC-column.

Chromatographic separation was performed on a 30 m x 0.25 mm, df 0.25 µm HP-5 MS capillary column (Agilent Technologies), using the following temperature programme: 50 °C for 45 min, 10 °C/min until 250°C, hold 1 min, and finally 12°C/min until 310°C, hold 6 min.

Preliminarily, full scan EI data were acquired to determine appropriate masses for selected-ion monitoring mode (SIM) used for PAHs and CBs quantitation. Two *m/z* ratios were considered for each analyte: the most abundant was used for quantitation, the other for confirmatory purposes (**Table 2.2)**. The analyses were performed under the following conditions: ionization energy: 70 eV; mass range: 40-300 amu; scan time: 3 scan/s; electron multiplier voltage: 2200 V. Signal acquisition and data handling were performed using a TurboMass software (Perkin Elmer). The investigated analytes and the respective *m/z* ratios are reported in **Table 2.2.**

Table 2.2 Investigated analytes and *m/z* ratios, underlined those used for quantitation

Analyte	**m/z**
CBS	
Chlorobenzene:	<u>112</u> 114
Dichlorobenzenes	<u>146</u> 148
Trichlorobenzenes	<u>180</u> 182
Tetrachlorobenzenes	214 <u>216</u>
Pentachlorobenzenes	<u>248</u> 250
Hexachlorobenzenes	284 <u>286</u>

Analyte	m/z
Naphtalene	128 129
Acenaphtylene	152 153
Acenaphtene	153 154
Fluorene	165 166
Phenanthrene	176 178
Anthracene	176 178
Fluoranthene	200 202
Pyrene	200 202

2.2.5 *TD-GC-MS Method Validation*

Method validation was performed according to EURACHEM guidelines [75] using nitrogen as blank matrix and following the same procedure reported in **paragraph 1.2.6**.

For all the analytes, the limits of detection and limits of quantification were calculated as signal-to-noise ratio, S/N=3 and S/N=5 respectively, using five replicates at the concentration of 1 $\mu g/m^3$.

Calibration curves (four concentration levels, three replicated measurements for each level) were evaluated in the 0.2-20 $\mu g/m^3$ range.

Repeatability and intermediate precision were calculated in terms of RSD % on two concentration levels i.e. 1 and 10 $\mu g/m^3$ by performing six replicated measurements for each level. Intermediate precision was estimated over three weeks verifying homoscedasticity of the data and performing the analysis of variance (ANOVA) at the confidence level of 95%.

Trueness was calculated in terms of relative recovery rate (RR%) at two concentration levels i.e. 1 and 10 $\mu g /m^3$ for each analyte; four replicated measurements were analyzed.

2.3 Results and Discussion

The aim of this cooperation project between Parma University, Salerno University and Stockholm University was the evaluation of the performances of new multipurpose TD-tubes for the TD-GC-MS analysis of SVOCs of environmental concern, like chlorobenzene derivatives and light polycyclic aromatic hydrocarbons (PAHs).

2.3.1 Carbon Sorbent Materials

A new non-granular carbon-based material (*patent pending*) is proposed as new sorbent for thermal desorption tubes.

Commercially available TD-tubes for VOCs and SVOCs analyses are based on the use of granular carbon-based sorbents (GCA), such as Carbotrap® and Carbosieve®, or polymeric materials, such as Tenax-TA® or Tenax-GR®.

Carbotrap® 300 tubes were used as reference, since they are proposed as trapping material for VOCs monitoring in EPA methods. More precisely, Carbotrap® 300 is a multi-bed sorbent material, consisting of Carbosieve® S-III carbon molecular sieve (CMS), Carbotrap C and Carbotrap B, made of porous granular carbon. Depending on the internal diameter, the pores can be classified in three main classes: macropores (>500 Å), mesopores (20–500 Å), and micropores (<20 Å).

Carbon molecular sieves are spherical highly porous carbon-based materials, characterized by higher relative adsorptive strength compared to spherical graphitized polymer carbon and graphitized carbon black sorbents. They are porous carbon skeletal frameworks obtained by the pyrolysis of a polymeric precursors. Carbosieve® S-III adsorbents have non-tapered pores and are suitable for trapping highly volatile compounds. Although hydrophobic, this material retains water during sampling, strongly decreasing the absorbance capability of the material.

Carbotrap® is made of graphitized carbon black (GCB). Generally, these sorbents are characterized by weaker relative adsorption strength compared to carbon molecular sieves. The material is granular, non-porous (in the case of Carbotrap® B and C) and the graphitization process results in a highly pure surface with enhanced adsorption properties, *via* aspecific, π-π and CH-π interactions.

Carbotrap® B and C are the most widely used GCBs, since they allow the trapping of analytes in a wide molecular weight, with Carbotrap® C suggested for the analysis of C_{12}–C_{20} hydrocarbons [76].

As reported, porous granular carbon structures are characterized by the presence of micro-, meso- and macropores (**Figure 2.5** left). This strongly affects both the adsorption and release capability of the material: in fact, it has to be taken into account that different porosities are characterized by different retention strength, possibly resulting in heterogeneous release of the adsorbed compounds. In addition, the presence of both mesopores and macropores lead to water condensation and droplets formation, thus reducing the adsorption capabilities of the material.

In the tested non-granular active carbon only micropores are present (**Figure 2.5** right), thus reducing the drawbacks related to the presence of water condensate, occurring *via* capillary condensation [77-79].

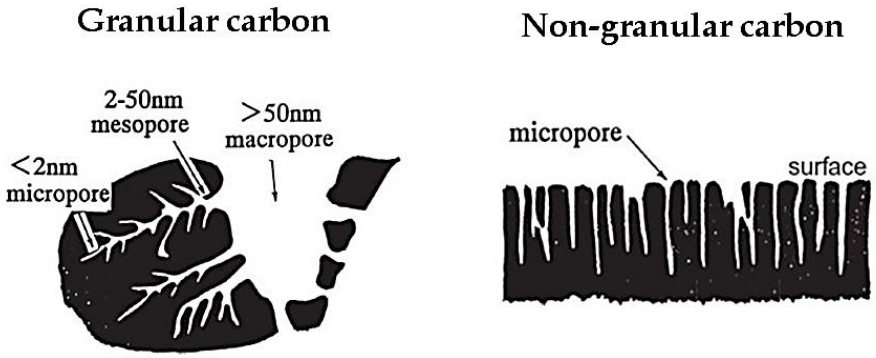

Figure 2.5 Schematic representation of granular (left) and non-granular (right) active carbon

Different absorption/desorption profiles are observed when GCA and NGCA are used as sorbent material (**Figure 2.26)**.

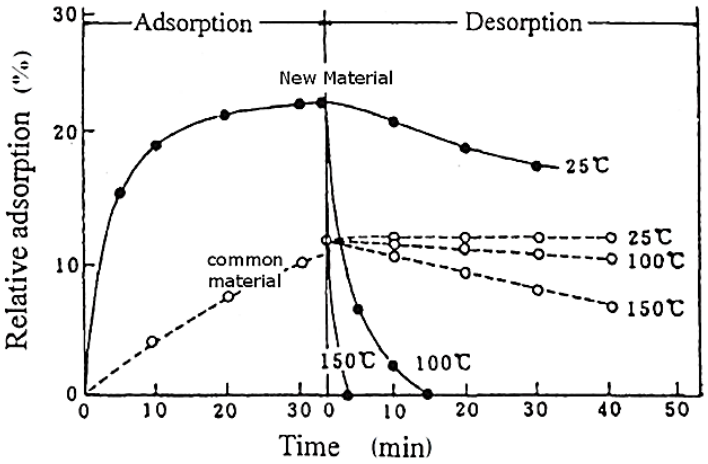

Figure 2.6 absorption and desorption profiles for granular (dotted) and non-granular (solid) active carbon

As shown in **Figure 2.6**, GCA is characterized by linear trends for both adsorption and desorption steps, thus requiring long analysis times. Moreover, by increasing the desorption temperature only a slight improvement in the release speed is obtained. By contrast, a logarithmic trend characterizes the adsorption profile of NGAC: under these conditions, the saturation of the sorbent material is reached in short times and higher relative adsorptions can be achieved. The release of the analytes follows an exponential trend, thus resulting in a faster desorption by increasing the temperature.

2.3.2 *NGAC Characterization*

In order to prove the suitability of the NGAC material for thermal desorption, the stability of the sorbent material was evaluated by means of thermogravimetric analyses. Since the material was stored in a non-dried environment, the material released the adsorbed water at 100°C, then it proved to be stable up to 700°C. The comparison between the release profiles after storage at 40% of relative humidity and under RT conditions (70% relative humidity) is shown in **Figure 2.7**. The difference of weight loss between the two curves is related to the amount of water absorbed and released in terms of different humidity levels.

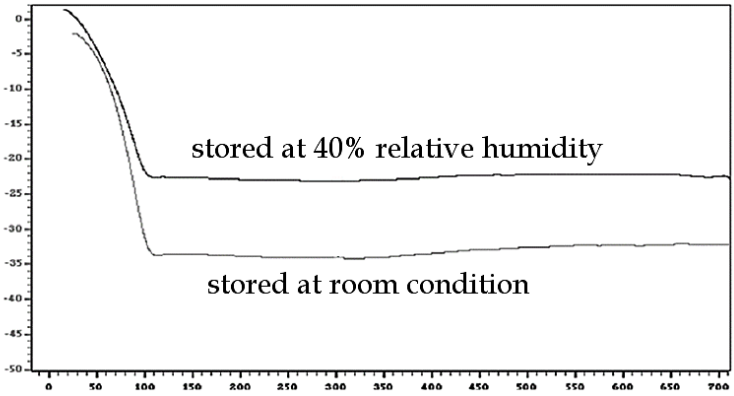

Figure 2.7: TGA of NGAC material stored at room condition and at 40% of relative humidity

Elemental analysis was also performed: the material was composed almost entirely by carbon, with a noticeable presence of oxygen.

The morphology of the material was investigated by scanning electron microscopy. The sorbent material is characterized by two different morphologies, as can be clearly seen in **Figure 2.8**.

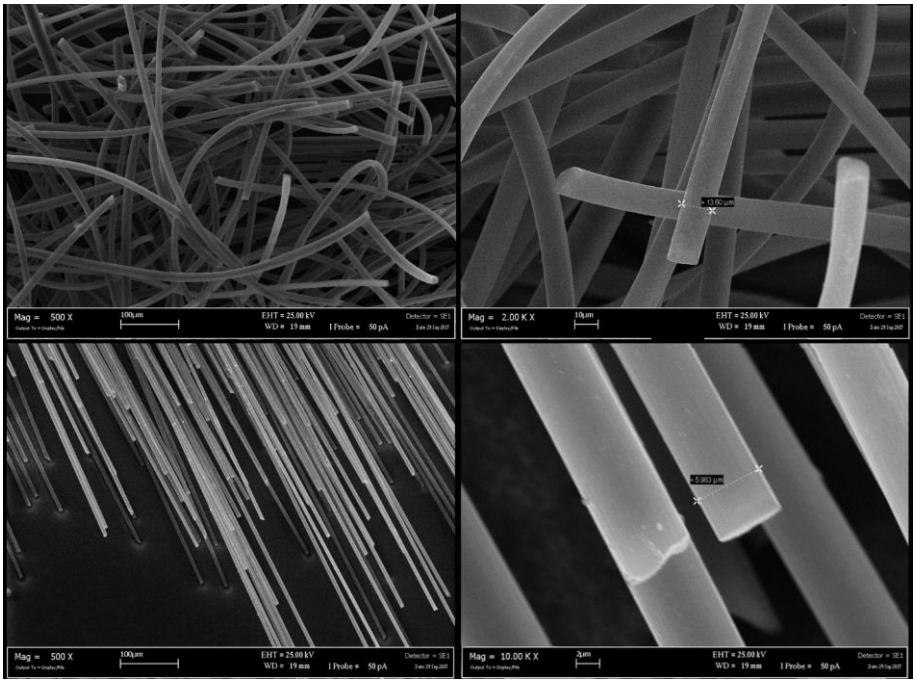

Figure 2.8 Scanning electron microscope images of the sorbent material

Two different carbon-based fibers can be observed: more precisely, disordered fibers (13.43±0.60 μm average diameter) and aligned fibers (6.00±0.12 μm diameter) are present. Previous unpublished studies proved that by using this multibed sorbent higher adsorption capabilities toward VOCs than those achieved by the use of TD tubes filled in with a single component can be obtained.

2.3.3 *SVOCs Analysis*

The target SVOCs were all the CBs and the following PAHs: naphthalene, acenaphtylene, acenaphtene, fluorene, phenanthrene, anthracene, fluoranthene, pyrene. These aromatic hydrocarbons were selected considering that heavier compounds are not present in the gas-phase since they are adsorbed on solid particulate. The sampling instrumental setup used for the analysis is depicted in **Figure 2.9**.

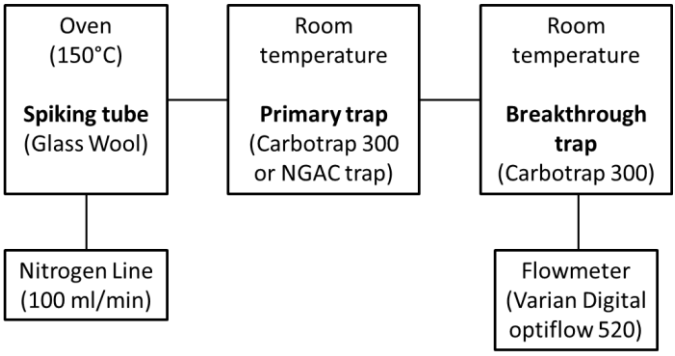

Figure 2.9 Schematic representation of the instrumental setup

As reported, the use of three different tubes was required:

1. **Spiking tube**: it is an empty stainless steel tube, containing glass wool, in which the analytes were spiked. The spiked tube was connected to the nitrogen line and heated in an oven; the sampling temperature was optimized at 150°C in order to obtain the complete vaporization of the target analytes from the glass wool.
2. **Primary Trap**: this trap, either Carbotrap® 300 or NGAC, was connected with the spiking tube and kept at room temperature. This is the trap considered for measuring the adsorbing capabilities of the materials.
3. **Breakthrough trap**: this trap was used in order to collect the gas from the primary trap, thus allowing the evaluation of the breakthrough volume

The oven temperature optimization was performed by analyzing the glass wool tube after the sampling: the temperature was increased starting from 90 °C, until no response for the targeted compounds was obtain. A subsequent optimization of the parameters related to the thermal desorption step was carried out with the final aim of obtaining the complete release of the analytes from both the primary trap and the cryo-trap. This was the major instrumental limitation: the analytes were strongly retained from Tenax, thus requiring long desorption times and high flows. For this reason, a high split ratio before the injection in the GC was required. The optimized TD parameters are reported in **Table 2.3**.

Table 2.3 optimized parameters in Turbomatrix 650 thermal disrober

Temperature (°C)		**Pneumatic (ml/min)**		**Time (min)**	
Valve	265	Desorption tube	50	Purge	1
Tube	400	Trap	1.8	Primary desorption	20
Transfer line	270	Column	1.8	Trap desorption	60
Trap sampling	-40	Split	6		
Trap desorption	300	% injected	23%		

Another instrumental issue was related to the length of the transfer-line (~1 m), with problems associated to peak broadening and carryover effects [74, 80].

The GC programme temperature was optimized in order to both obtain separate peaks for each analyte (except in the case of the 1,2,3,4- and 1,2,3,5-tetrachlorobenzene) and reduce the reported limitations. The GC run started 15 min after the beginning of the desorption of the cryo-trap; under these conditions the obtained chromatogram was the results of both GC separation and the analytes release from the Tenax-trap.

As can be clearly seen in **Figures 2.10** and **2.11**, the peaks of both CBs and PAHs were sharp and intense. No carryover effect was observed for both the primary trap and the Tenax cryo-trap. By the analysis of the breakthrough trap, no breakthrough was observed for both the sampled volumes (1 and 10 liters) in the 0.2-20 ng/m^3 range for both Carbotrap® 300 and NGAC.

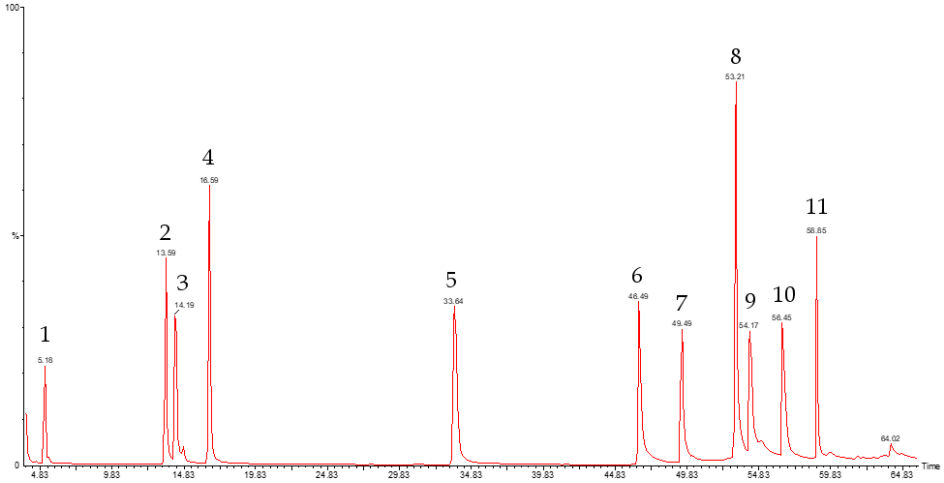

Figure 2.10 TD-GC-(SIM)MS analysis of a mixture of mixtures of CBs (10 ng spike): 1) monochlorobenzene; 2) 1,2-dichlorobenzene; 3) 1,3-dichlorobenzene; 4) 1,4-dichlorobenzene; 5) 1,2,3-trichlorobenzene; 6) 1,2,4-trichlorobenzene; 7) 1,3,5-trichlorobenzene; 8) 1,2,3,4- tetrachlorobenzene and 1,2,3,5-tetrachlorobenzene; 9) 1,2,4,5-tetrachlorobenzene; 10) pentachlorobenzene; 11) hexachlorobenzene

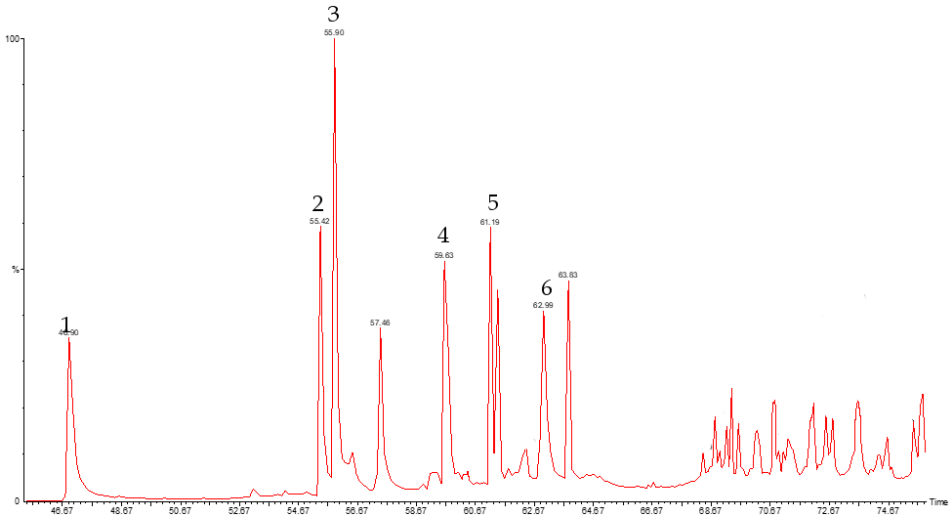

Figure 2.11 TD-GC-(SIM)MS analysis of a mixture of mixtures of PAHs (10 ng spike): 1) naphthalene; 2) acenaphthylene, 3) acenaphthene, 4) fluorene; 5) phenathrene; 6) pyrene+fluoranthene

The enrichment capabilities of the NGAC TD-tubes were compared with those of Carbotrap® 300 (**Figure 2.12**).

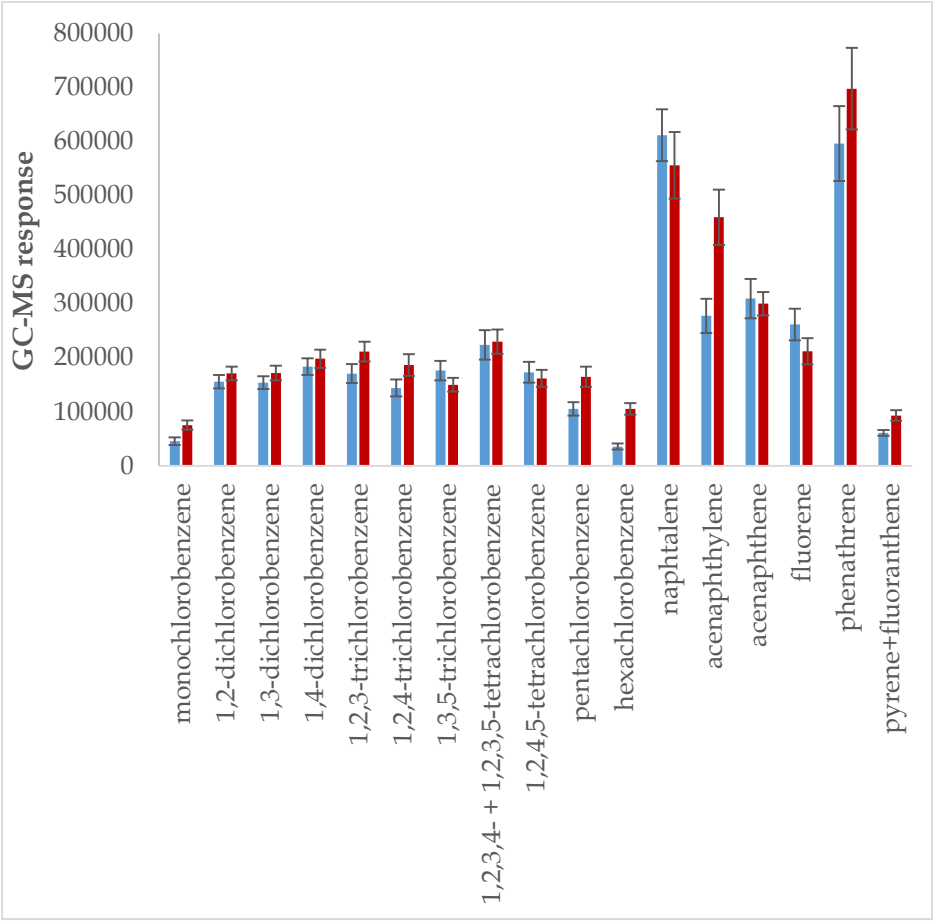

Figure 2.12 Enrichment capabilities of Carbotrap® 300 (blue) and NGAC (red) for the TD-GC-MS analysis of a mixtures of CBs and PAHs (10 ng spike, n=5)

As shown in **Figure 2.12**, under nitrogen the new NGAC sorbent material was characterized by extraction capabilities better or comparable to those achieved by the commercial trap.

Additional analyses were performed by extracting the target compounds (in the 0.2-20 $\mu g/m^3$ range) in presence of 30 and 70% relative humidity. The new material was able of extracting the SVOCs even when high percentages of relative humidity were tested. At the lower moisture level, no decrease in the extraction capabilities were observed compared to the analysis performed by

using only nitrogen as carrier gas, whereas at the highest level, an average reduction of 28% in the GC-MS responses was present. It has to be noticed that the observed decrease con be attributable also to the adsorption of the Tenax cryo-trap. By contrast, the commercial Carbotrap® tubes, even at the lower level of relative humidity, were clogged, failing the leak tests.

On the basis of the obtained results, it can be stated that by using the new TD-tube no filtering/drying unit is required, thus avoiding problems related to the possible adsorption of the analytes before the TD-trap.

Another important parameter affecting the extraction capabilities of the sorbent is the amount of material filling the TD-tube: commercially available multi-sorbent tubes contain about 240 mg of granular carbon. Our study proved that only 50 mg of the NGCA sorbent allowed to achieve higher or comparable extraction capabilities compared to the commercial devices.

2.3.4 Method Validation

Finally, method validation was performed following Eurachem guidelines [75], in order to prove the suitability of TD-GC-MS method based on the use of NGAC material for the determination of SVOCs in air at trace levels.

Excellent results in terms of LOD and LOQ values were achieved for all the investigated compounds (**Table 2.4**). The obtained values were lower than those reported in literature for PAHs [74] and CBs [70] respectively by using commercial coatings or those required by the EPA methods [63].

A good linearity was proven by applying Mandel's fitting test on two order of magnitude in 0.2-20 $\mu g/m^3$ range. Being the analytes present in mixture, the lowest level was selected by considering the highest LOQ value of the target analytes.

As for precision, good results were obtained in terms of both repeatability and intermediate precision, with RSD values always lower than 23% for the two concentration levels considered. Three different TD-tubes were used. In the case of intermediate precision, ANOVA showed that mean values were not significantly different among 3 month giving p values >0.05. The achieved repeatability was better than that achieved by using the Carbotrap® 300 (<30%).

Extraction recoveries were calculated for all the analytes at two concentration levels (1 and 10 $\mu g/m^3$), showing a good efficiency: recoveries ranging from

75±10 to 93±15 were obtained for CBs (n=5), whereas PAHs were characterized by recoveries in the 72±8 - 88±14 range (n=5).

Table 1.2: LOD and LOQ values (ng/m^3) of the NGAC TD-tube

Analyte	**LOD** (ng/m^3)	**LOQ** (ng/m^3)
monochlorobenzene	4	14
1,2-dichlorobenzene	2	6
1,3-dichlorobenzene	2	6
1,4-dichlorobenzene	2	6
1,2,3-trichlorobenzene	7	23
1,2,4-trichlorobenzene	7	22
1,3,5-trichlorobenzene	27	90
1,2,3,4- + 1,2,3,5-tetrachlorobenzene	2	5
1,2,4,5-tetrachlorobenzene	4	15
pentachlorobenzene	25	90
hexachlorobenzene	55	180
naphtalene	6	21
acenaphthylene	7	22
acenaphthene	18	60
fluorene	57	195
phenathrene	50	170
pyrene+fluoranthene	26	85

2.4 Conclusions

In this study the capabilities of new multipurpose absorbent tubes, using non granular active carbon (NGAC) were tested for the analysis of SVOCs and compared to those achieved by using commercially available multi-bed sorbent Carbotrap® 300.

More precisely, a TD-GC-MS method for the analysis of CBs and PAHs was developed and validated by following Eurachem guidelines. The developed NGAC TD-tubes proved to be suitable for the analyses of SVOCs in presence high humidity levels without requiring a drying/filtering unit. By contrast, clogging of the commercial TD-tubes was always observed.

LOQ in the 5-182 ng/m^3 range and in the 14-196 ng/m^3 range for CBs and PAHs respectively were obtained. A good linearity was demonstrated in the 0.2-20 μg/m^3 range. An acceptable precision in terms of repeatability and intermediate precision was achieved (CV<23%). A goody trueness was also obtained with recovery rates in the 72(±8)-93(±15)% range (n=5).

This research study had to face the following instrumental issues:

1. Frequent maintenance was required: the system was operating at the maximum allowed conditions, thus frequent turnover of the consumable parts, such as the *o*-rings was required;
2. Transfer line was too long, thus causing condensation and broadening phenomena;
3. Secondary trap material (Tenax) was not suitable for an immediate release of the SVOCs, leading to a slow release of the analytes. As a consequence, long analysis times were required
4. Separation of the analytes was obtained not only through GC-chromatography but also by the desorption from the secondary trap
5. The TD was not directed interfaced with the TurboMass software of the GC-MS, thus leading to frequent instrumental fail errors

Future studies will be devoted to improve the instrumental configuration (substitution of the Tenax in the cryo-trap and short transfer-line) and to analyze other classes of SVOCs.

2.5 Acknowledgments

Thanks to Prof. C. Crescenzi from University of Salerno for providing the material and Prof. C. Östman from Stockholm University for the supervision.

2.6 References

[1] C.J. Weschler, W.W. Nazaroff, *Semivolatile organic compounds in indoor environments*, Atmos. Environ., 42 (2008) 9018–9040

[2] T. Iwasaki, W. Miyazaki, A. Takeshita, Y. Kuroda, N. Koibuchi, *Polychlorinated biphenyls suppress thyroid hormone-induced transactivation,* Biochem. Bioph. Res. Co., 299 (2002) 384–388

[3] L.S. Birnbaum, D.F. Staskal, *Brominated flame retardants: cause for concern?*, Environ. Health Persp., 112 (2004) 9–17.

[4] R.R. Newbold, W.N. Jefferson, E. Padilla-Banks, *Long-term adverse effects of neonatal exposure to bisphenol A on the murine female reproductive tract*, Reprod. Toxicol., 24 (2007) 253–258.

[5] K.L. Howdeshell, *A model of the development of the brain as a construct of the thyroid system*, Environ. Health Persp., 110 (2002) 337–348.

[6] C.J. Weschler, W.W. Nazaroff, *SVOC partitioning between the gas phase and settled dust indoors*, Atmos. Environ., 44 (2010) 3609-3620.

[7] Y.F. Mao, Z. Li, W.Q. Tao, *Predicting emissions and transport of Semi-volatile organic compounds in indoor environments: a review on mechanistic models*, in: Indoor Air 2014-13th International Conference on Indoor Air Quality and Climate, Hong Kong, 2014, pp. 280-287.

[8] H. Xiao, F. Wania, *Is vapor pressure or the octanol–air partition coefficient a better descriptor of the partitioning between gas phase and organic matter?*, Atmos. Environ., 37 (2003) 6867-6878.

[9] B.A. Tichenor, *Characterizing Sources of Indoor Air Pollution and Related Sink Effects*, ASTM, West Conshohocken, PA, USA, 1996.

[10] K. Breivik, A. Sweetman, J.M. Pacyna, K.C. Jones, *Towards a global historical emission inventory for selected PCB congeners – a mass balance approach: 1. Global production and consumption.*, Sci. Total Environ., 290 (2002) 181–198.

[11] M. Khajeh, Y. Yamini, J. Hassan, *Trace analysis of chlorobenzenes in water samples using headspace solvent microextraction and gas chromatography/electron capture detection*, Talanta, 69 (2006) 1088–1094

[12] U.S. EPA, U.S. Environmental Protection Agency. *Chlorinated benzenes; Final Test Rule*, 40 CFR Part 799. Fed. Reg., 51 (1986) 24657.

[13] EC (European Community), *Council Directive 76/464/EEC on pollution caused by certain dangerous substances discharged into the aquatic environment of the Community*. Official J. (1976) L 129.

[14] EC (European Community), *Directive 2000/60/EC of the European Parliament and of the Council establishing a framework for Community action in the field of water policy*. Official J. (2000) L 327.

[15] Agency for Toxic Substances and Disease Registry (ATSDR). *Toxicological Profile for Chlorobenzene*. Public Health Service, U.S. Department of Health and Human Services, Atlanta, GA, USA, 1990.

[16] U.S. Department of Health and Human Services. Hazardous Substances Data Bank (HSDB, online database). National Toxicology Information Program, National Library of Medicine, Bethesda, MD, USA 1993.

[17] U.S. Environmental Protection Agency. *Updated Health Effects Assessment for Chlorobenzene. EPA/600/8-89/099. Environmental Criteria and Assessment Office, Office of Health and Environmental Assessment, Office of Research and Development*, Cincinnati, OH, USA 1989.

[18] http://www.inchem.org/documents/sids/sids/95501.pdf

[19] ATSDR (Agency for Toxic Substances and Disease Registry), *Toxicological Profile for 1,4-Dichlorobenzene*, ATSDR/TP-92/10, Atlanta, GA, USA, 1993.

[20] A.P. Leber, T. J. Benya, *Halogenated Benzene*, in, *Patty's Industrial Hygiene and Toxicology*, Fourth Edition, Volume II, Part B, John Wiley and Sons, Hoboken, NJ, USA, 1994.

[21] M. Morita, G. Ohi, *Para-dichlorobenzene in human tissue and atmosphere in Tokyo metropolitan area*, Environ. Pollut., 8 (1975) 269-274.

[22] U.S. Department of Health and Human Services, *Hazardous Substances Data Bank (HSDB, online database)*, National Toxicology Information Program, National Library of Medicine, Bethesda, MD, USA, 1993.

[23] U.S. Environmental Protection Agency, *Integrated Risk Information System (IRIS) on 1,2,4-Trichlorobenzene,* National Center for Environmental Assessment, Office of Research and Development, Washington, DC, USA, 1999.

[24] Agency for Toxic Substances and Disease Registry (ATSDR), *Toxicological Profile for Hexachlorobenzene (Update),* Public Health Service, U.S. Department of Health and Human Services, Atlanta, GA, USA, 1996.

[25] U.S. Environmental Protection Agency, *Deposition of Air Pollutants to the Great Waters, First Report to Congress*, EPA-453/R-93-055, Office of Air Quality Planning and Standards, Research Triangle Park, NC, USA, 1994.

[26] H. Shen, Y. Huang, R. Wang, D. Zhu, W. Li, G. Shen, B. Wang, Y. Zhang, Y. Chen, Y. Lu, H. Chen, T. Li, K. Sun, B. Li, W. Liu, J. Liu, S. Tao, *Global Atmospheric Emissions of Polycyclic Aromatic Hydrocarbons from 1960 to 2008 and Future Predictions*, Environ. Sci. Technol., 47 (2013) 6415–6424.

[27] M. Lee, *Analytical Chemistry of Polycyclic Aromatic Compounds*, Academic Press, Cambridge, MA, USA, 1981.

[28] S.A. Stout, S.D. Emsbo-Mattingly, G.S. Douglas, A.D. Uhlera, K.J. McCarthy, *Beyond 16 Priority Pollutant PAHs: A Review of PACs used in Environmental Forensic Chemistry*, Polycycl. Aromat. Comp., 35 (2015) 285-315.

[29] C. Achten, J.T. Andersson, *Overview of Polycyclic Aromatic Compounds (PAC)*, Polycycl. Aromat. Comp., 35 (2015) 177–186.

[30] K. Ravindra, L. Bencs, E. Wauters, J. de Hoog, F. Deutsch, E. Roekens, N. Bleux, P. Berghmans, R. Van Grieken, *Seasonal and site-specific variation in vapour and aerosol phase PAHs over Flanders (Belgium) and their relation with anthropogenic activities*, Atmos. Environ., 40 (2006) 771–785.

[31] M. Tobiszewski, J. Namieśnik, *PAH diagnostic ratios for the identification of pollution emission sources*, Environ. Pollut., 162 (2012) 110–119.

[32] D.H. Phillips, *Polycyclic aromatic hydrocarbons in the diet*, Mutat. Res. 443 (1999) 139-47.

[33] I.J. Keyte, R.M. Harrison, G. Lammel, *Chemical reactivity and long-range transport potential of polycyclic aromatic hydrocarbons – a review*, Chem. Soc. Rev., 42 (2013) 9333-9391.

[34] https://www.ncbi.nlm.nih.gov/books/NBK138705/pdf/Bookshelf_NBK138705.pdf

[35] EPA methods: https://www.epa.gov/sites/production/files/2015-07/documents/epa-8270d.pdf, https://www.epa.gov/sites/production/files/2015-12/documents/8275a.pdf

[36] SKC (2011) Guide to NIOSH/OISH/ASTM air sampling methods. www.skcinc.com/OSHA-NIOSH/default.asp.

[37] https://www.epa.gov/sites/production/files/2016-02/documents/to-10ar.pdf

[38] J. Lee, K. Huang, Y. Yu, M. Chen., *Laboratory retention of vapor-phase PAHs using XAD adsorbents*, Atmos. Environ., 38 (2004) 6185—6193.

[39] R. Barro, J. Regueiro, M. Llompart, C. Garcia-Jarez, *Analysis of industrial contaminants in indoor air: Part 1. Volatile organic compounds, carbonyl compounds, polycyclic aromatic hydrocarbons and polychlorinated biphenyls*, J. Chromatogr. A, 1216 (2009) 540–566.

[40] T. Staaf, C. Östman, *Indoor air sampling of organophosphate triesters using solid phase extraction (SPE) adsorbents*, J. Environ. Monit., 7 (2005) 344-348.

[41] E. Ghasemi, M. Sillanpää, *Optimization of headspace solid phase microextraction based on nano-structured ZnO combined with gas chromatography–mass spectrometry for preconcentration and determination of ultra-traces of chlorobenzenes in environmental samples*, Talanta, 130 (2014) 322-327.

[42] Y. Wang, J. Zhang, Y. Ding, J. Zhou, L. Ni, C. Sun, *Quantitative determination of 16 polycyclic aromatic hydrocarbons in soil samples using solid-phase microextraction*, J. Sep. Sci., 32(2009) 3951-3957.

[43] M. Khajeh, Y. Yamini, J. Hassan, *Trace analysis of chlorobenzenes in water samples using headspace solvent microextraction and gas chromatography/electron capture detection*, Talanta, 69 (2006) 1088–1094.

[44] A. Tor, *Determination of chlorobenzenes in water by drop-based liquid-phase microextraction and gas chromatography-electron capture detection*, J. Chromatogr. A, 1125 (2006) 129–132.

[45] H.J. Stan, N.H. Kirsch, *GC-FID Determination of Chlorobenzene Isomers in Methanogenic Batch-Cultures from River Sediments*, Int. J. Environ. An. Ch., 60 (1995) 33-40.

[46] B. Heinzow, S. Mohr, G. Ostendorp, M. Kerst, W. Körner, *PCB and dioxin-like PCB in indoor air of public buildings contaminated with different PCB sources – deriving toxicity equivalent concentrations from standard PCB congeners*, Chemosphere, 67 (2007) 1746–1753.

[47] Y. Wang, H.K. Lee, *Determination of chlorobenzenes in water by solid-phase extraction and gas chromatography–mass spectrometry*, J. Chromatogr. A, 803 (1998) 219 –225.

[48] C. Gu, H. Huang, J. Huang, Z. Jin, H. Zheng, N. Liu, M. Li, J. Liu, F. Meng, *Chlorobenzene sensor based on Pt-decorated porous single-crystalline ZnO nanosheets*, Sens. Actuators A Phys., 252 (2016) 96–103

[49] P.V.S. Ajay, J. Printo, D.S.C.G. Kiruba, L. Susithra, T. Kinoshita, S. Muthusamy, *Colorimetric sensors for rapid detection of various analytes,* Mater. Sci. Eng. C Mater. Biol. Appl., 78 (2017) 1231–1245.

[50] D.L. Poster, M.M. Schantz, L.C. Sander, S.A. Wise, *Analysis of polycyclic aromatic hydrocarbons (PAHs) in environmental samples: a critical review of gas chromatographic (GC) methods*, Anal. Bioanal. Chem., 386 (2006) 859–881

[51] B. Zhao, S. Zhang, Y. Zhou, D. He, Y. Li, M. Ren, Z. Xu, J. Fang, *Characterization and quantification of PAH atmospheric pollution from a large petrochemical complex in Guangzhou: GC-MS/MS analysis*, Microchem. J. 119 (2015) 140–144.

[52] G. Purcaro, S. Moret, M. Bucar-Miklavcic, L.S. Conte, *Ultra-high performance liquid chromatographic method for the determination of polycyclic aromatic hydrocarbons in a passive environmental sampler*, J. Sep. Sci. 35 (2012) 922–928.

[53] H.F. Nassar, N. Tang, T. Kameda, A. Toriba, M.I. Khoder, K. Hayakawa, *Atmospheric concentrations of polycyclic aromatic hydrocarbons and selected nitrated derivatives in Greater Cairo, Egypt*., Atmos. Environ, 45 (2011) 7352–7359.

[54] G. Mirivel, V. Riffault, J.C. Galloo*, Simultaneous determination by ultra-performance liquid chromatography-atmospheric pressure chemical ionization time-of-flight mass spectrometry of nitrated and oxygenated PAHs found in air and soot particles,* Anal. Bioanal. Chem., 397 (2010) 243–256.

[55] L. Hollosi, T. Wenzl, *Development and optimisation of a dopant assisted liquid chromatographic-atmospheric pressure photo ionisation-tandem mass spectrometric method for the determination of 15+ 1 EU priority PAHs in edible oils*, J. Chromatogr. A, 1218 (2011) 23–31.

[56] S.S. Cai, J.A. Syage, K.A. Hanold, M.P. Balogh, *Ultra Performance Liquid Chromatography-Atmospheric Pressure Photoionization-Tandem Mass Spectrometry for High-Sensitivity and High-Throughput Analysis of US Environmental Protection Agency 16 Priority Pollutants Polynuclear Aromatic Hydrocarbons*, Anal. Chem., 81 (2009) 2123–2128.

[57] D.B. Robb, M.W. Blades, *State-of-the-art in atmospheric pressure photoionization for LC/MS*, Anal. Chim. Acta, 627 (2008) 34–49.

[58] S.C.C. Lung, C.H. Liu, *Fast analysis of 29 polycyclic aromatic hydrocarbons (PAHs) and nitro-PAHs with ultrahigh performance liquid chromatography-atmospheric pressure photoionization-tandem mass spectrometry*, Sci. Rep., 5 (2015) Art. 12992, doi:10.1038/srep12992.

[59] D. Matschulat, A. Deng, R. Niessner, D. Knopp, *Development of a highly sensitive monoclonal antibody based ELISA for detection of benzo[a]pyrene in potable water*, Analyst, 130 (2005) 1078-1086.

[60] L.R. Dartnell, M.R. Patel, M.C. Storrie-Lombardi, J.M. Ward, J.P. Muller, *Experimental determination of photostability and fluorescence-based detection of PAHs on the Martian surface*, Meteorit. Planet. Sci., 47 (2012) 806–819.

[61] X.Y. Meng, Y.S. Li, Y. Zhou, Y.Y. Zhang, B. Qiao, Y. Sun, L. Yang, P. Hu, S.Y. Lu, H.L. Ren, J.H. Zhang, X.R. Wang, Z.S. Liu, *Real-time immuno-PCR for ultrasensitive detection of pyrene and other homologous PAHs*, Biosens Bioelectron., 70 (2015) 42–47.

[62] B. Lazarov, R. Swinnen, M. Spruyt, E. Goelen, M. Stranger, G. Desmet, E. Wauters, *Optimisation steps of an innovative air sampling method for semivolatile organic compounds*, Atmos. Environ. 79 (2013) 780–786.

[63] http://easlab.com/QC/EPA%20TO17%20Volatile%20Organic%20Compounds.pdf

[64] https://www.cdc.gov/niosh/docs/2003-154/pdfs/2549.pdf

[65] https://www.astm.org/DATABASE.CART/HISTORICAL/D6196-97.htm

[66] S.A. Idris, C. Robertson, M.A. Morris, L.T. Gibson, *A comparative study of selected sorbents for sampling of aromatic VOCs from indoor air*, Anal. Methods, 2 (2010) 1803–1809.

[67] A. Kumar, I. Víden, *Volatile organic compounds: sampling methods and their worldwide profile in ambient air*, Environ. Monit. Assess., 131 (2007) 301–321.

[68] L. Sampaolo, E. Pierini, A.R. Mastrogiacomo, *Evaluation of a new dualsorbent trap for organic pollutants of different volatility*, Chromatographia, 50 (1999) 680–684.

[69] G.K.S. Wong, S.J. Ng, R.D. Webster, *Quantitative analysis of atmospheric volatile organic pollutants by thermal desorption gas chromatography mass spectrometry*, Anal. Methods, 5 (2013) 219–230.

[70] A. Maceira, L. Vallecillos, F. Borrull, R.M. Marcé, *New approach to resolve the humidity problem in VOC determination in outdoor air samples using solid adsorbent tubes followed by TD-GC–MS*, Sci. Total Environ., 599–600 (2017) 1718–1727

[71] L. Dutaur, M.L. Riba, V. Simon, J. Namieśnik, L. Torres, *Improvement of analytical techniques for the determination of monoterpenes in atmospheric samples: water removal on K_2CO_3 and $CaCl_2$*, Chem. Anal., 43 (1998) 375–386.

[72] C.M. Karbiwnyk, C.S. Mills, D. Helmig, J.W. Birks, *Minimization of water vapor interference in the analysis of non-methane volatile organic compounds by solid adsorbent sampling*, J. Chromatogr. A, 958 (2002) 219–229.

[73] G.V. Martins, S. Martins, A.O. Martins, *Determination of gaseous polycyclicaromatic hydrocarbons by a simple direct method using thermaldesorption–gas chromatography–mass spectrometry*, Environ. Monit. Assess., 185 (2013) 6447–6457.

[74] Y. Li, Q. Xian, L. Li, *Development of a short path thermal desorption–gas chromatography/mass spectrometry method for the determination of polycyclic aromatic hydrocarbons in indoor air*, J. Chromatogr. A, 1497 (2017) 127–134.

[75] *The Fitness for Purpose of Analytical Methods: A Laboratory Guide to Method Validation and Related Topics*, EURACHEM Guide, 1st English ed., LGC Ltd., Teddington, U.K., 2014, http://www.eurachem.ul.pt.

[76] http://www.sigmaaldrich.com/content/dam/sigma-aldrich/docs/Supelco/Genera_Information/1/specialty-carbon-adsorbents-t410081.pdf

[77] E.Z. Pina-Salazar, K. Kaneko, *Adsorption of water vapor on mesoporosity-controlled singe wall carbon nanohorn*, Colloids and Interface Science Communications, 5 (2015) 8–11.

[78] K. Morishige, S. Kittaka, *Kinetics of Capillary Condensation of Water in Mesoporous Carbon: Nucleation and Meniscus Growth*, J. Phys. Chem. C, 119 (2015) 18287−18292.

[79] D. R. Ceratti, M. Faustini, C. Sinturel, M. Vayer, V. Dahirel, M. Jardat, D. Grosso, *Critical effect of pore characteristics on capillary infiltration in mesoporous films*, Nanoscale, 7 (2015) 5371–5382.

[80] B. Lazarov, R. Swinnen, M. Spruyt, E. Goelen, M. Stranger, G. Desmet, E.Wauters, *Optimisation steps of an innovative air sampling method for semivolatile organic compounds*, Atmos. Environ., 79 (2013) 780–786.

Chapter 3

A Rapid Microextration by Packed Sorbent-Liquid Chromatography-Mass Spectrometry Method for the Determination of Dexamethasone and Dexamethasone Disodium Phosphate in Aqueous Humor

The research study presented in this chapter has been published in Journal of Pharmaceutical and Biomedical Analysis: F. Bianchi, M. Mattarozzi, N. Riboni, P. Mora, S.A. Gandolfi, M. Careri, *A rapid microextraction by packed sorbent − liquid chromatography tandem mass spectrometry method for the determination of dexamethasone disodium phosphate and dexamethasone in aqueous humor of patients with uveitis*, J. Pharmaceut. Biomed., 142 (2017) 343–347.

3.1 Introduction

3.1.1 *Uvea and Uveitis*

The wall of the human eye consists of three distinct concentric layers, the outer layer (the transparent cornea and the opaque white sclera), the middle layer (the uveal tract, or simply uvea), and the inner layer (the retina) (**Figure 3.1**).

The prime functions of the uveal tract are the nutrition and gas exchange: uveal vessels directly perfuse the ciliary body and iris, to support their metabolic needs, and indirectly supply diffusible nutrients to the outer retina, sclera, and lens, which lack any intrinsic blood supply.

The uvea is composed of three parts: the iris anteriorly, an intermediate ciliary body, and the choroid posteriorly (**Figure 3.1**).

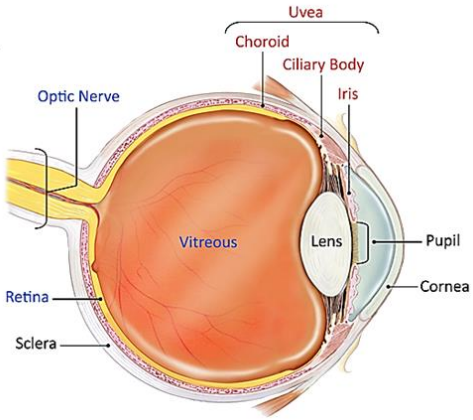

Figure 3.1 Eye schematic picture

1 The iris is the anterior part of the uvea, and forms a diaphragm over the lens. There is a hole in the center of the iris, known as the pupil. Pupil size is controlled by the light intensity entering the eye: it contracts under intensive light irradiation, and expands under low lighting, tuning the amount of light entering the lens and the posterior segment of the eye. The iris is exposed to both visible light and UV radiation and acts as a light screen in order to eliminate excessive light, sheltering both the choroid and ciliary body, also deeply pigmented.

2 The ciliary body: located between the iris and the choroid, is attached to the outer layer of the eye (the sclera). It extends for approximately 5-6 mm from the root of the iris to the beginning of the choroid. The structure

of the ciliary body is similar to the iris and its main function is the production of the aqueous humor, which fills the space in front of and behind the iris.

3 The choroid extends from the sclera to retina. The choroid is a layer of connective tissue, which consists of large amount of blood vessels. The main function of the choroid is to support and nourish the retina.

Uveitis, an inflammation of the uvea, can be differentiated in anterior, intermediate and posterior uveitis, depending on which part of the uvea is affected. Anterior uveitis starts suddenly and symptoms can last up to 8 weeks, whereas posterior uveitis develops gradually and can lasts for many years. Some forms of anterior uveitis are recurrent and can involve all the layers.

Uveitis is present all over the world with an incidence in the developed countries ranging between 15 and 20 cases per 100,000 people/year. Even if this disease has been observed in patients of any age, it represents a significant burden of disease during both early adulthood and in an age range from the 50s to the 60s [2].

Cataract is a common complication in patients affected by uveitis: some forms of uveitis commonly feature cataract as part of the disease process; in addition, topical, periocular, or systemic corticosteroids used to treat uveitis can result in cataract formation. Eye surgery in uveitic eyes has considerable potential for postoperative worsening or relapsing of intraocular inflammation:

1 Infectious causes of uveitis have to be identified in order to treat them before performing any surgery;
2 Infectious causes may influence perioperative care and antibiotic prophylaxis [3];
3 Many forms of uveitis are associated with systemic diseases that may require systemic treatments;
4 The surgical outcome may be influenced by the type of uveitis.

Thus, optimal treatment of cataract requires an accurate management of uveitis, including appropriate diagnostic workup and scrupulous attention to preoperative preparation, intraoperative technique, and postoperative management.

In patients with a history of noninfectious uveitis (idiopathic or related to a systemic autoimmune disease), the control of inflammation requires a greater focus on perioperative prophylaxis by corticosteroids administration [4].

3.1.2 *Corticosteroids*

Corticosteroids are potent anti-inflammatory and immunosuppressive agents. They are also used in order to stabilize the blood-retina barrier by affecting the expression of molecules involved in ion and water flux, as well as enhancing tight junction integrity, making them good agents for reducing macular edema.

Corticosteroids have been used to treat uveitis from the beginning of 1950s [5,6]. These drugs provide several advantages: they are inexpensive, fast acting and potent, thus making them excellent candidates for therapy of virtually all patients with noninfectious ocular inflammatory diseases.

The mechanisms whereby corticosteroids exert their anti-inflammatory effects are both complex and incompletely understood [7].

Corticosteroids administration can be performed topically, regionally, or systemically [8]:

- Systemic corticosteroids, although efficient in controlling inflammation, are associated with numerous side effects such as adrenal suppression and osteoporosis, thus are considered as a poor choice for long-term use [9].
- Periocular corticosteroids are used to treat patients affected by chronic or recurrent inflammation which do not tolerate systemic therapy. The main drawback associated to their use is the need of repeated injections in a 2 to 4-month interval, thus leading to potential risk of globe perforation, orbital fibrosis, orbital fat prolapses, and ptosis [10].
- Intravitreal injection is another modality of intraocular delivery but the effect is transient (its activity expires in several months) and present the risk of vitreous hemorrhage and retinal detachment [11,12].
- Topical administration of anti-inflammatory corticosteroids is usually preferred over systemic administration due to higher ocular drug concentrations with minimal systemic adverse events.

The ophthalmic topical treatment by using eye-droplets, however, is affected by several drawbacks in terms of pharmaceutical formulations (i.e. solubility,

stability, and preservation) and clinical limitations (i.e. limited efficacy, corneal/scleral permeability, systemic toxicity and compliance). Furthermore, within two minutes after instillation over 80% of the topical product is expelled from the eye *via* the nasolacrimal drainage system, thus limiting ocular penetration of the drug [13].

In uveitis, penetration of the drug into the aqueous humor in fact, is a key parameter in order to assess clinical efficacy, due to poor tissue permeability [14, 15]: topical administration can reach the anterior segment, but it is less effective in reaching the posterior segment. Oral or intravenous administration can reach the posterior segment, but are associated with non-specific accumulation of the drug in other organs, thus resulting in related adverse effects. In addition, the blood-retina barrier hinders drugs diffusion into the posterior segment [15].

In order to overcome these limitations and allow the delivery of medication to both anterior and posterior uvea, the release of medication from both biocompatible and biodegradable polymers and non-biodegradable matrices has been tested and approved by the FDA [16]. Implants are introduced into the vitreous humor through an incision in the ocular *pars plana* located between the lens and the retina.

Currently, three implant has been approved for posterior segment to treat severe non-infectious posterior segment non-infectious uveitis: Ozurdex™ (Allergan Inc.), a fully biocompatible system having dexamethasone as active principle, with a therapeutic action of 6–9 months [17], and two non-biodegradable implants, i.e. Vitrasert™ (Bausch & Lomb), lasting 6 months [18], and Retisert™ (Bausch & Lomb), carrying fluocinolone acetonide, a corticosteroid with approximately 2 years life time [19]. The main drawback affecting the non-biocompatible implants is that they require the removal from the eye after reservoir depletion, carrying all the risk associated to surgery.

3.1.3 Dexamethasone

Dexamethasone (DEX) (**Figure 3.2**) is a very potent glucocorticoid, about 30 times more than cortisone, and one of the most prescribed worldwide drug for uveitis treatment [20].

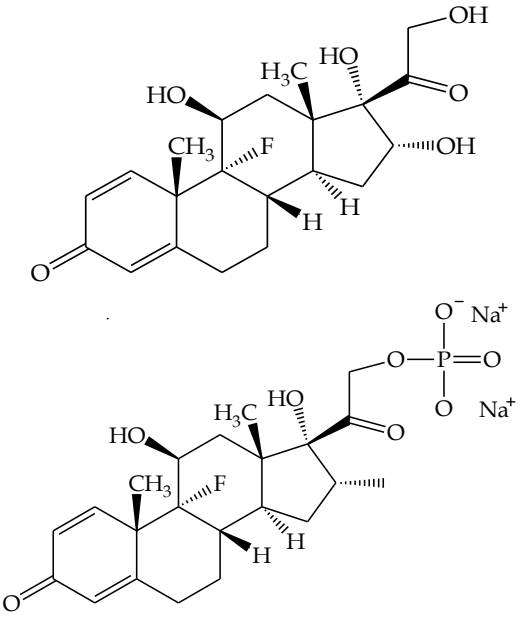

Figure 3.2: Molecular structure of dexamethasone (left) and dexamethasone disodium phosphate

DEX has been widely used in order to treat a plethora of ocular diseases, thus including both anterior and posterior segment inflammation, or as immunosuppressive agent during the postoperative management and prevention of corneal graft rejections [21]. It is prescribed in form of ophthalmic eye drops, suspensions or ointments for topical administration [22]. Due to the low water solubility, dexamethasone is usually replaced by dexamethasone disodium phosphate (DEX-SP) (**Figure 3.2**) [23] characterized by higher hydrophilicity, and easily hydrolysable to free active dexamethasone by phosphatase [24].

An effective treatment of the uveitis infections requires that dexamethasone reaches the targeted site, thus achieving and maintaining the therapeutic concentration of about 1 μg/ml [25], but, due to the poor permeability of DEX and DEX-SP towards the corneal epithelium, in topical administration, less

than 3% of the instilled dose usually reaches the aqueous humor [26]. This concentration in the vitreous humor is even lower when the drug is administered *via* ophthalmic solution: only 0.001% is expected to reach the posterior segment, at least one order of magnitude less than those is achieved through periocular injections, in the 0.01–0.1% range [26]. Moreover, dexamethasone is characterized by a very short half-life in aqueous humor, i.e. 3–6 h [27], thus requiring frequent administrations.

Despite all these limitations, topical administration remains ideally preferable, carrying less side effects and risks compared to systemic or intraocular treatments.

The analysis of DEX and DEX-SP in aqueous humor requires

- high selectivity in order to avoid the detection of possible interferences, able to coelute or interfere during the ESI ionization step, thus invalidating the quantitative analysis
- high sensitivity: low LODs and LOQs have to be achieved due to the low concentration levels of the analytes in the samples
- be suitable for the analysis of the low sample volumes: only small amount of biological sample can be collected during surgery (up to tens of μl).

3.1.4 *Sample treatment and MS-methods: state of art*

GC–MS [28,29], LC–MS [29,30], LC–MS^n [29-33] and liquid chromatography-diode array detection (LC-DAD) [29,34] have been used to analyze dexamethasone in different biological matrices, such as blood, urine and humor aqueous. Compared to the GC analysis, LC has the advantage of direct analysis of samples without derivatization.

Respect to LC-DAD analysis, LC–MS and LC–MS/MS are able to provide lower detection limits (at sub-ng/l level) and better selectivity [29]. Moreover, LC-MS is superior in terms of selectivity, thus reducing false positives in complex matrices.

Despite the excellent performances of LC-MS, in order to obtain high recoveries and minimize the presence of interfering compounds, steroids extraction and clean-up procedures have to be applied prior to the detection step.

Liquid-liquid extraction has been proposed for the quantitative determination of dexamethasone in humor aqueous [33]. However, this technique is often laborious and requires toxic solvents. Moreover, they are usually affected by low recovery rates, due to the possible formation of emulsions.

Solid phase extraction (SPE) has been widely used for steroids extraction from aqueous samples [34,35] but this technique is incompatible with the low sample volumes that can be collected.

To overcome this limitation and avoid or reduce the use of solvents, researchers developed new methods based on microextraction techniques for the determination of steroid hormones both in biological and environmental samples.

Among them, SPME has been used to detect steroid hormones in both water [36] and biological samples [37-39].

Molecularly imprinted polymers (MIP) are synthetic stables polymers presenting recognition sites complementary to template molecules in terms of size, shape and arrangement of functional groups. These sites are capable of binding the target molecule with a high selectivity in presence of interfering compounds in complex matrices. MIPs have been also applied for developing new SPME coatings for steroid extraction [40,41]. However, MIPs present several drawbacks, i.e. limited number of functional groups able to interact with target molecules and slow binding kinetics.

In-tube SPME (it-SPME) is an extraction method derived from SPME: an open tubular fused-silica capillary presenting an inner surface coating is used as extraction device [42]. Analytes in liquid samples are extracted and concentrated into the stationary phase by repeated draw/eject cycles of sample solution, thus allowing the analysis of low sample volumes. it-SPME has been used for simultaneous determination of endocrine disruptors [43] in water and steroids from human urine samples [44].

Quick, Easy, Cheap, Effective, Rugged and Safe extraction (QuEChERS) is a recently developed technique based on the following steps:

1. homogenized samples are extracted by using an organic solvent
2. an aliquot of the extraction solvent is cleaned up using dispersive SPE
3. the cleaned extracts are analyzed by using the proper instrumental technique

The QuEChERS procedure is characterized by small amounts of both sample and solvent, short extraction times and high extraction efficiency of polar compounds. Moreover, it is very cheap and simple, thus allowing its use for high throughput analyses demand. It has been used for steroids extraction in herbal medicines [45,46], biological tissues [47,48] and milk [49].

Microextraction by packed sorbent (MEPS) was proposed by Abdel-Rehiet al. in 2004 [50,51]. It is suitable for the treatment of small sample volumes and it is characterized by high selectivity and recovery rate, thus it can be successfully applied for the analysis of humor aqueous.

3.1.5 *MEPS Procedure*

Microextraction by packed sorbent is a new miniaturized form of SPE: it can be considered as a green sample pretreatment technology, since it reduces sample handling time and solvent consumption. It is suitable for a wide range of sample volumes (from few µL to several mL) and can be easily coupled with both LC and GC.

Typical MEPS is designed in syringe format: in homemade MEPS, the sorbent is packed inside a syringe (50–500 µL), whereas in commercial devices, the sorbent (1-4 mg) is set in a small cartridge called barrel insert and needle (BIN) (**Figure 3.3**).

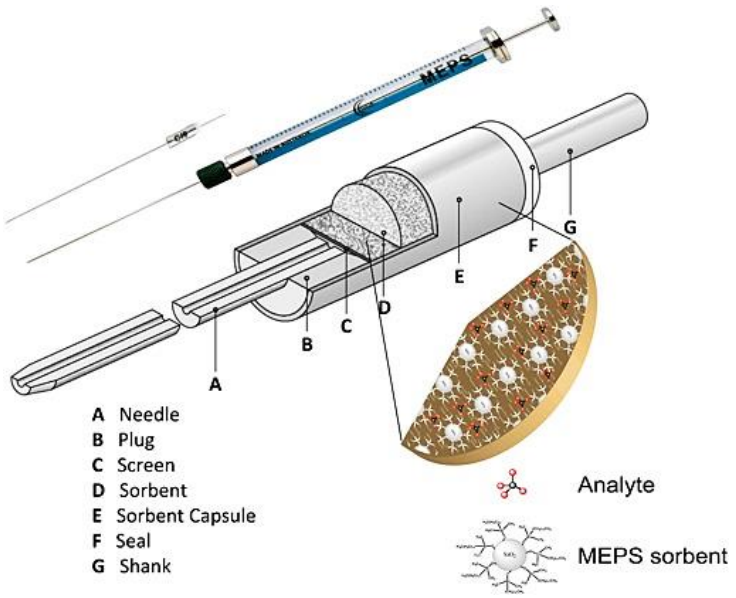

Figure 3.3 Scheme the MEPS syringe and MEPS-BIN [52]

Since the MEPS procedure was very promising, the technology moved from the simple syringe packaging of the firsts MEPS to their full automation and incorporation in PAL systems, thus the extraction can be performed manually, semi or fully automatically (**Figure 3.4**).

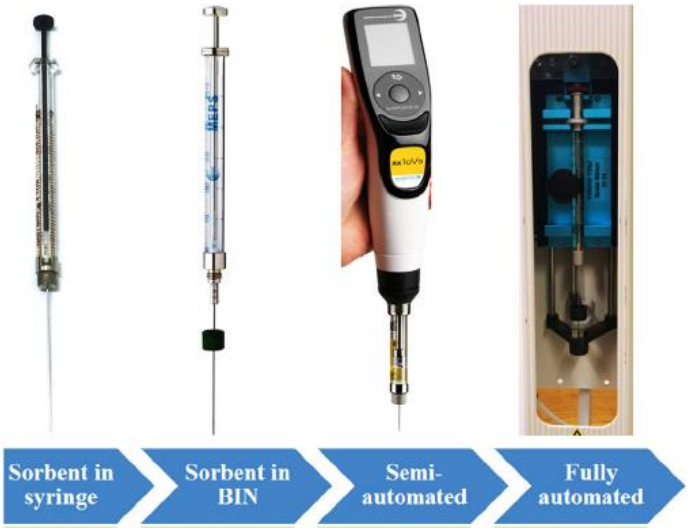

Figure 3.4 Scheme the MEPS systems, from manual to fully automated treatment [53]

The main advantage of the MEPS procedure is the possibility to perform sample extraction, washing, concentration, elution and injection by using the same device (**Figure 3.5**). All these steps require small amounts of both solvent and sample volume, thus being very interesting for biological, food and environmental applications.

The MEPS extraction procedure can be summarized as follows:

1. Conditioning of the sorbent by using methanol, water or buffer solutions is performed in order to activate the binding sites of the adsorbent.
2. Sample loading can be performed directly or with several loading/discharging cycles in order to concentrate the analytes on the sorbent material. The sample volume has to be optimized in order to obtain the best compromise between good analytical performances and extraction recoveries.

   The sampling flow, ranging from 10 to 20 µl/sec, is of a paramount importance: the use of low flows allows to increase the interaction

between the analytes and the adsorbent and decrease the presence of bubbles inside the syringe.

3. Washing: this step allows to remove interfering compounds from the MEPS by using a proper eluent. Small volumes of solvent (usually 50-100 µl) are required, thus suiting the need of green chemistry. The washing step can be performed either by the same solvent used during the sampling or a new eluent capable of maximizing the extraction of the interferences from the MEPS.
4. Elution: the analytes are eluted from the sorbent material. Organic solvents such as methanol, ethanol, isopropanol, acetonitrile are commonly used, pure or mixed or buffered with acidic or basic solutions. The choice of the correct eluent is crucial and has to be performed by considering: i) physiochemical character of the analytes ii) types of interactions between the analytes and the MEPS material; iii) compatibility with the mobile phase or volatility in the case of subsequent LC or GC coupling analyses.
   Several cycles of elution can be applied in order to reach the complete recovery of the analytes from the MEPS.
5. Final washing: washing of the MEPS sorbent after the elution of the analytes is recommended in order to avoid any carryover effect.

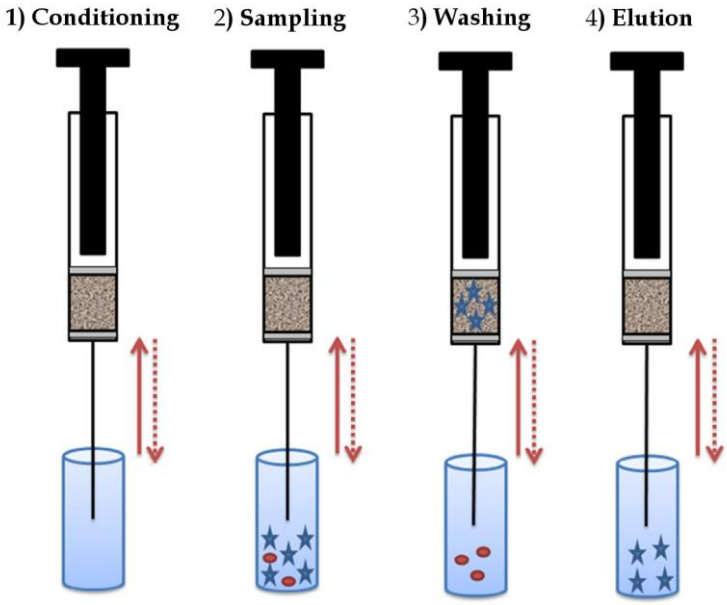

Figure 3.5 Schematic representation of the MEPS procedure

When analytes have to be extracted from complex matrices, a pretreatment of the sample could be necessary: dilution, centrifugation and precipitation are usually applied in order to prevent clogging of the MEPS device, volume understatement and formation of particulate. Moreover, in the case of biological samples, protein precipitation is usually required prior to the MEPS extraction [54] in order to avoid BIN clogging and backpressure problems.

As in SPE, the MEPS sorbent material is the core of the extraction procedure: the stationary phase has to be selective toward the adsorption of the target molecules, not retaining the interfering compounds.

Several commercially available sorbents have been developed, thus including:

- unmodified silica SIL (SIL)
- alkyl-functionalized silica: ethyl (C_2), octyl (C_8), octadecyl (C_{18})
- copolymer microspheres of styrene-divinylbenzene (PS-DVB)
- ion-exchange stationary phase: benzene sulfonic acid-functionalized silica, a strong cationic exchange for the extraction of organic amines (mixed mode 80% C_8 and 20% SCX); n-propyl trimethylammonium-based ligand, a strong anionic exchange sorbent used for separation of carboxylic compounds (SAX);

The core of all materials (except PS-DVB copolymer) is silica microspheres with mean particle size of 45 µm and pore size of 60 Å.

The MEPS procedure has been successfully applied for the extraction of steroids from water [55,56], saliva [57], plasma [57], blood [57] and urine samples [57,58].

The present research study is devoted to the development and validation of a fast, efficient, sensitive, reliable and high throughput MEPS-based methodology combined with LC–MS^2 for the simultaneous determination of dexamethasone and dexamethasone sodium phosphate in human aqueous humor from patients affected by uveitis after topical administration of the drug. Owing to the limited amount of sample volume available, the MEPS procedure was selected in order to perform extraction, clean-up and pre-concentration of the investigated analytes in a single device, thus increasing the speed of the analysis and minimizing the possibility of sample losses. This method was designed in order to be a valuable tool for clinical studies to assess the reliability of dexamethasone administration in patients affected by uveitis.

3.2 Materials and Methods

3.2.1 *Chemicals and materials*

Dexamethasone-21 disodium phosphate salt (> 98% purity), dexamethasone (≥ 98% purity), acetic acid (99% purity), ammonium acetate (98% purity) and methanol (> 99.9% purity) were purchased from Merk S.p.A. (Milan, Italy). C_2, C_8 and C_{18} MEPS BIN were acquired from SGE Analytical Science (Milton Keynes, UK).

3.2.2 *Aqueous humor sampling*

Following respective ethics committee approval, patients with a history of uveitis requiring cataract surgery were divided into two groups of perioperative steroidal supplementation.

Group A (topical prophylaxis alone): from 4 days before surgery: disodium dexamethasone 0.15% eye drops (4 instillations/day).

Group B (topical + oral prophylaxis): from 4 days before surgery: oral dexamethasone (0.05 mg/Kg/day, in a single dose in the morning), and adjunctive topical treatment as in the group A, as detailed in a previous report [59].

A total of 15 patients per group were involved. The day of surgery the patients were asked to put one drop of dexamethasone 0.15% in the operating eye just before moving to the Hospital (2–4 h before surgery). Cataract extraction was performed on all patients through standard pharmacoemulsification technique with foldable hydrophobic acrylic lens implantation, under topical or local anaesthesia (peribulbar injection). After cutting the corneal limbus, before the filling of the anterior chamber of the eye with viscoelastic matrix, an aliquot part of the aqueous humor (at least 50 µL, depending on the anatomy and the clinical characteristics of the eye) was drawn with a suitable sterile syringe with flat needle. This withdrawal did not change the modalities and the prognosis of surgery, being the aqueous humor normally dispersed on the surgical field. The liquid was quickly transferred in a microcentrifuge tube and stored at -80 °C.

From subjects who agreed to enter the study, written informed consent was obtained according to the tenets of the Declaration of Helsinki.

3.2.3 *Experimental design and optimization of the MEPS procedure*

The experiments were carried out on blank aqueous humor samples spiked with DEX and DEX-SP both at 3 µg/l. A 2^2 two-levels full factorial design (FFD) [60] was carried out by investigating the effects of both loading and eluting cycles. In both cases, low and high levels were 5 and 25 cycles, respectively. Standard solutions of both analytes at 3 µg/l were used. A F-test comparing the experimental and calculated responses at the center of the experimental domain was performed to evaluate the existence of relevant quadratic effects and a star design was added to the factorial design experiments [61]. The final regression models were then calculated using the Central Composite Design (CCD) experiments, obtained both from the FFD and the star design and used to find the optimal extraction conditions by using the multicriteria method of the desirability functions [62-64].

All statistical analyses were carried out by using the statistical package SPSS Statistics 24.0 (IBM, Milano, Italy).

3.2.4 *MEPS procedure*

A commercial e-Vol® equipped with a C18 BIN was used for MEPS extraction. Prior to extraction, each BIN was activated by using 4 × 50 µL of methanol and 2 × 50 µL of water. 50 µL of aqueous humor were drawn up and down through the BIN 19 times. Then, the analytes were eluted with 10 × 26 µL of methanol and analyzed by LC–MS^2. After extraction, 10 wash cycles each with 10 × 50 µL of methanol were used to clean the sorbent material and to avoid carryover effects. Both a fill and injection speed of 1 arbitrary unit were used.

3.2.5 *LC–MS^2 analysis*

Chromatographic separation was performed on a HPLC system (Thermo Electron Corporation, San Josè, CA, USA) coupled with a LTQ XL linear ion trap mass spectrometer (Thermo Electron Corporation) equipped with a pneumatically assisted electrospray interface. The system was controlled by the Xcalibur software (Thermo Electron Corporation).

The mobile phase was delivered by the Surveyor chromatographic system (Thermo Electron Corporation) equipped with a 200-vial capacity sample tray. A volume of 20 µL of each extract was injected into a GEMINI C_{18} 100 mm x 2.0 mm, 3 µm, 110 Å column (Phenomenex, Torrance, California, USA),

equipped with a C_{18} security guard cartridge and thermostated at 25 °C, at a flow rate of 250 µL/min.

The mobile phase consisted of solvent A (methanol) and solvent B (5 mM ammonium acetate, pH = 4.2). The initial condition was 40% solvent A and 60% solvent B. A linear gradient was performed with mobile phase A increasing from 40 to 90% within 1 min. After 7 min the mobile phase was returned to the initial conditions and re-equilibrated for 2 min. The sheath gas (nitrogen, 99.99% purity), the auxiliary gas (nitrogen, 99.99% purity) and the sweep gas (nitrogen, 99.99% purity) were delivered at flow rates of 30, 10 and 5 arbitrary units, respectively.

Optimized conditions of the source were set as follows: ESI voltage, 4.5 kV; capillary voltage, 30 V; capillary temperature, 300°C; tube lens, 100 V.

DEX-SP and DEX were analyzed in multiple reaction monitoring (MRM) mode using an electrospray probe in the positive ionization mode with a collision energy of 30 V.

The following transitions were monitored:

- DEX SP: *m/z* 517 → *m/z* 499 (used for quantitation)
  m/z 517 → *m/z* 479
  m/z 517 → *m/z* 395
- DEX: *m/z* 393 → *m/z* 373 (used for quantitation)
  m/z 393 → *m/z* 355
  m/z 393 → *m/z* 337

3.2.6 *Validation*

Validation was carried out under the optimized conditions, to meet the acceptance criteria for bioanalytical method validation [65]. Aqueous humor samples extracted from patients submitted to cataract surgery not treated with DEX-SP were used as blank matrix.

For both the analytes, the lower limit of quantification (LOQ) was calculated as signal-to-noise ratio, S/N = 5, using five independent samples and tested for accuracy and precision to meet the previously cited international criteria.

The calibration curves were evaluated on six concentration levels in the LOQ–150 µg/l range, performing two replicated measurements for each level. Lack-of-fit and Mandel's fitting test were performed to check the goodness of fit

and linearity. The significance of the intercept (significance level 5%) was established by running a Student *t*-test.

Precision in terms of both within-run and between-run precision was calculated in terms of RSD% on three concentration levels (LOQ, 3 and 70 µg/l), performing five replicates at each level. Between-run precision was estimated over three days testing for homoscedasticity among the data and performing the analysis of variance (ANOVA) at the confidence level of 95%. Accuracy was calculated in terms of recovery rate (RR%) as follows:

$R.R.\% = c_1/c_2\ 100$

where c_1 is the measured concentration and c_2 is the concentration calculated from the quantity spiked into the sample. Three different concentration levels (LOQ, 3 and 70 µg/l) with five replicated measurements were analyzed.

Method selectivity was assessed by testing for interference 10 blank aqueous humor samples. Finally, stability was evaluated in terms of both long-term and bench-top storage, and processed sample stability. Three replicates at the LOQ and at 70 µg/l were always performed.

3.3 Results and Discussion

The aim of the present research study was to develop an analytical method for the detection of dexamethasone and dexamethasone sodium phosphate in aqueous humor. This steroid is one of the most prescribed drug worldwide for uveitis clinical treatment. Topical administration of ophthalmic solutions is preferred, since less side-effect are present, but several studies proved that the amount of dexamethasone in aqueous humor is far lower compared to therapeutic concentration required. Thus the need of developing a fast and high-throughput analysis for clinical evaluation of dexamethasone administration in patients affected by uveitis.

3.3.1 LC-MS² chromatographic conditions

Preliminary assays based on literature [31] were performed in order to achieve optimal chromatographic performances by testing different LC columns and mobile phase conditions, tuning the ESI parameters and selecting the MRM transition of the target analytes.

To achieve optimized chromatographic resolution, peak sharpness and signal intensity, two reversed phase HPLC columns, having a C_{18} stationary phase, namely KINETEX (100 mm x 2.1 mm, 2.6 µm, 100 Å, Phenomenex®) and GEMINI (100 mm x 2.0 mm, 3 µm 110 Å, Phenomenex®) were tested. Both proved to be suitable for the elution of the DEX and DEX-SP in short LC runs. GEMINI HPLC column was preferred, being characterized by sharper peaks and a decrease in the backpressure.

Optimization of the mobile phase flow was achieved by performing analyses in the 200-300 µl/min range, thus allowing to select the best compromise between the analysis times and the backpressures (250 µl/min). The optimization of the mobile phase composition allowed the detection of both DEX and DEX-SP in a short time (7 min).

The analysis of standard solutions of both DEX and DEX-SP in flow injection mode allowed to optimize the ESI ion source tuning parameters and select the MRM transitions.

MRM detection was performed in order to increase the sensibility of the analysis, thus obtaining very low LODs and LOQs. Since ESI is a soft ionization, the molecular protonated ion was the most intense, thus it was

selected as parent ion. Four collision energies were tested, i.e. 20, 25, 30, 35 V in order to magnify the most abundant transition maintaining two transitions for confirmatory purposes. The best compromise between fragmentation and sensibility was obtained by operating at 30 V.

The monitored transitions are reported in **Table 3.1.**

Table 3.1: MRM transitions. The ion used for quantitation are highlighted

DEX					
Parent ion					
		393	$[M+H]^+$		
Product ion					
373	$[M+F]^+$	355	$[M+H-HF- H_2O]^+$	337	$[M+H-HF- 2H_2O]^+$
DEX-SP					
Parent ion					
		517	$[M+H]^+$		
Product ion					
499	$[M+H-H_2O]^+$	479	$[M+H-HF- H_2O]^+$	395	$[M+H-HF- NaPO_3]^+$

3.3.2 MEPS extraction optimization

As reported in **paragraph 3.1.2,** several techniques have been applied for the extraction of DEX and DEX-SP from biological samples. The collection of humor aqueous during surgery treatment of cataracts allows to obtain only small sample volumes (at least 50 µL), thus MEPS was chosen as extraction technique.

In order to obtain a high repeatability, the extractions were performed by using a semi-automatic commercially available eVol device. This tool allowed not only a better control of the loading volumes, but also an accurate control of the fill/injection speed.

Preliminary investigations were performed by using different MEPS sorbent, namely C_2, C_8 and C_{18} BINs, in order to maximize the extraction yield (**Figure 3.6**).

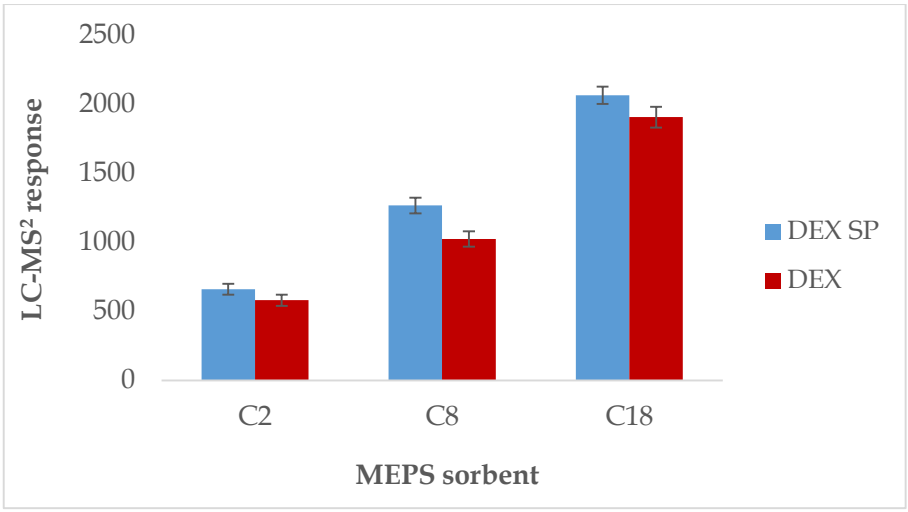

Figure 3.6 MEPS sorbent selection (n=3).

In accordance with a study performed by Anizan et al. [58], C_{18} sorbent material was characterized by the highest extraction yields. The optimization of the eluting solvent was also optimized: acetonitrile (ACN), methanol (MeOH), and a mixture 1:1 of methanol and ethyl acetate (MeOH : EtAc), were tested (**Figure 3.7**).

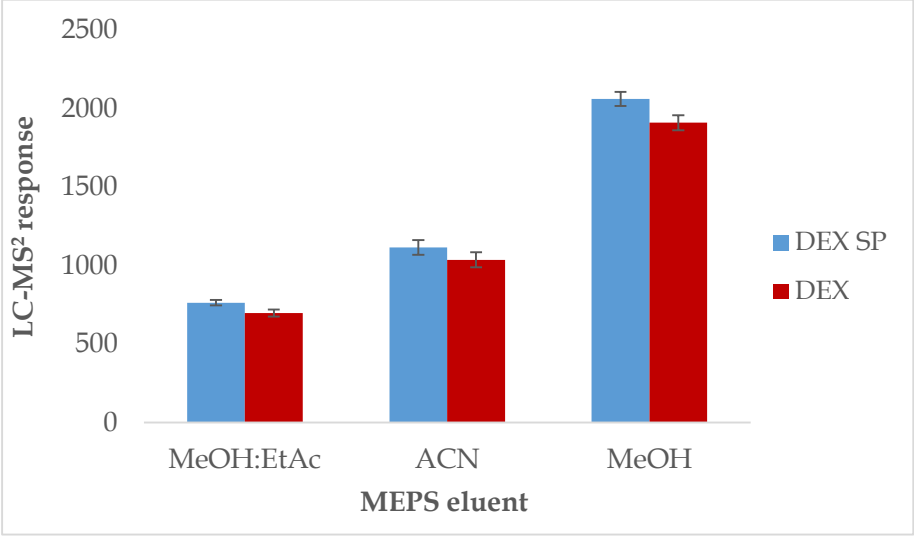

Figure 3.7 MEPS eluting solvent selection (n=3).

Pure MeOH proved a higher elution capability compared to the other solvents for both DEX and DEX-SP. The performed tests demonstrated that a fill/injection speed of 1 a.u. was the optimum for both sampling and eluting, since the viscosity of the matrix led to volume mismatched due to bubbles formations when higher flows were used.

In order to investigate the effects of both loading and eluting cycles and optimize the MEPS extraction, full factorial design (FFD) was performed.

Compared to the OVAT (one-variable-at-the-time) method, FFD is an exhaustive approach of the experimental design that allows to vary the levels of all factors at the same time instead of one at a time, thus considering each possible interaction occurring between the factors. It requires to measure responses at all combinations of the factor levels.

The experimental domain (the domain determining the factor levels) was defined taking into account that a minimum number of loading cycles (n=5) has to be performed in order to promote the interactions among the analytes and the sorbent material. Again, the minimum of cycles required for analyte elution was set to 5, thus ensuring high extraction rates for both DEX and DEX-SP from the MEPS BIN. As for the top level, it has to be considered that as the number of cycles increases, the extraction time get longer, thus a maximum of 25 cycles was considered for both sampling and eluting step.

Repeatability of measurements was assessed by performing 4 replicates at the center of the experimental domain.

Since FFD considers only linear responses of the factors in the domain, the presence of curvature in the response surface has to be tested for both the analytes by using a central composite design (CCD): CCD contains an imbedded factorial design with center point and additional *star points* experiments that allow the estimation of curvature (**Figure 3.8**).

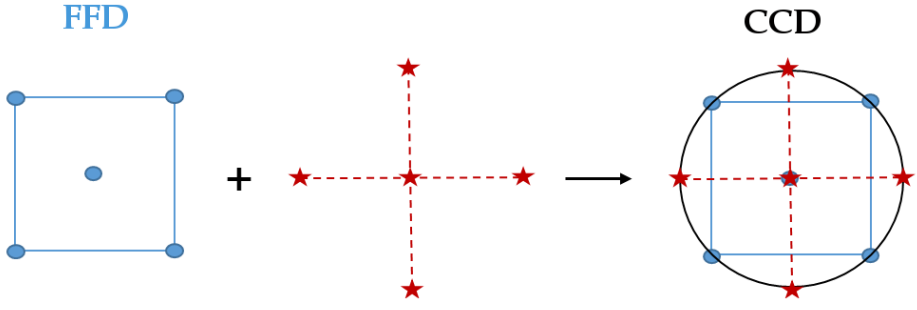

Figure 3.8: CCD design obtained by FFD (blue) and star points (red)

In order to find the optimal experimental conditions, the desirability function approach was applied.

This method is based on the idea that the quality of a process that has many features is completely unacceptable if one of them is outside of a *desirable* limit. The aims of the desirability function are: i) calculate the operating conditions (factor levels) that ensure compliance with the criteria of all the involved responses; ii) provide the best compromising conditions in the desirable joint response [66]. Derringer's desirability function [67] allows to convert the multiple responses into a single one, combining the individual responses into a composite function, that has to be optimized.

In a first step, an individual desirability function d_i ($\hat{y}_i$) for each response $\hat{y}_i(k)$ is attributed by the analyst. Desirability values are assigned between 0 and 1, where $d_i(\hat{y}_i)=0$ is an undesirable response, and $d_i(\hat{y}_i)=1$ represents the ideal response.

Different models (linear, stepwise, logarithmic, exponential, sigmoid…) can be used, depending on the optimization criteria adopted, within an acceptable range of response, between an upper and a lower acceptable value.

Once all the factors and responses are transformed in single desirability functions, they are combined in a unique function named *global desirability* (D) in order to obtain the best joint responses using the following equation:

$$D = (d_1^{r_1} x\ d_2^{r_2} x \ldots\ldots x\ d_n^{r_n})^{\frac{1}{\sum r_i}} = \left(\prod_{i=1}^{n} d_i^{ri} \right)^{\frac{1}{\sum r_i}}$$

where r_i is the importance of each variable relative to the others.

D is formulated in order to provide very quick and reliable results:

- if one of the responses (j) is more important than others, $r_j>1$, thus increasing its weight in the global desirability;
- if one of the responses is completely undesirable, $d_i(\hat{y}_i)=0$ ➔ D=0;
- If D≠0 ➔ all the variables which are being simultaneously optimized can be considered to have a desirable value.

The optimization procedure implies to maximize D in order to obtain the best values for all the single desirabilities $d_i(\hat{y}_i)$, thus predicting the values that the different responses can assume at the optimal factors combination by using the fitted models.

The optimal experimental conditions for the MEPS extraction were obtained in correspondence to a number of loading cycles = 19, with a global desirability D = 0.90 and very good single desirability values. Thus, the developed procedure proved to be suitable for the simultaneous extraction of DEX and DEX-SP. As for the eluting cycles, taking into account that samples containing higher amounts of corticosteroids compared those used in the CCD could be analyzed, a number of cycles n = 10 was chosen in order to ensure the complete elution of the analytes.

The model obtained for both DEX and DEX-SP, R^2 fitting parameter (used to assess the fitting between the model and the experimental data), and single desirability values are reported in **Table 3.2**.

Table 3.2 Regression coefficients and single desirability of the polynomial functions calculated using the forward method (± standard error)

Analyte	**CCD model**	**R^2**	**d**
DEX	$y = 4500\ (\pm100) + 800\ (\pm100)\ x_1 - 1200\ (\pm200)\ x_1^2$	0.89	0.92
DEX-SP	$y = 2990\ (\pm90) + 420\ (\pm90)\ x_1 - 730\ (\pm130)\ x_1^2$	0.87	0.89

The optimization of the MEPS procedure allowed to obtain extraction yields higher than 85% and excellent selectivity toward DEX and DEX-SP.

3.3.3 Method Validation

The method was validated following the guidelines for the validation of bioanalytical methods [65].

The obtained parameters are reported in **Table 3.3**.

Table 3.3 Validation parameters of the MEPS-LC-MS^2 method

Analyte	**LOQ** (µg/l)			**Linearity Range** (µg/l)		
DEX	0.5			LOQ-150		
DEX-SP	0.7			LOQ-150		
Precision						
	Within run (RSD%)			Between run (RSD%)		
	Level 1 LOQ	Level 2 3µg/l	Level 3 70µg/l	Level 1 LOQ	Level 2 3µg/l	Level 3 70µg/l
DEX	12	10	6	14	12	5
DEX-SP	13	8	4	16	13	6
Accuracy (RR%, n=5)						
	Level 1 LOQ		Level 2 3µg/l		Level 3 70µg/l	
DEX	105±10		95±5		97±3	
DEX-SP	119±25		91±6		99±4	

The obtained LOQ values, 0.5 and 0.7 µg/l for DEX and DEX-SP respectively, demonstrated the suitability of the developed MEPS-LC-MS^2 method to quantify the analytes at trace levels.

The method proved to be selective, since no interference from exogenous or other endogenous compounds were observed.

By applying Mandel's fitting test, a good linearity was proven for more than two order of magnitude, in LOQ-150 µg/l range.

The accuracy of the method was demonstrated in terms of recovery rate in the 91(±6)–119(±25)% (n=5) range, whereas extraction yields higher than 85% were always obtained.

Satisfactory precision was observed both in terms of within-run and between-run precision with RSD always lower than 16% also at the LOQ levels, thus meeting the guidance criteria[76].

No problems related to the long-term stability of the stock solutions were observed: in fact, ANOVA performed on data obtained by the analysis of standard solutions daily prepared from the stock solutions did not show any significant differences ($p > 0.05$) up to 7 months, provided that the stock solutions were stored at −20°C. Bench-top stability was evaluated by the analysis of standard solutions maintained at room temperature up to 12 h at three concentration levels: student *t*-test, showed no significant differences ($p > 0.05$) between the mean responses. It was not possible to assess the freeze and thaw stability since the low sample volumes were not enough in order to perform freeze and thaw cycles. Finally, no significant differences between the responses obtained from the same samples analyzed just after the MEPS extraction and after 10 h were present, thus proving the processed sample stability. Being the developed method characterized by a short LC run (7 min), 10 hours was considered the longest period until completion of the analysis.

3.3.4 *Real Sample Analysis*

The analysis of aqueous humor samples from patients with a history of uveitis requiring cataract surgery was performed by the developed MEPS-LC-MS^2 method. Neither DEX nor DEX-SP were detected in samples from group A and B, respectively. The obtained results were explained by considering the time elapsed from the drop instillation: even thought a previous study reported that DEX could be detected up to 12 h after instillation [28], several research publications demonstrated a drastic decrease in the concentration of the analytes in a very short time after the administration [23,27,58,68, 69].

The obtained data reinforce the evidence regarding the short half-life of both DEX and DEX-SP in aqueous humor and the lack of reliability of corticosteroids topical administration *via* eye droplets in patients affected by uveitis.

As previously mentioned, research is showing a great interest in newly developed ophthalmic drug carriers for topical administration, as the use of cyclodextrin-poloxamer aggregates. The developed method could be used to assess the suitability of these new drug administrations to reach the active intraocular concentrations of DEX and DEX-SP.

3.4 Conclusions

A rapid and reliable MEPS-LC–MS^2 method for the determination of dexamethasone disodium phosphate and dexamethasone in humor aqueous was developed and validated. The use of MEPS extraction was of paramount importance due to the low sample volumes available.

Experimental design and desirability functions approach allowed the optimization of the MEPS procedure, reaching extraction yield up to 85% and an excellent selectivity toward the extraction of the target analytes, since no interfering compound was present.

The method is suitable for the simultaneous determination of both DEX and DEX-SP at trace levels. Therefore, the proposed method has to be considered as a valuable tool for clinical studies in order to assess reliability of dexamethasone administration in patients affected by uveitis.

3.5 Acknowledgments

Thanks to Dr. M. Mattarrozzi and Prof. M. Careri from the department of SCVSA, UNIPR for the HPLC-MS analyses. Thanks to Dr. P. Mora and Prof. S.A. Gandolfi from the Department of Medicine and Surgery, UNIPR.

3.6 References

[1] F.A. Jakobiec, *Ocular anatomy, embryology and teratology*, Harper & Row, Philadelphia, USA, 1982.

[2] E. Miserocchi, G. Fogliato, G. Modorati, F. Bandello, *Review on the world wide epidemiology of uveitis*, Eur. J. Ophthalmol., 23 (2013) 705–717.

[3] R.N. Van Gelder, T.K. Leveque, *Cataract surgery in the setting of uveitis*, Curr. Opin. Ophthalmol., 20 (2009) 42–45.

[4] M. Jancevski, C.S. Foster, *Cataract and uveitis*, Curr. Opin. Ophthalmol., 21 (2010) 10–14.

[5] E.H. Steffensen Corticotropin, cortisone, and hydrocortisone in treatment of ocular disease, JAMA 150 (1952) 1660–1664.

[6] M. Raizman, *Corticosteroid therapy of eye disease. Fifty years later*, Arch. Ophthalmol., 114 (1996) 1000–1001.

[7] E.T. Cunningham, J.D. Wender, *Practical approach to the use of corticosteroids in patients with uveitis*, Can. J. Ophthalmol., 45 (2010) 352-358.

[8] G.J. Jaffe, D. Martin, D. Callanan, P.A. Pearson, B. Levy, T. Comstock, *Fluocinolone acetonide implant (Retisert) for noninfectious posterior uveitis: thirty-four-week results of a multicenter randomized clinical study,* Ophthalmology, 113 (2006) 1020-1027.

[9] M. Taban, C.Y. Lowder, P.K. Kaiser, *Outcome of fluocinolone acetonide implant (Retisert) reimplantation for chronic noninfectious posterior uveitis*, Retina, 28 (2008) 1280-1288.

[10] K G. Falavarjani, Q.D. Nguyen, *Adverse events and complications associated with intravitreal injection of anti-VEGF agents: a review of literature*, Eye, 27 (2013) 787–794.

[11] K.M. Sampat, S.J. Garg, *Complications of intravitreal injections*, Curr. Opin. Ophthalmol. 21 (2010) 178-183.

[12] J.W. Shell, *Ophthalmic drug delivery systems. Survey of ophthalmology*, 29 (1984) 117–128.

[13] K. Lee, A. Park, S. Jang, Y.R. Chung, *Elevation of intraocular pressure after inadvertent dexamethasone implant injection into the lens*, Can. J. Ophthalmol., 51(2016) 103–105.

[14] T.L. Comstock, H. H. DeCory, *Advances in Corticosteroid Therapy for Ocular Inflammation: Loteprednol Etabonate*, Int. J. Infl., 2012, article 789623, doi:10.1155/2012/789623.

[15] K. Hosoya, M. Tachikawa, *Inner blood-retinal barrier transporters: role of retinal drug delivery*, Pharm. Res., 26 (2009) 2055-65.

[16] S. R. Chennamaneni, C. Mamalis, B. Archer, Z. Oakey, B. K. Ambati, *Development of a novel bioerodible dexamethasone implant for uveitis and postoperative cataract inflammation*, J. Control. Release, 167 (2013) 53-59.

[17] Allergan Inc. *Allergan receives FDA approval for Ozurdex® as treatment option for noninfectious uveitis affecting the posterior segment of the eye*, 2010.
http://agn.client.shareholder.com/releasedetail.cfm?ReleaseID=511060

[18] Bausch & Lomb. Vitrasert® (ganciclovir intravitreal implant) 4.5 mg.
http://www.bausch.co.nz/en_US/ecp/pharma/product/vitrasert.aspx

[19] D.G. Callanan, G.J. Jaffe, D.F. Martin, P.A. Pearson, T.L. Comstock, *Treatment of posterior uveitis with a fluocinolone acetonide implant: three-year clinical trial results*, Arch. ophthalmol., 126 (2008) 1191–1201.

[20] J. Rodríguez Villanueva, I. Bravo-Osuna, R. Herrero-Vanrell, I.T. Molina Martínez, M. Guzmán Navarro, *Optimising the controlled release of dexamethasone from a new generation of PLGA-based microspheres intended for intravitreal administration*, Eur. J. Pharm. Sci., 92 (2016) 287–297.

[21] Q. Pan, Q. Xu, N.J. Boylan, N.W. Lamb, D.G. Emmert, J.C. Yang, L. Tang, T. Heflin, S. Alwadani, C.G. Eberhart, W.J. Stark, J. Hanes, *Corticosteroid-loaded biodegradable nanoparticles for prevention of corneal allograft rejection in rats*, J. Control. Release 201 (2015) 32–40.

[22] A. Thakur, R.S. Kadam, U.B. Kompella, *Influence of Drug Solubility and Lipophilicity on Transscleral Retinal Delivery of Six Corticosteroids*, Drug Metab. Dispos., 39 (2011) 771-781.

[23] C. Cagini, F. Cometa, G. Torroni, A. Pellegrino, R. Pellegrino, G.M. Cavallini, *Dexamethasone disodium phosphate penetration into the human aqueous humor after topical application*, Curr. Eye Res., 41 (2016) 897–899.

[24] P. Rohdenwald, H. Mollmann, J. Barth, J. Rehder, H. Derendorf, *Pharmacokinetics of dexamethasone and its phosphate ester*, Biopharm. Drug Dispos., 8 (1987) 205–212.

[25] E. Barcia, R. Herrero-Vanrell, A. Dìez, C. Alvarez-Santiago, I. Lòpez, M. Calonge, *Downregulation of endotoxin-induced uveitis by intravitreal injection of polylactic-glycolic acid (PLGA) microspheres loaded with dexamethasone*, Exp. Eye Res., 89 (2009) 238–245.

[26] J.R. Villanueva, L.R. Villanueva, M.G. Navarro, *Pharmaceutical technology can turn a traditional drug, dexamethasone into a first-line ocular medicine. A global perspective and future trends*, Int. J. Pharm., 516 (2017) 342–351.

[27] C.N. McGhee, *Pharmacokinetics of ophthalmic corticosteroids*, Br. J. Ophthalmol., 76 (1992) 681–684.

[28] D. Watson, M.J. Noble, G.N. Dutton, J.M. Midgley, T.M. Healey, *Penetration of topically applied dexamethasone alcohol into human aqueous humor*, Arch. Ophthalmol., 106 (1988) 686–687.

[29] J. Aufartova, C. Mahugo-Santana, Z. Sosa-Ferrera, J.J. Santana-Rodriguez, L. Novakova, P. Solich, *Determination of steroid hormones in biological and*

environmental samples using green microextraction techniques: an overview, Anal. Chim. Acta, 704 (2011) 33–46.

[30] L. Li, P. Ma, J. Wei, K. Qian, L. Tao, *LC-ESI–MS method for the determination of dexamethasone acetate in skin of nude mouse*, J. Chromatogr. B, 933 (2013) 44–49.

[31] M. Zhang, G.A. Moore, B.P. Jensen, E.J. Begg, P.A. *Bird, Determination of dexamethasone and dexamethasone sodium phosphate in human plasma and cochlear perilymph by liquid chromatography/tandem mass spectrometry*, J. Chromatogr. B, 879 (2011) 17–24.

[32] C. Shu, T. Zeng, S. Gao, T. Xia, L. Huang, F. Zhang, W. Chen, *LC-MS/MS method for simultaneous determination of thalidomide, lenalidomide, cyclophosphamide, bortezomib, dexamethasone and adriamycin in serum of multiple myeloma patients*, J. Chromatogr. B, 1028 (2016) 111–119.

[33] R. Earla, S.H.S. Boddu, K. Cholkar, S. Hariharan, J. Jwala, A.K. Mitra, *Development and validation of a fast and sensitive bioanalytical method for the quantitative determination of glucocorticoids – Quantitative measurement of dexamethasone in rabbit ocular matrices by liquid chromatography tandem mass spectrometry*, J. Pharm. Biomed., 52 (2010) 525–533.

[34] M.A. Saracino, C. Iacono, L. Somaini, G. Gerra, N. Ghedini, M.A. *Raggi, Multi-matrix assay of cortisol, cortisone and corticosterone using a combined MEPS-HPLC procedure*, J. Pharm. Biomed. Anal., 88 (2014) 643-648.

[35] Z.D. Jauković, S.D. Grujić, I.V. Matić Bujagić, M.D. Laušević, *Determination of sterols and steroid hormones in surface water and wastewater using liquid chromatography-atmospheric pressure chemical ionization-mass spectrometry*, Microchem. J., 135 (2017) 39-47.

[36] B.G. Keevil, *LC–MS/MS analysis of steroids in the clinical laboratory*, Clin. Biochem., 49 (2016) 989-997.

[37] Z. Zhang, H. Duan, L. Zhang, X. Chen, W. Liu, G. Chen, *Direct determination of anabolic steroids in pig urine by a new SPME–GC–MS method*, Talanta, 78 (2009) 1083-1089.

[38] K. Saito, K. Yagi, A. Ishizaki, H. Kataoka, *Determination of anabolic steroids in human urine by automated in-tube solid-phase microextraction coupled with liquid chromatography–mass spectrometry*, J. Pharmaceut. Biomed., 52 (2010) 727-733.

[39] L. Yang, T. Luan, C. Lan, *Solid-phase microextraction with on-fiber silylation for simultaneous determinations of endocrine disrupting chemicals and steroid*

hormones by gas chromatography-mass spectrometry, J. Chromatogr. A, 1104 (2006) 23-32.

[40] L. Qiu, W. Liu, M. Huang, L. Zhang, *Preparation and application of solid-phase microextraction fiber based on molecularly imprinted polymer for determination of anabolic steroids in complicated samples*, J. Chromatogr. A, 1217 (2010) 7461-7470.

[41] T. Jiang, L. Zhao, B. Chu, Q. Feng, W. Yan, J.M. Lin, *Molecularly imprinted solid-phase extraction for the selective determination of 17β-estradiol in fishery samples with high performance liquid chromatography*, Talanta, 78 (2009), 442-447.

[42] R. Eisert, J. Pawliszyn, *Automated In-Tube Solid-Phase Microextraction Coupled to High-Performance Liquid Chromatography*, Anal. Chem., 69 (1997) 3140-3147.

[43] Y. Wen, B.S. Zhou, Y. Xu, S.W. Jin, Y.Q. Feng, *Analysis of estrogens in environmental waters using polymer monolith in-polyether ether ketone tube solid-phase microextraction combined with high-performance liquid chromatography*, J. Chromatogr. A, 1133 (2006) 21-28.

[44] K. Saito, K. Yagi, A. Ishizaki, H. Kataoka, *Determination of anabolic steroids in human urine by automated in-tube solid-phase microextraction coupled with liquid chromatography-mass spectrometry*, J. Pharm. Biomed. Anal., 52 (2010) 727-733.

[45] N. Klinsunthorn, A. Petsom, T. Nhujak, *Determination of steroids adulterated in liquid herbal medicines using QuEChERS sample preparation and high-performance liquid chromatography*, J. Pharmaceut. Biomed., 55 (2011) 1175–1178.

[46] W. Pormsila, D. Jityongchai, W. Tesphon, *A Modified Quechers Extraction for the Determination of Dexametasone*, ESJ, 10 (2014) 138-144.

[47] C. Pouech, M. Tournier, N. Quignot, A. Kiss, L. Wiest, F. Lafay, M.M. Flament-Waton, E. Lemazurier, C. Cren-Olivé, *Multi-residue analysis of free and conjugated hormones and endocrine disruptors in rat testis by QuEChERS-based extraction and LC-MS/MS*, Anal. Bioanal. Chem., 402 (2012) 2777–2788.

[48] A.S.P. Boggs, T.B. Schock, L.H. Schwacke, T.M. Galligan, J.S. Morey, W.E. Mc Fee, J.R. Kucklick, *Rapid and reliable steroid hormone profiling in Tursiops truncatus blubber using liquid chromatography tandem mass spectrometry (LC-MS/MS)*, Anal. Bioanal. Chem., 409 (2017) 5019-5029.

[49] X. Tan, Z. Li, L. Deng, S. Zhao, M. Wang, *Analysis of 13 kinds of steroid hormones in raw milk using modified QuEChERS method combined with UPLC-QTOF-MS*, J. Integr. Agr., 15 (2016) 2163-2174.

[50] M. Abdel-Rehim, Z. Altun, L. Blomberg, *Microextraction in packed syringe(MEPS) for liquid and gas chromatographic application. Part I −determinationof local anesthetics in human plasma samples using gaschromatography-mass spectrometry*, J. Chromatogr. B, 801 (2004) 317–321.

[51] M. Abdel-Rehim, Z. Altun, L. Blomberg, *Microextraction in packed syringe(MEPS) for liquid and gas chromatographic application. Part II−determination of ropivacaine and its metabolites in human plasma samplesusing MEPS with liquid chromatography/tandem mass spectrometry*, J. Mass. Spectrom., 39 (2004) 1488–1493.

[52] https://www.researchgate.net/figure/262574135_fig3_Figure-2-Schematic-overview-of-the-micro-extraction-by-packed-sorbent-MEPS-syringe-and

[53] L. Yanga, R. Said, M. Abdel-Rehim, *Sorbent, device, matrix and application in microextraction by packedsorbent (MEPS): A review*, J. Chrom. B, 1043 (2017) 33–43.

[54] P.L. Kole, G. Venkatesh, J. Kotecha, R. Sheshala, *Recent advances in sample preparation techniques for effective bioanalytical methods*, Biomed. Chromatogr., 25 (2011) 199-217.

[55] G. Grueiro Noche, M.E. Fernández Laespad, J.L. Pérez Pavón, B. Moreno Cordero, S. Muniategui Lorenzo, *Microextraction by packed sorbent for the analysis of pharmaceutical residues in environmental water samples by in situ derivatization-programmed temperature vaporizer–gas chromatography–mass spectrometry*, J. Chromatogr. A, 1218 (2011) 9390-9396

[56] A. Prieto, S. Schrader, M. Moeder, *Determination of organic priority pollutants and emerging compounds in wastewater and snow samples using multiresidue protocols on the basis of microextraction by packed sorbents coupled to large volume injection gas chromatography–mass spectrometry analysis*, J. Chromatogr. A 1217 (2010) 6002-6011.

[57] M.A. Saracino, C. Iacono, L. Somaini, G. Gerra, N. Ghedini, M.A. Raggi, *Multi-matrix assay of cortisol, cortisone and corticosterone using a combined MEPS-HPLC procedure*, J. Pharmaceut. Biomed., 88 (2014) 643-648.

[58] S. Anizan, E. Bichon, F. Monteau, N. Cesbron, J.P. Antignac, B. Le Bizec, *A new reliable sample preparation for high throughput focused steroid profiling by gas chromatography–mass spectrometry*, J. Chromatogr. A, 1217 (2010) 6652-6660

[59] P. Mora, S. Gonzales, S. Ghirardini, P. Rubino, J.G. Orsoni, S.A. Gandolfi, F. Majo, Y. Guex-Crosier, *Perioperative prophylaxis to prevent recurrence following cataract surgery in uveitic patients: a two-centre, prospective, randomized trial*, Acta Ophthalmol., 94 (2016) 390–394.

[60] E.P. Box, W.G. Hunter, J.S. Hunter, *Statistics for Experimenters: An Introduction to Design, Data Analysis, and Model Building*, first ed., John Wiley & Sons, Hoboken, NJ, USA, 1978.

[61] A.I.J.A. Khuri Cornell, *Response Surfaces*, first ed., Marcel Dekker, New York, NY, USA, 1987.

[62] R. Carlson, *Design and Optimization in Organic Synthesis*, third ed., Elsevier, Amsterdam, Netherland, 1992.

[63] F. Bianchi, M. Careri, A. Mangia, M. Mattarozzi, M. Musci, *Experimental designfor the optimization of the extraction conditions of polycyclic aromatichydrocarbons in milk with a novel diethoxydiphenylsilane solid-phasemicroextraction fiber*, J. Chromatogr. A, 1196–1197 (2008) 41–45.

[64] M. Mattarozzi, M. Milioli, F. Bianchi, A. Cavazza, S. Pigozzi, A. Milandri, M.Careri, *Optimization of a rapid QuEChERS sample treatment method forHILIC-MS2analysis of paralytic shellfish poisoning (PSP) toxins in mussels*, Food Control., 60 (2016) 138–145.

[65] Guidance for Industry, Bioanalytical Method Validation, US Department of Health and Human Services, Food and Drug Administration, 2001, 2017, https://www.fda.gov/downloads/Drugs/Guidances/ucm368107.pdf

[66] R.H. Myers, D.C. Montgomery, *Response Surface Methodology: Process and Product Optimization Using Designed Experiments,* Wiley Series in Probability and Statistics), Wiley, New York, NY, USA, 2009.

[67] G. Derringer, R.Suich, *Simultaneous Optimization of Several Response Variables*, J. Qual. Technol., 12 (1980) 214–219.

[68] K. Araki-Sasaki, O. Katsuta, H. Mano, T. Nagano, M. Nakamura, *The effects of oral and topical corticosteroid in rabbit corneas*, BMC Ophthalmol., 16 (2016) 160–166.

[69] X. Huang, S. Liu, Y. Yang, Y. Duan, D. Lin, *Controllable continuous subtenon drug delivery of dexamethasone disodium phosphate to ocular posterior segment in rabbit*, Drug. Deliv., 24 (2017) 452–458.

Chapter 4

Sol-gel Coated Ion Sources for Direct Electron Ionization – Liquid Chromatography Coupling

The research study presented in this chapter has been published in Analytica Chimica Acta: N. Riboni, L. Magrini, F. Bianchi, M. Careri, A. Cappiello, *Sol-gel coated ion sources for liquid chromatography-direct electron ionization mass spectrometry*, Anal. Chim. Acta, 978 (2017) 35-41.

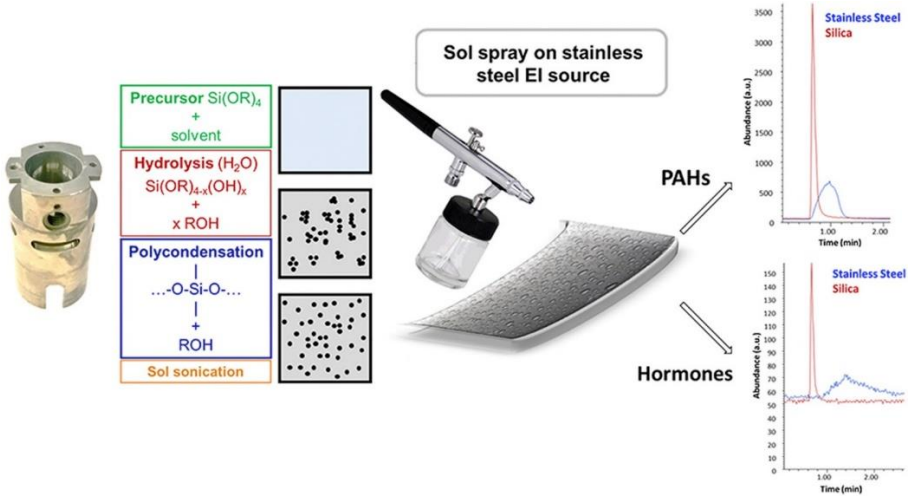

4.1 Introduction

4.1.1 Mass Spectrometry

Mass spectrometry is a powerful analytical tool for both quantitative and qualitative applications. It is used in chemistry and biology to determine the structure of unknown compounds [1], for proteomic applications [2-3] and DNA characterization [4]. In analytical chemistry is one of the most used techniques in order to detect pollutants and contaminants at low concentration levels. Sophisticated and sensitive MS instruments are hyphenated with separation techniques such as gas and liquid chromatography or capillary electrophoresis (CE) in order to analyze complex matrices.

During the past 40 years several MS ionization sources have been developed, starting from Electron Ionization (EI), moving to Electrospray (ESI) and Matrix-Assisted Laser Desorption/Ionization (MALDI) [5], and from Desorption Electrospray Ionization (DESI) [6] to Direct Analysis in Real Time (DART) [7].

In all the cases, the key process in a MS instrumentation is the ionization: the analytes have to be converted into charged ions by i) subtracting or adding electrons (forming a radical ion ($M^{\bullet\pm}$), ii) with the subtraction or addition of protons, generating either positive $(M+H)^+$ or negative $(M-H)^-$ ions, iii) forming adducts $(M+X)^\pm$, or iv) transferring charged species. Depending on both the chemical and physical properties and the stability of the targeted molecule and of the obtained ion, different form or amount of energy have to be applied.

Soft ionization techniques require the use of low energy in order to generate preferentially the molecular ion, thus preserving the structure of the analyte. These techniques are particularly suitable for the analysis of large or polar molecules and require additional stages of fragmentation for structure characterization. On the other side, hard ionization involves more energetic transitions, in order to promote fragmentation, required for qualitative analysis and enhanced structure elucidation.

Ionization can be performed in gas, liquid, or solid phases. EI ionization is applied in the gas phase, thus its use is devoted to compounds characterized by high volatility and thermal stability. By contrast, ESI ionization occurs in

liquid phase through low-energy chemical processes: ions are formed by solvents removal and electrostatic expulsion. MALDI ionization occurs via laser ablation of analytes in a solid matrix or nonvolatile liquid phase.

4.1.2 *Electron Ionization*

Electron Ionization (EI) was the first ionization method applied in MS, developed by Dempster in 1918 [8]. This kind of ionization occurs in the gas phase, through the interactions between the analytes and high-energy electrons. The energy surplus, not directly involved in the ionization process, is responsible for extensive fragmentation of the molecules, thus usually the molecular ion is either not present or characterized by low intensity.

Electrons are emitted *via* thermionic emission by heating a wire filament under high-vacuum conditions, then they are accelerated by an electric field toward the anode, reaching a kinetic energy of 70 eV. The analytes are introduced in the ion source as neutral molecules with a perpendicular orientation respect to the electron beam (**Figure 4.1**). The electron moving close to a gas-phase molecule in a low pressure (10^{-5}-10^{-6} torr) environment, causes distortion and fluctuation in the electric field around the neutral molecules and induces ionization (generation of a positive radical ion, $M^{\bullet +}$). 70 eV electrons energy not only generates the molecular ion but also is enough to induce covalent bond dissociation, thus producing fragments known as second-generation product ions. The obtained cations are then directed towards the mass analyzer by a repeller electrode.

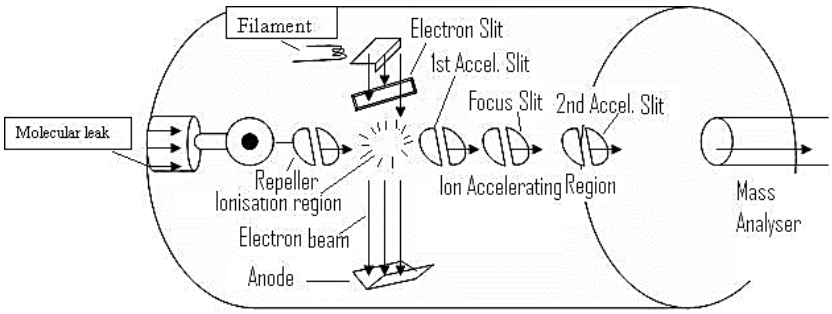

Figure 4.1 Scheme of an EI ion source

The probability of a successful ionization event increases with electron energy up to 70 eV. Over this value, the impact section of the ionization process starts

retreating, and electron–molecule interactions become weaker and unproductive. The number of ions produced is directly proportional to the analyte pressure in the ion source (related to the analyte concentration in the injected sample), thus allowing quantitative measurements.

Recombination and adducts generation is impossible because of the lack of inter-molecular interaction during the ionization, so this process depends only on the structure and energy content within the isolated molecule. EI spectra are the result of intramolecular reactions and are not influenced by matrix effect. The main advantage of this ion source is the fragmentation pattern, highly reproducible, characteristic of each analyte and, as already stated, not affected by matrix effect: a direct comparison between the obtained mass spectra and libraries containing thousands of reference is possible, thus allowing qualitative analysis of unknown compounds.

4.1.3 *Liquid Chromatography - Mass spectrometry*

In the last few decades, many efforts have been devoted to develop new interfaces for LC-MS, overcoming the apparent incompatibility between liquid chromatography and mass spectrometry. Some important features have to be considered:

- Solvent restriction: the mobile phase is made by different components and additive. Moreover, an eluent gradient can be applied in order to perform an exhaustive separation of the analytes. Separation and ionization of analytes often depend on antagonist mobile-phase components.
- LC involves high-pressure liquid phase, whereas the MS analyzer operates only under high-vacuum conditions, thus requiring that only small amounts of solvent could enter in the mass spectrometer.
- Sample restriction: analytes may vary dramatically in weight, polarity and stability, thus leading to a huge variability in terms of response and system requirements on both interface and mass spectrometer.

The development of soft ionization techniques moved liquid chromatography closer to mass spectrometry, thus allowing the improvement of powerful instrumentations for new and more challenging analytical applications. Atmospheric pressure ionization (API) interfaces have been successfully

coupled with LC. The main advantage of these ion sources is their possibility to handle a broad range of different substances.

In an ESI source (**Figure 4.2**), the ionization of the sample is obtained at atmospheric pressure in the liquid phase: the eluent is nebulized by a capillary needle, acting as inlet into the apparatus. The stainless steel needle is surrounded by an electrode that retains a steady voltage (± 2-5 kV), charging the solvent droplets. Desolvation is performed through the use of a nitrogen flow and the possible heating, thus reducing the droplet size: the increment in electric field density induces an increase in surface tension, until a breakdown limit, known as the *Rayleigh limit*. Once this limit has been passed, the droplet divides into smaller units of either positive or negative charge, depending on the applied voltage. This process is referred to as either coulombic explosion or *Taylor Cone*. The process continues until the molecular ions have reached the entrance of the mass analyzer.

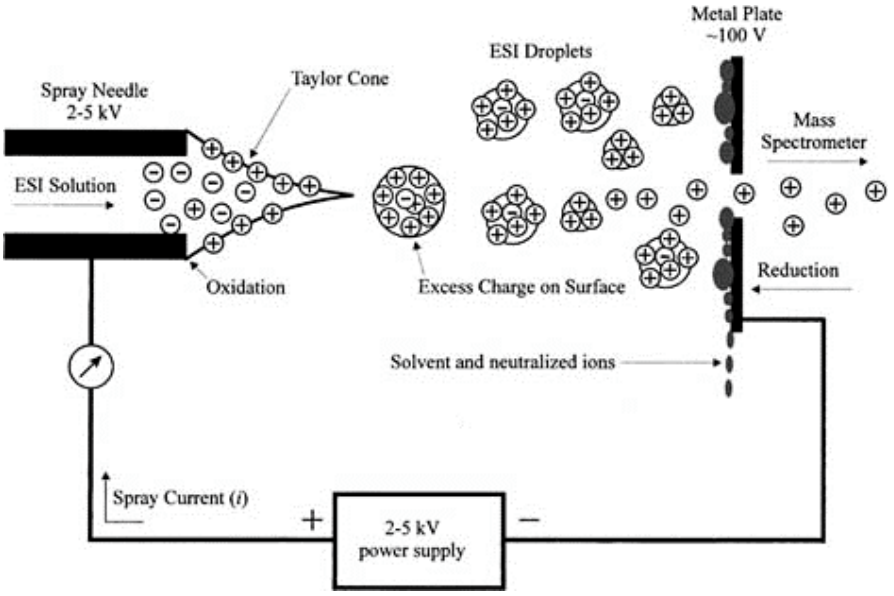

Figure 4.2 Scheme of an ESI ion source

This ionization process is considered soft in terms of energy: normally, little or no fragmentation is observed. Both positive and negative-ion spectra can be obtained. Moreover, multi-charged ions can be formed, therefore an ESI spectrum can be characterized by ions carrying multiple charges, thus

reducing their mass-to-charge ratio compared to the respective mono-charged species.

Several restrictions are present:

1. Polarity is a key factor in order to obtain a satisfactory response: API interfaces often rely on simple acidic or basic chemical processes to ionize the analytes in the liquid phase, thus requiring the use of polar eluent or additives.
2. Variation in the mobile-phase composition has an enormous influence in the response of the analytes, leading to signal suppression or exaltation or nonlinear responses.
3. All the species involved in the process may compete during the ionization process, suppressing the signal of other chemical species (matrix effect).
4. The ideal conditions for sample ionization are often in conflict with the composition of the mobile phase chosen for optimizing the component separation. Post-column addition of suitable modifiers can be performed in order to improve ionization and enhance signal response. This greatly affects the analysis of unknown or complex samples, when ionization cannot be optimized for all the components.
5. Fragmentation is very limited and does not produce sufficient data for an accurate characterization, so tandem mass spectrometry of unknown compounds for structure elucidation has to be performed. However, it is difficult to create MS^n reference electronic libraries, because the processes involved in the collision-induced dissociation are influenced by unpredictable and hard-to-replicate events.
6. Common buffers such as phosphate, borate and tris(hydroxymethyl)aminomethane cannot be used: even at trace levels they could interfere with the ESI process. Only volatile buffers such as ammonium acetate are feasible for the ESI ionization. Moreover, excess of cations like Na^+, K^+, and detergents, such as PEG, often suppress the ESI signals.

On the other hand, API techniques are excellent for the analysis of compounds in a wide molecular weights range. Moreover, the possibility of achieving extremely high sensitivity, in the low-picogram range, paved the way to the development of proteomics, metabolomics, doping, environmental and food analyses.

4.1.4 HPLC-MS Coupling with Electron Ionization

The major advantage of EI mass spectra relies on their reproducibility and the high fragmentation pattern. These spectra are highly informative, thus allowing structure elucidation and the analysis of unknown compounds by the comparison of the experimental spectra with those collected in electronic libraries (such as the NIST library [9]). Moreover, a deconvolution of unresolved chromatographic peaks can be performed by using proper algorithms (i.e. AMDIS [10]).

EI ionization conditions (gas phase, high temperature, low pressure) are particularly suitable for gas chromatographic coupling, but the presence of high amount of solvent is critical. Being the operating conditions of LC and EI, very different, in developing new interfaces, a compromise between the different reciprocal requirements has to be found.

The first on-line combination of LC and EI, called the *moving belt interface*, was performed more than 40 years ago: the typical flow rate of HPLC columns was too high for full introduction of the liquid phase into the MS ion source (0.3-1.0 ml/min), thus requiring to eliminate the majority of the eluate. This interface was based on a rotating system able to both evaporate the solvents and transport the solute into the high-vacuum region for vaporization [11] (**Figure 4.3**).

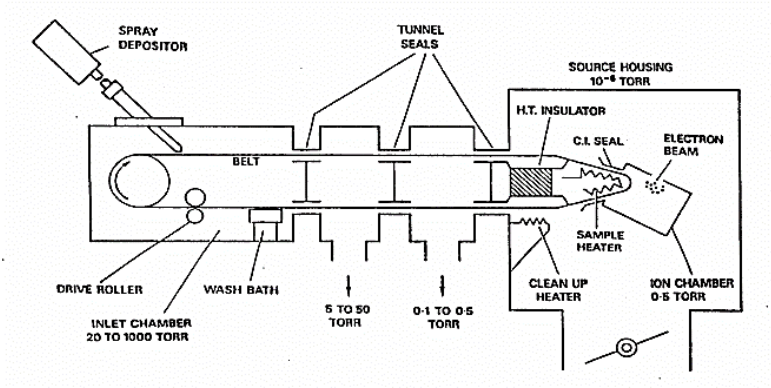

Figure 3.3 Scheme of moving belt interface

Many drawbacks were observed, so it was replaced by the particle beam interface (PB) (**Figure 4.4**). The operating conditions of PB rely on the formation of an aerosol, followed by a rapid heating, thus allowing the evaporation and elimination of the solvent vapors. Instead of free charged

droplets, PB aerosol evaporation creates a beam of solute particles (particle beam) that can be vaporized and ionized in the EI ion source.

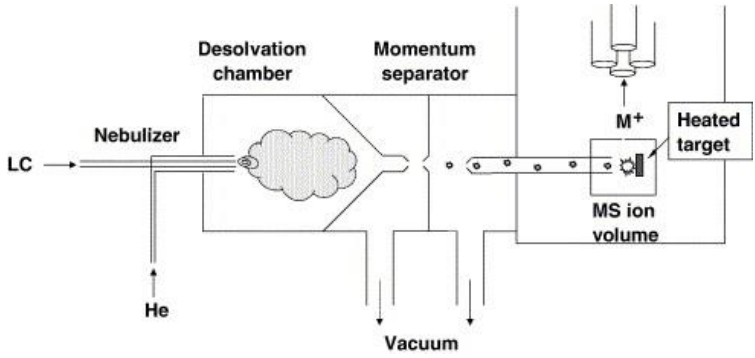

Figure 4.4 Scheme of a Particle Beam interface

The PB was designed for high-flow-rate HPLC columns and small particles were rarely obtained. In addition, when water was present in the mobile phase, many wet solute particles were lost by contact with the interface walls, leading to several drawbacks, in particular in the reverse-phase mode, such as scarce sensitivity, signal instability, and limited linearity.

In the past 20 years several attempts were performed in order to develop new interfaces exploiting eluent-jet formation [13], chemical ionization (CI) [14] and supersonic molecular beams [15].

The reduction of the eluent flow rate to 1–5 µl/min in the interface is the focal point for the Cap-EI source, developed in 2000 by the research group of A. Cappiello [16]. This ion source was developed in collaboration with Waters and is based on a typical PB interface carrying a new nebulizer and a simplified hardware (**Figure 4.5**): since the amount of the solvent is drastically reduced, the interface can be simplified without altering the solute transport efficiency.

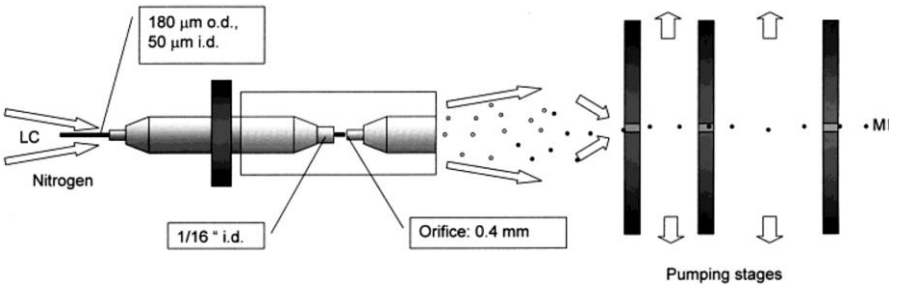

Figure 4.5 Scheme of a Cap-EI ion source [16]

The original PB interface was equipped with a pure pneumatic nebulizer (**Figure 4.6** left), in which the eluent from the LC column is forced to pass into a capillary surrounded by a helium flow: the liquid stream increases the linear velocity and breaks up into small aerosol droplets. Their size is related on both the composition of the mobile phase used in LC and the interface temperature. A mixture of solute particles, solvent vapors, and helium should pass through the nozzle at the end of the desolvation chamber.

In the Cap-EI the nebulization mechanism is based on a high-velocity gas jet coaxial with the liquid stream (**Figure 4.6** right). In this nebulizer, the gas passes through a ring-shaped passage, increasing its speed and promoting the formation of a very small and homogeneous aerosol. The new nebulizer is no longer influenced by the volatility of the solvents used in the mobile phase and operates at ambient temperature. In addition, the sensitivity is significantly improved compared to PB.

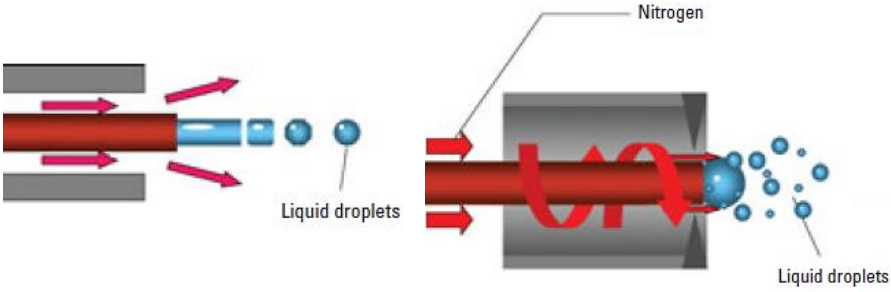

Figure 4.6 Scheme of a Cap-EI nebulizer

4.1.5 *Direct-EI ion source*

Recently, the development of new and reliable nanoscale LC columns (nanoLC) allowed to obtain excellent separation capabilities with reduced mobile phase flows (hundreds of nl/min). The great decrease of liquid amount used in LC boosted the research toward new, simpler and robust interfaces between LC and EI.

Cappiello et al. developed a new, simple interface call Direct-EI [17,18], characterized by only a minimal instrumentation adjustment with respect to the Cap-EI nebulizer: more precisely, the nanoLC eluent is driven directly into the EI source (**Figure 4.7**).

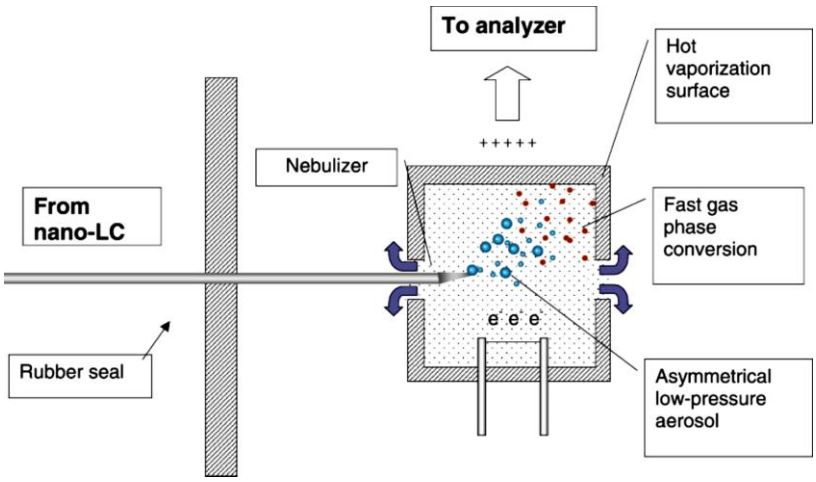

Figure 4.7 Scheme of a Direct-EI ion source [18]

By using this new nano-system is possible to squeeze all the interfacing processes into the small volume of the EI ion source chamber. The flow rate accepted by the interface has a maximum of 800 nl/min but the optimum range is 200-400 nl/min, depending on both the mobile phase and the analyzed sample. The lowest flow rate required for generating a fine and homogeneous aerosol is 100 nl/min [19].

By using this interface, the aerosol is generated inside the ion source in high-vacuum conditions at the high operation temperature typical of the EI ion source (250-350°C), thus resulting in an almost instantaneous droplet desolvation and solute vaporization prior to the ionization. The entire process takes place in the ion chamber and no modifications of the original EI ion source are required (**Figure 4.8**). The micronebulizer consists of a cone-shaped tip slightly bent sideways and an orifice of ~5 µm, protruding 1 mm into the ion source. An additional opening, opposite to the nebulizer tip, increases solvent vapor removal and avoids any ion–molecule reaction. Neither the electron path nor the electric fields are influenced by the interface presence into the ion chamber. The high temperature of the ion source has a double function in the ionization process: increases the solvent vaporization and converts the solute at the gas phase upon contact with the hot stainless steel surface (**Figure 4.9**). Once the particles reach the hot metal, the heat leads to their complete gas-phase conversion. However, if the heating process is not sufficiently fast, thermal decomposition of the most thermally sensitive analytes can occur.

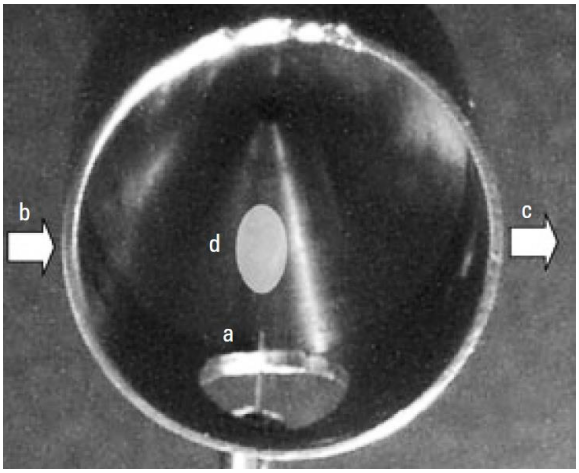

Figure 4.8 Picture of a Direct-EI ion source, a: nano-flow nebulizer, b→c: electron current, d: aerosol generation area [17]

The very small particles generated by the Direct-EI interface are characterized by an increased surface-to-mass ratio in order to promote their vaporization, thus reducing possible decomposition phenomena and increasing the number of possible detectable analytes. The source operative conditions have to be optimized during the method development and evaluated case by case.

Finally, the vaporized molecules are ionized by the electron beam of the EI source, and the generated ions are directed towards the mass analyzer by the repeller.

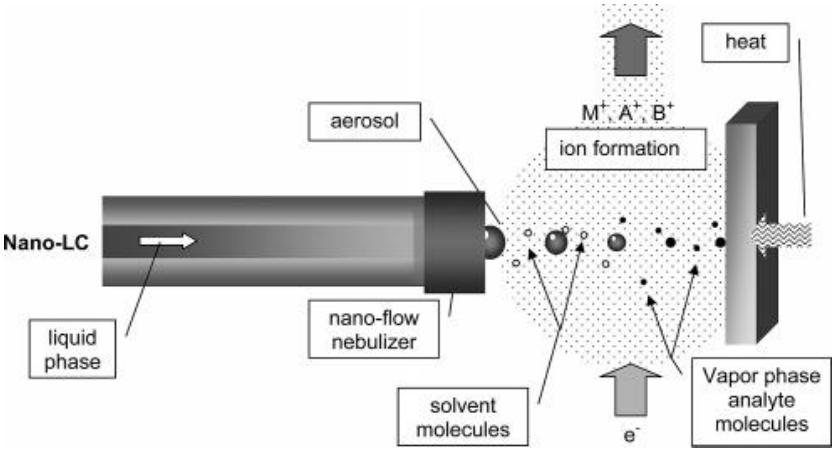

Figure 4.9 Scheme of the Direct-EI ionization process [20]

The interface between the LC and the EI is the nebulizer itself, connected to the analytical nano-LC-column by a 30-µm i.d. capillary tubing, kept insulated from the heated source in order to avoid premature mobile-phase vaporization, thus resulting in pressure-related problems and possible solute degradation.

The major advantages are the extreme compactness and simplicity of the interface: the lack of any peculiar solute transport mechanism avoids sample losses, enhances the sensitivity and extends the range of possible applications. Peak profile is highly reproducible and high quality and informative mass spectra are generated. Direct-EI is also compatible with the presence of high concentrations of nonvolatile buffers in the mobile phase, thus requiring only a frequent ion source cleaning.

4.1.6 Direct-EI ion source vs ESI

The LC can be coupled either with API sources and Direct-EI. Advantages and drawbacks are briefly summarized: ESI, being an environmental pressure ionization, is immediately suitable for coupling with LC, thus not requiring high vacuum conditions typical of the EI source. The Direct-EI source, despite the easy hardware adjustment, not only offers an excellent solution to overcome this pressure gap, but use the high-vacuum conditions in order to desovate and vaporize the analytes.

API sources are characterized by the possibility of detecting analytes in a wide mass range, whereas the EI is excellent for low molecular weight analytes: the detection of heavy molecules can be very tricky, being very hard to vaporize.

In ESI the ionization of the analytes is performed in the liquid phase, thus resulting in a strong dependence between the ionizability of the analyte and the physio-chemical properties of the spray. Polarity, solubility and polarizability of the analyte and the composition of the mobile phase are key parameters in order to promote the ionization. Moreover, strong ion-ion and ion-molecule interactions in the charged droplets can be present between solvent, analytes and interfering compounds, thus leading to strong matrix effects in complex samples, with possible signal increase or suppression, non-linear responses and adducts formation. In EI, the ionization of the analytes occurs in gas-phase, regardless their chemical background (only thermal stability is required), therefore no intermolecular interaction is present, leading to the absence of matrix effect in the Direct-EI source. As example,

atrazine MS analysis in absence and in presence of fulvic acid by using the two sources is shown in **Figure 4.10** [20]**.**

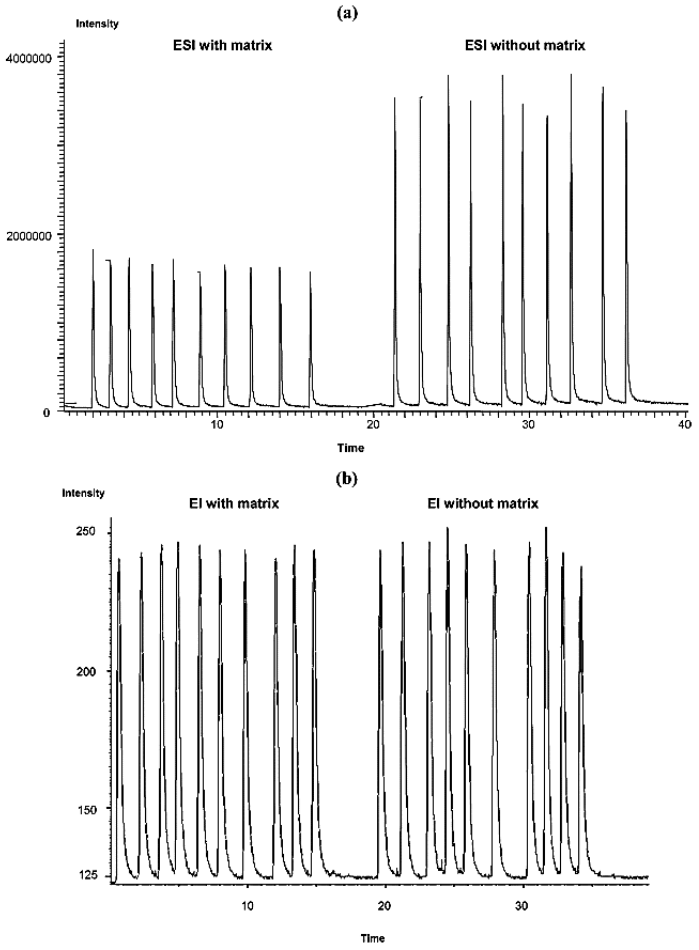

Figure 4.10 Evaluation of matrix effect on atrazine in presence (right) and without (left) of fulvic acid as matrix in ESI (a) and EI (b) [20]

Direct-EI LC-MS obtained spectra are comparable with those obtained by GC-EI-MS (**Figure 4.11**).

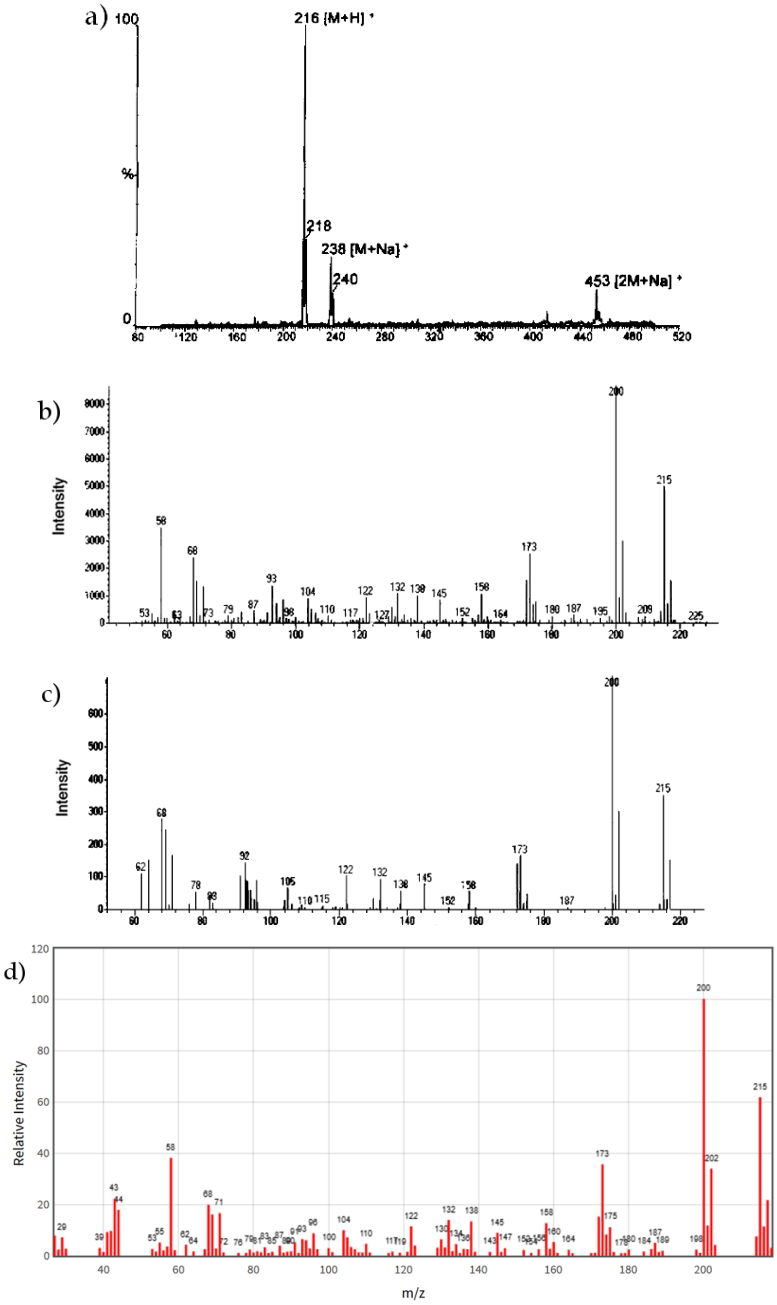

Figure 4.11 Spectra obtained by the analysis of atrazine in a) ESI-MS, b) GC-MS, c) Direct-EI-MS [20] and d) reference in NIST library

The characteristics of the two ion sources are summarized in **Table 4.1**.

Table 4.1 Comparison between API and EI features

ESI	EI
• Ambient pressure • Analysis of a wide range of molecular weights (proteins, complexes…) • Ionization related to the physio-chemical properties of the analytes • Strong ion-ion and ion-molecule interactions • Solvent and buffer restriction • Matrix effect (signal suppression, exaltation, non-linear response) • Soft ionization → no or low fragmentation (molecular ion)	• High vacuum condition (≈10^{-5} torr) • Suitable for molecules < 1000 Da • No toleration for extraneous substances • Ionization *via* high energy electrons • Absence of ion-ion and ion-molecule interactions • Absence of matrix effects • No post-column adjustments • Hard ionization → very high fragmentation → structural information • High reproducible spectrum → online libraries and matching algorithms

4.1.7 *Direct-EI ion source vaporization surface*

The vaporization of the analytes in a Direct-EI source occurs on the surface of the ionization chamber: the nanodroplets reach the hot metal surface that allows a complete gas-phase conversion of the solute. The material of the ion source surface is a key issue for the detection of analytes characterized by high-polarity and high-molecular weight, thus requiring high-source temperatures to be vaporized.

The typical EI ion source is made by 316 stainless steel. Although this material proved suitable for GC-MS analysis, several studies [21,22] proved that it is not totally inert and difficulties in the detection of some analytes by using Direct-EI LC-MS have been reported.

Major problems have been reported during the analysis of thermally labile and heavy or polar compounds: adsorption and thermal degradation phenomena on the SS surface affect both sensitivity and repeatability of the analysis.

Compounds characterized by high molecular weight require higher temperatures to be vaporized, thus the contact between these molecules and the surface could last too long, leading to possible analyte degradation and peak broadening. The detection of polar compounds can also be a challenge because of their possible dipolar and chemical interaction with the metal surface, thus resulting in peak tailing and lack of reproducibility.

In this context, the research group led by A. Cappiello tested the use of commercially available ceramic materials, sprayed onto the surface of a typical EI source [23]. The resulting coating was able to improve the detection of high-molecular weight and high-boiling compounds, but several limitations were highlighted: the coating was very thick and polishing occurred after few analyses.

4.1.8 Sol-gel technology

Sol-gel technology is a valid alternative to the typical coating procedures: it is a low-temperature chemical process capable of developing a great variety of inorganic networks from silicon or metal alkoxide monomer precursors $M(OR)_4$ and $R_nM(OR)_{4-n}$ on stainless steel [24]. Sol–gel protective coatings have shown excellent chemical stability for metal substrates. Moreover, the sol–gel method is an environmentally friendly technique for surface protection, thus replacing toxic pretreatments traditionally used for developing coatings on stainless steel. The morphology and the chemical composition of the developed material can be tuned by selecting proper solvents, precursors, stabilizers and catalyzers and by optimizing the reaction conditions, such as precursor concentrations, deposition method, drying heating temperature and gelation time.

The sol-gel reaction steps (**Figure 4.12**) can be summarized as follows:

1. Alcoxide dissolution in a proper solvent, usually an alcoholic solution carrying the same –R group of the alcoxide, with a stabilizer if required;
2. Hydrolysis of the alcoxide M-OR groups by adding water and, if necessary a catalyzer, (acid, base or fluoride) leading to the formation of hydroxyl M-OH groups;
3. Polycondensation, formation of M-O-M bonds and release of water and/or alcohol. During the coating process, the hydroxyl-alcoxides interact also with the hydroxyl groups present on the metal substrate,

such as Fe-OH, through hydrogen bonding. The formation of strong Fe-O-M bonds takes place during the gelation process and the followed high temperature heating [25].

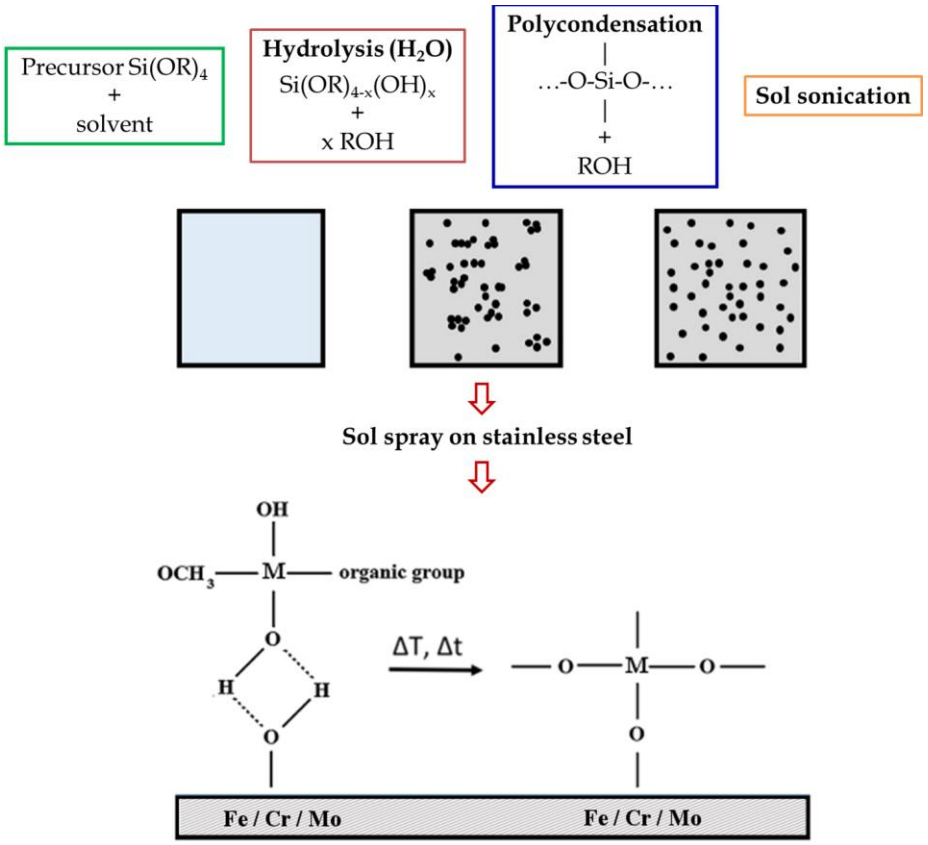

Figure 4.12 Schematic representation of reaction in the interface between the iron surface and the coating

In literature, several inorganic and organometallic networks have been developed in order to protect stainless steel from corrosion and chemical reactions. The most used and promising materials are based on silica, titania and zirconia alkoxides.

- **Silica**: silica coatings can be developed from a plethora of alcoxide precursors ($Si(OR)_4$ and $R'_nSi(OR)_{4-n}$), carrying different organic R and R' groups [26-28]. R' functionalization provides additional properties to the hybrid network compared to the inorganic system. However, these organic branches, being polymer monomers or

organic chains, usually are not very stable to high temperatures, leading to possible cracks formation, coating exfoliation or burning. On the contrary, unfunctionalized silica coatings proved a great thermal resistance and chemical inertness: smooth, crack-free and homogeneous morphologies have been obtained on stainless steel surfaces [29-32].

- **Titania**: Titania coatings have been used for widespread environmental applications because of their biological and chemical inertness, long-term stability, low electron conductivity and heat resistance [33]. TiO_2 has three structural phases: anatase, rutile and brookite. Anatase is a metastable phase and exhibits the best photocatalytic activity while the most stable rutile phase is less active. Brookite is rare compared to anatase and rutile and characterized by photocatalytic activity. Titania coatings of anatase and rutile were developed for stainless steel protection.
- **Zirconia**: ZrO_2 has an expansion coefficient very close to bulk stainless steel, thus could reduce the formation of cracks during high temperature process and improve the mechanical resistance of the coatings [34,35]. Moreover, ZrO_2 is also characterized by good chemical and excellent thermal stability. ZrO_2 coating on stainless steel provide anti-corrosion properties, thus increasing the lifetime of the material [35].

The group of analytical chemistry of the University of Parma proved the suitability of the sol-gel approach for both sample treatment and MS applications, with the development of materials characterized by high thermal and chemical stability, controlled morphology and high purity [36-39].

3.1.9 Coating of the Direct-EI ion source

The aim of this research, carried out in collaboration with Prof. A. Cappiello (University of Urbino) and Agilent Technology, was to develop and test new coatings for Direct-EI LC-MS applications, whose requirements are reported below:

1. Thermal stability: the ion source operative temperature is in the 250-350°C range
2. High inertia: no reaction, bonding or chemical modification of the analytes must occur by their interactions with the coating
3. Stability under high vacuum conditions: the coating has to be characterized by a very strong adhesion to the stainless steel
4. Controlled morphology: the coating surface has to be smooth, homogeneous and crack-free. The morphology of the coating is of a pivotal importance in order to favor the vaporization of the analytes. Any porosity has to be avoided, being able to cause compounds retention and carryover effect. The thickness uniformity ensures no electric and magnetic field distortions, as well as homogeneous heating and no hot points presence inside the ion chamber;
5. High flexibility: the ion source has to bear the strong mechanical stress due to stainless steel expansion.

In this study, we developed and tested the performances of three different coatings, i.e. silica, titania and zirconia. The coatings were synthesized by sol-gel technology and sprayed inside the bare stainless steel EI ion source. The coated ion sources were used for Direct-EI LC-MS analysis of environmental pollutants, i.e. polycyclic aromatic hydrocarbons (PAHs) and steroids. Then the study of three parameters related to the peak quality (i.e. peak width, area and peak delay) and the limit of detections, obtained by operating at different source temperatures, allowed to assess the improvement in the detection of the target compounds.

4.2 Material and Methods

4.2.1 Chemicals and materials

All reagents, naphthalene, and indeno1,2,3(c-d)pyrene (used as model compounds for PAHs), mestranol, diethylstilbestrol, 17-βestradiol, 17-α-ethynylestradiol, (used as model compounds for hormones) and solvents were purchased by Sigma Aldrich. EI SS ion sources were from Agilent Technologies (Palo Alto, CA, USA).

4.2.2 Coating synthesis

All the sol-gel coatings were previously tested on 316 SS plates in order to optimize the sol formulation and the spraying and heating conditions, by considering the morphology of the coating, its adhesion and the mechanical and thermal resistance.

The following optimized sols were obtained:

1. Silica-based coating: 2 ml TEOS were mixed with 1.7 ml of poly(dimethylsiloxane) hydroxy terminated (OH-TSO), 200 µl of absolute ethanol and 400 µl of acetic acid. The solution was sonicated at room temperature overnight.
2. Titania-based coating: 3080 µl of absolute ethanol were mixed with 190 µl of ethyl acetoacetate (EtAcAc), 1 ml of titanium (IV) tetrabutoxide, 40 µl of water. The solution was sonicated overnight, then OH-TSO was added (200 µl/ml of solution). Sonication was then performed for 2 h.
3. Zirconia-based coating: 2 ml of a 0.25M solution of zirconium isopropoxide in distilled isopropanol were mixed with 115 µl of EtAcAc; sonication was carried out for 3 h. 15 µl of water were carefully added under sonication in 30 min. The resulting transparent solution was sonicated overnight, then OH-TSO was added in a 200 µl/ml of solution ratio. Sonication was then performed for 2 h.

All the sols were stable in closed vials up to one month.

4.2.3 *Ion source coating*

Chemical etching was performed by dipping the stainless steel ion sources in HF (22%, v/v) at 50° C, for 60 min followed by HNO_3 (33% w/w) at 50 °C for 30 min. The sols were preliminary sonicated for 30 min, then sprayed under spinning at 3000 rpm by using a commercial airbrush onto the inner surface of the ion volume of the ion source. Finally, the ion sources were air-dried overnight at room temperature keeping the spinning in order to keep the homogeneity of the coating. Final heating was performed in a programmed oven from 50 °C to 350 °C (heating rate 2 °C/min). The temperature of 350 °C was maintained for 2 h in order to remove the organic component, promote the iron-gel bond formation and promote coating hardening. Two coated ion sources were prepared for each kind of sol-gel based material.

4.2.4 *Coating characterization*

Thermogravimetric analysis (TGA) was performed on a TGA 7 instrument (Perkin-Elmer, Waltham, MA, USA) over the temperature range 30-400 °C (heating rate: 5 °C/min) under inert atmosphere (N_2).

Infrared spectra were recorded using a FT-IR Nicolet 5700 spectrometer (Thermo Fisher Scientific, Inc., Waltham, MA, USA), equipped with an ATR Smart Orbit TM, operating between 4000 and 400 cm^{-1}.

Coating thickness and surface morphology were investigated by using environmental scanning electron microscopy (ESEM) with a Leica 430i instrument (Leica, Solms, Germany).

Coating bleeding was investigated by performing scan analyses in the 60-500 *m/z* range using the 90:10 (v:v) acetonitrile:water (ACN:H2O) mobile phase.

4.2.5 *Nano flow-Direct-EI LC-MS analysis*

All the analyses were performed on a nanoHPLC 1100 series combined with EI 5975 mass spectrometer (Agilent Technologies) under the following conditions: flow injection analysis, 90:10 (*v/v*) ACN:H2O mobile phase, flow rate: 300 nL/min, injection volume: 10 nL, analyte concentration: 100 ng/ml.

The MS was operated in the selected ion monitoring (SIM) mode by recording the current of the following ions:

- *m/z* 128 for naphthalene
- *m/z* 276 for indeno1,2,3(c-d)pyrene
- *m/z* 227 for mestranol
- *m/z* 268 for diethylstilbestrol
- *m/z* 272 for 17-α-ethynylestradiol
- *m/z* 296 for 17-β-estradiol

under the following ion source temperatures: 250, 300 and 350 °C.

Signal stability and repeatability in terms of intermediate precision were evaluated over three days using two ion sources. Three replicate measurements at each level for each effect (i.e day and temperature) were performed. Analysis of variance (ANOVA) was used to determine statistically significant differences between the mean responses obtained over 3 days.

Limit of detections (LODs) were calculated from the signal-to-noise ratios obtained by the analysis of the standard solutions: LOD = 3 S/N

4.3 Results and Discussion

The coatings were developed by sol-gel technology on stainless steel ion sources with the final aim of improving the Direct-EI LC-MS detection of environmental pollutants i.e. PAHs and hormones. The analytes were selected in order to simulate the common difficulties observed in the use of Direct-EI LC-MS, i.e. detection of high-boiling and polar compounds.

4.3.1 *Chemical etching*

In order to provide hydroxyl groups on the SS ion surface suitable for the inter-condensation reactions with the sol-gel networks and to remove surface contaminants and impurities, chemical etching of the substrate was performed. Several etching solutions (**Table 4.2**) were tested, according to literature [40,41] and previous knowledge. 316 SS plates were etched by using different mixtures and a reference silica sol was sprayed onto the samples. The coatings were then heated by using the conditions reported in **paragraph 4.2.3**.

Table 4.2 Etching mixture

Name	Reagent	% w/w	Solvent	Immersion Temperature	Etching time
Kellers	HNO_3 HCl HF	1.6 0.2 0.4	Water	25°C	10 s – 1 min
Kroll	HNO_3 HCl	3.6 0.7	Water	25°C	15 s – 2 min
Nital	HNO_3	7.6	Ethanol	25°C	1 - 10 min
Picral	Picric acid	48	Ethanol	25°C	1 - 10 min
Piranha	H_2SO_4 H_2O_2	70 9	-	90°C	30 min
HF	HF	22	Water	50°C	60 min
	HNO_3	33	Water	50°C	30 min
HCl	HCl	18	Water	25°C	10 min
Alkaline	NaOH	10	Water	70°C	30 min

The efficacy of the chemical etchings was evaluated by the analysis of both the morphology of the coatings (homogeneity and presence of cracks) and its adhesion towards the SS surface. **Figure** 3**.13** depicts one representative sample per etching mixture.

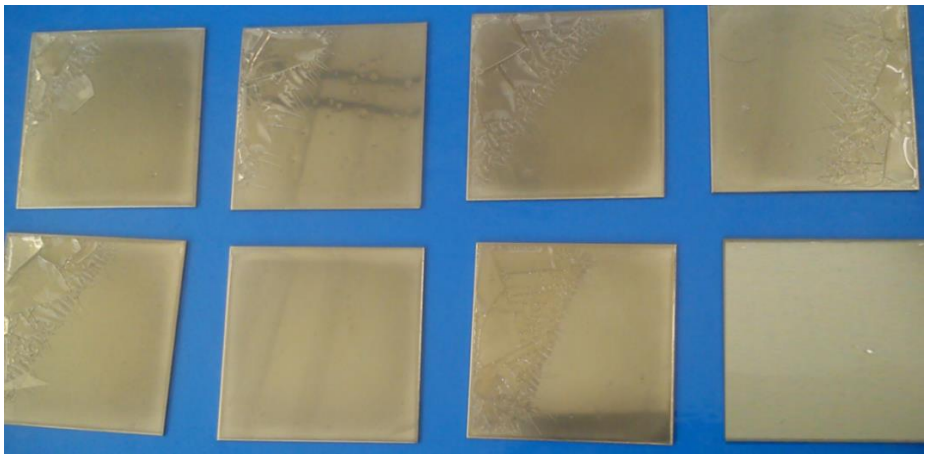

Figure 4.13 Samples etched SS surfaces, form top-left to bottom-right: Alkaline, Nital, Picral, Kroll, Piranha, HCl, Kellers and HF etching

As clearly shown in **Figure** 4**.13**, the best coatings were those deposited on HCl- and HF-etched surfaces.

HCl etching was performed by full immersion of the sample in HCl solution (18% w/w) at room temperature for 10 minutes. Then the surface was washed with distilled water, in order to remove the excess of acid that can act as additional catalyzer during the sol-gel reaction. The morphology of the SS surface was not modified during the entire process.

HF etching was performed by using HF (22% w/w) solution at 50°C: after immersion, the SS sample changed the color from its natural shiny gray to black and the surface morphology from smooth to rough. The HF solution turned from transparent to green, due to the formation of iron, molybdenum and chromium fluorides. By leaving the plates under ambient condition, an orange layer, due to the presence of iron oxides was observed. A passivation step was therefore required: the samples were dipped in a nitric acid (33%) solution. The treated samples were stable at ambient conditions as-well-as the untreated stainless steel: the nitric reaction restored the corrosion resistant properties by creating a passivation layer on the steel surface. The surface was

characterized by high roughness and the deposited coating was strongly adherent, more than in any other etched samples.

The different appearance of the surface after the etchings can be clearly seen in **Figure 4.14**.

Figure 4.14 Etched SS surfaces: HCl (left) and HF (right)

Moving from plane SS plates to the inner surface of the ion sources, only the HF etching proved to be suitable for depositing homogeneous, crack-free and adhered sol-gel coatings. In fact, the mechanical strain led to cracks formation and coatings exfoliation when HCl etching was performed.

4.3.2 *Sol-gel coating*

Sol-gel materials were synthetized starting from the corresponding metal alkoxides, optimizing sol mixtures reported in literature for silica [42], titania [43,44] and zirconia [35].

In order to avoid cracks and increase the adhesion capabilities of the material poly(dimethylsiloxane) hydroxy terminated was added. The use of this plasticizer was required since preliminary experiments performed on silica-based materials, obtained by using several alcoxides (TEOS, methyltriethoxysilane and ethyltriethoxysilane) did not allow to achieve stable, homogeneous and crack-free coatings.

OH-TSO overcame all the mentioned limitations and was fully integrated in the inorganic network: the hydroxyl terminated chains can be involved in the polycondensation reaction (**Scheme 4.1**).

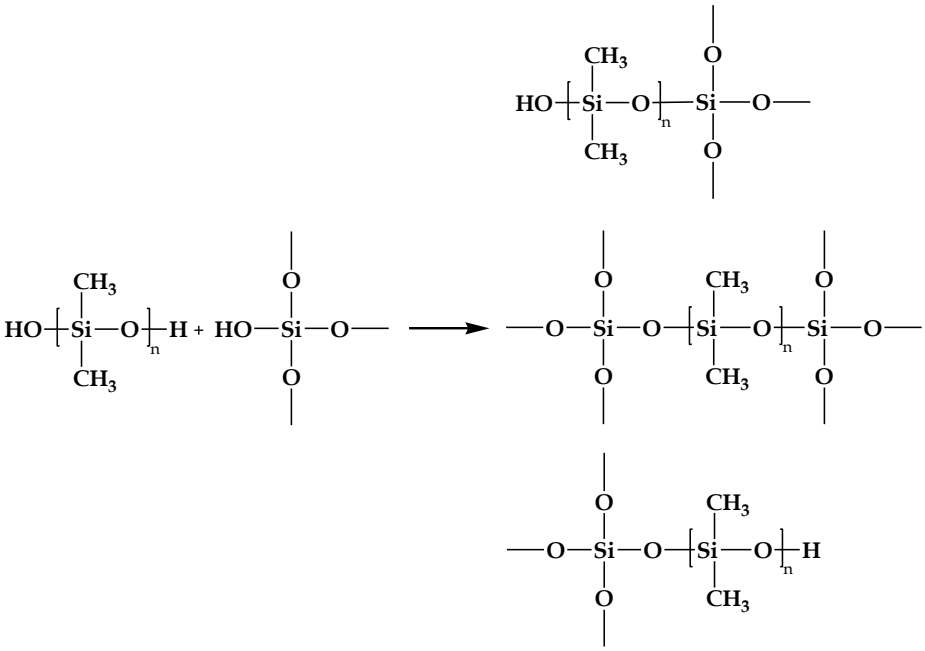

Scheme 4.1 OH-TSO possible reaction with growing silica gel

The OH-TSO presence inside the gel provided excellent conformational freedom to the inorganic network: the coatings containing the plasticizer were stable up to 350°C and able to bear the mechanical stress, thus providing homogeneous and crack-free surfaces.

Sonication of the sols allowed to obtain homogeneous solutions, disrupting condensation hotspots, thus increasing the lifetime of the sols up to 1 month.

As discussed in **paragraph 4.1.8**, during the sol-gel polycondensation reactions, hydroxyl groups of the hydrolyzed precursors and plasticizer interact with the SS surface, thus allowing the formation of M'-O-M (M=Si, Ti, Zr, M'=Fe, Cr, Mo) bonds.

Hybrid coatings from modified silanes have been widely used to obtain organic–inorganic hybrid materials, characterized by excellent corrosion resistance for metal substrates [24]. Moreover, by changing the organic functionalization and the ratio functionalized/unfunctionalized precursor is possible to tune the mechanical and chemical characteristics of the coating, i.e. flexibility, adhesion, chemical inertness, hydrophobicity…

We tested two different hybrid materials: methacrylate- and phenyl-based materials, widely proposed as protective coatings on stainless steel [28].

Hybrid methacrylate coatings are characterized by high hydrophobicity and a crosslinking *via* methacrylate polymerization [27,30,31,45].

Based on the literature we developed and tested the following sols:

1. 3-(Trimethoxysilyl)propyl methacrylate, ethanol, hydrochloridric acid, water
2. 3-(Trimethoxysilyl)propyl methacrylate, TEOS, methanol, hydrochloridric acid, water
3. 3-(Trimethoxysilyl)propyl methacrylate, TEOS, methanol, acetic acid, water

Several functionalized/unfunctionalized alcoxides, catalyzer/precursor and solvent/precursor ratios and plasticizer additions were experimented. In all the cases, due to the presence of an organic cross-linking, the material was not stable to the ion source operative temperatures, showing cracks and burning of the coating.

Phenyltrimethoxysilane (PTMS) has been also proposed in order to develop sol-gel coatings both for SS protection [26] and for Solid-Phase Microextraction [38,39]. The phenyl groups allowed to obtain not only coatings characterized by higher hydrophobicity compared those developed from TEOS, but also materials able to interact *via* π electrons. The possible interactions toward the aromatic analytes could lead to retain these compounds.

Three mixture based on our group's previous studies were developed:

1. TEOS (895 µl), PTMS (1054 µl), H_2O (430 µl), HCl 0.6 M (24 µl), ethanol (1 ml), TSO-OH (500 µl)
2. TEOS (1338 µl), PTMS (1584 µl), H_2O (1295 µl), HCl 0.6 M (48 µl), TSO-OH (850 µl)
3. TEOS (1338 µl), PTMS (1584 µl), H_2O (1295 µl), HCl 0.6 M (48 µl), TSO-OH (850 µl), ethanol (1 ml)

The coatings were affected by several drawbacks: exfoliation, lack of adhesion and high porosity were present, thus resulting not suitable for Direct-EI LC-MS application.

The coating technique was another key parameter: spray coating allowed the deposition of the sol only in the region involved in the desolvatation, vaporization and ionization processes, included between the beginning of the source body and the drawout plate of the ion source (**Figure 4.15**).

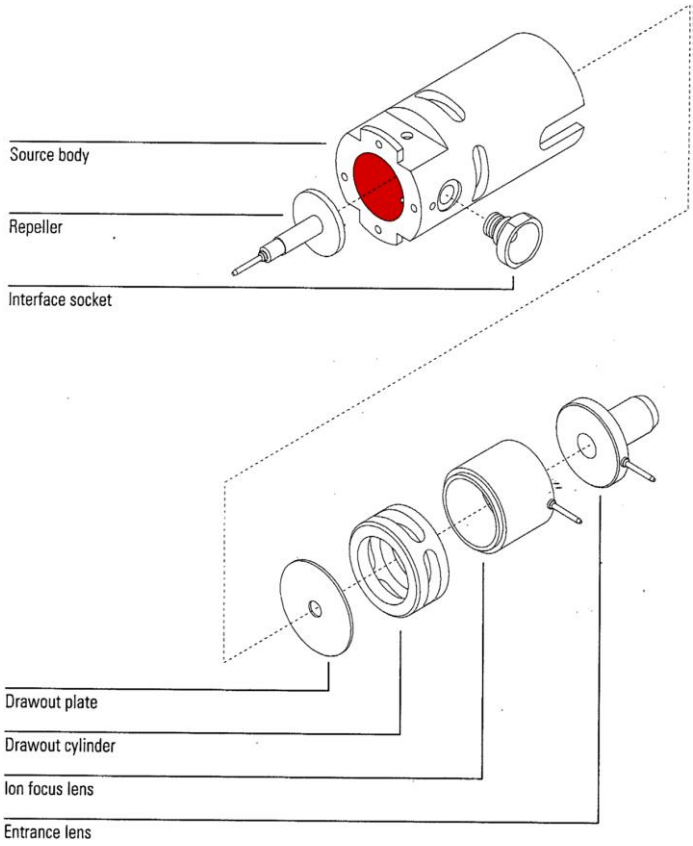

Figure 4.15 Schematic representation of the EI ion source body. The coated surface is depicted in red.

The sources were spinned at 3000 rpm during the spray deposition and the gelation step, in order to obtain very homogeneous and thin coatings. They were air-dried overnight at room temperature and finally heated in oven. The heating programme was optimized: a very slow heating rate (2 °C/min) from 50 °C to 350 °C was applied to avoid cracking and exfoliation phenomena. The temperature of 350 °C, the highest operation temperature of the ion source, was maintained for 2 h. This step was necessary to ensure the complete evaporation of the organic component, i.e. residual solvents, catalyzers and organic sub-products, promote the iron-gel bond formation and the coating hardening. The obtained coatings are shown in **Figure 4.16**, both on SS plates (HCl and HF etching) and inside the ion source (only HF etching).

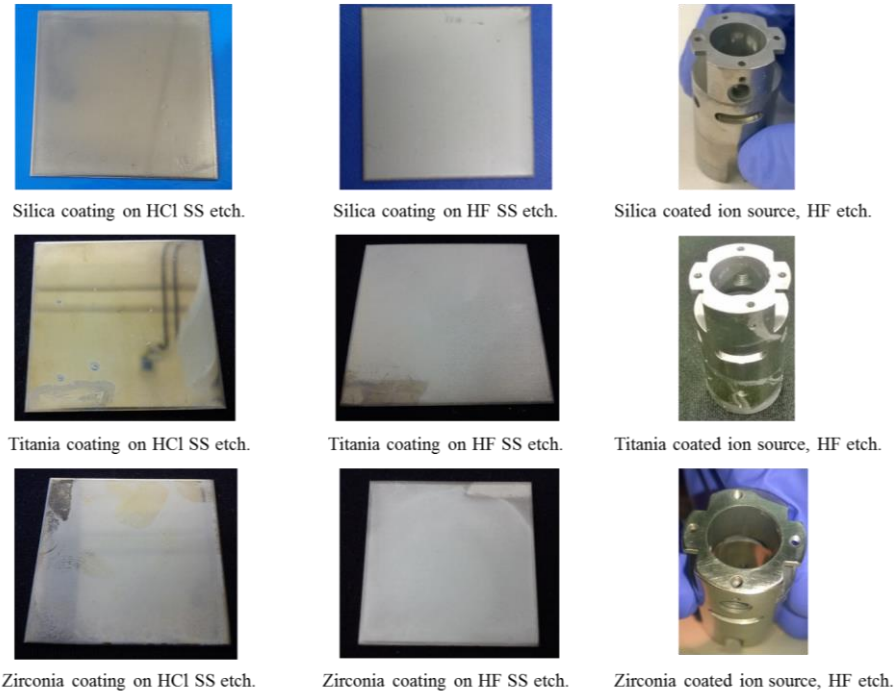

Figure 4.16 photographs of the developed coatings on SS plates and ion sources

4.3.3 *Coating characterization*

Powder samples of sol-gel materials were investigated by IR spectroscopy. The spectrum of silica-based (**Figure 4.17**) material showed bands at 2966 cm^{-1}, 2913 cm^{-1} and 1411 cm^{-1} which can be ascribed to the asymmetric and symmetric stretching and to the bending of the -CH_3 bonds, respectively. The band at 1260 cm^{-1} can be related to the bending of the Si-CH_3 group, whereas the signal at 1002 cm^{-1} can be attributed to Si-O-Si asymmetric stretching. Finally, bending vibrations of Si-O-Si bonds were observed between 850 and 760 cm^{-1} [29, 30, 46-49].

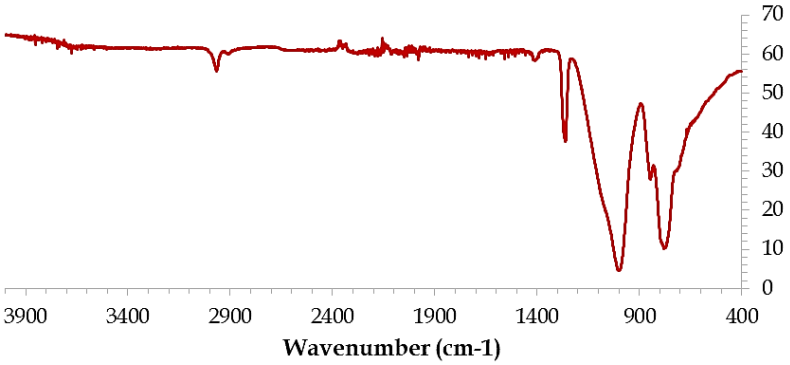

Figure 4.17 FT-IR spectra of the silica-based material

Similarly, the titania-based (**Figure 4.18**) coating showed bands at 2965 cm^{-1}, 2911 cm^{-1} and 1410 cm^{-1}, ascribed to the asymmetric and symmetric stretching and to the bending of the -CH_3 bonds. Signals at 1265 cm^{-1} and 1003 cm^{-1} were related to the bending of the Si-CH_3 group and to Si-O-Si asymmetric stretching, respectively. Bands in the 800-450 cm^{-1} region were attributed to Ti-O and Ti-O-Ti bonds [50,51].

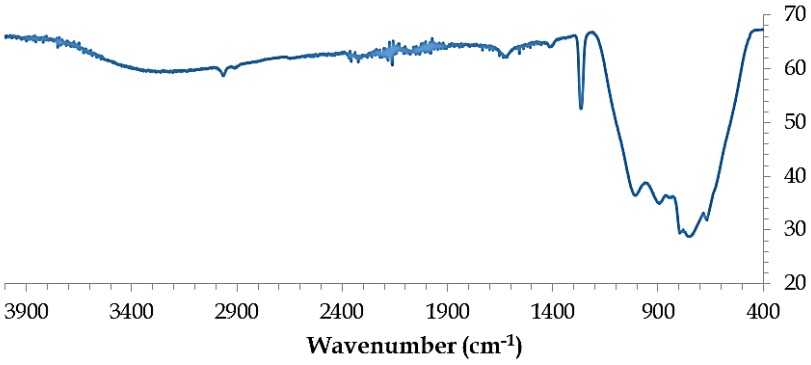

Figure 4.18 FT-IR spectra of the titania-based material

It has to be noticed that the presence of common bands between the silica-based and the titania-based coatings can be ascribed to the use of the plasticizer. As expected, these bands are also present in the case of the zirconia-based material (**Figure 4.19**). Additional bands observed between 1565 and 1455 cm^{-1} could be associated to stretching Zr-O-C bonds, whereas Zr-O-Zr species are observed below 720 cm^{-1} [52-54].

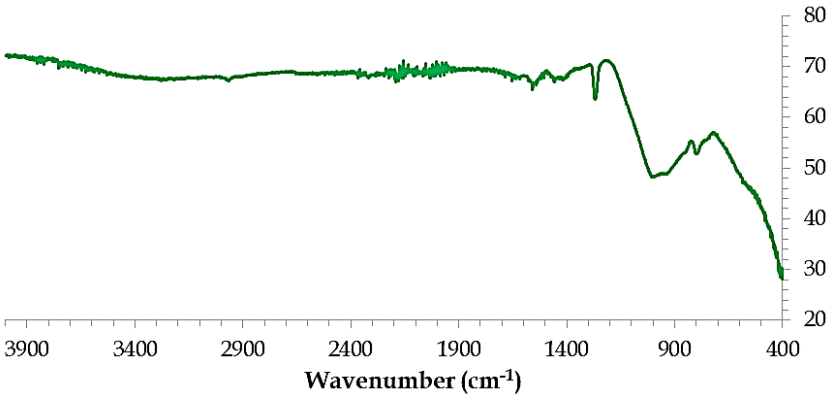

Figure 4.19 FT-IR spectra of the zirconia-based material

The thermal behavior of the silica-, titania- and zirconia-based coatings was recorded by means of TGA (**Figure 4.20-4.22**). Excellent thermal stabilities were obtained for all the materials: negligible weight losses were shown up to 350-400°C.

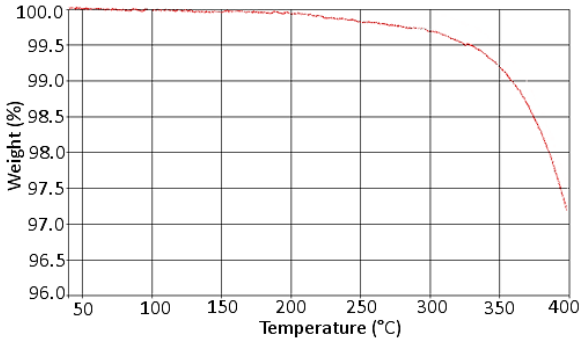

Figure 4.20 Thermogravimetric analysis of the silica-based coating under nitrogen

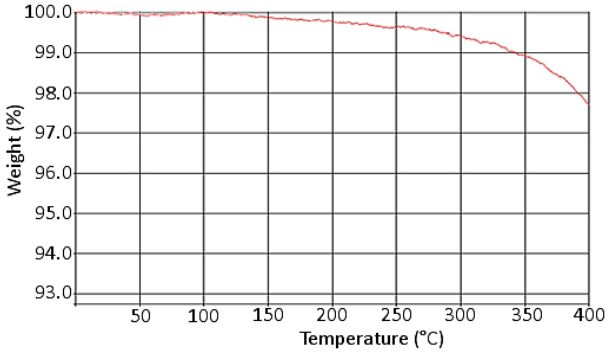

Figure 4.21 Thermogravimetric analysis of the titania-based coating under nitrogen

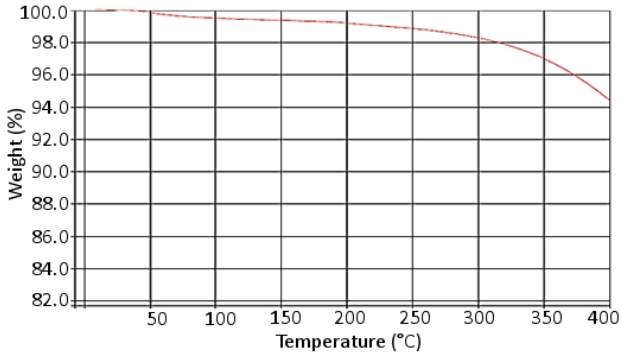

Figure 4.22 Thermogravimetric analysis of the Zirconia-based coating under nitrogen

The thermal resistance has also to be proven in a long-term period, being the coatings developed on ion sources working continuously under vacuum conditions at high operation temperatures. To assess long-term stability, additional TGAs were recorded on materials kept for 2 weeks at 300°C (an example is shown in **Figure 4.23**). The achieved results were very satisfactory, since no significant change in the TGA profile was observed.

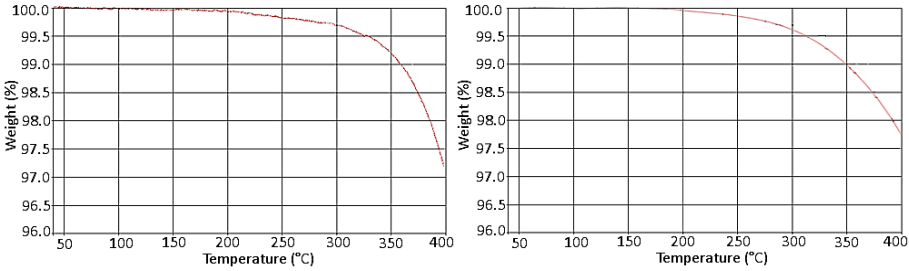

Figure 4.23 Thermogravimetric analyses of the silica-based coating under nitrogen: left) prior the use; right) after 15 days at the ion source operating temperature (300°C)

The thermal stability of the materials was also assessed by investigating the bleeding of the coated sources at the operating conditions: no significant bleeding was observed for all the developed coatings, not only for short-term periods, but also when long-term stability was evaluated.

The morphology of the developed coatings was investigated by Environmental Scanning Electron Microscopy under different magnifications (**Figure 4.24**).

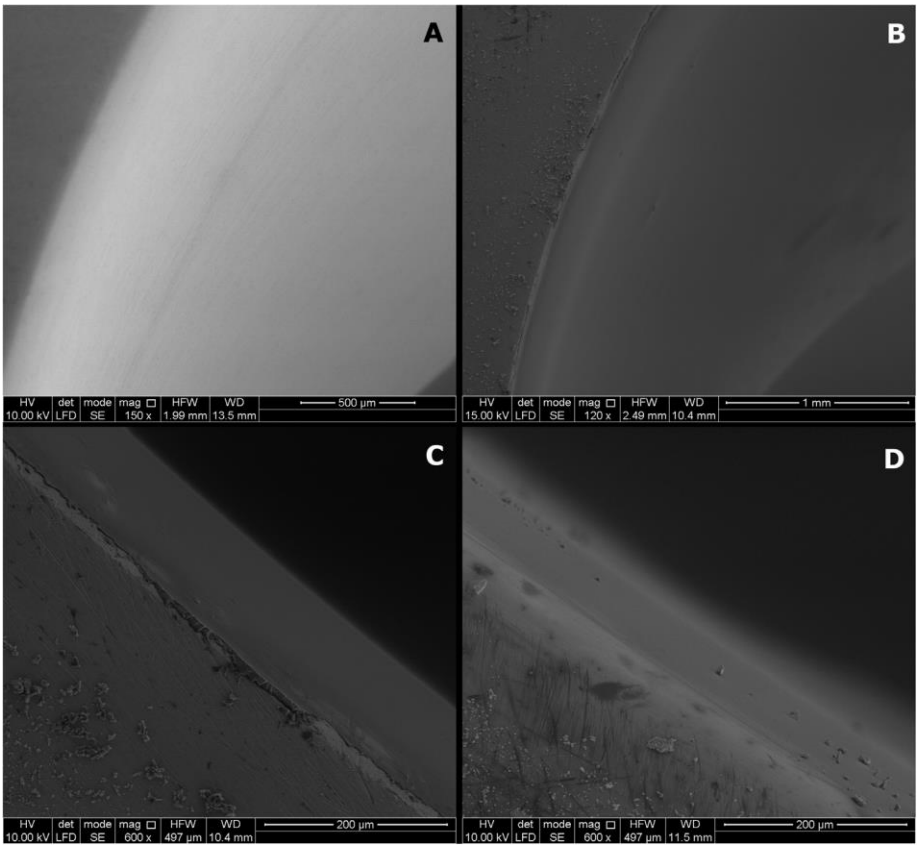

Figure 4.24 ESEM micrographs of: A) bare SS ion source, B) silica-, C) titania-, D) zirconia-coated ion sources

In **Figure 4.24,** significant examples of the developed coatings (B-D) are compared to the bare SS ion source (A). All the coatings were characterized by homogeneous, smooth and crack-free layers. The ESEM analysis allowed to evaluate the thicknesses of the developed coatings, obtained by performing 4 measurements per ion source, for 2 different ion sources. Silica coating was characterized by an average thickness of 9 ± 1 µm, titania of 11 ± 2 µm zirconia of 6 ± 1 µm, thus no significant or very slight differences between the coatings were present. This aspect was crucial in order to compare the analytical performances of the different coated ion sources: only the presence of interactions between the analytes and the different sol-gel materials affected the analytical parameters.

The coatings thickness depends on the number of times the sols are sprayed inside the ion source, thus different coating thickness can be obtained. This

parameter is of paramount importance: heavy thicknesses led to cracking phenomena and to the release of particulate and sol-gel components inside the ion source, jeopardizing the correct use of the mass spectrometer. On the contrary, the use of very thin films led to shorten the lifetime of the coatings.

In addition to both the thermal resistance related to the high operation temperature of the ions sources and the related mechanical stress due to the steel expansion, the coating has to be characterized by an excellent adhesion towards the SS since the ion source works under high vacuum conditions (10^{-5} torr). In order to assess the bearing to void conditions, as a preliminary investigation, the coatings were heated at 350°C in a flask connected to a vacuum line. Then the coating morphology was investigated *via* ESEM analysis: silica-, titania- and zirconia-based materials proved excellent adhesions on the SS surface, since no morphology changes were observed.

Additional investigations were performed by studying the morphology of the coatings after Direct-EI LC-MS analyses. Again, no significant modification of the sol-gel surface was observed (**Figure 4.25**)

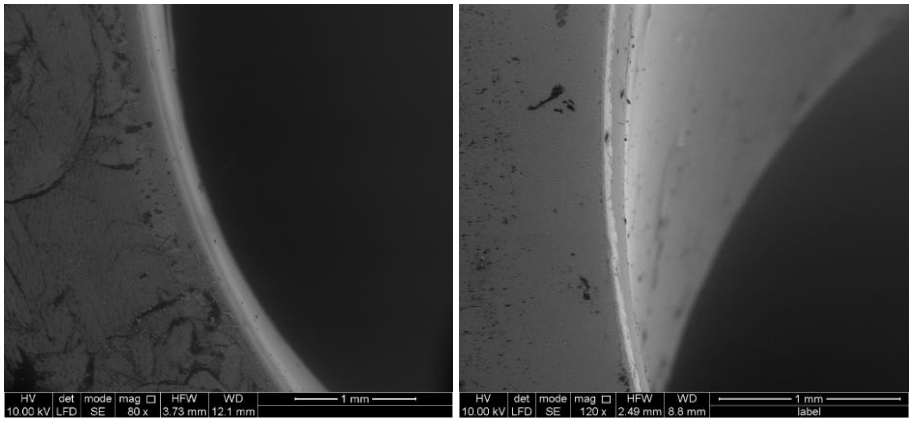

Figure 4.25 ESEM micrographs of the silica coated ion source before (left) and after (right) the Direct-EI LC-MS analyses.

4.3.4 Direct-EI LC-MS analysis of PAHs and hormones

The capabilities of the developed coatings were tested toward the analysis of environmental pollutants, i.e. PAHs and hormones.

PAHs are generated from both natural and anthropogenic sources, typically during incomplete combustion [55]. This class includes compounds characterized by carcinogenic, mutagenic, immunologic and reproductive effects, thus the risks for human health [56]. PAHs can be transported in air for hundreds of kilometers, to regions far away from the sources, thus are considered as emerging contaminants. Currently, PAHs in environmental matrices are analyzed both by GC-MS [57] and HPLC-MS [58].

The analysis of hormones is of pivotal importance for environmental analyses, since in the lasts 50 years, a dramatic increase in the use of pharmaceutical drugs has been occurred, both for human diseases treatment and animal husbandry. The active component of the drugs often are hormones, which can alter metabolic and physiological functions even at low concentrations, thus they are considered endocrine disrupting compounds. The presence of these drugs were assessed in surface and groundwater, soil and sediment with concentrations in the ng-µg/l range, causing a major impact on the environment, therefore they are considered as new emerging contaminants [59-62]. Due to the public health risk, a growing interest in monitoring hormones has occurred, leading to development of new methods from institutions such as EPA Method 539 [63].

The developed methods for the detection of PAHs and hormones by using LC-MS API ion sources are time consuming and require MS^n analyses for quantitation. The use of the Direct-EI LC-MS could lead to the development of more simple and rapid methods, not affected by matrix effect, thus allowing to simplify the sample treatment.

Six analytes, namely naphthalene, indeno1,2,3(c-d)pyrene, mestranol, diethylstilbestrol, 17-βestradiol, 17-α-ethynylestradiol were selected as reference compounds among the PAHs and the hormones, respectively (**Figure 4.26**). Among PAHs, indeno1,2,3(c-d)pyrene is characterized by high molecular weight and the presence of several condensed aromatic rings. Due to the high boiling point, adsorption and interaction phenomena can occur by using SS ion source, thus producing peak broadening and tailing. By contrast, naphthalene, being the most volatile compound, is characterized by good detection parameters by using a bare ion source.

The analysis of the hormones is very challenging because of their high polarity and boiling temperatures. The structure of the analytes presents aromatic rings, multiple bonds and hydroxyl groups that can interact with the SS surface.

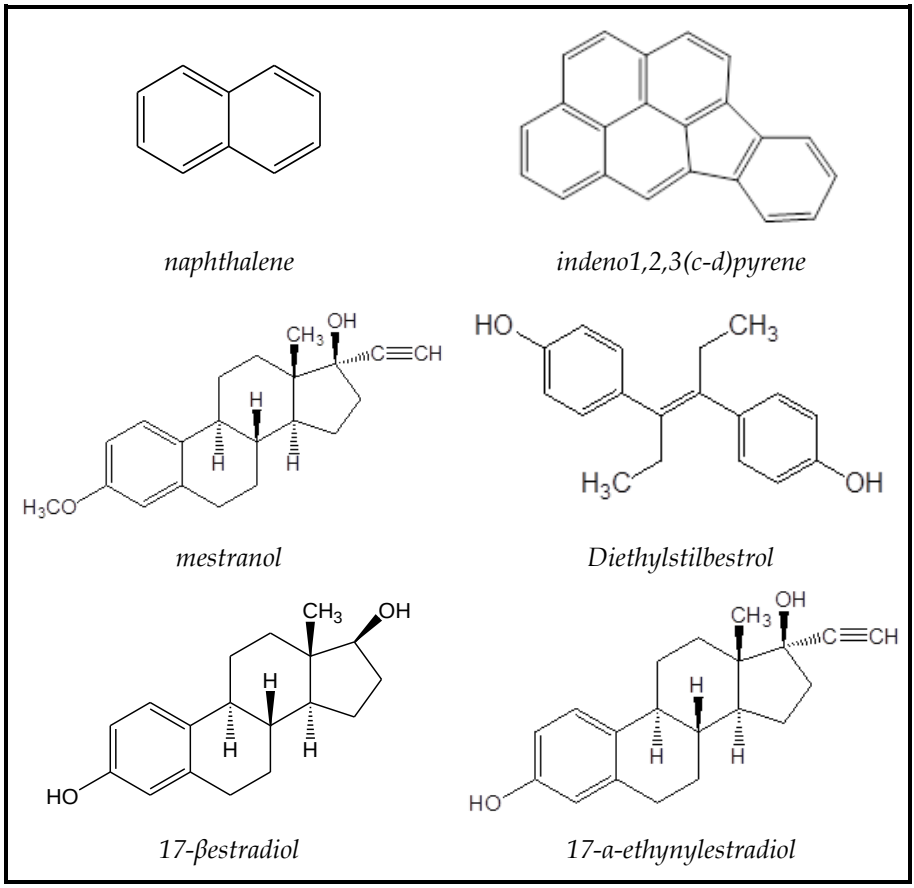

Figure 4.26 Structure of the analytes

All the analyses were performed in flow injection. A schematic representation of the utilized instrumental configuration is reported in **Figure 4.26**. This apparatus allowed to inject a fixed volume (10 nl) of the analyte solutions after the chromatographic column. This configuration was set in order to mimic the full Direct-EI LC-MS analysis, but the obtained peaks were related only to the ion source performances, being not influenced by any chromatographic separation.

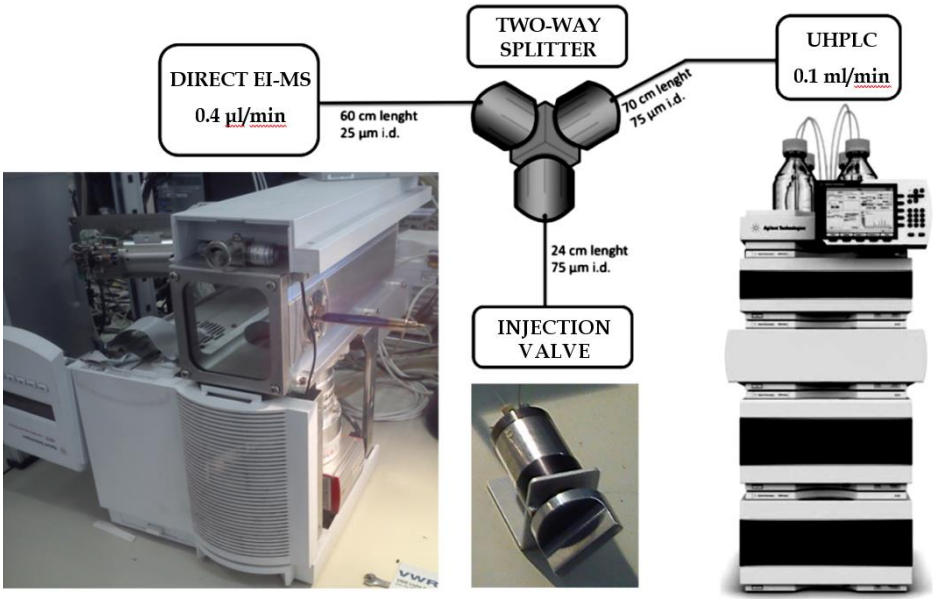

Figure 4.27 Schematic representation of the instrumental setup

The performances of the different coated ion sources were studied by evaluating three parameters related to peak quality, i.e. peak width, peak delay and peak area.

1. **peak width**: this parameter highlights the presence of undesired broadening and tailing phenomena. These effects can be related to the presence of interactions between the analytes and the ion source surface, leading to the retention of the molecules and increasing the width of the peaks. Both the average value and the relative standard deviation (RSD%) have to be considered: the first is related to the shape of the peak, the second to the reproducibility of the signal.
2. **peak delay**: it measures the time required by the analytes to be detected. Only the relative standard deviation (RSD%) has been considered, since this value can be associated to possible delays in the detection of molecules interacting with the surface of the ion source.
3. **peak area:** differences in peak area among different coatings can suggest the retention of the analytes on the surface of the ion source. Being adsorbed on the walls of the ionization chamber, these molecules cannot be detected, thus a decrease in the sensitivity can occur. The RSD% is of paramount importance because it is related to the repeatability of the analyses.

The obtained peak parameters for PAHs analyses are reported in **Table 4.2.**

Table 4.2 Peak parameters for PAHs analysis by using silica-, titania- and zirconia-coated ion sources

PEAK WIDTH mean ± dev. st. (RSD%)				
T °C	**S. Steel**	**Silica**	**Titania**	**Zirconia**
		Naphthalene		
250	0.100±0.008 (8)	0.100±0.002 (2)	0.100±0.003 (3)	0.35 ± 0.12 (22)
300	0.100±0.005 (5)	0.100±0.003 (6)	0.100±0.003 (3)	0.30 ± 0.06 (15)
350	0.100±0.004 (4)	0.100±0.002 (2)	0.100±0.016 (16)	0.200±0.028 (14)
		Indeno1,2,3(c-d)pyrene		
250	n.d.	0.300±0.010 (3)	n.d.	n.d.
300	1.200±0.900 (75)	**0.100±0.002 (2)**	3.7 ± 2.1 (56)	0.51 ± 0.37 (72)
350	0.400±0.250 (63)	0.100±0.009 (9)	0.700±0.120 (17)	0.350±0.028 (8)
AREA mean ± dev. st. (RSD%)				
T °C	**S. Steel**	**Silica**	**Titania**	**Zirconia**
		Naphthalene		
250	60000±8000 (13)	63000±2000 (3)	38000±4000 (11)	23000±13000 (57)
300	60000±5000 (8)	**65000±4000 (6)**	38000±2000 (5)	29000±8000 (28)
350	63000±3000 (5)	69000±5000 (7)	38000±13000 (34)	37000±9000 (24)
		Indeno1,2,3(c-d)pyrene		
250	n.d.	132000±10000 (8)	n.d.	n.d.
300	127000±16000 (13)	**155000±7000 (5)**	38000±2000 (5)	21000±11000 (52)
350	140000±22000 (16)	161000±7000 (4)	93000±7000 (8)	56000±18000 (32)
PEAK DELAY RSD%				
T °C	**S. Steel**	**Silica**	**Titania**	**Zirconia**
		Naphthalene		
250	14.1	1.2	3.9	14.6
300	15.5	**1.1**	3.7	9.8
350	17.4	1.4	4.7	5.7
		Indeno1,2,3(c-d)pyrene		
250	n.d.	1.0	n.d.	n.d.
300	27.3	**0.9**	3.7	15.3
350	25.2	1.4	4.6	1.6

n.d. not detected or not useful for quantitation

As expected, no significant improvements were observed for naphthalene: being characterized by a low molecular weight, this analyte can be easily vaporized, thus reducing potential interaction with the SS surface. The detection of naphthalene was feasible also when low working temperatures were used, i.e. 250°C, obtaining sharp signals. However, the silica coating allowed an improvement of the repeatability, as can be seen by the decrease of the RDS%.

Indeno1,2,3(c-d)pyrene is characterized by a molecular weight two fold higher than that of naphthalene, and presents some difficulties in terms of vaporization. By using the bare SS ion source signal suppression and broad signals occurred, also by operating at the highest possible instrumental temperature (350°C). By contrast, by using the silica-based coating, sharp peaks were obtained also at low temperature. Optimal results were achieved at 300°C, while good signals were observed at 250°C.

Titania- and zirconia-based materials did not show any significant improvement in the peak quality compared to the bare SS source.

A comparison between the peaks obtained for naphthalene and indeno1,2,3(c-d)pyrene by using SS sources and the coated sources is reported in **Figure 4.28**.

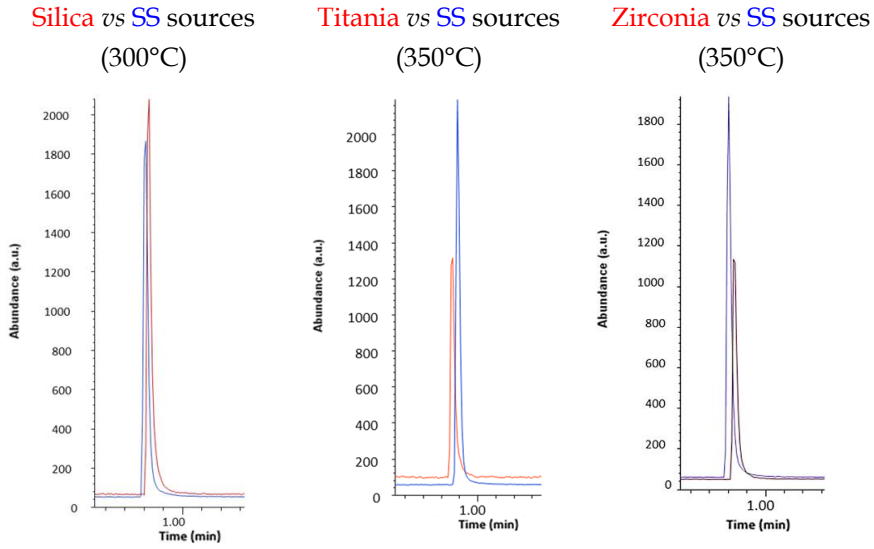

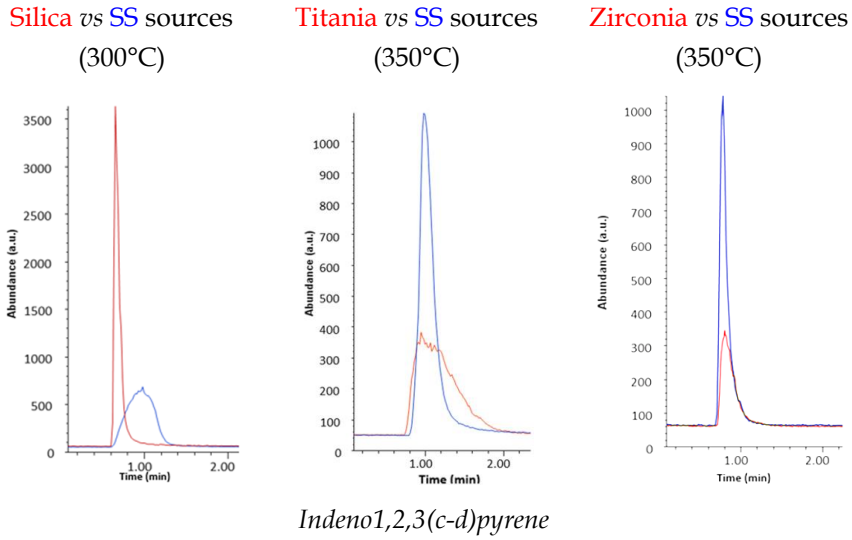

Figure 4.28 PAHs peaks comparison between coated and SS ion sources

As for hormones the obtained analytical parameters are reported in **Table 4.3**;

Table 4.3 Peak parameters for hormones analysis by using silica-, titania- and zirconia-coated ion sources

		PEAK WIDTH mean ± dev. st. (RSD%)		
T °C	**S. Steel**	**Silica**	**Titania**	**Zirconia**
		Mestranol		
250	n.d.	0.100±0.007 (7)	n.d.	n.d.
300	0.800±0.520 (65)	**0.100±0.004 (4)**	0.760±0.322 (42)	n.d.
350	0.100±0.050 (50)	0.100±0.011 (11)	0.100±0.011 (11)	0.100±0.007 (7)
		Diethylstilbestrol		
250	n.d.	0.100±0.003 (3)	n.d.	n.d.
300	0.910±0.530 (58)	**0.100±0.003 (3)**	1.000±0.420 (42)	n.d.
350	0.100±0.050 (50)	0.100±0.008 (8)	0.210±0.045 (21)	0.120±0.025 (21)
		17-β-estradiol		
250	n.d.	0.100±0.007 (7)	n.d.	n.d.
300	1.380±0.660 (48)	**0.100±0.005 (5)**	1.31 ± 0.46 (36)	n.d.
350	0.360±0.210 (58)	0.100±0.010 (10)	0.230±0.048 (21)	0.100±0.013 (13)
		17-α-ethynilestradiol		
250	n.d.	0.100±0.013 (10)	n.d.	n.d.
300	1.000 ± 0.530 (53)	**0.100±0.004 (4)**	n.d.	n.d.
350	0.300±0.170 (57)	0.100±0.009 (9)	0.330±0.068 (21)	0.150±0.019 (13)

AREA mean ± dev. st. (RSD%)				
T °C	**Stainless Steel**	**Silica**	**Titania**	**Zirconia**
		Mestranol		
250	n.d.	17200±1800 (10)	n.d.	n.d.
300	47000±15000 (32)	**22500±300 (1)**	28000±18000 (63)	n.d.
350	67500±6500 (10)	22310±380 (2)	36000±21000 (57)	13950±770 (6)
		Diethylstilbestrol		
250	n.d.	10520±710 (7)	n.d.	n.d.
300	28000±10000 (36)	**15800±1100 (7)**	20000±10000 (50)	n.d.
350	40300±4400 (11)	9900±500 (5)	39000±21000 (55)	8750±830 (9)
		17β-estradiol		
250	n.d.	8490±620 (7)	n.d.	n.d.
300	23300±3400 (15)	**12320±650 (5)**	11200±6200 (56)	n.d.
350	25500±3800 (15)	9150±430 (5)	20000±9800 (49)	5900±1100 (18)
		17-α-ethynil estradiol		
250	n.d.	3540±460 (13)	n.d.	n.d.
300	7400±2200 (30)	**5120±490 (10)**	n.d.	n.d.
350	7700±1300 (17)	4200±290 (7)	6200±3500 (56)	2100±610 (29)

PEAK DELAY RSD%				
T °C	**S. Steel**	**Silica**	**Titania**	**Zirconia**
		Mestranol		
250	n.d.	1.4	n.d.	n.d.
300	12.0	**0.5**	7.1	n.d.
350	14.0	1.2	5.0	1.5
		Diethylstilbestrol		
250	n.d.	1.1	n.d.	n.d.
300	8.8	**0.4**	5.1	n.d.
350	13.9	0.7	3.1	2.1
		17-β-estradiol		
250	n.d.	1.2	n.d.	n.d.
300	29.5	**0.3**	10.0	n.d.
350	15.3	0.8	3.0	1.5
		17-a-ethynilestradiol		
250	n.d.	1.3	n.d.	n.d.
300	37.5	**1.2**	n.d.	n.d.
350	15.0	1.2	8.8	3.6

n.d. not detected or not useful for quantitation

The use of a bare SS ion source did not provide peaks useful for quantitation purposes: the peaks were very broad and tailed. The detection of the analytes at 250°C was not feasible, resulting in a complete signal suppression. Hormones are characterized not only by high boiling temperatures, but also by a very high polarity: due to the presence of both hydroxyl groups and multiple bonds, the analytes strongly interact with the SS ion source walls, leading to adsorption phenomena. Moreover, the analyses performed by bare ion source were affected by very low repeatability also when high temperature were used: the RSD% were above 50% for peak width, in the 10-36% range for peak area and between 8.8% and 37.5% for peak delay. The variability was so high that data were not suitable for quantitative analyses.

The silica coatings allowed to reach a noticeable improvement in the detection of hormones: peak width was widely reduced, thus obtaining sharp peaks also for 17-β-estradiol and 17-α-ethynilestradiol, the analytes characterized by the worst performances when the SS ion source was used (**Figure. 4.29** and **Table 4.3**). Similarly, to PAHs, the best analytical performances were obtained by operating at the ion source temperature of 300°C. A noteworthy increase in terms of repeatability was achieved: RSD% lower than 5% for peak width, 10% for peak area and 1.2% for peak delay were obtained. It has also to be noticed that the detection of all the analytes was feasible also by operating at 250°C.

Finally, both titania- and zirconia-based coatings did not show any significant improvement compared to the bare SS ion source (**Figure. 4.29** and **Table 4.3**).

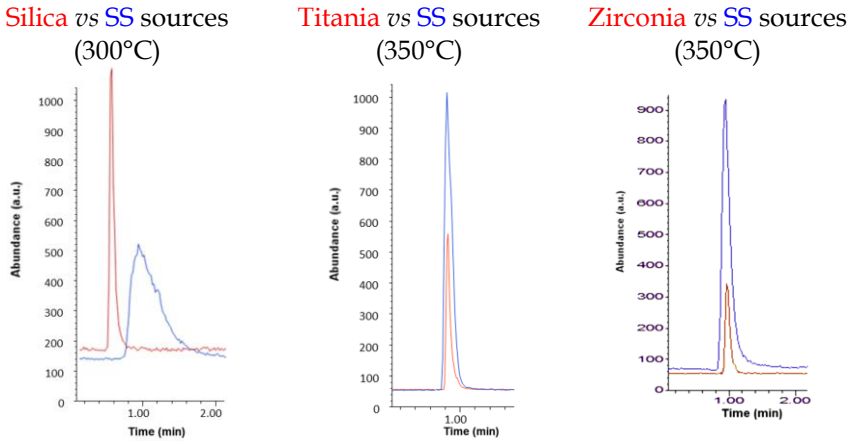

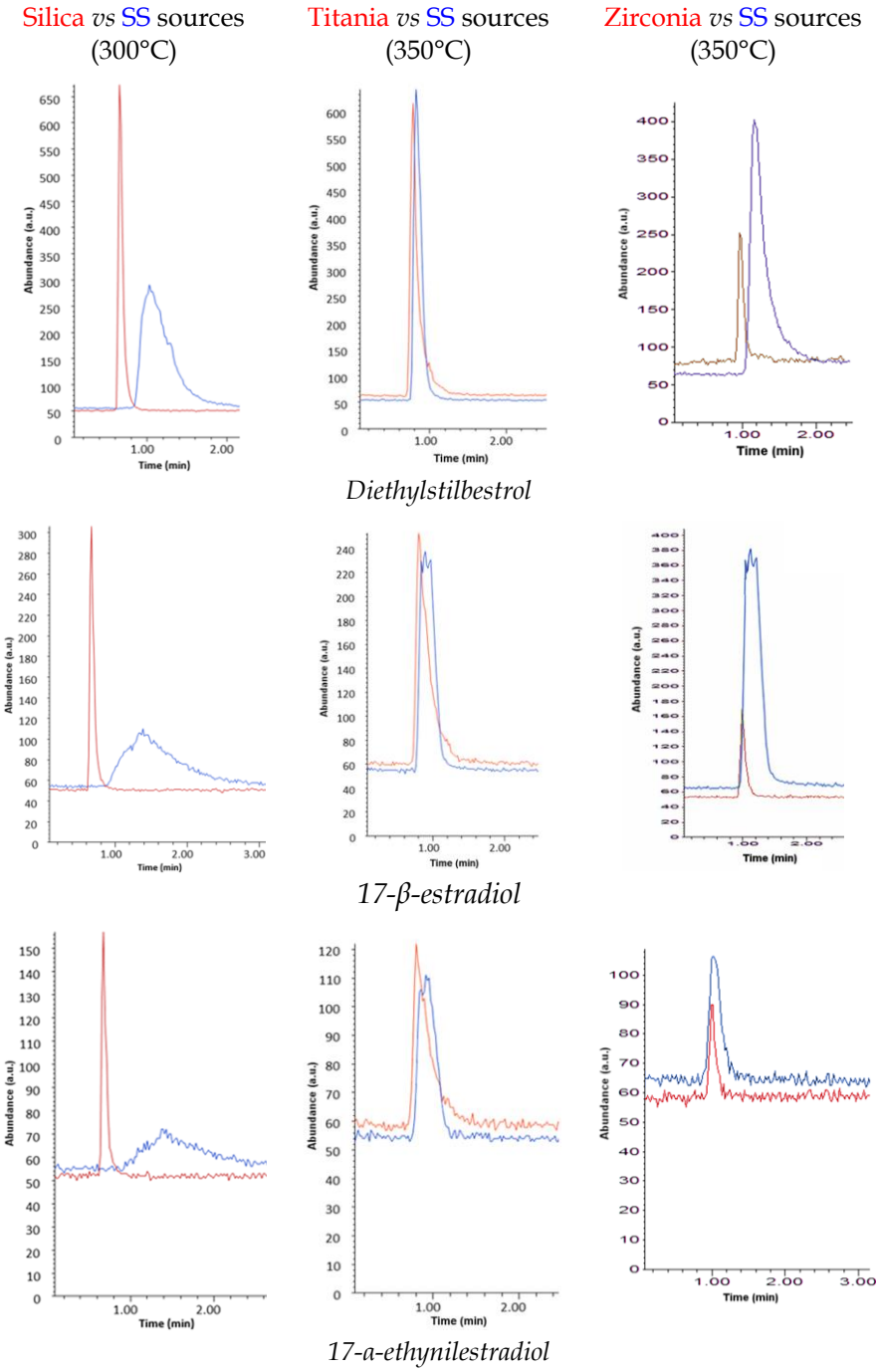

Figure 4.29 Hormones peaks comparison between coated and SS ion sources

Noticeable improvements in the detection of the investigated compounds were achieved for both PAHs and hormones by using the silica-based ion source and by operating at the ion source temperature of 300 °C.

The use of sol-gel coatings allowed to improve the inertness of the ion source, thus reducing both absorption phenomena and chemical reactivity of the SS surface, by limiting the presence of metal active sites able to interact with the analytes. These finding are in accordance with previous studies dealing with the application of inert sol-gel materials on SS components of MS instruments [64-66].

Noteworthy improvement in terms of repeatability was achieved, especially for the hormones analysis: RSD% values always lower than 9 and 13% were obtained both for PAHs and hormones respectively, for all the investigated temperatures, whereas the SS source was characterized by RSD% up to 63% at 350°C. Taking into account that the experiments were carried out by using two ion sources on different days the results achieved by using silica-based coating can be considered satisfying.

Owning to the improvements achieved in terms of peak shape, also the signal-to-noise ratios showed a great increase. Sharp peaks were characterized by high S/N ratio: by operating at 300 °C, the silica-based coating provided S/N ratios up to 16 times higher than those achieved by using the uncoated ion source.

S/N ratios can be used in order to calculate the LODs of the developed method. The achieved results are reported in **Table 4.4**.

Table 4.4 Detection limits (ng/µl) for PAHs and hormones using the Direct-EI LC-MS technique

	LOD (ng/µl)					
	SS (300°C)	SS (350°C)	Silica (300°C)	Silica (350°C)	Titania (350°C)	Zirconia (350°C)
naphtalene	0.4	0.3	**0.3**	0.4	0.7	0.3
indeno 1,2,3 (c-d)pyrene	1.9	1.1	**0.1**	0.2	3.0	3.4
mestranol	2.1	1.6	**0.8**	1.2	0.5	1.0
diethylstilbestrol	1.3	0.8	**0.4**	0.8	0.5	2.1
17-β-estradiol	3.6	1.3	**0.9**	1.0	1.4	2.8
17-a-ethynilestradiol	18	5.3	**2.7**	4.3	5.0	9.7

Taking into account that the reported LOD values were calculated by using standard solutions, further studies will be carried out to evaluate the performances of the silica-based ion source using real matrices.

Finally, as for the ion source cleaning, no problems were observed when cleaning with different solvents was performed, whereas strong mechanical polishing could damage the surface of the coating.

4.4 Conclusions

The Direct-EI LC-MS interface can be considered an interesting approach for coupling LC-MS and electron ionization. However, since strong interactions are present between the SS surface of the ion source and compounds characterized by high molecular weight and polarity, peak broadening, tailing, signal suppression and thermal decomposition can occur.

In this research study, the use of sol-gel technology was proposed in order to develop inorganic coatings able to increase the chemical inertness of the ion sources. The main challenges were related to both the high thermal and mechanical resistance, as well as to the strong adhesion of the coating to the metal surface.

Three materials based on silica, titania and zirconia were sprayed in the ion source section devoted to the vaporization process. The coatings were characterized in terms of chemical composition, *via* IR analysis, and morphology, by using ESEM. The optimized coated sources were tested for the Direct-EI LC-MS determination of PAHs and the hormones. Three peak parameters were investigated by working at different ion source temperatures.

Excellent performances were achieved by using the silica-based coating both in terms of peak shape and intensity, if compared to the bare material and the other coatings. Moreover, the use of the silica-coated ion source showed an excellent improvement in terms of repeatability, with RSD% <9% for PAHs and <11% for hormones respectively, at 300°C.

Finally, all the investigated analytes could be detected at lower operating temperatures compared to the bare SS ion source.

By contrast, titania- and zirconia-coatings did not provide significant improvements compared to the SS ion source.

Recently, the research group of A. Cappiello developed a new interface, based on the Direct-EI LC-MS, called liquid-EI [67], where the vaporization of solutes and mobile phase takes place at atmospheric pressure into a specifically designed region, called "vaporization microchannel", before entering the high-vacuum ion source. Based on the results of the silica-coated ion source, a fused silica liner, placed inside the vaporization microchannel, acts as an inert vaporization surface speeding up the gas-phase conversion of low volatile molecules, thus reducing the possibility of any memory effect.

4.5 Acknowledgements

Thanks to the UNIURB LC-MS, research group, Department of Pure and Applied Sciences for the collaboration and the hospitality: Prof. A. Cappiello, Prof. P. Palma, Prof. G. Famiglini, Dr. V. Termopoli and Dr. L. Magrini. Thanks also to Agilent Technology for providing the prototype and the SS ion sources.

4.6 References

[1] T. Kind, O. Fiehn, *Advances in structure elucidation of small molecules using mass spectrometry*, Bioanal. Rev., 2 (2010) 23–60.

[2] R. Aebersold, M. Mann, *Mass-spectrometric exploration of proteome structure and function*, Nature, 537 (2016) 347–355.

[3] A. Politis, F. Stengel, Z. Hall, H. Hernández, A. Leitner, T. Walzthoeni, C.V. Robinson, R. Aebersold, *A mass spectrometry–based hybrid method for structural modeling of protein complexes*, Nat. Methods, 11 (2014) 403–406.

[4] J.R. Edwards, H. Ruparel, J. Ju, *Mass-spectrometry DNA sequencing*, Mutat. Res. 573 (2005) 3-12.

[5] A. El-Aneed , A. Cohen, J. Banoub, Mass Spectrometry, *Review of the Basics: Electrospray, MALDI, and Commonly Used Mass Analyzers*, Appl. Spectrosc. Rev., 44 (2009) 210-230.

[6] D.R. Ifa, C. Wu, Z. Ouyang, R.G. Cooks, *Desorption electrospray ionization and other ambient ionization methods: current progress and preview*, Analyst, 135 (2010) 669–681.

[7] J.H. Gross, *Direct analysis in real time - a critical review on DART-MS*, Anal. Bioanal. Chem., 406 (2014) 63-80.

[8] A.J. Dempster, *A new Method of Positive Ray Analysis,* Phys. Rev., 11 (1918) 316–325.

[9] Wiley Registry 11th Edition / NIST 2017 Mass Spectral Library, by Wiley, NIST, September 2017.

[10] M.R. Meyer, F.T. Peters, H.H. Maurer, *Automated mass spectral deconvolution and identification system for GC-MS screening for drugs, poisons, and metabolites in urine*, Clin. Chem., 56 (2010) 575-84.

[11] S.J. Stout, A.R. daCunha, *Simplified Moving-Belt Interface for Liquid Chromatography/Mass Spectrometry*, Anal. Chem., 57 (1985) 1783-1786.

[12] W.V. Ligon, B.S. Dorn, *Particle Beam Interface for Liquid Chromatography/Mass Spectrometry*, Anal. Chem., 62 (1990) 2573-2580.

[13] C.E. Kientz, A.G. Hulst, A.L. De Jong, E.R.J. Wils, *Eluent Jet Interface for Combining Capillary Liquid Flows with Electron Impact Mass Spectrometry*, Anal. Chem., 68 (1996) 675-681.

[14] R.J. Dijkstra, B.L.M. Van Baar, C.E. Kientz, W.M.A. Niessen, *An eluent–jet interface for chemical ionization mass spectrometry and coupling of microcolumn liquid chromatography with electron ionization mass spectrometry*, Rapid. Commun. Mass Sp., 12 (1998) 5–10.

[15] A. Amirav, O. Granot, *Liquid chromatography mass spectrometry with supersonic molecular beams*, J. Am. Soc. Mass Spectrom., 11 (2000) 587–591.

[16] A. Cappiello, M. Balogh, G. Famiglini, F. Mangani, P. Palma, *An efficient liquid chromatography--mass spectrometry interface for the generation of electron ionization spectra*, Anal. Chem., 72 (2000) 3841-3846.

[17] A. Cappiello, G. Famiglini, F. Mangani, P. Palma, *A Simple Approach for Coupling Liquid Chromatography and Electron Ionization Mass Spectrometry*, J. Am. Soc. Mass. Spectrom., 13 (2002) 265–273.

[18] A. Cappiello, G. Famiglini, P. Palma, A. Siviero, *Liquid Chromatography-Electron Ionization Mass Spectrometry: fields of application and evaluation of the performance of a Direct-EI Interface*, Mass Spectrom. Rev., 24 (2005) 978– 989.

[19] A. Cappiello, G. Famiglini, F. Mangani, P. Palma, A. Siviero, *Nano-high-performance liquid chromatography–electron ionization mass spectrometry approach for environmental analysis*, Anal. Chim. Acta, 493 (2003) 125–136.

[20] A. Cappiello, G. Famiglini, E. Pierini, P. Palma, H. Trufelli, *Advanced Liquid Chromatography-Mass Spectrometry Interface Based on Electron Ionization*, Anal. Chem. 79 (2007) 5364-5372.

[21] J.J. Brocks, J.M. Hope, *Tailing of chromatographic peaks in GC-MS caused by interaction of halogenated solvents with the ion source*, J. Chromatogr. Sci., 52 (2014) 471-475.

[22] W. D'Autry, K. Wolfs, S. Yarramraju, A. Van Shepdael, J. Hoogmartens, E. Adams, *Characterization and improvement of signal drift associated with electron ionization quadrupole mass spectrometry*, Anal. Chem., 82 (2010) 6480-6486.

[23] L. Magrini, G. Famiglini, P. Palma, V. Termopoli, A. Cappiello, *Boosting the detection potential of liquid chromatography-electron ionization mass*

spectrometry using a ceramic coated ion source, J. Am. Soc. Mass Spectrom., 27 (2015) 153-160.

[24] D. Wang, G.P. Bierwagen, *Sol–gel coatings on metals for corrosion protection*, Prog. Org. Coat., 64 (2009) 327–338.

[25] D. Balgude, A. Sabnis, *Sol–gel derived hybrid coatings as an environment friendly surface treatment for corrosion protection of metals and their alloys*, J. Sol–Gel Sci. Technol., 64 (2012) 124–134.

[26] N. Kumar, A.Jyothirmayi, K.R.C. Soma Raju, R. Subasri, *Effect of functional groups (methyl, phenyl) inorganic–inorganic hybrid sol–gel silica coatings on surface modified SS316*, Ceram. Int., 38 (2012) 6565–6572.

[27] E. Certhoux, F. Ansart, V. Turq, J.P. Bonino, J.M. Sobrino, J. Garcia, J. Reby, *New sol–gel formulations to increase the barrier effect of a protective coating against the corrosion of steels*, Prog. Org. Coat., 76 (2013) 165– 172.

[28] T. P. Chou, C. Chandrasekaran, S. Limmer, C. Nguyen, G. Z. Cao, *Organic-inorganic sol-gel coating for corrosion protection of stainless steel*, J. Mater. Sci. Lett., 21 (2002) 251– 255.

[29] D.C.L. Vasconcelos, J.A.N. Carvalho, M. Mantel, W.L. Vasconcelos, *Corrosion resistance of stainless steel coated with sol-gel silica*, J. Non-Cryst. Solids, 273 (2000) 135-139.

[30] S.M. Hosseinalipour, A. Ershad-langroudi, A. Nemati Hayati, A.M. Nabizade-Haghighi, *Characterization of sol–gel coated 316L stainless steel for biomedical applications*, Prog. Org. Coat., 67 (2010) 371–374.

[31] T.P. Chou, C. Chandrasekaran, S.J. Limmer, S. Seraji, Y. Wu, M.J. Forbess, C. Nguyen, G.Z. Cao, *Organic-inorganic hybrid coatings for corrosion protection*, J. Non-Cryst. Solids, 290 (2001) 153-162.

[32] T. Nakagawa, M. Soga, *A new method for fabricating water repellent silica films having high heat-resistance using the sol-gel method*, J. Non-Cryst. Solids, 260 (1999) 167-174.

[33] N. Barati, M.A. Faghihi Sani, Z. Sadeghian, H. Ghasemi, *Titania Nanostructured Coating for Corrosion Mitigation of Stainless Steel*, Prot. Met. Phys. Chem. S., 50 (2014) 371–377.

[34] M. Atik, P. Neto, L.A. Avaca, M.A. Aegerter, *Sol-gel thin films for corrosion protection*, Ceram. Int., 21 (1995) 403-406.

[35] H. Li, K. Liang, L. Mei, S. Gu, S.Wang, *Corrosion Protection of Mild Steel by Zirconia Sol-Gel Coating*, J. Mater. Sci. Lett., 20 (2001) 1081-1083.

[36] M. Careri, L. Elviri, A. Lorenzi, A. Mangia, A. Penna, G. Predieri, *Improved silica xerogel film processing for MALDI-TOF-MS quantitative analysis of peptides and small molecules*, J. Sol-Gel Sci. Technol., 60 (2011) 359-365.

[37] F. Bianchi, M. Mattarozzi, P. Betti, F. Bisceglie, M. Careri, A. Mangia, L. Sidisky, S. Ongarato, E. Dalcanale, *Innovative cavitand-based sol-gel coatings for the environmental monitoring of benzene and chlorobenzenes via solid-phase microextraction*, Anal. Chem., 80 (2008) 6423-6430.

[38] F. Bianchi, F. Bisceglie, M. Careri, S. Di Berardino, A. Mangia, M. Musci, *Innovative sol-gel coatings for solid-phase microextraction: development of fibers for the determination of polycyclic aromatic hydrocarbons at trace level in water*, J. Chromatogr. A, 1196-1197 (2008) 15-22.

[39] M. Mattarozzi, F. Bianchi, F. Bisceglie, M. Careri, A. Mangia, G. Mori, A. Gregori, *Planar solid-phase microextraction-ion mobility spectrometry: a diethoxydiphenylsilane-based coating for the detection of explosives and explosive taggants*, Anal. Bioanal. Chem., 399 (2011) 2741-2746.

[40] R. Cheraghali, S.H. Moradi, M. Ghoranneviss, P. Aberomand Azar, S.A. Khorrami, *Etching of 316L Stainless Steel by Different Chemical Etchant Solutions for the Growth of Carbon Nanotubes by Thermal Chemical Vapour Deposition*, Asian J. Chem., 23(2011) 2833-2836.

[41] L. Li, V. Breedveld, D.W. Hess, *Creation of superhydrophobic stainless steel surfaces by acid treatments and hydrophobic film deposition*, ACS Appl. Mater. Inter. 4 (2012) 4549-4556.

[42] M. Atik, P. De Lima Neto, L. A. Avaca, M. A. Aegerter, J. Zarzycki, *Protection of 316L stainless steel against corrosion by SiO_2 coatings*, J. Mater. Sci. Lett., 13 (1994) 1081-1085.

[43] N. Barati, M.A. Faghihi Sani, H. Ghasemi, Z. Sadeghian, S.M.M. Mirhoseini, *Preparation of uniform TiO2 nanostructure film on 316L stainless steel by sol–gel dip coating*, Appl. Surf. Sci., 255 (2009) 8328–8333.

[44] H. Cheraghi, M. Shahmiri, Z. Sadeghian, *Corrosion behavior of TiO_2–NiO nanocomposite thin films on AISI 316L stainless steel prepared by sol–gel method*, Thin Solid Films, 522 (2012) 289–296.

[45] T. P. Chou, C. Chandrasekaran, G. Z. Cao, *Sol-gel-derived hybrid coating for corrosion protection,* J. sol-gel Sci. Techn., 26 (2003) 321-327.

[46] M. Houmard, E.H.M. Nunes, D.C.L. Vasconcelos, G. Berthomé, J.C. Joud, M. Langlet, W.L. Vasconcelos, *Correlation between sol–gel reactivity and wettability of silica films deposited on stainless steel*, Appl. Surf. Sci., 289 (2014) 218–223.

[47] H. Aguiar, J. Serra, P. González, B. León, *Structural study of sol–gel silicate glasses by IR and Raman spectroscopies*, J. Non-Cryst. Solids, 355 (2009) 475–480.

[48] J. Niu, D. Yang, J. Sha, J.N. Wang, M. Li, *Infrared spectra of silicon nanowires*, Mater. Lett., 61 (2007) 894–896.

[49] P. Innocenzi, Infrared spectroscopy of sol–gel derived silica-based films: a spectra-microstructure overview, J. Non-Cryst. Solids, 316 (2003) 309–319.

[50] D.C.L. Vasconcelos, E.H.M. Nunes, A.C.S. Sabioni, J.C.D. da Costa, W.L. Vasconcelos, *Structural Characterization and Corrosion Behavior of Stainless Steel Coated with Sol-gel Titania*, J. Mater. Eng. Perf., 21 (2012) 411–417.

[51] D.C.L. Vasconcelos, E.H.M. Nunes, A.C.S. Sabioni, P.M.P. Vasconcelos, W.L. Vasconcelos, *Optical characterization of 316L stainless steel coated with sol–gel titania*, J. Non-Cryst. Solids, 358 (2012) 3042–3047.

[52] F. L. Perdomo, P. De Lima-Neto, M.A. Aegerter, L.A. Avaca, *Sol-Gel Deposition of ZrO2 Films in Air and in Oxygen-Free Atmospheres for Chemical Protection of 304 Stainless Steel: A Comparative Corrosion Study*, J. Sol-Gel Sci. Techn., 15 (1999) 87–91.

[53] E. Nouri, M. Shahmiri, H.R. Rezaie, F. Talayian, *Investigation of structural evolution and electrochemical behaviour of zirconia thin films on the 316L stainless steel substrate formed via sol–gel process*, Surf. Coat. Techn., 205 (2011) 5109–5115

[54] M. Atik, C. R.'Kha, P. De Lima Neto, L. A. Avaca, M. A. Aegerter, J. Zarzycki, *Protection of 316L stainless steel by zirconia sol-gel coatings in 15% H_2SO_4 solutions*, J. Mater. Sci. Lett.., 14 (1995) 178-181.

[55] ATSDR. *Toxicological profile for polycyclic Aromatic Hydrocarbons (PAHs), update.* Agency for Toxic Substances and Drug Registry (ATSDR), Chapt. 1, Washington, DC, USA, 1995.

[56] https://archive.epa.gov/epawaste/hazard/wastemin/web/pdf/pahs.pdf

[57] M. Bates, P. Bruno, M. Caputi, M. Caselli, G. de Gennaro, M. Tutino, *Analysis of polycyclic aromatic hydrocarbons (PAHs) in airborne particles by direct sample introduction thermal desorption GC/MS*, Atmos. Environ., 42 (2008) 6144–6151.

[58] S.C.C. Lung, C.H. Liu, *Fast analysis of 29 polycyclic aromatic hydrocarbons (PAHs) and nitro-PAHs with ultrahigh performance liquid chromatography-atmospheric pressure photoionization-tandem mass spectrometry*, Sci. Rep., 5 (2015), article 12992, doi:10.1038/srep12992.

[59] R. López-Serna, S. Pérez, A. Ginebreda, M. Petrović, D. Barceló, *Fully automated determination of 74 pharmaceuticals in environmental and waste waters by online solid phase extraction–liquid chromatography-electrospray–tandem mass spectrometry*, Talanta, 83 (2010) 410–424.

[60] A. C. Naldi, P. B. Fayad, M. Prévost, S. Sauvé, *Analysis of steroid hormones and their conjugated forms in water and urine by on-line solid-phase extraction coupled to liquid chromatography tandem mass spectrometry*, Chem. Cent. J., 10:30 (2016) doi: 10.1186/s13065-016-0174.

[61] N.H. Torres, M.M. Aguiar, L.F.R. Ferreira, J.H.P. Américo, A.M. Machado, E.B. Cavalcanti, V.L. Tornisielo, *Detection of hormones in surface and drinking water in Brazil by LC-ESI-MS/MS and ecotoxicological assessment with Daphnia magna*, Environ. Monit. Assess., 187: 379 (2015), doi: 10.1007/s10661-015-4626-z.

[62] M. Henriques, V. Vale Cardoso, A. Mourão Rodrigues, E. Ferreira, M. João Benoliel, C.M.M. Almeida, *Simultaneous Determination of Ten Endocrine Hormone Disrupters in Water Using SPE/LC-(ESI)MS-MS*, J. Water. Resource Prot., 2 (2010) 818-829.

[63] G.A. Smith, A.D. Zaffiro, M.L. Zimmerman, D. J. Munch, *EPA Method 539: Determination of Hormones in Drinking Water by Solid Phase Extraction (SPE) and Liquid Chromatography Electrospray Ionization Tandem Mass Spectrometry (LC-ESI-MS/MS)*, https://nepis.epa.gov/Exe/ZyPDF.cgi/P100J76V.PDF?Dockey=P100J76V.PDF

[64] J.J. Brocks, J.M. Hope, *Tailing of chromatographic peaks in GC-MS caused by interaction of halogenated solvents with the ion source*, J. Chromatogr. Sci., 52 (2014) 471-475.

[65] W. D'Autry, K. Wolfs, S. Yarramraju, A. Van Shepdael, J. Hoogmartens, E. Adams, *Characterization and improvement of signal drift associated with electron ionization quadrupole mass spectrometry*, Anal. Chem., 82 (2010) 6480-6486.

[66] R.D. Brittain, M. Wang, US 5633497 A, Varian Associates, Inc, 1997.

[67] V. Termopoli, G. Famiglini, P. Palma, M. Piergiovanni, A. Cappiello, *Atmospheric Pressure Vaporization Mechanism for Coupling a Liquid Phase with Electron Ionization Mass Spectrometry*, Anal. Chem. 89 (2017) 2049−2056.

Chapter 5

New Materials for Desorption Electrospray Ionization-High Resolution Mass Spectrometry: Determination of New Psychoactive Substances

5.1 Introduction

5.1.1 New Psychoactive Substances

New psychoactive substances (NPS) are a very large group of drugs of abuse not fully controlled by international conventions. Being considered as a major threat to the public health, the United Nation Office of Drugs and Crimes (UNODC) and the European Monitoring Centre for Drugs and Drug Addiction (EMCDDA) are paying increasing attention toward their monitoring [1]. *Designer drugs* is the term that was traditionally associated to synthetic drugs: now it has been widen to include psychoactive substances that mimic the effects of the controlled illicit drugs (*recreational drugs*), thus circumventing common controls.

Most of the NPS were synthesized and patented in the second half of XX century, especially between the '60s and the '70s, by pharmaceutical societies: they are able to produce effects similar to those created by known illicit substances through slight chemical modification of their chemical structure. On the market they are known as *legal highs*, *herbal highs*, *research chemicals* or *bath salts*. By the end of 2016, EMCDDA monitored on the EU market more than 620 new psychoactive substances, 66 of which were detected for the first time in Europe in 2016 [2]. These substances are not controlled by international drug laws and include synthetic cannabinoids, stimulants, opioids and benzodiazepines (**Figure 5.1**). In most cases, they are marketed as *legal replacements* for illicit drugs, being labelled as *not for human consumption*.

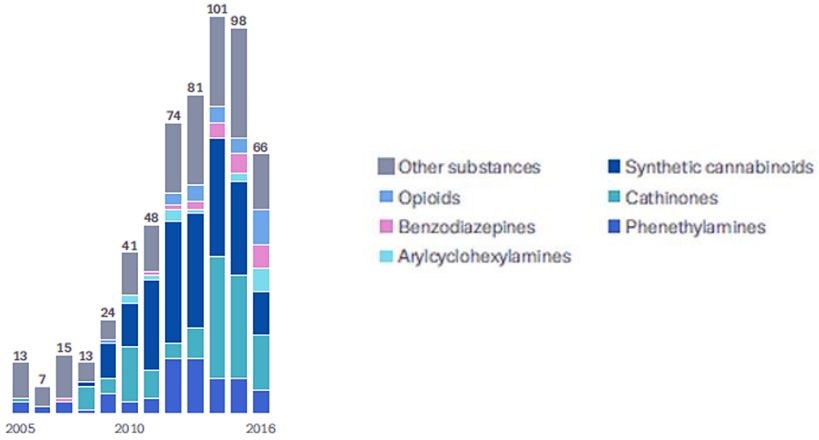

Figure 5.1 number and categories of new psychoactive substances notified to the EU Early Warning System for the first time, in the 2005-2016 period [2].

In 2016, new drugs were reported to the EU Early Warning System at a rate of one per week: among them, the new psychoactive substances, notably synthetic cathinones and cannabinoids, are establishing a foothold in the drug market, being very cheap and widespread through chronic drug users. To overcome this phenomenon, several European countries have introduced blanket bans, extended or adapted existing laws, and devised new legislation to target both the producers and retailers.

NPS are mostly produced in bulk quantities by chemical and pharmaceutical companies in China as intermediate products of pharmaceuticals, then they are shipped to Europe, where they are processed into the final products, packaged and sold. Reported studies [2] have demonstrated their increased production in clandestine European laboratories.

The last decade was characterized by a noticeable growth of online drug marketplaces, leading to a parallel market.

The accessibility to the so-called deep-web is attracting great interest by both inspection bodies and institutions, due to the presence of several illegal activities such as drug and human trafficking. Various strategies are used to conceal both transactions and the physical locations of servers, thus including browsers, such as Tor and I2P, able to hide the computer's internet protocol address, cryptocurrencies, such as bitcoins, and encrypted communication between sellers and customers. Most sales in the dark-net markets are drug-related: data from 2013 suggested that drug sales were responsible for more than 90% of the total economic revenue of deep-web marketplaces.

One of the major issue of the NPS is the lack or the dearth of information about their adverse effects that usually include anxiety, paranoia, hallucinations, seizures, hyperthermia and cardiotoxicity [3]. Moreover, compared to the other drugs, the age of the consumers is one of the most alarming data: the consumers are mostly teenagers in school age (**Figure 5.2**) [2].

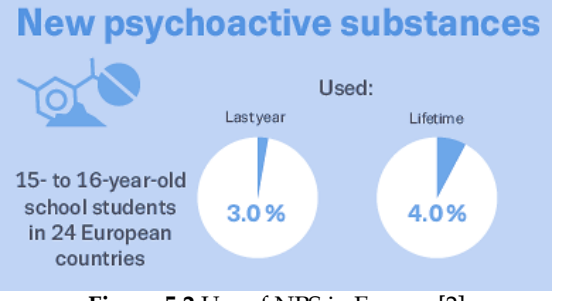

Figure 5.2 Use of NPS in Europe [2]

Since the NPS class encloses a wide range of compounds, the division in sub-classes can be useful in order to summarize the properties and the effects of the different drugs of abuse:

1. Synthetic cannabinoids

These substances mimic the effects of Δ-9-tetrahydrocannabinol (THC) that is the major responsible for the psychoactive effect of cannabis. Since 2008, producers in Europe imported bulk powders of synthetic cannabinoids mixed with dried plant material in order to create hundreds of different *legal high* products, sold as *legal replacements* for cannabis or *herbal smoking mixtures*. Synthetic cannabinoids are the largest group of new substances monitored by the EMCDDA, thus including compounds characterized by very different structures: 169 synthetic cannabinoids were reported since 2008, 11 of them in the sole 2016 and 24 in 2015 [2]. In addition, forensic data suggest that the majority of the synthetic cannabinoids in powder are processed and packaged in Europe. Whereas cannabis and THC are controlled by international drug control treaties and laws, synthetic cannabinoids are subject to controls only at the national level: they are considered legalized in several countries, thus allowing their public distribution, especially on web markets.

HU-210 and HU-211 (**Figure 5.3**) enantiomers are synthetic analogues of THC, thus they are regarded as *classical cannabinoids*. The main issue of these NPS is the considerably high effect, at least 100 times higher than THC.

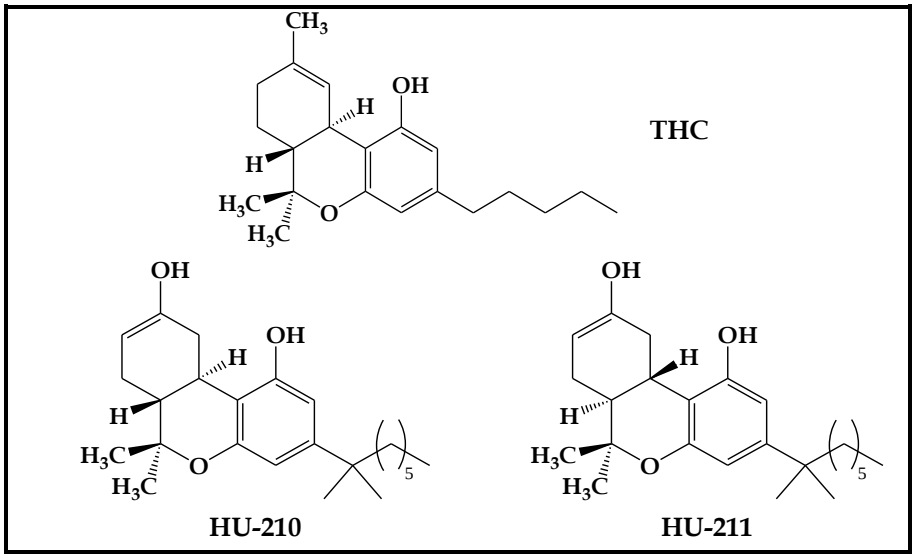

Figure 5.3 Structure of HU-210

Other synthetic cannabinoids, unrelated to THC and structurally different, have also emerged on the market.

Cyclohexylphenols or 3-arylcyclohexanols (known as CP compounds) are *non-classical cannabinoids*, developed as potential analgesics in the 1980s. CP-47,497 showed an activity from 3 to 28 times higher compared the natural cannabis. An emergence in several countries was reported for the abuse of CP-47,497 and CP-47,497-C8 (**Figure 5.4**).

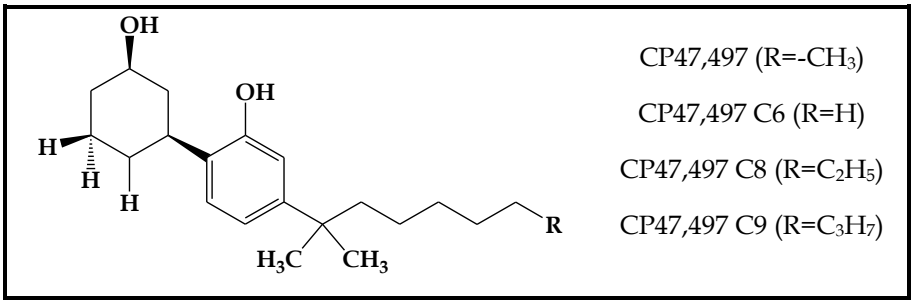

Figure 5.4 Structure of most common non-classical cannabinoids

The JWHs are aminoalkylindole and phenylacetylindoles compounds (**Figure 5.5**) developed J.W. Huffman (the drugs have been named by using the initials of their discoverer) during his research studies focused on metabolites and analogues of THC. JWH-018 is the most widespread synthetic cannabinoid, considered three times more potent than THC, acting as a cannabinoid agonist at both the CB1 and CB2 receptors. The side-alkyl chain of the JWHs strongly affects their effect: compared to JWH-018, JWH-019, the hexyl homologue is slightly less potent, whereas JWH-073 (butyl homologue) and JWH-020 (heptyl- homologue) are characterized by a noticeable loss of activity.

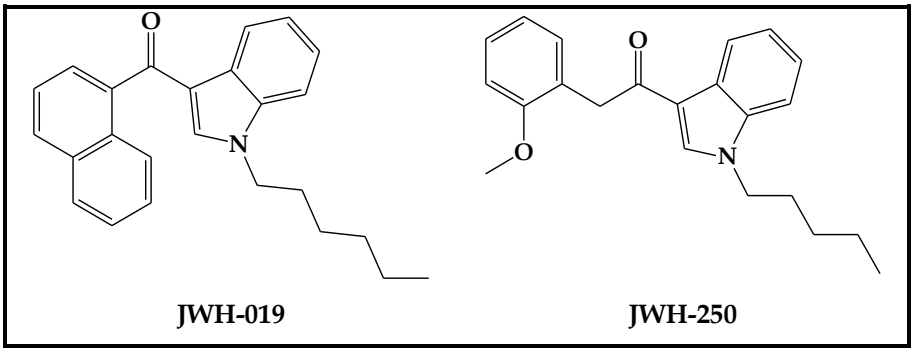

Figure 5.5 Structure of aminoalkylindole (JWH-018) and phenylacetylindoles (JWH-250)

Data regarding human toxicity of synthetic cannabinoids are limited: as in the case of several other NPS, these drugs are sold in mixture containing several chemicals at different concentrations: under these conditions, it is very hard to assess substance-specific effects. The knowledge on the toxicity is related to scientific reports and clinical observations: cardiovascular problems [4,5], psychological disorders [6,7], suicide tendencies [8], and carcinogenic potential of drug's metabolites [9] have been reported.

2. Synthetic cathinones

These compounds are chemically related to cathinone, a natural stimulant extracted from *Catha edulis*. Synthetic cathinones have similar effects to the phenethylamine drugs (such as amphetamine and methamphetamine), but, according to EMCCDA, they are characterized by lower potency. They present of a β-keto group on the side chain of the phenethylamines (**Figure 5.6**).

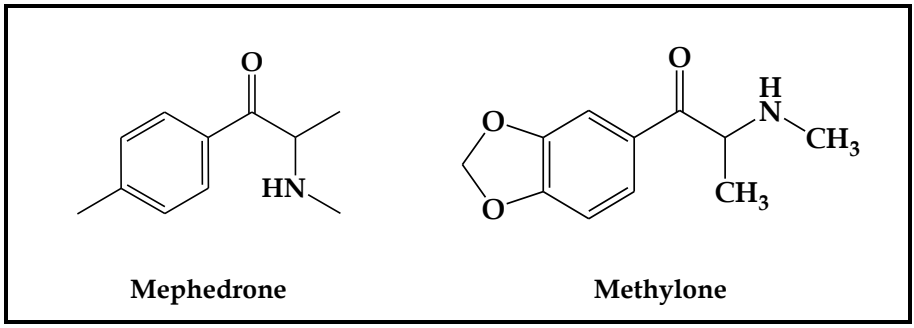

Figure 5.6 Structure of the two most common synthetic cathinone: mephedrone and methylone

Synthetic cathinones are the second largest group of new drugs monitored by the EMCDDA: 118 are the compounds identified until now, with 14 compounds detected for the first time in 2016. In 2015, they accounted for one third of the total number of seizures, i.e. over 1.8 tons of drugs, generally in powder form.

4-methylmethcathinone or mephedrone (4-MMC) was first synthesized in 1929 but it was rediscovered in 2007, when several reports of its use as psychoactive drug emerged, first in Israel and then in other countries, such as Australia, Scandinavia, Ireland and the United Kingdom [10]. Up to 2010, methylone and mephedrone were identified as the most common substances of use in this group in Europe. Mephedrone was then declared illicit in several

countries, thus including EU and USA, therefore several chemically-related compounds, such as 2-MMC and 3-MMC were developed and dealt in most countries as legal substitutes.

Some synthetic cathinones have been patented as pharmaceuticals: methylone was proposed as antidepressant and antiparkinsonian agents [11], whereas diethylcathinone and pyrovalerone were used as appetite suppressants, before assessing abuse and dependency in chronic users [12].

These compounds are present as mixture in several products: they are sold, in both powders or pills and capsules, as *research chemicals, plant food*, *bath salts*, *glass cleaner, meow meow* or *ecstasy*. They can be assumed *via* ingestion, especially mixed with alcohol, or injected in the bloodstream.

Few reports on the toxicity of synthetic cathinones exist, mostly related to user reports and clinical observations. The latter reported that the most common symptom include cardiac and psychiatric problems, especially related to neurological agitation, ranging from mild agitation to severe psychosis [13].

Studies of patients under the influence of mephedrone have demonstrated the presence of sympathomimetic effects, thus including tachycardia and hypertension, as well as psychoactive effects, usually related to amphetamine derivatives abuse [14]. Additional adverse effects are associated to central nervous, nasal/respiratory and cardiovascular systems. Several deaths related to the abuse of synthetic cathinones have been reported.

In Italy, the annual parliament relation on drugs of abuse of the *Dipartimento Politiche Antidroga* highlighted that 1.2% of the students in the 15-19 age, assumed mephedrone or related drugs at least once.

3. Ketamine and ketamine derivatives

Ketamine (**Figure 5.7**) was synthesized as an anaesthetic in 1962 and patented in 1963 in Belgium as a medical alternative to phencyclidine. The use as new psychoactive substance dates back to the 1980s and 1990s. It is frequently sold as *ecstasy* or under the street names *of K, ket, special K, kit kat, cat valium, zer'* and others [15]. Pharmaceutical preparations of ketamine include solutions, powders and capsules.

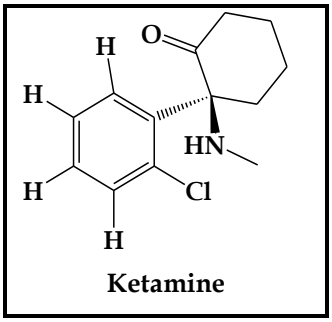

Figure 5.7 Chemical structure of Ketamine

Ketamine and phencyclidine have similar biological actions: they are able to both affect different central neuronal activities [16,17] and stimulate the cardiovascular system [18], thus increasing the heart rate and blood pressure and leading to tachycardia and hypertension. Moreover, neurotoxicity of ketamine substances can be increased by assuming other substances, thus including phencyclidine (known as *angel dust*) and alcohol [19].

Psychological dependence, anxiety, changes of perception and persistent impairment of attention and recall have been reported [20]. Physiological effects include visual and auditory anomalies [21] and impairment of motor functions [21]. Chronic ketamine use has been reported to result in potential lasting memory and cognitive dysfunctions [19].

5.1.2 NPS Abuse in Italy

In Italy, from the 2009, the *Sistema Nazionale di Allerta Precoce per le droghe* of the *Dipartimento Politiche Antidroga, Presidenza del Consiglio dei Ministri*, has performed a constant monitoring on NPS occurrence, by cooperating with the *Sistema di Allerta* (labs, emergency rooms, hospitals, toxicological studies, law enforcements…) and the EMCDDA. This collaboration has led to the registration of 280 NPS and reported 70 acute poisoning cases related to new psychoactive drug assumption [22].

A radical modification of the legislation was performed in 2011, thus introducing the scheduling of cathinones and synthetic cannabinoids of the napthoylindole and phenylacetylindole families as illegal classes of substances, as opposed to individual substances [23-26].

In 2017, the annual relation of the Parliament on drug addiction of the *Dipartimento Politiche Antidroga* highlighted that 33.5% of the interviewees in

the 15-64 age admitted the use of psychoactive drugs at least once, whereas 10% reported the abuse in the current year. These percentage increases noticeably when the class is restricted to the young population, in the 15-34 age range. The percentage related to the NPS abuse within the year is 1.4%, increasing to 2.5% in the restricted class.

5.1.3 *Driving under the Influence of Drugs: an EU Challenge*

The mobility provided by road transport is one of the most important benefit in the modern world but it is affected by a dramatic drawback: more than 28 000 people die on European roads each year. Many of the accidents are caused by drivers whose performance were altered by the use of psychoactive substances, thus including alcohol, illicit drugs and psychoactive pharmaceuticals.

When the Action Programme was introduced in EU in 2003, it was estimated that about 25% of fatalities on European roads were related to the use of alcohol, but comparable studies regarding the abuse of illicit drugs or psychoactive substances were not present.

For this reason, in 2006, the DRUID (Driving under the Influence of Drugs, Alcohol and Medicines) project was carried out, with the aim of estimating the size of the problem and examining the possible countermeasures. The prevention of driving under the influence of drugs was included as one of the key actions in the recent EU drugs action plan for the 2013–2016 period.

As reported in the circular letter 300/A/3213/15/109/421 of 27th of April 2015, driving under the influence of psychoactive substances is one of the major issues for the EU, which required the attention of all the Member States, in order to reduce the occurrence of road incidents for the 2010-2020 period.

In Italy, excellent achievements have been obtained in terms of control tests for alcohol abuse, by contrast the assessment of drug intake while driving is still considered very challenging.

In order to comply with the EU standards that require strictly road safety controls of drivers, new organizational arrangements were adopted in order to both increase and improve the control activities, thus including the deployment of the State Police labs for the analyses of sampled body fluids.

A key issue is the development of both new sampling methods to be performed *on the road* during routine control activities, as well as new rapid

screening methods able to assess the presence of drugs in body fluids at trace levels.

By the beginning of 2015, road controls are performed by the State Police in collaboration with clinicians in order to assess the presence of both physical and psychological alterations of drivers, by using qualitative tests able to detect drugs of abuse in human oral fluid (**Figure 5.8**).

Figure 5.8 Quantisal™ Oral Fluid Collection Device and Alere DDS2 mobile test system used by the State Police

In case of positive results, adjunctive samples are collected and sent to the *Centro Ricerche di Laboratorio e Tossicologia Forense della Polizia di Stato*, where they are analyzed by a using a proper GC-MS method.

Several studies have been performed in order to demonstrate the suitability of road tests for the detection of drugs of abuse in oral fluids. The main project, performed between 2010 and 2011, was called TOXTEST. It involved 12 Italian cities, with the aim to assess the performances of 4 commercial kits for the determination in oral fluids of the most commonly used drugs of abuse, i.e. opioids, cocaine, benzodiazepines, amphetamine, methamphetamine and cannabinoids.

The results achieved proved that the device *Drugtest 5000* was characterized by the best performances in terms of limits of detection and reliability. However, it has to be pointed out that the range of detectable substances by using these devices is very limited, since only the most common drugs of abuse are monitored, whereas the new psychoactive drugs are undetected.

5.1.4 Sample Collection and Pretreatment

Saliva is a biological fluid secreted by the salivary glands, which composition is made by over 99% of water, whereas the remaining 1% comprises electrolytes (especially sodium, potassium, calcium, chloride, magnesium, bicarbonate, and phosphate), mucus, white blood cells, epithelial cells, glycoproteins, enzymes, antimicrobial agents and lysozyme [27].

The oral fluid sampling is mostly performed by devices using a swab collector that is put in the driver's mouth is able to withdraw 1 ml (± 10%) of oral fluid in few minutes. Since drug abusers are usually characterized by low salivation the use of saliva collectors is required.

Quantisal™ Oral Fluid Collection Device (**Figure 5.9**) is one of the most used tool, presenting a colorimetric indicator that ensures the collection of an oral fluid volume suitable for screening, confirmatory and repeat testing.

Once the sampling is performed, the swab is stored in a plastic test tube containing a buffer solution, able to stabilize both the drug and metabolites specimen, thus allowing to perform confirmatory analyses within 24 h.

Figure 5.9 Quantisal™ Oral Fluid Collection Device

Sample pretreatment is usually required in order to avoid the presence of interfering analytes, especially peptides and proteins. Several extraction methods have been proposed in literature, such as liquid-liquid [28], SPE [29,30], SPME [31] and MEPS [32,33]. The latter is characterized by several advantages as reported in **Chapter 3**.

5.1.5 NPS Analysis

NPS and their metabolites are a wide group of organic compounds characterized by multiple, active, and polar functional groups, thus derivatization is often required when GC-MS analyses are performed, in order to both reduce tailing of polar compounds and improve the detectability of the investigated compounds [34]. GC-MS analysis has been used for the detection of JWH [35,36], CP [37] and AM and UR [38] compounds.

Detection is mostly carried out by MS detector, even if FID detector has also been proposed [39,40]. One of the main drawback of GC analysis is that some NPS can undergo thermal degradation processes [41].

LC-MS and LC-MS/MS are the most applied techniques for NPS analyses: both ESI [42,43] and APCI [44] have been used as ionization techniques.

The use of capillary electrophoresis and UV detection for the determination of synthetic cannabinoids was first reported in 2012 [45]. In order to improve the identification capabilities of the method, Akamatsu et al. [46] proposed the use of CE coupled with MS/MS detector.

Screening techniques based on mass spectrometry have also been proposed by using MALDI [47] and DART [48,49]. These techniques are very attractive for forensic laboratories since high throughput analyses can be performed.

Finally, immunoassay tests were also proposed for the screening of the NPS both in urine [50] and saliva [51].

5.1.6 Desorption Electrospray Ionization Mass Spectrometry

DESI is a new ambient ionization technique, proposed in 2004 by G. Cook [52] and commercialized by Prosolia Inc. It is usually coupled with mass spectrometry to be used as screening technique since it is characterized by the possibility to record the mass spectra in only few seconds, working at ambient pressure and temperature, thus maintaining an efficient ionization. It provides the typical advantages related to the high-resolution mass spectrometry (HRMS) such as univocal identification of the compounds, low detection limits and possibility to perform analysis of complex mixture by MS/MS. The major feature of DESI is the possibility to analyze directly the sample, thus requiring no or very simple sample pretreatment, leading to fast analysis, low costs and use of small amounts of organic solvents.

DESI can be applied on solid, liquid or gas samples: solid samples can be directly analyzed, whereas liquid samples are deposited on a proper surface and evaporated, and gas samples are adsorbed on solid materials.

The DESI analysis is characterized by feature typical of both electrospray and desorption/ionization analyses (such as MALDI), overcoming the respective limitations: the ESI analysis requires the presence of a liquid sample, whereas the MALDI analysis is performed on materials in which the samples are co-crystallized within a matrix and deposited on a proper surface [53]. Both techniques require sample pretreatment, which is usually inapplicable in in-situ analysis, whereas DESI, being suitable for the direct analysis, is ideal for high throughput and screening purposes.

The DESI source is a high-velocity pneumatically assisted ESI source, generating charged micro-droplets by the application of a proper potential on the ESI needle (**Figure 5.10**). The jet is directed towards the probe surface: the impact of the primary droplets leads to the formation of a micrometer-size thin solvent film, to the solvation of the sample at the liquid-solid interface and to the generation of an electrostatic field. The spray allows the formation of secondary droplets, containing the analytes, expelled from the film solvent by electrostatic repulsions [54]. These droplets are then desolvated and ionized in the gas-phase, as in the traditional ESI analysis. Finally, the ions are collected by the MS inlet. Since the ionization process is very close to the electrospray, the spectra obtained by using these techniques are comparable: similarly to ESI, DESI mass spectrometry is considered as a soft ionization technique, usually preserving the molecular ion.

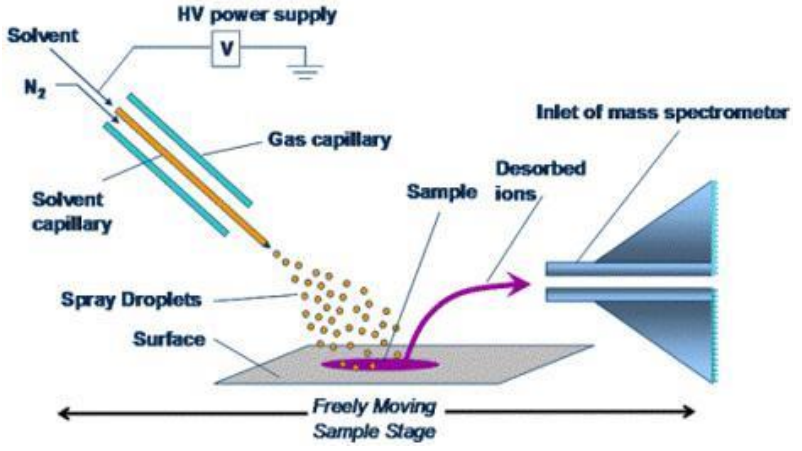

Figure 5.10 Schematic representation of a DESI source

Several studies regarding the formation of secondary droplets, the generation of the electrostatic field and the ionization phenomena were published [55,56]. Fluid dynamics simulation were performed in order to describe the interactions of the primary droplets of the spray and the probe surface, which lead to the formation of the secondary droplets [55] (**Figure 5.11**).

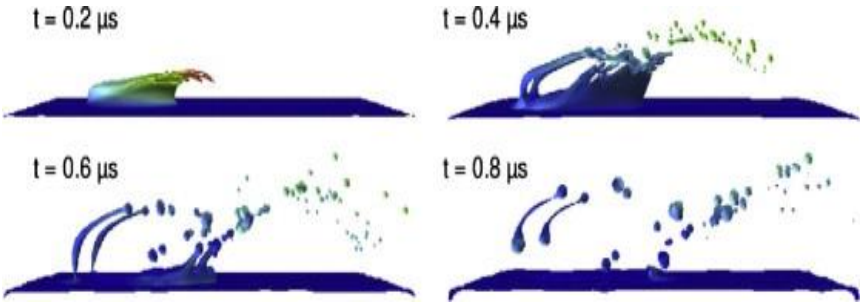

Figure 5.11 Fluid dynamics simulation at different times [55]

Venter et al. [56] calculated that a droplet characterized by 3 µm diameter, reaches the probe surface with a speed of 100 m/s, which means that the kinetic energy is 500 MeV. Once it hits the supporting material, this energy is turned into heat, thus increasing the local temperature of the surface, leading to the formation of secondary droplets.

Takats et al [57] demonstrated that the DESI source is strongly influenced by the dielectric constant of both the substrate material and the spray. The comparison of several substrates commercially available, i.e. polytetrafluorethylene (PTFE), polymethylmethacrylate, porous silica, demonstrated that the probe material has a major impact on the ionization of the deposited analytes. Besides the dielectric and thermal constant, the interaction between the analytes and the surface at the liquid-solid interface and the hydrophobicity of the material lead to modification of both signal intensity and stability[57]. The latter is strongly influenced by the different crystallization of the analytes on the surface and the consecutive desorption/solvation phenomenon in the sprayed solvent. Nanoporous silicon and ultra-thin layer chromatography plates have also been proposed as DESI supports [58].

DESI-MS is a very promising technique, suitable for the analysis of a wide range of analytes, characterized by different physical and chemical properties.

Among the field of application, pharmaceutical analysis is one of the most studied [59]: experiments on pharmaceuticals and drugs in their final form, such as pills or tablets, can be performed, since no pretreatment is required. The analysis of metabolites and active principles can be achieved also in tissues and cells, as well as in body fluids, such as urine, saliva and blood. In-vivo analysis of plants is also possible, by directing the spray onto the sample.

Forensic analysis is another noticeable field of application of the DESI analysis [60,61]: gunshot residues, explosives, toxic substances and chemical warfare agents have been detected with both high sensibility and selectivity, in very short times and without sample pretreatment.

DESI-MS imaging can also be performed for the analysis of solid samples, thus allowing analyte mapping as well as the determination and distribution of unknown compounds. The main applications are related to the analysis of body tissues [62,63] in order to assess the presence, distribution and targeting of drugs and their metabolites.

The main advantages of DESI imaging are reported below:

1. It does not require radioactive and radiolabeled compounds
2. It can be achieved on very small samples i.e. tissues characterized by diameters less than 300 μm
3. Excellent limits of detection can be achieved by using high resolution mass spectrometry (HRMS)
4. The limits of detection can be further increased by MRM analysis for detecting targeted compounds.

Recently, the research is focusing on the development of miniaturized DESI sources coupled with portable mass spectrometers, in order to obtain systems characterized by high accuracy and sensibility for in-situ analysis [64].

The aim of this research study is the development and the validation of a screening method suitable for the determination of NPS in human saliva for high-throughput analyses. It combines MEPS extraction of the sample with DESI-HRMS in order to obtain a fast method characterized by high sensitivity and selectivity. The study was performed in collaboration with Stockholm University and KTH Royal Institute of Technology of Stockholm.

This study is part of the project entitled *Parma contro le nuove droghe* project funded by Fondazione Cariparma, carried out in cooperation with the Department of Medicine and Surgery, University of Parma.

5.2 Materials and Methods

5.2.1 Chemicals and materials

Ketamine HCl (1000 mg/l in methanol), and mephedrone HCl (1000 mg/l in methanol) were purchased from Lipomed (Arlesheim, Switzerland). UR-144 (100 mg/l in methanol), Spice Cannabinoid Mix (100 mg/l in acetonitrile), Spice Cannabinoid Mix 2 (100 mg/l in acetonitrile), 2-propanol (99.9%), acetonitrile – ACN (99.8%), dichloromethane - DCM (> 99%), ammonium hydroxide (33% in water) were from Merk (Milan, Italy). Ketamine d_4 HCl (100 mg/L in MeOH) was purchased from LGC (Teddington, UK). Methanol – MeOH (> 99.9%) was from J.T. Baker (PA, U.S.A.). Deionized water was obtained by using a MilliQ element A10 System (S. Francisco, CA, USA).

5.2.2 Standard Solutions and Real Sample Pretreatment

The stock solutions were maintained in dark at -18°C.

Standard solutions were obtained by dilution in H_2O:MeOH 1:1 and a volume of 2 µl was spiked on the DESI supports. Deuterated ketamine was used as internal standard (IS) at a concentration of 1 mg/l.

The analysis of real samples was performed by spiking blank saliva obtained from 5 different individuals with NPS in the 0.1-10 mg/l range.

The spiked saliva was diluted with 200 µl of MeOH in order to obtain protein precipitation. The samples were frozen at -18°C for 15 min, sonicated for 15 min at ambient temperature and finally centrifuged at 11 000 x g for 10 min. The supernatant was collected and centrifuged in order to guarantee the complete precipitation of proteins.

5.2.3 Experimental Design and Optimization of the MEPS Procedure

Preliminary investigations were performed by using different MEPS sorbents (C_{18} and M1) and eluents (NH_4OH 50mM in MeOH and a mixture 78:20:2 of DCM: 2-propanol:NH_4OH).

A 2^2 two-levels FFD was carried out by investigating the effects of both loading and eluting cycles. In both cases, low and high levels were 5 and 25 cycles, respectively. Blank saliva was used as matrix. The analytes were spiked at the concentration of 10 mg/l. Five analytes were considered as

model compounds, i.e. ketamine, mephedrone, UR-144, JWH-250 and JWH-08. Four replicates were performed at the center of the experimental domain in order to evaluate the experimental error.

The significance of the loading/eluting effects was evaluated by using the statistical package SPSS Statistics v.23.0 (IBM, Milano, Italy).

The optimal extraction conditions were obtained by using the multicriteria method of the desirability functions.

5.2.4 GC-MS analysis

In order to optimize the MEPS procedure, GC-MS analyses of the spiked saliva were performed using a HP 6890 Series Plus gas chromatograph (Agilent Technologies, Palo Alto, CA) equipped with a MSD 5973 mass spectrometer (Agilent Technologies). Helium was used as the carrier gas at a constant flow rate of 1 mL/min; the gas chromatograph was operated in splitless mode for 1 min with the PTV injector (Agilent Technologies) maintained at the temperature of 300 °C and equipped with a 1.5 mm i.d. multi-baffled liner (Agilent Technologies).

Chromatographic separation was performed on a 30 m × 0.25 mm, df 0.25 µm MDN-5S capillary column (Supelco, Bellerofonte, USA), using the following temperature programme: initial temperature 120 °C hold 1 min, 30 °C/min up to 240 °C, 10°C/min up to 290°C, hold 5 min, 10°C up to 310, hold 13 min.

The transfer line and source were maintained at the temperatures of 220 and 150 °C, respectively. Preliminarily, full scan EI data were acquired to determine appropriate masses for selected-ion monitoring mode under the following conditions: ionization energy: 70 eV; mass range: 45-400 amu; scan time: 3 scan/s; electron multiplier voltage: 2165 V. Signal acquisition and data handling were performed using the HP Chemstation (Agilent Technologies).

The *m/z* ratios related to the model compounds are reported in **Table 5.1**.

Table 5.1 m/z ratios of the investigated analytes. Highlighted the ratios used for quantitation

Analyte	***m/z***
Mephedrone	58, 91, 119
Ketamine	180, 152, 209
UR-144	214, 296, 311
JWH-250	335, 214, 144
JWH-081	371, 314, 354

5.2.5 Optimized MEPS Procedure

A commercial e-Vol® equipped with a C_{18} BIN was used for MEPS extraction. Prior to extraction, each BIN was activated by using 5 × 50 µL of MeOH and 5 × 50 µL of water. 50 µL of saliva sample loaded in the BIN using 5 loading cycles. Then, the analytes were eluted with 25 × 25 µL of DCM:2-propanol:NH_4OH and analyzed by DESI-HRMS. After extraction, 10 × 50 µL washing cycles were performed in order to avoid carryover effects.

Both fill and injection speeds of 1 arbitrary unit were used.

5.2.6 DESI-HRMS Analysis

All the mass spectra were recorded by a LTQ Orbitrap XL hybrid FTMS instrument (Thermo Finnigan, San Jose, CA, USA), equipped with Xcalibur 2.0. software, in automatic gain control mode. The injection time in the ionic trap is 250 ms, 1 microscan was recorded for each spectrum.

All the experiments were performed by using an Omni Spray™ (Prosolia, Inc., Indianapolis, IN, USA) DESI source operating in positive ion mode, with a point-to-point oscillating acquisition mode.

The experimental conditions are reported in **Table 5.2**:

Table 5.2: DESI operative conditions

solvent flow	1 µl/min
spray voltage	4 kV
Tube lens voltage	100 V
capillary voltage	15 V
capillary temperature	250 °C
nitrogen pressure	8,5 bar
incident angle	50°
collection angle	40°
tip-to-surface distance (d1)	1,7 mm
inlet-to-surface distance (d2)	0,5 mm
tip-to-inlet distance (d3)	3,6 mm
spray tip length (d4)	1 mm

The sample plate was positioned on a movable stage with 1-D automatic control movement (x axis). CCD cameras are mounted on the source in order to visually monitor the sample position and the spray alignment.

Preliminarily, full-scan accurate mass spectra in the 150–400 amu range were acquired to determine the appropriate masses for each analyte. Identification and quantitation of target compounds was performed using the accurate mass of the analytes within a mass window of 5 ppm. Quantitation was performed by using the extracted ion chromatograms of the *m/z* value corresponding to the protonated ion of each investigated compound, as reported in **Table 5.3**.

Table 5.3: monitored ions and corresponding *m/z* ratios

Analyte	Ion	Theoretical *m/z*	Measured *m/z*	Δm *(ppm)*
Ketamine	$[M+H]^+$	238.09959	238.09921	0.62
Ketamine d_4	$[M+H]^+$	242.12443	242.1483	0.66
Mephedrone	$[M+H]^+$	178.12267	178.12267	0.12
UR-144	$[M+H]^+$	312.23257	312.23199	0.23
JWH-250	$[M+H]^+$	336.19666	336.19666	0.25
JWH-200	$[M+H]^+$	385.19073	385.19073	0.28
HU-211	$[M+H]^+$	387.28986	387.28986	0.27
CP47,497	$[M+H]^+$	319.26508	319.26508	0.23
CP47,497 C8	$[M+H]^+$	333.27853	333.27853	0.25
JWH-122 and JWH-019	$[M+H]^+$	356.20157	356.20157	0.27
AM-2211	$[M+H]^+$	360.17566	360.17566	0.26
JWH-081	$[M+H]^+$	372.19556	372.19556	0.28

Different spraying solvents were tested, i.e. H_2O:MeOH (1:1 and 3:1) and H_2O:AcN (1:1 and 3:1); followed the optimization of the geometrical parameters of the DESI source. Polytetrafluoroethylene (PTFE) commercially available slides (Prosolia, Inc., Indianapolis, IN, USA) and three materials made of polylactide (PLA), developed by KTH Royal Institute of Technology of Stockholm, were tested as DESI supports.

5.2.7 *New DESI Supports Characterization*

The developed materials were characterized by AFM and SEM analyses. AFM analyses were performed on a PARK XE-100, Park Systems (Mannheim, Germany). The images were acquired in tapping mode with a scan rate of 0.5 Hz and a 50 × 50 μm window. SEM characterization was performed on a Leica 430i (Leica, Solms, Germany).

5.2.8 Method Validation

Validation was carried out under the optimized conditions, by following the Guidance for Industry – Bioanalytical Method Validation the Food and Drug Administration (FDA) [65]. Saliva from 5 individuals was used as blank matrix and spiked with the investigated NPS.

Both LODs and quantification LOQs were measured by using blank saliva spiked with the minimum concentration of the analytes able to provide signals significantly different from the baseline. Five replicates using independent samples were performed.

The calibration curves were evaluated on six concentration levels in the 0.1–10 mg/l range for ketamine and mephedrone and in the 0.5-10 mg/l range for UR-144, Mix Spice 1 and 2. Deuterated ketamine as was used as IS, at the concentration of 1 mg/l. Blank sample (matrix sample processed without IS) and zero sample (matrix sample processed with IS) were also analyzed. Three replicated measurements for each level were performed.

Lack-of-fit and Mandel's fitting tests were performed to check the goodness of fit and linearity, whereas the significance of the intercept (significance level 5%) was established by running a Student *t*-test.

Repeatability and intermediate precision were calculated in terms of CV% on three concentration levels: LOQ, 1 and 10 mg/l for all the analytes except UR-144, which was studied at LOQ, 5 and 10 mg/l. Five replicate measurements *per* level were performed. Intermediate precision was estimated over three days verifying homoscedasticity of data and performing the analysis of variance (ANOVA) at the confidence level of 95%.

Trueness was calculated in terms of recovery rate (RR%) as follows:

$$R.R.\% = c_1/c_2 \cdot 100$$

where c_1 is the measured concentration and c_2 is the concentration calculated from the quantity spiked into the sample. Three different concentration levels (LOQ, 1 and 10 mg/l for all the analytes except UR-144, which was studied at LOQ, 5 and 10 mg/l) with five replicated measurements were analyzed.

Finally, freeze and thaw stability was evaluated by three different cycles at two different concentration levels, i.e. LOQ and 10 mg/l (three replicate measurements). Moreover, short-term stability of the biological samples at LOQ and 10 mg/l was studied at ambient temperature for 24 h. Long-term stability was evaluated for 15 days by storing the spiked samples at -18°C.

Two concentration levels, i.e. LOQ and 10 mg/l, 3 replicates per sample were considered. Stock solution stability was evaluated for 6 months at -18°C and for 6 h at room temperature.

5.3 Results and discussion

The aim of this research study was the development and validation of a DESI-HRMS method for the detection of new psychoactive substances in saliva both for screening and quantitation purposes. The use of high-resolution mass spectrometry allows the univocal identification of the targeted compounds, thus not requiring any chromatographic separation of the analytes.

5.3.1 DESI-HRMS Optimization

Preliminary analyses were performed in order to obtain the accurate *m/z* ratios by full-scan acquisition of mass spectra of standard solutions at 10 mg/l.

The use of additives to promote ionization was tested: solutions of NaCl (0.1-50 mM) and formic acid (0.01-1%) were added to the sample with the aim of promoting the formation of $[M+Na]^+$ and $[M+H]^+$ adducts, respectively. By operating under these conditions, no signal improvements were observed; moreover, by increasing the concentration of the formic acid within the sample or using more acid in the spray solution, a dramatic boost of the noise was present. Therefore, preliminary analyses were performed by using H_2O:MeOH 1:1 standard solutions and monitoring the protonated molecular ion for all the NPS (**Table 5.3**).

Being able to affect both the ionization yield and the ions recovery by the MS inlet, the following source parameters were optimized [66]:

1. Spray composition
2. Spray flow
3. Acquisition mode
4. Geometrical parameters
5. Supporting material

1. Spray Composition

This parameter has a major influence on the formation, dimension and charge of liquid films, primary and secondary droplets, thus affecting both the ionization yield and the focalization of the spray. Moreover, the interaction among spray, analytes and surface can be tuned by changing the DESI spray composition, thus influencing the desorption of the analytes from the supporting material.

Four different spray compositions were tested, i.e. MeOH:H_2O 1:1 and 1:3 and AcN:H_2O 1:1 and 1:3; the results are reported in **Figure 5.12.**

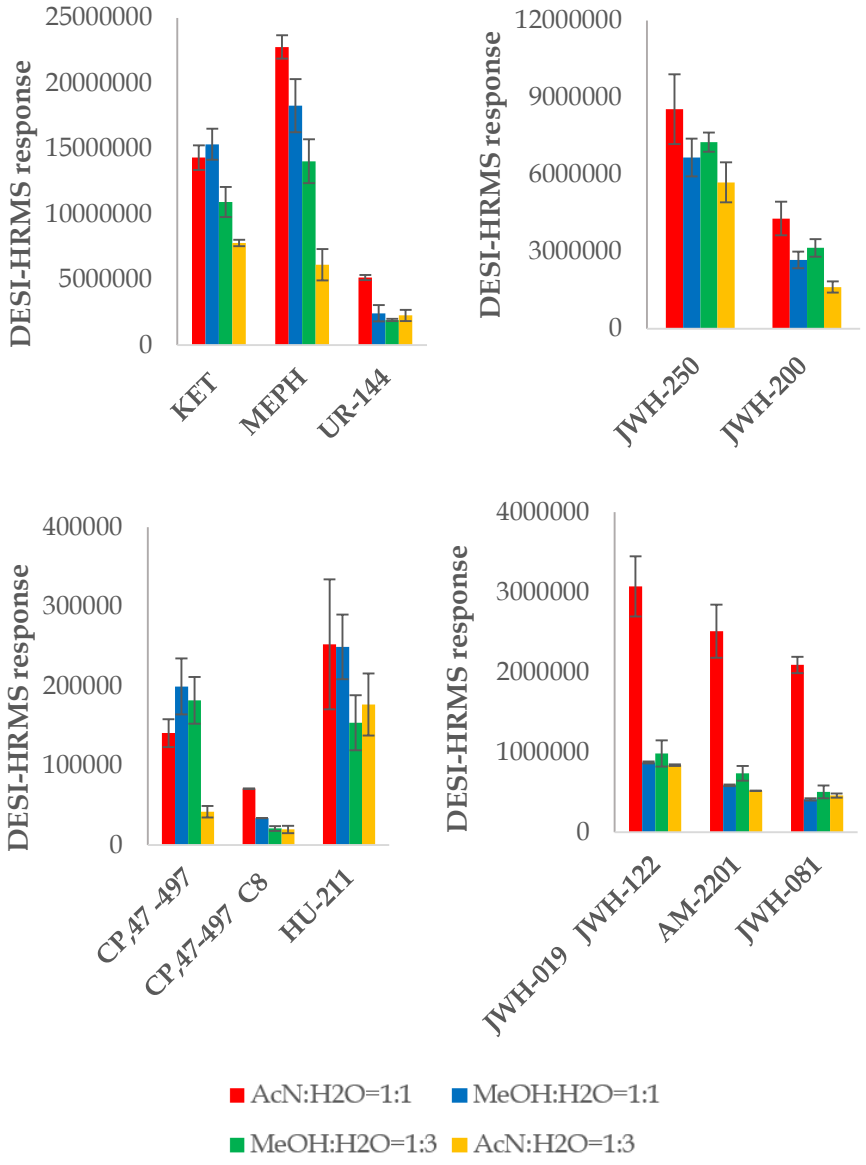

Figure 5.12 Histograms related to the spray optimization

The data highlighted the strong effect of the spray composition: the best global results were achieved by using AcN:H_2O 1:1 mixture, with increased responses especially for Spice Cannabinoid Mix 2 analytes.

2. Spray Flow

The spray flow has a noticeable impact on the equilibrium of the gas-liquid interface: it affects both the dimension and the speed of the primary microdroplets, thus influencing the formation of the liquid film on the DESI support and consequently the solubilization of the analytes, as well as the emission of secondary droplets.

Two different spray flows were tested, i.e. 1 and 2 µl/min: the data obtained showed a decrease in the DESI-HRMS responses by increasing the flow. This behavior can be explained by taking into account that high flows can lead to a decrease in the spray focusing capability. On the basis of these findings, the flow was set at 1 µl/min.

3. Acquisition Mode

The Omni Spray™ software allows to perform DESI analyses in different acquisition modes:

- **Scanning**: this acquisition mode allows the continuous scan in the x-direction of the DESI slide, at a constant speed (µm/s). This mode is affected by low recoveries and the possibility to push the analytes along the slide, leading to cross-contamination phenomena. This usually occurs when the spiked sample is characterized by high viscosity and drying struggling. Since saliva is affected by both the mentioned drawbacks, scanning mode was immediately discarded.
- **Point-to-point fixed acquisition**: the software can generate a grid of monitoring points and the DESI source is automatically moved on each specific positions of the slide. The spray is maintained for a well-defined time, properly chosen by the analyst, on one of these fixed points, and then it automatically moves to the next.
- **Point-to-point oscillating acquisition**: this acquisition mode is similar to the previous one but the source is not maintained on a fixed position, swinging about the points in the grid. In this case the center spot position, the oscillating distance and the number of oscillations can be set by the analyst.

The analyses performed by using point-to-point fixed acquisition mode resulted in low responses and poor repeatability compared to the oscillating

acquisition. These phenomena can be explained by considering the high variability in centering exactly the sample spotted on the DESI support.

The obtained data demonstrated that the point-to-point oscillating acquisition mode allowed to obtain the best performances in terms of both sensibility and repeatability. Therefore, this acquisition mode was selected for sample analysis. It has to be noticed that only 1 minute of acquisition per spotted sample is required, thus ensuring a very rapid screening, mandatory for high-throughput analyses.

4. Geometrical parameters

The geometrical parameters related to the position of both the DESI tip and the MS inlet with respect to the DESI support were also optimized. As shown in **Figure 5.13** α and d_1 affect the ionization of the analytes and the generation of secondary droplets, whereas β, d_2 and d_3 influence the ions collection.

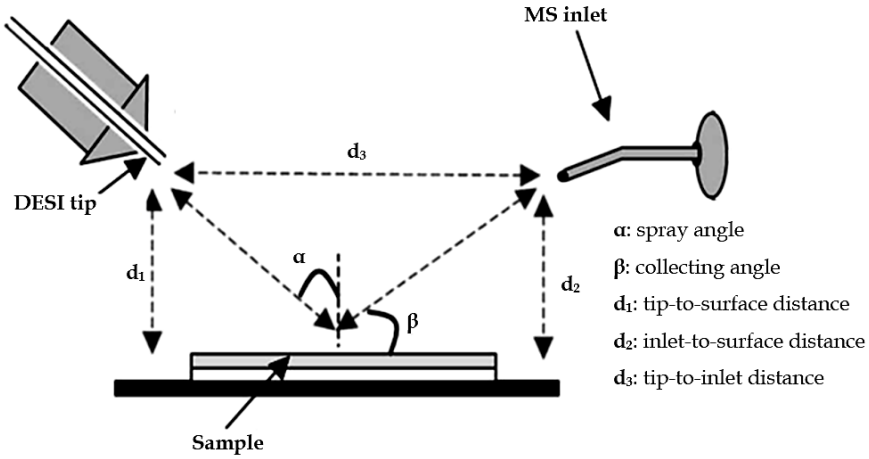

Figure 5.13 Schematic representation of the geometrical parameters in a DESI source

The standard DESI parameters are: α=54.5°, β=45.5°, d_1=5 mm e d_3=3 mm. The optimization was performed by changing the α angle and monitoring the DESI-HRMS responses; the other parameters were changed accordingly (**Figure 5.14**).

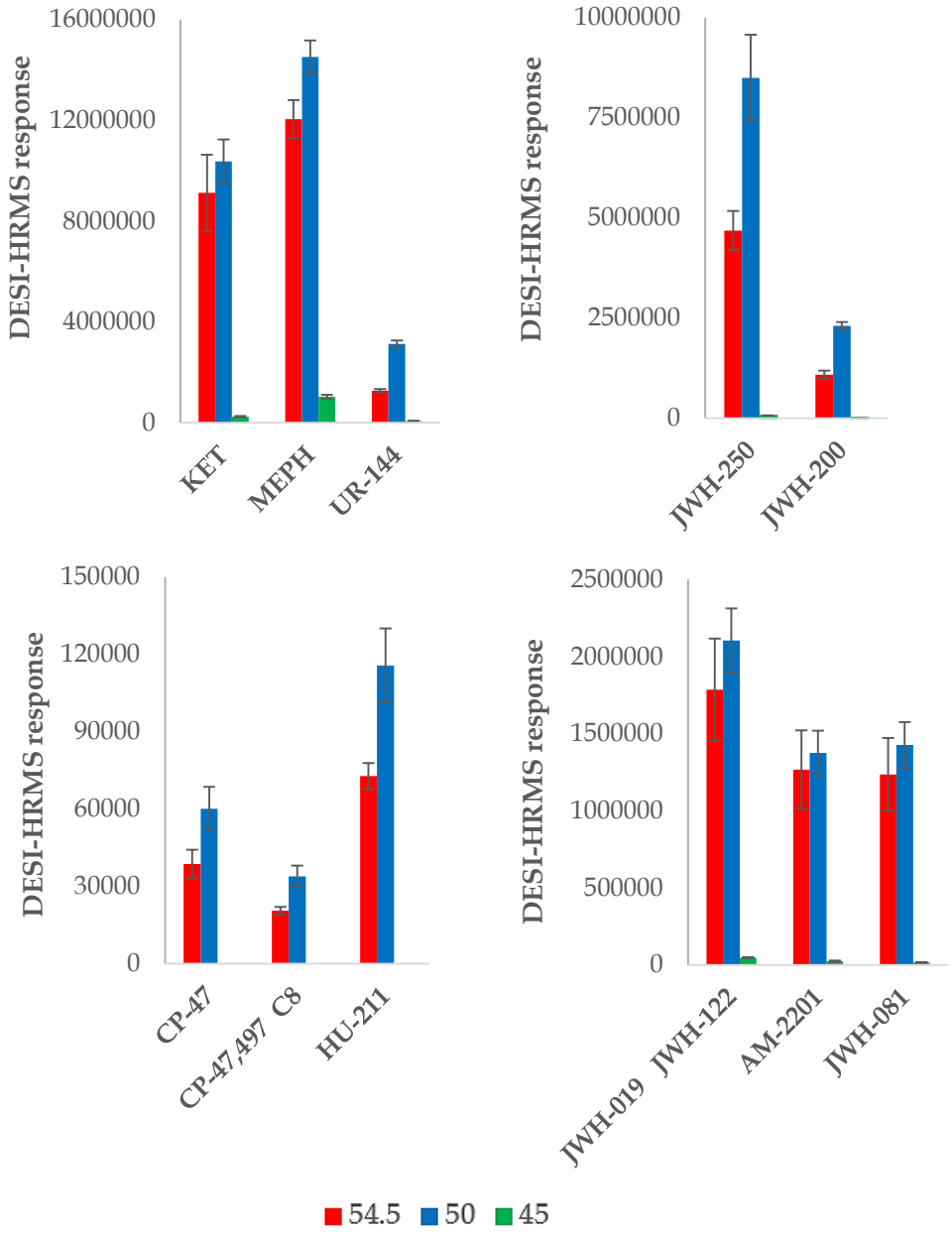

Figure 5.14 Histograms related to the α angle optimization

The best results were achieved by decreasing the α angle from 54.5° to 50°, whereas further angle decline lead to obtain low or no responses. This can be explained taking into account that at 50°, the generation of the secondary

droplets is promoted but at 45° the spray is too tilted to promote the solubilization of the analytes. In addition, possible difficulties in the collection of the ions could occur, thus α was set at 50°. The geometrical optimized parameters are reported in **Table 5.2**.

5. Supporting Material

The physiochemical properties of the slide surface are able to affect the adsorption/solubilization of the analytes, thus strongly influencing the ionization of the investigated compounds and the repeatability of the analyses.

The optimization of the supporting material was performed by using four different materials: PTFE commercially available slides (Prosolia) and three PLA-based films developed by KTH Royal Institute of Technology of Stockholm (**Figure 5.15**). PTFE is usually proposed for DESI analyses since it is an inert polymer, characterized by a wrinkled surface and high hydrophobicity. The solvent-surface and analyte-surface interactions are very weak, thus promoting the desorption and the solubilization of the analytes, increasing both DESI-HRMS responses and signal stability. Moreover, PTFE slides commercially available are characterized by the presence of a grid, which assist the solution spotting and the automation of the analysis when point-to-point acquisition mode is performed.

The PLA-based film tested were respectively: PLA (unmodified polylactide), PLA A and PLA B (functionalized polylactides). The PTFE grid was duplicated under these films in order to assist both sample spotting and acquisition. The films were then stacked on microscope slides

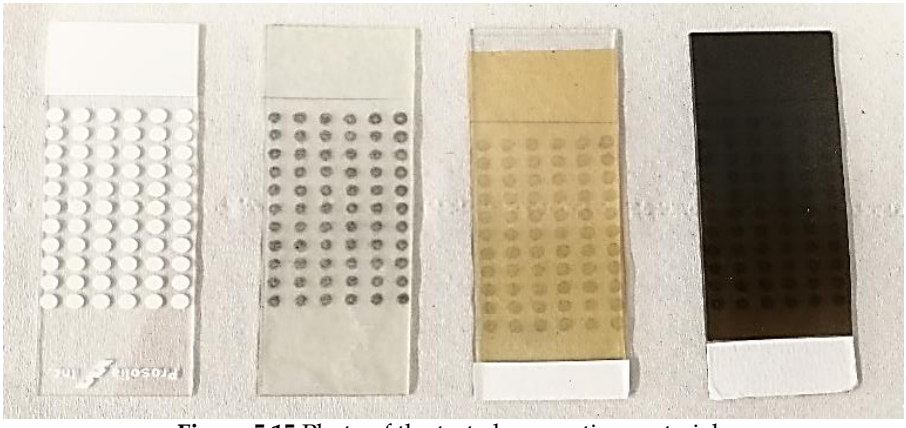

Figure 5.15 Photo of the tested supporting materials

The hydrophobicity of the different materials was assessed in order to evaluate their affinity toward the analytes and the spray solvent. It is also related to the drying time, the liquid film formation and the secondary droplets generation.

The contact-angle measurements were performed by spotting 2 µl of deionized water (3 replicates) on the tested surfaces; the calculated angles are reported in **Table 5.4**.

Table 5.4: Contact angles and standard deviation measured for the different materials

Material	Contact angle (°)
PTFE	131 (±1)
PLA	72 (±1)
PLA A	70 (±1)
PLA B	83 (±4)

The obtained data highlighted that the PLA-based materials were characterized by higher hydrophilicity compared to the PTFE slides, leading to higher wettability by both spotted solution and DESI spray.

Then the four supporting materials were tested for the DESI analysis of NPS standard solutions at two concentration levels, i.e. 0.1 and 1 mg/l. 2 µl were spotted on the DESI support, performing 5 replicate measurements at each level (**Figure 5.16**).

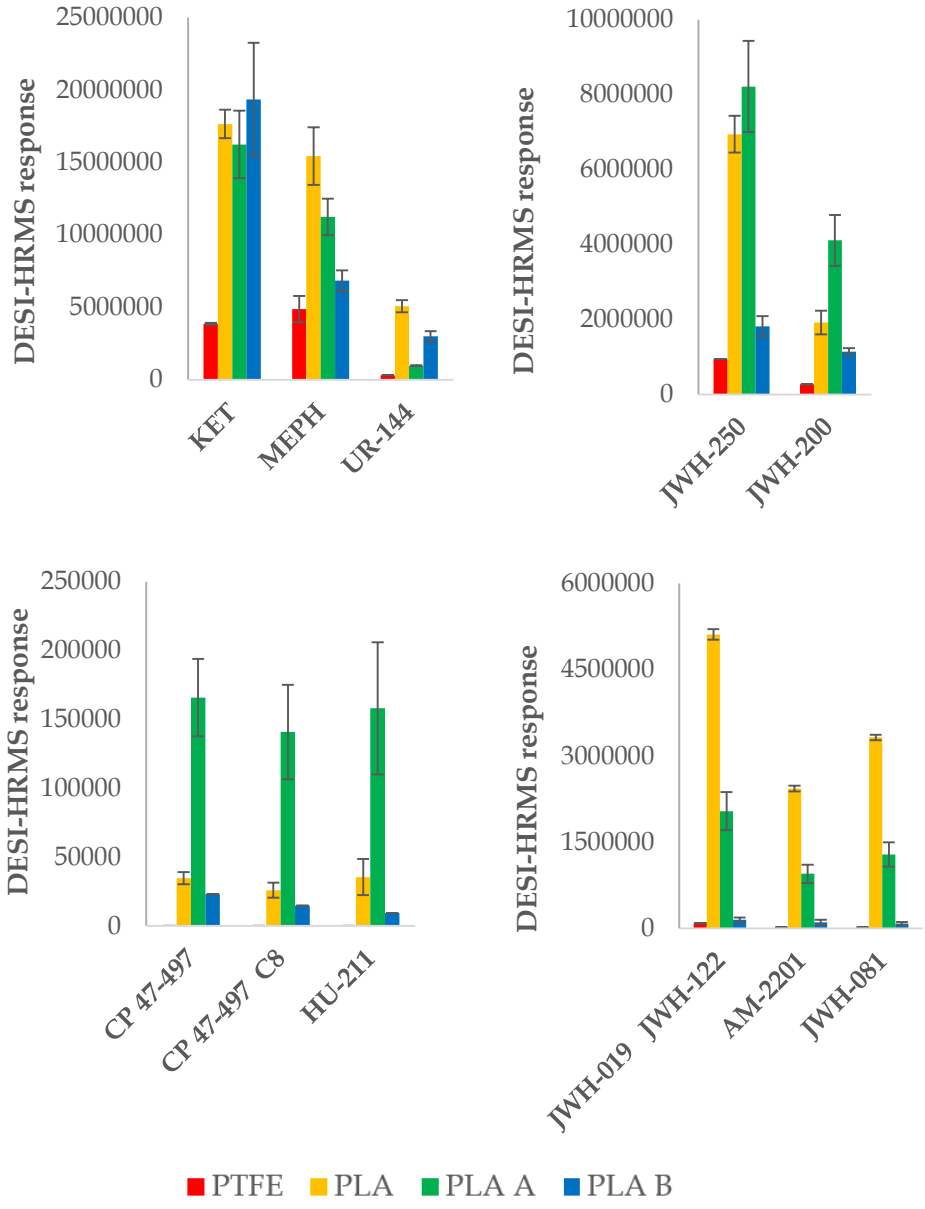

Figure 5.16 DESI-HRMS responses of the different analytes (1 mg/l) by using different supporting materials

The use of different supporting materials strongly affects the ionization of the analytes. Unfunctionalized PLA showed the best performances in terms of both signal intensity and repeteability for ketamine, mephedrone, UR-144,

JWH-019, JWH-122, AM-2201 and JWH-081 analyses, whereas PLA A allowed to obtain signal enhancements for HU-221, CP 47-497 and its analogue CP 47-497 C_8. However, it has to be pointed out that these analytes can be detected only at high concentration (above 1 mg/l). Since the italian law requires zero-tolerance for drivers under the effects of psychoactive drugs, in order to reach the lowest limits of detection, only unfunctionalized PLA was considered for method validation.

In addition, PLA allowed to obtain reproducible signals, with CV% always lower than 20% (**Figure 5.17)**.

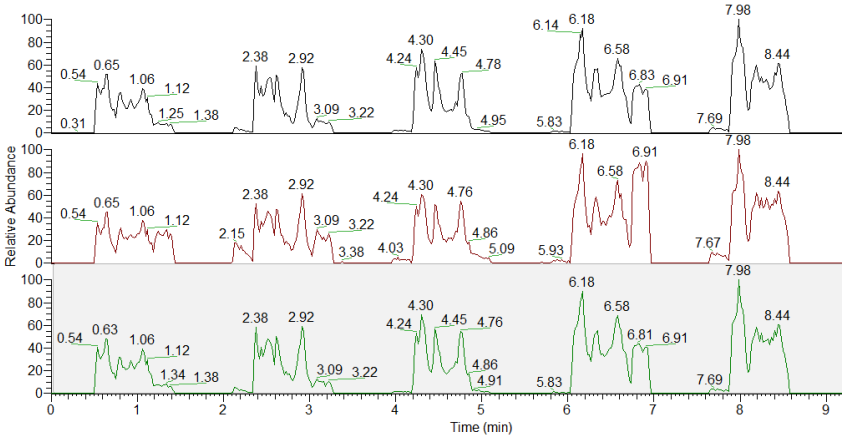

Figure 5.17 DESI-HRMS signals of JWH-019 + JWH-122, AM-122 and JWH-081 (0.1 mg/l), n=5

PLA film was characterized by both AFM and SEM analyses. AFM showed the presence of PLA grains on the material surface (**Figure 5.18**).

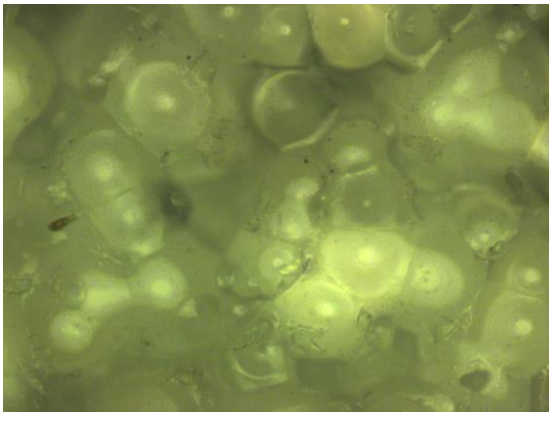

Figure 5.19 Photograph of the PLA surface obtained by AFM

Their depth was > 5 μm, too high to be analyzed by AFM (**Figure 5.19**).

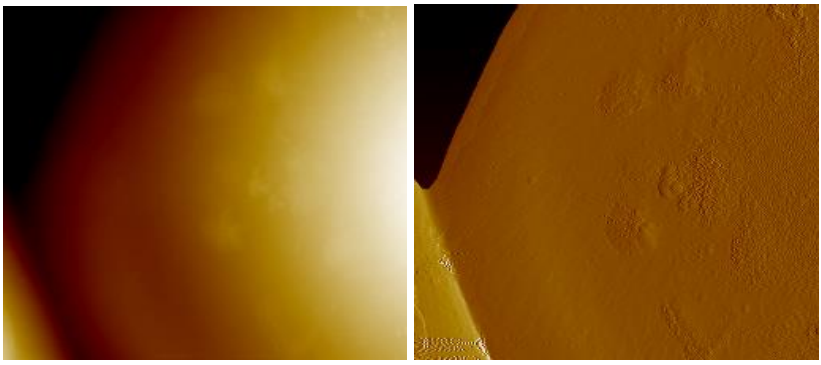

Figure 5.19 AFM topographic image (left) and signal-error (right) of two adjacent granules

SEM analyses confirmed the presence of a wrekled surface, charcaterized by the presence of *fused* polymer grains. The thickness of the material was 82.4 (±7.9) μm, calculated considering 3 different supports and 5 points per picture (**Figure 5.20**).

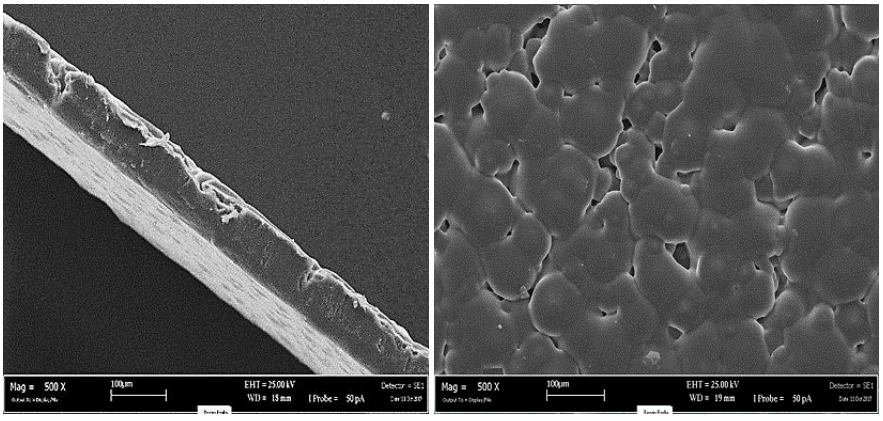

Figure 5.20 SEM micrographies of the support: lateral view (left) and surface morphology (right)

5.3.2 *MEPS Procedure Optimization*

Saliva is a very complex matrix, composed by electrolytes, blood and epithelial cells and proteins: several research studies proved that NPS analysis in ESI is affected by strong matrix effect [67]. DESI-HRMS analyses performed on spiked saliva samples confirmed the presence of a strong matrix effect, since no analyte was detected in untreated saliva, thus requiring a

pretreatment step before the analysis. This phenomenon could be explained taking into account the presence of proteins and peptides that are able to influence the analytes adsorption/desorption on the slide surface. In addition, their solubilization in the spray can cause the clogging of the MS inlet.

In order to overcome these difficulties a MEPS approach was followed.

A commercial e-Vol® was used for NPS extraction from saliva, by using fill and injection speed of 4 arbitrary units: higher flows were discharged since bubbles' formation inside the MEPS syringe was observed, thus causing poor repeatability.

In order to optimize the extraction conditions, five analytes were considered as model compounds, i.e. ketamine, mephedrone, UR-144, JWH-250 and JWH-08 spiked in saliva. The NPS were extracted by MEPS and analyzed by GC-MS technique.

Two different sorbent materials were tested: C_{18} and M1 (a mixed resin 80% C_8 and 20% SCX cationic exchanger) (**Figure 5.21**).

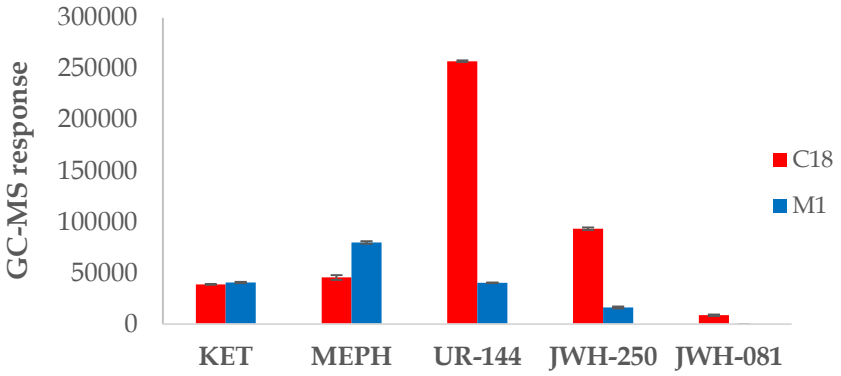

Figure 5.21 MEPS sorbent optimization

The obtained data highlighted that the C_{18} sorbent was characterized by the best extraction capabilities. A washing step was also tested, by using different solutions, in order to remove possible interfering compounds, but a noteworthy decrease in signal intensities occurred, due to the removal of the analytes from the MEPS stationary phase. Therefore, no washing step was performed.

The elution of the analytes was evaluated by using two different eluting solutions, i.e. NH_4OH 50mM in MeOH (A) and a mixture 78:20:2 of DCM: 2-

propanol:NH_4OH (B). Eluent B was characterized by the best extraction capabilities for all the investigated analytes, as reported in **Figure 5.22**.

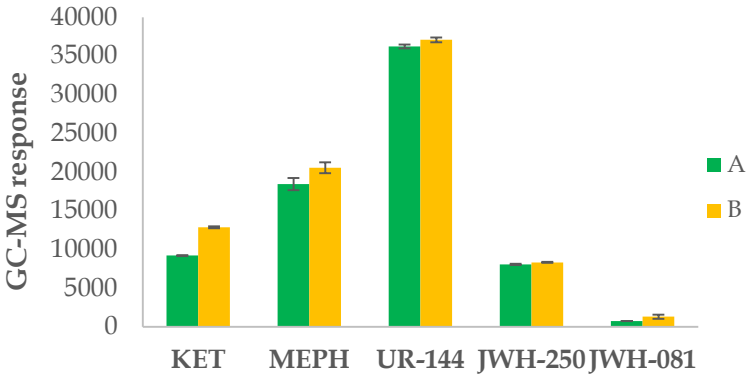

Figure 5.22 MEPS eluent optimization: NH4OH 50mM in MeOH (A) and a mixture 78:20:2 of DCM: 2-propanol:NH4OH (B)

The loading and eluting cycles were optimized by using a 2^2 FFD, following the procedure described in **Chapter 3**, using the condition reported in **Paragraph 5.2.3**.

The model obtained for the investigated compounds, R^2, and single desirability values are reported in **Table 5.5**. The optimum was reached when 5 loading cycles and 25 eluting cycles were used, thus obtaining a global desirability of D= 0.87 and excellent single desiderabilities, in the 0.71-0.95 range.

Table 5.5 Regression coefficients and single desirabilities of the polynomial functions calculated using the forward method (± standard error)

Analyte	CCD model	R^2	d
Ketamine	$y = 12630\ (\pm 590) - 3200\ (\pm 460)\ x_1$	0.94	0.93
Mephedrone	$y = 7100\ (\pm 1100) - 3290\ (\pm 960)\ x_1 - 4300\ (\pm 1500)\ x_1\ x_2$	0.93	0.92
UR-144	$y = 68200\ (\pm 6500) - 17000\ (\pm 12000)\ x_1\ x_2$	0.86	0.85
JWH-250	$y = 35100\ (\pm 3600) + 7700\ (\pm 3800)\ x_2$	0.92	0.95
JWH-081	$y = 6130\ (\pm 430) + 970\ (\pm 450)\ x_2$	0.82	0.71

The results showed that a low number of loading cycles were sufficient in order to promote the adsorption of the analytes on the MEPS sorbent, whereas 25 eluting cycles were required in order to assess the complete recovery of the extracted analytes, highly retained on the C_{18} resin.

The optimized MEPS conditions were applied during method validation.

5.3.3 *MEPS-DESI-HRMS Method Validation*

The validation of the MEPS-DESI-HRMS method was performed by following the guideline for bioanalytical methods [65].

It has to be noticed that HU-221, CP47-497 and CP47-497 C_8 analytes were detected in extracted MEPS saliva only at concentration higher than 10 mg/l, thus the proposed method is not suitable for their detection at low concentration levels; therefore, they were not considered during the validation step.

LODs and LOQs are reported in **Table 5.6**.

Table 5.6 Limit of detection and limit of quantitation of the investigated NPS

Analyte	**LOD** (mg/l)	**LOQ** (mg/l)
Ketamine	0.05	0.1
Mephedrone	0.05	0.1
UR-144	0.50	1.0
JWH-250	0.25	0.5
JWH-200	0.25	0.5
JWH-019 and JWH-122	0.25	0.5
AM-2201	0.25	0.5
JWH-081	0.25	0.5

The results showed the developed method is suitable for the analysis of the investigated drugs of abuse at low concentration levels. In a previous study, Cheng et al [68] observed that the concentration of NPS in oral fluids and urine was far higher compared to the LOQs obtained in this method.

The linearity was assessed by using Mandel's test over two orders of magnitude, i.e. LOQ-10 mg/l, for all the investigated analytes, with the exception of UR-144 (**Table 5.7**). Six concentration levels, blank and sample

and zero sample were considered (three replicates *per* level). Student *t*-tests proved that all intercepts were not significantly different from zero (significance level 5%) for all the analytes.

Table 5.7 Linearity range and regression coefficients of the MEPS-DESI-HRMS method

Analyte	**Range** (mg/l)	**a** (±s.d.)
Ketamine	0.1 - 10	0.860 (± 0.013)
Mephedrone	0.1 - 10	0.819 (±0.010)
UR-144	1 - 10	1.562 (±0.014)
JWH-250	0.5 - 10	2.560 (±0.044)
JWH-200	0.5 - 10	0.303 (±0.006)
JWH-019 and JWH-122	0.5 - 10	2.612 (±0.055)
AM-2201	0.5 - 10	0.709 (±0.015)
JWH-081	0.5 - 10	1.724 (±0.022)

Method precision was evaluated in terms of both repeatability (**Table 5.8**) and intermediate precision (**Table 5.9**) on three concentration levels, performing five replicates at each level; intermediate precision was estimated over three days.

Table 5.8 Repeatability (CV%) of the developed MEPS-DESI-HRMS method

Analyte	**Repeatability** (CV%)		
	Level 1 LOQ	Level 2 1 or 5 mg/l	Level 3 10 mg/l
Ketamine	3.2	3.0	3.0
Mephedrone	10.4	7.2	4.9
UR-144	15.9	10.6	1.5
JWH-250	5.0	4.1	1.7
JWH-200	9.1	11.3	12
JWH-019 and JWH-122	11.2	6.7	2.2
AM-2201	11.3	8.4	1.2
JWH-081	1.4	2.8	3.2

Table 5.9 Intermediate precision (CV%) of the developed MEPS-DESI-HRMS method

Analyte	**Intermediate Precision** (CV%)		
	Level 1 1 mg/l	Level 2 1 or 5 mg/l	Level 3 10 mg/l
Ketamine	9.6	8.2	7.3
Mephedrone	19.0	12.3	5.1
UR-144	18.8	13.2	9.4
JWH-250	15.6	12.9	9.3
JWH-200	19.4	14.8	14.5
JWH-019 and JWH-122	19.0	11.8	9.6
AM-2201	18.7	10.0	6.2
JWH-081	19.0	13.6	9.4

The analyses were always characterized by CV% lower than 20%, thus a good precision was achieved.

Recovery rate was calculated at three concentration levels, by analyzing five replicates measurements (**Figure 5.10**).

Table 5.10 Recovery rates of the developed MEPS-DESI-HRMS method

Analyte	**Recovery Rate** (±s.d.)		
	Level 1 1 mg/l	Level 2 1 or 5 mg/l	Level 3 10 mg/l
Ketamine	120 (±4)	105 (±4)	99 (±3)
Mephedrone	102 (±1)	100 (±2)	100 (±5)
UR-144	102 (±2)	101 (±6)	100 (±1)
JWH-250	62 (±6)	78 (±5)	100 (±2)
JWH-200	87 (±12)	91 (±8)	100 (±1)
JWH-019 and JWH-122	101 (±2)	100 (±3)	100 (±2)
AM-2201	80 (±8)	88 (±6)	100 (±1)
JWH-081	86 (±1)	93 (±4)	100 (±1)

The method accuracy showed recovery rates in the 62-120% for the lowest concentration level, whereas recovery rates above 100% were obtained at 10 mg/l. These data are in accordance with the FDA guidelines.

The biological sample solutions were stable for three freeze/thaw cycles if stored at -18°C and thawed at ambient temperature for a 6h period: ANOVA proved did not show significant differences among the mean values (p>0.05). Short-term stability was demonstrated at two concentration levels along 24 h at ambient temperature, whereas the long-term stability of the biological samples was evaluated for 15 days at -18°C, a period far longer compared to the time usually elapsed between the sampling and the analysis of the real samples. No significant differences in the responses were obtained for all the analytes both for short and long-term analyses.

Stock solution stability for 6 months at -18°C and for 6h at room temperature was also demonstrated.

5.4 Conclusions

This research study was carried out in order to meet the European and Italian demand to monitor and prevent driving under the influence of drugs abuse: a simple and rapid screening method for the detection of new psychoactive substances at low concentration in oral fluids was developed.

DESI-HRMS allowed high throughput analyses characterized by both high sensibility and selectivity. Very short analysis times and low costs can be achieved.

The first step was the optimization of the DESI conditions i.e. acquisition mode, spray composition, spray flow, geometrical parameters and supporting material. An unfunctionalized PLA support developed by KTH Royal Institute of Technology of Stockholm proved to be characterized by the best performances compared to both commercially available PTFE slides and other functionalized materials.

Since the analysis of NPS was affected by strong matrix suppression, a MEPS extraction of the spiked saliva samples was performed. The extraction was optimized for five model compounds by experimental design and multicriteria method of desirability functions.

The method was validated by following the FDA guidelines: the obtained LOQs, linearity and accuracy proved the suitability of the method for the analysis of road-collected samples.

Since the research is focusing on the development of the miniaturized DESI-MS instruments, the developed method could be considered as a first step in order to provide valuable tools for the analysis of NPS abuse in drivers.

5.5 Acknowledgement

Thanks also to Prof. M. Hakkarainen from the KTH Royal Institute of Technology of Stockholm for providing the supporting materials.

5.6 References

[1] UNODC, *The challenge of new psychoactive substances. A Report from the Global SMART Programme,* March 2013.
http://www.unodc.org/documents/scientific/NPS_2013_SMART.pdf/

[2] European Monitoring Centre for Drugs and Drug Addiction, *European Drug Report: Trends and Developments*, 2017.
http://www.emcdda.europa.eu/system/files/publications/4541/TDAT17001ENN.pdf_en

[3] C.R. Harris, A. Brown, *Synthetic cannabinoid intoxication: a case series and review*, J. Emerg. Med., 44 (2013) 360-366.

[4] G. McIlroy, L. Ford, J.M. Khan, *Acute myocardial infarction, associated with the use of a synthetic adamantyl-cannabinoid: a case report*, BMC Pharmacol. Toxicol., 17 (2016) doi: 10.1186/s40360-016-0045-1

[5] A. Mir, A. Obafemi, A. Young, C. Kane, *Myocardial infarction associated with use of the synthetic cannabinoid K2*, Pediatrics, 128 (2011) 1622-1627.

[6] H. Müller, H.B. Huttner, M. Köhrmann, J.E. Wielopolski, J. Kornhuber, W. Sperling, *Panic attack after spice abuse in a patient with ADHD*, Pharmacopsychiatry, 43 (2010) 152-3.

[7] S. Every-Palmer, *Synthetic cannabinoid JWH-018 and psychosis: an explorative study*, Drug Alcohol Depend., 117 (2011) 152-157.

[8] E. Ludger, K. Krueger, R. Lindigkeit, H.M. Schiebel, T. Beuerle, *Synthetic cannabinoids in "spice-like" herbal blends: First appearance of JWH-307 and recurrence of JWH-018 on the German market*, Forensic Sci. Int., 22 (2012) 216-222.

[9] J. Nakajima, D. Nakae, K. Yasukawa, *Structure-dependent inhibitory effects of synthetic cannabinoids against 12-O-tetradecanoylphorbol-13-acetate-induced inflammation and skin tumour promotion in mice*, J. Pharm. Pharmacol., 65 (2013) 1223-1230.

[10] J.P. Kelly, *cathinone derivatives: a review of their chemistry, pharmacology and toxicology*, Drug Test. Anal., 3 (2011) 439-453.

[11] P. Jacob, A.T. Shulgin, *Patent WO9639133 1996, 19 CA 126: 117961*, Neurobiogical Technologies Inc, USA.

[12] P. Meltzer, D. butler, J.R. Deschamos, B.K. Madras, *(4-methylphenyl)-2-pyrrolidin-1-yl-pentan-1-one (pyrovalerone) analogues: a promising class of monoamine uptake inhibitors*, J. Med. Chem, 49 (2006) 1420-1432.

[13] J.M. Prosser, L.S. Nelson, *The Toxicology of Bath Salts: A Review of Synthetic Cathinones*, J. Med. Toxicol., 8 (2012) 33-42.

[14] D.M. Wood, S. Davies, M. Puchnarewicz, J. Button, R. Archer, H. Ovaska, J. Ramsey, T. Lee, D. W. Holt, P.I. Dargan, *Recreational Use of Mephedrone (4-Methylmethcathinone, 4-MMC) with Associated Sympathomimetic Toxicity*, J. Med. Toxicol., 6 (2010) 327–330.

[15] EMCDDA, *Report on the risk assessment of ketamine in the framework of the joint action on new synthetic drugs*, Belgium, 2012.

[16] F. Liu, M.G. Paule, S. Ali, C. Wang, *Ketamine-induced neurotoxicity and changes in gene expression in the developing rat brain*, Curr. Neuropharmacol., 9 (2011) 256-261.

[17] J. Kanungo, E. Cuevas, S.F. Ali, M.G. Paule, *Ketamine induces motor neuron toxicity and alters neurogenic and proneural gene expression in zebrafish*, J. Appl. Toxicol., 33 (2013) 410-417.

[18] M. Johnstone, *The cardiovascular effects of ketamine in man*, Anaesthesia, 31 (1976) 873-882.

[19] C.J.A. Morgan, CM. Dodds, H. Furby, F. Pepper, J. Fam, T.P. Freeman, E. Hughes, C. Doeller, J. King, O. Howes, J.M. Stone, *Long-Term Heavy Ketamine Use is Associated with Spatial Memory Impairment and Altered Hippocampal Activation*, Front. Psychiatry, 5 (2014), article 149, doi: 10.3389/fpsyt.2014.00149.

[20] H.R. Pal, N. Berry, R. Kumar, R. Ray, *Ketamine dependence*, Anaesth. Intensive Care, 30 (2002) 382-384.

[21] D. Umbricht, L. Schmid, R. Koller, F.X. Vollenweider, D. Hell, D.C. Javitt, *Ketamine-induced deficits in auditory and visual context-dependent processing in healthy volunteers: implications for models of cognitive deficits in schizophrenia*, Arch. Gen. Psychiatry, 57 (2000) 1139-1147.

[22] http://www.politicheantidroga.gov.it

[23] Ministero della Salute. D.M.16 giugno 2010. *Aggiornamento delle tabelle contenenti l'indicazione delle sostanze stupefacenti e psicotrope relative a composizioni medicinali, di cui al decreto del Presidente della Repubblica 9 ottobre 1990, n. 309 e successive modificazioni ed integrazioni con l'inserimento delle*

sostanze denominate JWH-018, JWH-073 e Mefedrone, G.U. Serie Generale, n. 146 del 25 giugno 2010.

[24] Ministero della Salute. Decreto 18 luglio 2007. *Aggiornamento delle tabelle contenenti l'indicazione delle sostanze stupefacenti e psicotrope e relative composizioni medicinali, di cui al decreto del Presidente della Repubblica del 9 ottobre 1990, n. 309, e successive modificazioni ed integrazioni, recante il testo unico delle leggi in materia di disciplina degli stupefacenti e sostanze psicotrope e di prevenzione, cura e riabilitazione dei relativi stati di tossicodipendenza*, G.U. Serie Generale, n. 173 del 27 luglio 2007.

[25] Ministero della Salute. D.M. 11 maggio 2011. *Aggiornamento e completamento delle tabelle contenenti l'indicazione delle sostanze stupefacenti e psicotrope, di cui al decreto del Presidente della Repubblica 9 ottobre 1990, n. 309 e successive modificazioni ed integrazioni. Inserimento nella tabella I delle sostanze 3,4-metilendiossipirovalerone (MDPV), JWH-250, JWH-122 ed analoghi di struttura derivanti dal 3-fenilacetilindolo e dal 3-(1-naftoil)indolo*.

[26] Ministero della Salute. D.M. 29 Dicembre 2011. *Aggiornamento delle tabelle contenenti l'indicazione delle sostanze stupefacenti e psicotrope, di cui al decreto del Presidente della Repubblica 9 ottobre 1990, n. 309 e successive modificazioni ed integrazioni. Inserimento nella tabella I della sostanza Butilone o bk-MBDB, di taluni analoghi di struttura derivanti dal 2-amino-1-fenil-1-propanone e della sostanza AM-694 e analoghi di struttura derivanti dal 3-benzoilindolo,* G.U. Serie Generale, n. 3 del 04 gennaio 2012 as modified by the Decreto 11 giugno 2012, G.U. Serie Generale, n. 142 del 20 giugno 2012.

[27] V. de Almeida Pdel, A.M. Grégio, M.A. Machado, A.A. de Lima, L.R. Azevedo, *Saliva composition and functions: a comprehensive review*, J. Contemp. Dent. Pract., 9 (2008) 72-80.

[28] I. Zancanaro, R. Pereira Limberger, P.O. Bohel, M. Kerpel dos Santos, R.B. De Boni, F. Pechansky, E. Dutra Caldas, *Prescription and illicit psychoactive drugs in oral fluid – LC–MS/MS method development and analysis of samples from Brazilian drivers*, Forensic Sci. Int., 223 (2012) 208–216.

[29] A. de Castro, B. Pineiro, E. Lendoiro, A. Cruz, M. López-Rivadulla, *Quantification of selected synthetic cannabinoids and Δ9-tetrahydrocannabinol in oral fluid by liquid chromatography–tandem mass spectrometry*, J. Chromatogr. A, 1295 (2013) 99– 106.

[30] C. Coulter, M. Garnier, C. Moore, *Synthetic Cannabinoids in Oral Fluid*, J. Anal. Toxicol., 35 (2011) 424-430.

[31] N. Fucci, N. De Giovanni, M. Chiarotti, *Simultaneous detection of some drugs of abuse in saliva samples by SPME technique*, Forensic Sci. Int., 134 (2003) 40-45.

[32] A.M. Ares, P. Fernàndez, M. Regenjo, A.M. Fernàndez, A.M. Carro, R.A. Lorenzo, *A fast bioanalytical method based on MEPS and UPLC-MS/MS for determining new psychoactive substances in oral fluid*, 174 (2017) 454-461.

[33] M. Sergi, C. Montesano, S. Odoardi, L. Mainero Rocca, G. Fabrizi, D. Compagnone, R. Curini, *MEPS coupled to LC-MS for the rapid and sensitive determination of cannabinoids in oral fluids*, 1301 (2013) 139-146.

[34] N.D. Danielson, P.A. Gallagher, J.J. Bao, *Chemical reagents and derivatization procedures in drug analysis*, in: R.A. Meyers (Ed.), *Encyclopedia of Analytical Chemistry*, John Wiley & Sons Ltd., Chichester, UK, 2000.

[35] V. Gambaro, S. Arnoldi, S. Bellucci, E. Casagni, L. Dell'Acqua, L. Fumagalli, M. Pallavicini, G. Roda, C. Rusconi, E. Valoti, *Characterization of in vitro metabolites of JWH-018, JWH-073 and their 4-methyl derivatives, markers of the abuse of these synthetic cannabinoids*, J. Chromatogr. B, 957 (2014) 68–76.

[36] A. Grigoryev, A. Melnik, S. Savchuk, A. Simonov, V. Rozhanets, *Gas and liquid chromatography–mass spectrometry studies on the metabolism of the synthetic phenylacetylindole cannabimimetic JWH-250, the psychoactive component of smoking mixtures*, J. Chromatogr. B, 879 (2011) 2519–2526.

[37] B.F. Thomas, B.R. Martin, *In vitro metabolism of ()-cis-3-[2-hydroxy-4-(1,1-dimethylheptyl)phenyl]-trans-4-(3-hydroxypropyl)cyclohexanol, a synthetic bicyclic cannabinoid analog*, Drug Metab. Dispos., 18 (1990) 1046–1054.

[38] B. Moosmann, S. Kneisel, U. Girreser, V. Brecht, F. Westphal, V. Auwärter, *Separation and structural characterization of the synthetic cannabinoids JWH-412 and 1-[(5-fluoropentyl)-1H-indol-3yl]-(4-methylnaphthalen-1-yl) methanone using GC–MS, NMR analysis and a flash chromatography system*, Forensic Sci. Int., 220 (2012) e17–e22.

[39] K. Simolka, R. Lindigkeit, H.-M. Schiebel, U. Papke, L. Ernst, T. Beuerle, Analysis of synthetic cannabinoids in spice-like herbal highs: snapshot of the German market in summer 2011, Anal. Bioanal. Chem., 404 (2012) 157–171.

[40] K. Tsujikawa, T. Yamamuro, K. Kuwayama, T. Kanamori, Y.T. Iwata, H. Inoue, Thermal degradation of a new synthetic cannabinoid QUPIC during analysis by gas chromatography–mass spectrometry, Forensic Toxicol., 32 (2013) 1–7.

[41] I. Möller, A. Wintermeyer, K. Bender, M. Jübner, A. Thomas, O. Krug, W. Schänzer, M. Thevis, Screening for the synthetic cannabinoid JWH-018 and its major metabolites in human doping controls, Drug Test. Anal., 3 (2011) 609–620.

[42] S. Kneisel, P. Bisel, V. Brecht, S. Broecker,M.Müller, V. Auwärter, Identification of the cannabimimetic AM-1220 and its azepane isomer (N-methylazepan-3- yl)-3-(1-naphthoyl)indole in a research chemical and several herbal mixtures, Forensic Toxicol., 30 (2012) 126–134.

[43] S. Dresen, S. Kneisel, W. Weinmann, R. Zimmermann, V. Auwärter, *Development and validation of a liquid chromatography–tandem mass spectrometry method for the quantitation of synthetic cannabinoids of the aminoalkylindole type and methanandamide in serum and its application to forensic samples*, J. Mass Spectrom., 46 (2011) 163–171.

[44] S. Dresen, S. Kneisel, W. Weinmann, R. Zimmermann, V. Auwärter, *Development and validation of a liquid chromatography–tandem mass spectrometry method for the quantitation of synthetic cannabinoids of the aminoalkylindole type and methanandamide in serum and its application to forensic samples*, J. Mass Spectrom., 46 (2011) 163–171.

[45] R. Gottardo, A. Bertaso, J. Pascali, D. Sorio, G. Musile, E. Trapani, C. Seri, G. Serpelloni, F. Tagliaroa, *Micellar electrokinetic chromatography: a new simple tool for the analysis of synthetic cannabinoids in herbal blends and for the rapid estimation of their log P values*, J. Chromatogr. A, 1267 (2012) 198–205.

[46] S. Akamatsu, T.S. Mitsuhashi, *MEKC–MS/MS method using a volatile surfactant for the simultaneous determination of 12 synthetic cannabinoids*, J. Sep. Sci., 37 (2014) 304–307.

[47] R. Gottardo, A. Chiarini, I. Dal Prà, C. Seri, C. Rimondo, G. Serpelloni, U. Armato, F. Tagliari, *Direct screening of herbal blends for new synthetic cannabinoids by MALDI-TOF MS*, J. Mass Spectrom., 47 (2012) 141–146.

[48] R.A. Musah, M.A. Domin, R.B. Cody, A.D. Lesiak, A.J. Dane, J.R.E. Shepard, *Direct analysis in real time mass spectrometry with collision-induced dissociation for structural analysis of synthetic cannabinoids*, Rapid Commun. Mass Spectrom., 26 (2012) 2335–2342.

[49] A.D. Lesiak, R.A. Musah, M.A. Domin, J.R.E. Shepard, *DART-MS as a preliminary screening method for herbal incense: chemical analysis of synthetic cannabinoids*, J. Forensic Sci., 59 (2014) 337–343.

[50] O. Beck, L. Rausberg, Y. Al-Saffar, T. Villen, L. Karlsson, T. Hanssonc, A. Helander, *Detectability of new psychoactive substances, 'legal highs', in CEDIA, EMIT, and KIMS immunochemical screening assays for drugs of abuse*, Drug Test Anal., 6 (2014) 492-499.

[51] W.C. Rodrigues, P. Catbagan, S. Rana, G. Wang, C. Moore, *Detection of Synthetic Cannabinoids in Oral Fluid Using ELISA and LC–MS-MS*, J. Anal. Toxicol., 37 (2013) 526 –533.

[52] Z. Takàts, J. M. Wiseman, B. Gologan, R. G. Cooks, *Mass spectrometry sampling under ambient conditions with desorption electrospray ionization*, Science, 306 (2004) 471-473.

[53] V. V. Laiko, M. A. Baldwin, A. L. Burlingame, *Atmospheric pressure matrix-assisted laser desorption/ionization mass spectrometry*, Anal. Chem., 72 (2000) 652-657.

[54] F. Zancanaro, F. Zivolic, D. Favretto, S. D. Ferrara, R. Seraglia, P. Traldi, *Pneumatically assisted desorption/ionization: Some thoughts on the possible ionization mechanisms*, J. Mass Spectrom., 45 (2010) 411-420.

[55] A. B. Costa, R. G. Cooks, *Simulated Splashes: Elucidating the Mechanism of Desorption Electrospray Ionization Mass Spectrometry*, Chem. Phys. Lett., 464 (2008) 1-3.

[56] A. Venter, P.E. Sojka, R. G. Cooks., *Droplet Dynamics and Ionization Mechanisms in Desorption Electrospray Ionization Mass Spectrometry*, Anal. Chem, 78 (2006) 8549-8555.

[57] Z. Takats, J. M. Wiseman, R. G. Cooks, *Ambient mass spectrometry using desorption electrospray ionization (DESI): instrumentation, mechanisms and applications in forensics, chemistry, and biology*, J. Mass Spectrom., 40 (2005) 1261-1275.

[58] T. J. Kauppila, N. Talaty, P. K. Salo, T. Kotiaho, R. Kostiainen, R. G. Cooks, *New surfaces for desorption electrospray ionization mass spectrometry: porous silicon and ultra-thin layer chromatography plates*, Rapid Commun. Mass Spectrom., 20 (2006) 2143-2150

[59] Y. Yang, J. Deng, *Analysis of pharmaceutical products and herbal medicines using ambient mass spectrometry*, Trend. Anal. Chem., 82 (2016) 68-88.

[60] M. Morelato, A. Beavis, P. Kirkbride, C. Roux, *Forensic applications of desorption electrospray ionisation mass spectrometry (DESI-MS)*, Forensic Sci. Int., 226 (2013) 10-21.

[61] M. Morelato, A. Beavis, A. Ogle, P. Doble, P. Kirkbride, C. Roux, *Screening of gunshot residues using desorption electrospray ionisation–mass spectrometry (DESI–MS)*, Forensic Sci. Int., 217 (2012) 101-106.

[62] J.M. Wiseman, D.R. Ifa, Y. Zhu, C.B. Kissinger, N.E. Manicke, P.T. Kissinger, R.G. Cooks, *Desorption electrospray ionization mass spectrometry: Imaging drugs and metabolites in tissues*, P. Natl. Acad. Sci. USA, 105 (2008) 18120-18125.

[63] N.E. Manicke, A.L. Dill, D.R. Ifa, R.G. Cooks, *High resolution tissue imaging on an orbitrap mass spectrometer by desorption electro-spray ionization mass spectrometry (DESI-MS),* J. Mass Spectrom., 45 (2010) 223-226.

[64] C. Chen, T. Chen, X. Zhou, R. Kline-Schoder, P. Sorensen, R.G. Cooks, Z. Ouyang, *Design of Portable Mass Spectrometers with Handheld Probes: Aspects of the Sampling and Miniature Pumping systems*, J. Am. Soc. Mass Spectrom., 26 (2015) 240-247

[65] *Guidance for Industry, Bioanalytical Method Validation*, US Department of Health and Human Services, Food and Drug Administration, 2001, 2017, https://www.fda.gov/downloads/Drugs/Guidances/ucm368107.pdf

[66] Z. Takats, J. M. Wiseman, R. G. Cooks, *Ambient mass spectrometry using desorption electrospray ionization (DESI): instrumentation, mechanisms and applications in forensics, chemistry, and biology*, J. Mass Spectrom., 40 (2005) 1261-1275.

[67] A. de Castro, B. Piñeiro, E. Lendoiro, A. Cruz, M. López-Rivadulla, *Quantification of selected synthetic cannabinoids and Δ9-tetrahydrocannabinol in oral fluid by liquid chromatography–tandem mass spectrometry*, J. Chromatogr. A 1295 (2013) 99–106.

[68] W.C. Cheng, K.M. Ng, K.K. Chan, V.K.K. Mok, B.K.L. Cheung, *Roadside detection of impairment under the influence of ketamine – Evaluation of ketamine impairment symptoms with reference to its concentration in oral fluid and urine*, Forensic Sci. Int., 170 (2007) 51–58.

Chapter 6

Odorant Binding Protein-Functionalized Superparamagnetic Nanoparticles for Biomedical Applications

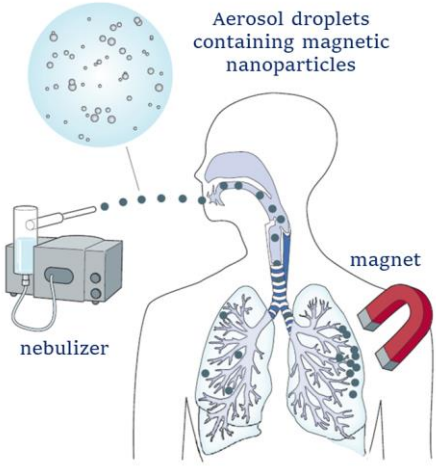

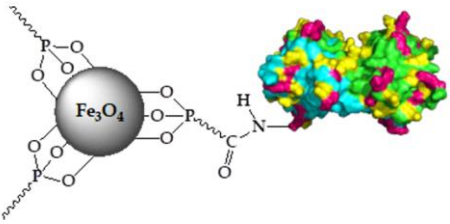

6.1 Introduction

6.1.1 Nanoparticles in Medicine

Nanoparticles (NPs) are materials with overall dimensions under 100 nm: they are also defined as *zero-dimensional nanomaterials*, since all their dimensions are in the nanoscale, opposing to the so-called *one-dimensional nanomaterials*, which have one dimension larger than the nanoscale (nanowires and nanotubes), and *two-dimensional nanomaterials*, which have two dimensions larger than the nanoscale (self-assembled monolayer films and nanoplates).

Peculiar properties characterize and differentiate the NPs from the bulk material: the latter has constant physical properties regardless of its size, whereas, size-dependent properties have been observed in nanomaterials. In fact, in bulk materials the percentage of atoms on the surface is not significant if compared to the total number of atoms, thus the properties of the material derive from the bulk. In the nanoscale, the ratio surface/volume of the atoms is significant and the properties of the nanomaterials can be tuned by changing their dimensions.

From the beginning of the year 2000, the development of nanomaterials has become one of the most attractive and innovative field of research in chemistry, physics and medicine. Numerous syntheses have been proposed by combining different types of materials, ranging from metals, alloys, metal oxides and semiconductive materials to a large variety of organic and inorganic networks [1], such as silica [2] and polymers [3]. Different nanostructures can be combined into larger superstructures by triggered or spontaneous assembly, further increasing the potential of the nanotechnology.

The main advantage of the nanomaterials is the possibility of engineering the systems with a bottom-up approach, thus tuning all the characteristics of the material (**Figure 6.1**):

1 Inorganic, organic and organometallic materials have been synthetized. The chemical composition of the material is of paramount importance since it is related to the nanostructure's properties and reactivity. Moreover, it is possible to develop hybrid materials characterized by the presence of a core, usually a metal or a metal oxide, and organic or

inorganic coatings, in order to exploit the features of the different building blocks.

2 Nanomaterials have been synthetized in several configurations, such as spherical NPs, dendrimers, liposomes, nanorods… It is possible to tune the physical properties of the material, such as shape and morphology, by tuning the reaction conditions and using chemical templates.

3 Size has a great influence on colloidal stability, specific surface area, optical properties, in vivo behavior and cellular uptake. In the 1–100 nm size range, the dispersion of nanoparticles in solution is derived from both electrostatic repulsion/attraction phenomena, related to the surface charge and the ionic strength of the solvent, and steric effects, tuned by the length of surface ligands.

4 The surface of the NPs can be modified by using proper functionalization in order to provide specific properties to the material, such as hydrophobicity, surface charge and presence of functional groups.

5 It is possible to functionalize the nanomaterials with ligands in order to reach specific targets, such as proteins, enzymes and peptides.

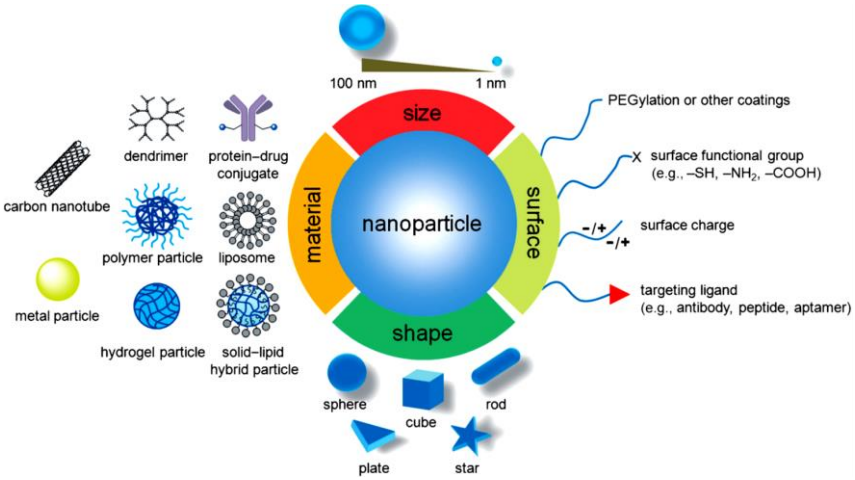

Figure 6.1 NPs functionalization

In addition to the properties tunability, the other main advantage of the NPs is the large surface-to-volume ratio compared to traditional delivery vehicles, thus being an important advantage in the nanomedicine with higher loading of the drug/active principle.

Nanomedicine refers to the medical application of nanotechnology: NPs are characterized by a size range comparable with the dimensions of biomolecules such as antibodies, membrane receptors, nucleic acids and proteins. Moreover, due their high surface/volume ratio and the possibility of modulating their properties, nanomaterials are considered as powerful tools for imaging, diagnosis and therapy. Nanoparticles developed from both inorganic and bioorganic precursors such as phospholipids, lipids, lactic acid, dextran, chitosan, have been proposed for medical applications.

A rapid summary of the nanoparticles used in medicine is reported below and represented in **Figure 6.2**:

- **Inorganic nanoparticles**: Au, Ni, Pt and TiO_2 nanoparticles are used in medicine. Gold nanoparticles (< 50 nm) are one of the most studied nanomaterials: they can be synthetized in different geometries, such as nanospheres, nanoshells, nanorods or nanocages. Moreover, gold NPs are characterized by localized surface plasmon resonant properties, i.e. the irradiation of light results in photons emission characterized by the same frequency in all directions, since the conduction electrons are driven by the associated electric field to a collective oscillation at a resonant frequency. Gold nanoparticles are therefore excellent labelling biosening units and can be detected by numerous techniques, such as optic absorption, fluorescence and electric conductivity [4,5]. Moreover, they can be used as nanocarriers, since the surface can be easily functionalized with drugs, linkers, ligands, antibodies and aptamers [4,5].
- **Quantum dots** (QDs) are fluorescent semiconductive nanocrystals (2–10 nm) that show size- and composition-tunable emission spectra and high quantum yield. All these characteristics make QDs excellent contrast agents for imaging and labels for bioassays [6].
- **Core-shell nanoparticles** are organic, inorganic or hybrid systems characterized by a core, usually inorganic, coated with another material (polymer, linker, metal). In biological applications core-shell nanoparticles have major advantages over bare nanoparticles, thus including less cytotoxicity [7], higher biocompatibility, better conjugation with biomolecules and increased chemical stability [8]. The coating is usually made of polymers that: i) provide biocompatibility to the nanomaterial; ii) improve the dispersion in body fluids by increasing the hydrophilicity of the system and the cellular uptake. The use of coatings

allows to enhance the release of the drug at its targeted site by specific degradation of the biopolymer under specific conditions of ionic strength, temperature, and pH [9-11].

Core/shell nanoparticles are also extensively used for bioimaging: the contrast magnification is provided by the core material, whereas the coating allows NPs targeting and biocompatibility. The shell thickness can be tuned to provide both adequate contrasting properties and binding to the target biomolecule and increasing the cyto-compatibility [12].

- **Liposomes** are phospholipid vesicles (50–100 nm) that are characterized by a bilayer membrane structure, mimicking biological membranes, and an internal aqueous phase. They are classified according to the number of layers into multi-, oligo- or uni-lamellar. They are amphiphilic, thus enabling the transport of both hydrophilic drugs entrapped within their aqueous interior and hydrophobic drugs dissolved into the membrane. Owing to their physicochemical characteristics, liposomes show excellent half-life in blood circulation, penetration and diffusion properties. Moreover, their surface can be functionalized with proper ligands in order to increase drug delivery targeting [13].
- **Dendrimers** are highly branched synthetic polymers (< 15 nm) with layered architectures constituted of a central core, an internal region and numerous terminal groups that determine the material properties. Dendrimers of different nature have been synthetized, characterized by different solubility and biological activity. They are excellent drug and imaging nanocarriers and, due to their highly branched structure, surface/volume ratio and surface functional groups, a high concentration of active principle can be loaded on dendrimers [14,15].
- **Carbon nanotubes** are formed by coaxial graphite sheets (< 100 nm diameter). These structures can be either single- (one graphite sheet) or multi-walled coated nanotubes (several concentric graphite sheets). They exhibit excellent strength and electrical properties and are efficient heat conductors, thus are suitable for biosensing applications. Carbon nanotubes can be functionalized in order to obtain drug nanocarriers and tissue-repair scaffolds [16,17]. Moreover, they have been demonstrated promising features for neuronal interfacing applications, due to their unique mechanical and electrical properties. Such devices are currently

tested for the treatment of a wide range of conditions such as stroke, schizophrenia and Parkinson's disease [18].

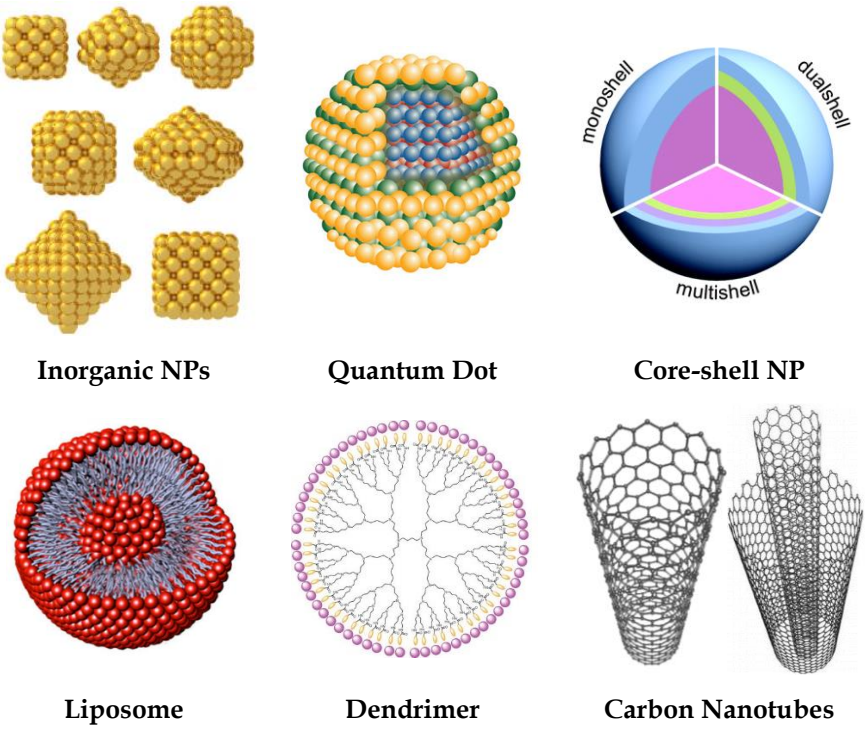

Figure 6.2 Graphic summary of common NPs used in medicine

In-vivo imaging is of pivotal importance for medical diagnosis, emerging as an essential technique to develop targeted therapies. Combining multiple imaging methods is required in order to collect more data as possible to obtain an accurate diagnosis, as in the case of tumors, brain diseases and biodistribution studies. New generations of hybrid nanomaterials that combine multiple imaging functionalities are extremely promising in order to obtain dynamic images, even at the cellular level. Noticeable progresses have been recently achieved by combining several techniques, such as optical imaging (OI), single-photon emission computed tomography (SPECT), positron emission tomography (PET), X-ray computed tomography (CT) and magnetic resonance imaging (MRI) [19,20].

Paramagnetic and superparamagnetic nanoparticles have been used as contrasting agents in MRI in order to magnify the imaging contrast [19]. QDs

are being used in two-photon induced photoluminescence [21], whereas NPs possessing radioactivity have been proposed in PET [22,23].

Multimodal nanoparticles [24] have been developed to be detected simultaneously by different imaging techniques, such as both MRI and OI (such as fluorescence microscopy): they incorporate both luminescent functionalities and the paramagnetic core (magnify the MRI signals), thus reaching a high sensitivity, which is typical of OI and 3D imaging of biological nanostructures and processes at cellular resolution (i.e. MRI detection). These NPs are characterized by shorter imaging time compared to classical pharmaceuticals, since only one contrast agent is required in order to perform different imaging analyses. They have reduced risk of exposure and a very high radiolabeling efficiency can be achieved in a short time, thus reducing the costs of the treatment.

To overcome the limitations and drawbacks of conventional drug administration, i.e. limited effectiveness, poor biodistribution, lack of sensitivity, strong side effects and toxicity, targeted drug delivery systems have been proposed: the drug/active principle is loaded onto functionalized nanocarriers, reaching the specific target, thus increasing its effectiveness and minimizing undesirable side effects [25]. Local delivery results in increased concentration of the drug only in the targeted cell, thus reducing its overall concentration.

Obviously, the design of a drug delivery system requires the evaluation of stability, shelf life, biocompatibility, biodistribution, targeting, functionality and ways of incorporation.

Nanoparticles can also enhance the bioavailability of water-insoluble drugs by their incorporation in the nanosystem, allow large payloads, and protect the therapeutic agents from physiological barriers, thus avoiding the drug hydrolytic or enzymatic degradation and body clearance.

Nanocarriers used for medical applications have to be biocompatible and nontoxic, thus liposomes, solid lipids nanoparticles, dendrimers, polymers, silica, carbon materials and magnetic nanoparticles have been proposed as drug delivery systems. Drugs can be either encapsulated in the nanoparticle's structure (liposomes, nanospheres and mesoporous polymeric nanoparticles), or grafted onto their surface.

The design of multifunctional nanoparticles (**Figure 6.3**) significantly can improve the cell targeting: in fact, classic nanoparticles provide a single function, whereas multifunctional nanoparticles combine different functionalities in a single nanomaterial. For example, the surface of a drug-loaded NP can be functionalized with a proper ligand able to provide targeting toward a specific cell or tissue.

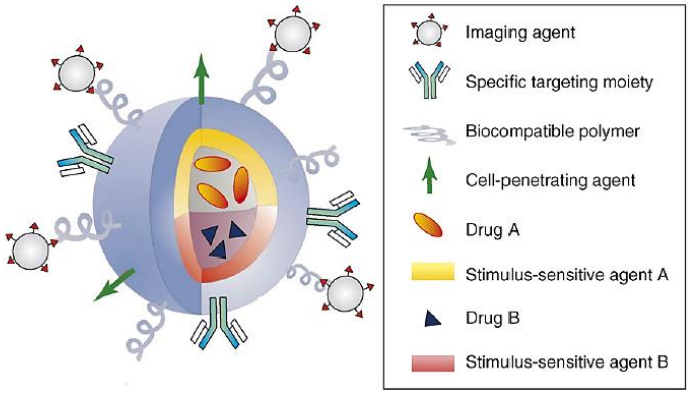

Figure 6.3 Schematic representation of a multifunctional NP

Cell-specific targeting occurs via active or passive mechanism:

- In active targeting, the functionalization by using *targeting ligands* allows to achieve ligand–receptor interactions [26-28]. Due to the high complexity of biological systems, a large variety of targeting ligands has been developed, thus including small *baiting* molecules, receptors, oligosaccharides, peptides, proteins, antibodies and nucleic acids. Active targeting can be also achieved through a manipulation of physical stimuli (i.e. temperature, pH, magnetism).
- Passive targeting is based on drug accumulation in the areas around the tumor with leaky vasculature [29]. The major drawback of passive targeting is that a large amount of administered nanoparticles is known to accumulate in non-targeted organs, especially in liver, spleen, and kidneys.

Once the drug-nanocarrier conjugate reaches the target, the drug is released through changes in physiological environment such as temperature, pH, ionic strength, or via an enzymatic activity.

Undesirable effects of nanoparticles strongly depend on their hydrodynamic size, shape, concentration, chemical composition (especially surface

chemistry), route of administration, reaction of the immune system and residence time in the bloodstream.

6.1.2 Superparamagnetic Nanoparticles

Among the different types of nanocarriers, superparamagnetic nanoparticles are one of the most studied class in medical research, for applications in cancer theranostics, imaging and drug delivery. They are characterized by a size range of 1–20 nm and exhibit a unique form of magnetism called superparamagnetism [30].

In macroscopic ferromagnetic materials, the spins of unpaired electrons undergo spontaneous magnetization if their energy is lowered by aligning with spins in neighboring atoms. To decrease the overall energy of the system, multiple magnetic domains are present and in absence of an external magnetic field, the overall magnetization is zero. The size of these domains is determined by the energy balance occurred in the creation of a new energy domain. By applying a magnetic field, the domains align their spin through the direction of the field. After the external field removal, a residual magnetization (M_r) is present: in order to change the domain orientation additional energy is required (H_c), thus ferromagnetic materials are characterized by hysteresis curves (**Figure 6.4**).

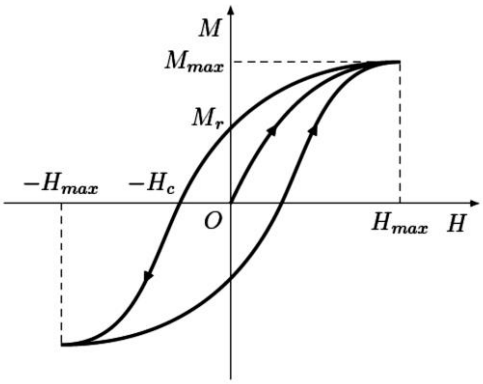

Figure 6.4 Hysteresis curve of a ferromagnetic material

A paramagnetic material is characterized by no magnetic moment in external zero field, whereas a weak magnetic moment is induced by a magnetic field. The induced moment is in the same direction as the applied field, and it increases with the magnetic field until a saturation value. At low fields, the

magnetization increment is linear, following Curie's law, which states that magnetization scales directly with field and inversely with temperature (**Figure 6.5**).

Paramagnetic domains do not have strong interactions, thus, after the removal of the external magnetic field, low activation energy is required to restore a random orientation, thus returning to a zero overall magnetic moment: paramagnetic materials do not present hysteresis (**Figure 6.5**).

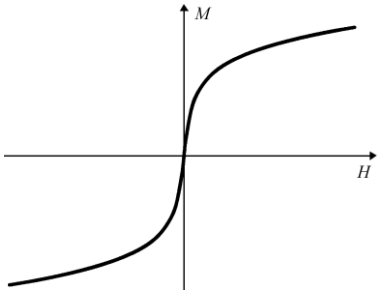

Figure 6.5 magnetization curve in paramagnetic materials

The characteristic size of the magnetic domain depends on the chemical composition and structure of the material. The size of the NPs can be lower than the characteristic domain dimension, thus each nanoparticle is a single magnetic domain (**Figure 6.6**). Single domain ferromagnetic and ferromagnetic NPs can be characterized by a new type magnetism, the superparamagnetism. A transition temperature between superparamagnetism and ferromagnetism is present and it is directly proportional to the characteristic size of the domain.

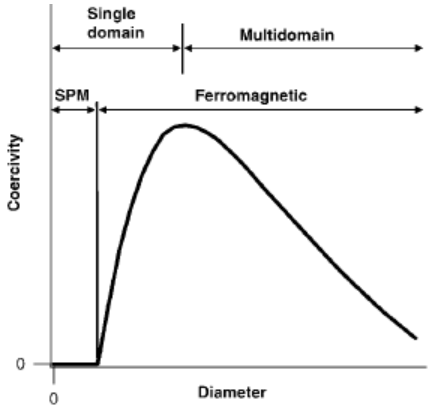

Figure 6.6 Superparamagnetic (SPM)/ferromagnetic behavior and single/multiple domain in function of the size of the NP

Superparamagnetic materials are characterized by the same behavior of paramagnetic materials, i.e. they follow Curie's law, they have zero magnetic moment after the magnetic field removal and similar magnetization curves, whereas the saturation magnetization is comparable to that of ferromagnetic materials (**Figure 6.7**). The spin reorientation is related to the temperature: below a limit called blocking temperature, the thermal energy is not sufficient to guarantee the random reorientation of the spins, thus the single domain NPs become ferromagnetic.

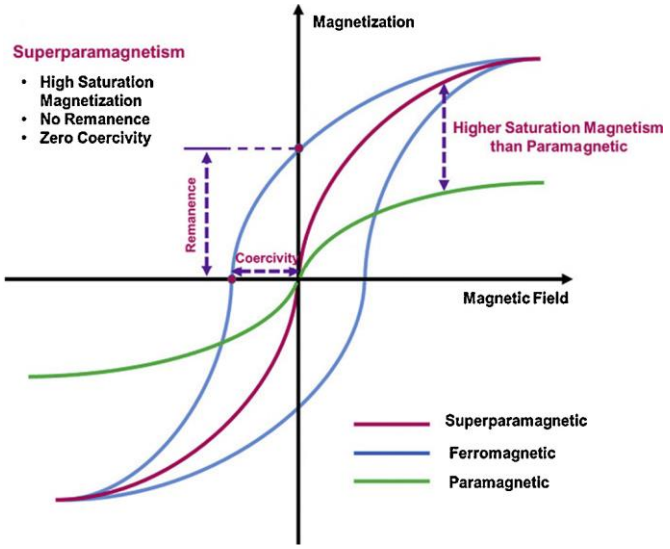

Figure 6.7 magnetization curves of ferromagnetic, paramagnetic and superparamagnetic materials

As previously reported, after the external field removal, zero overall magnetization is reached: thermal energy rearranges the magnetic domains spins (the NPs) in a random orientation, thus no additional energy is required to demagnetize the system. The superparamagnetic nanoparticles become highly dispersed when the magnetic field is switched off: this feature is of paramount importance since NPs aggregates are recognized and engulfed by macrophages, being removed from the body and removing the carried drug.

Superparamagnetic nanoparticles are also characterized by high magnetic susceptibility; therefore, it is possible to drive the nanoparticles by using an external low magnetic field.

6.1.3 Superparamagnetic Iron-Oxide Nanoparticles

Since the introduction of magnetism in medicine in the 1960s [31] research has been focused on the development of new magnetic particles and drug vectors, in order to increase the drug concentration in blood vessels, reduce early clearance from the body and minimize nonspecific cell interactions. This aspect has a major importance in drug-design, since it allows to minimize the side effects and to increase the internalization efficiency within target cells, thus reducing the total dose required, while maintaining the drug efficacy [32, 33].

Superparamagnetic iron oxide nanoparticles (SPIONs) are mainly based on α-Fe_2O_3 (hematite), γ-Fe_2O_3 (maghemite) and Fe_3O_4 (magnetite) nanoparticles with an inorganic core in the 1-20 nm size range.

Among the SPIONs, magnetite and maghemite nanoparticles are the most studied in medical research for biomedical applications. They can be coated by organic, inorganic and hybrid coatings and functionalized with drugs, DNA, imaging agents and targeting molecules (antibodies, small molecules, membrane cell penetrating agent and guests for bioreceptors). SPIONs can also be included in liposomes, thus obtaining *magnetoliposomes*, which combine agglomeration capabilities with superparamagnetic features [34].

By applying a magnetic field, SPIONs provide a stronger and more rapid magnetic response compared to bulk materials: superparamagnetic nanoparticles are able to drive drugs to a specific target site (biomolecule or cell) in the body under the influence of an external magnetic field (**Figure 6.8**). After its removal, SPIONs do not retain residual magnetism at ambient temperature, thus they have less tendency to agglomerate, being easily redispersed in body fluids and tissues. This has a noticeable importance, since the uptake by leukocytes can be strongly reduced, thus increasing the drug half-life.

The use of nanoparticle in medicine is related to their ability to circulate in the bloodstream, thus avoiding their uptake by macrophages, particularly in the reticuloendothelial system.

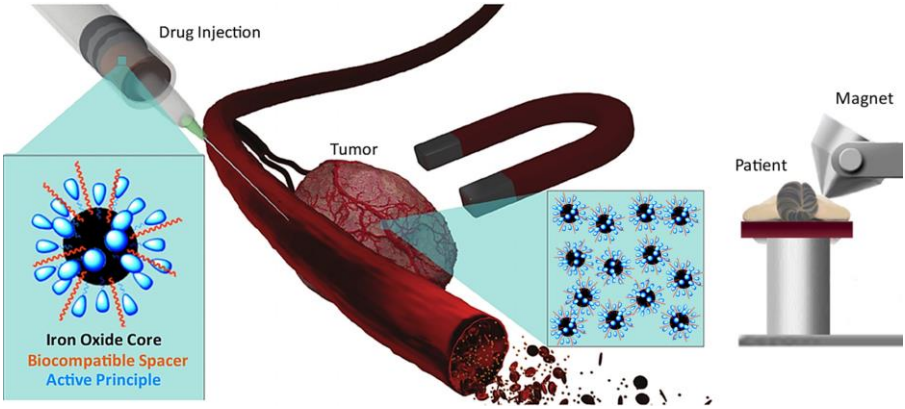

Figure 6.8 Magnetic drug delivery

The size of nanoparticles largely determines their half-life and their uptake: NPs characterized by sizes less than 10 nm are mainly removed by renal clearance, whereas particles larger than 200 nm become concentrated in liver and spleen (leading to possible bioaccumulation and bio-toxicity) or removed by phagocytic cells, thus reducing their plasma concentrations. Moreover, SPIONs characterized by a particle size less than 2 nm are not suitable for medical use, due to the increased capability of diffusing through cell membranes, damaging intracellular organelles and exhibiting potentially toxic effects. Nanoparticles the 10–100 nm range are ideal for biomedical applications, due to the longer circulation times and drug half-life.

NPS shape determines the extent to which the NP interacts with membrane receptors and hence the degree of internalization. The shape of nanoparticles can be tuned by changing reactant, templating agents and reaction conditions. Shi et al. modelled the particle–cell interaction by considering the diffusion and absorption of rod-like and spherical NPs through the membrane of a spherical cell [35]. The results showed that the internalization of the NPs is strongly affected the contact angle, related to their shape, whereas their endocytosis does not depend on the absorption mechanism [36].

Moreover, nanoparticle shape has a noticeable influence in the rate of macrophage uptake [37]: spherical SPs internalization in macrophages is favored over nanoparticles characterized by high aspect ratios.

As the size of iron oxide reaches the nanorange, the ions on the surface of nanoparticles gain a noticeable importance in determining the magnetic properties: the oxidation state of the iron ion on the surface of the nanoparticle

is extremely sensitive to the surrounding environment and can have a potential effect on the shape of the nanoparticles. For instance, iron ions in the trivalent state lead to synthetize spherical nanoparticles, whereas metal ions in the divalent state lead to the preferred formation of nanorods [38].

The first step to design and develop uniform and stable SPIONs is the synthesis of the core material, since it determines the morphology and the magnetic properties of the material. The most commonly used methods for preparation of uniform SPIONs in solution are co-precipitation, micro-emulsion and the use of organometallic precursors in organic solvent decomposition.

Magnetite and maghemite nanoparticles can be synthesized through the co-precipitation of Fe^{2+} and Fe^{3+} aqueous salt solutions by addition of nitrates [39] or bases [40]. The control of size, shape and composition of nanoparticles depends on the anion, Fe^{2+} and Fe^{3+} ratio, pH and ionic strength of the media [41]. Conventionally, magnetite is prepared by adding ammonium hydroxide in an oxygen-free environment to an aqueous mixture of Fe^{2+} and Fe^{3+} chloride at a 1:2 molar ratio, thus resulting in black magnetite precipitation in a 9-14 pH range.

Iron oxide nanoparticles can be oxidized, thus affecting the physical and chemical properties of the SPIONs. In order to prevent the oxidation by environmental oxygen and agglomeration, Fe_3O_4 nanoparticles are usually coated with either an organic or inorganic layer during the precipitation step.

The size of magnetic nanoparticles prepared by the co-precipitation method mainly depends on the pH and ionic strength of the precipitating solution. It has been demonstrated that as the pH and ionic strength of the medium increases, the size of the particles decreases [42]. These parameters not only affect the size of the nanoparticles, but also determine the electrostatic potential on the surface of these nanoparticles.

Smaller and more uniform nanoparticles can be synthesized by the micro-emulsion approach by using iron precursors like ferrous and ferric chloride. The aqueous phase is dispersed as reverse micelle in the oil phase, acting as nanoreactors, providing a confined space that limits the growth and agglomeration of nanoparticles during their synthesis, thus regulating both their size and surface properties [43].

Finally, the synthesis of monodispersed magnetic nanoparticles in the 3-20 nm range by thermal degradation and reduction of iron (III) acetylacetonate [44] in phenyl ether or benzyl alcohol [45] in the presence of alcohol, oleic acid, and oleylamine at temperatures ranging from 170 to 265°C have been reported. These nanoparticles are characterized by enhanced magnetic susceptivity.

The surface charge of nanoparticles is related to their colloidal stability: high positive or negative zeta potentials allow high dispersion stability resulting in the absence agglomeration. It also determines their biodistribution, since it is an important parameter affecting internalization of the nanoparticles in the target cells. Uncoated SPIONs are internalized into cells by different mechanisms, demonstrating surface-dependent particle endocytosis behavior [46]. Particles characterized by a hydrophobic surface present many drawbacks, thus including aggregation due to hydrophobic interactions, adsorption on protein surface and engulfment in circulating macrophages, resulting in their clearance from plasma [47]. Therefore, they are characterized by low circulation time.

Nanoparticle surface can be engineered by using hydrophilic and biocompatible polymer coatings such as polyethylene glycol, chitosan and dextran. The presence of terminal hydroxyl or amino functional groups allows to avoid nanoparticles engulfment by reticuloendothelial cells or circulating macrophages, thus reaching higher therapeutic efficacy due to increased residence time in blood [48]. Surface engineering of magnetic nanoparticles with different functional groups makes them suitable for a wide variety of biomedical applications.

Coating of SPIONs allows to:

1. reduce the aggregation tendency of the uncoated particles, their polydispersity and increase the colloidal stability
2. protect the iron ions on the surface of the NP from the oxidation
3. provide functional groups on the NP surface for further conjugation with targeting ligands, antibodies and drug active principle
4. increase drug half-life in blood by avoiding clearance by the reticuloendothelial system
5. enhance the biocompatibility of the SPION by using biocompatible polymers

6. increase their uptake efficiency by target cells: biopolymers such as PEG can enhance the internalization of NP in target cells, exploiting both the presence of functional groups, such as hydroxyl and amino [49], and targeting ligands able to interact with membrane protein.

SPIONs can be coated either during or after their synthesis, thus obtaining in both cases uniform coatings. The coating thickness has a strong influence since it influences NPs magnetization [50].

The nanoparticles can be loaded with a drug in order to be used as magnetic carriers, thus increasing the therapeutic effect in a specific area of the body. Obviously, the active principle has to be protected from the surrounding physiological environment and has to be released just in the target tissue.

The loading can be achieved by conjugation on the surface of the nanoparticle, co-encapsulation in a larger system, or adsorption in mesoporous materials.

The conjugation is performed by chemical bond or non-covalent interactions, such as hydrogen bond, electrostatic interaction and coordination of metal ions. Covalent linkage to a specific substituent enhances both the loading capability and stability of the material. This procedure usually requires the use of linkers, spacers and coupling agents, thus leading to multistep reactions (**Figure 6.9**).

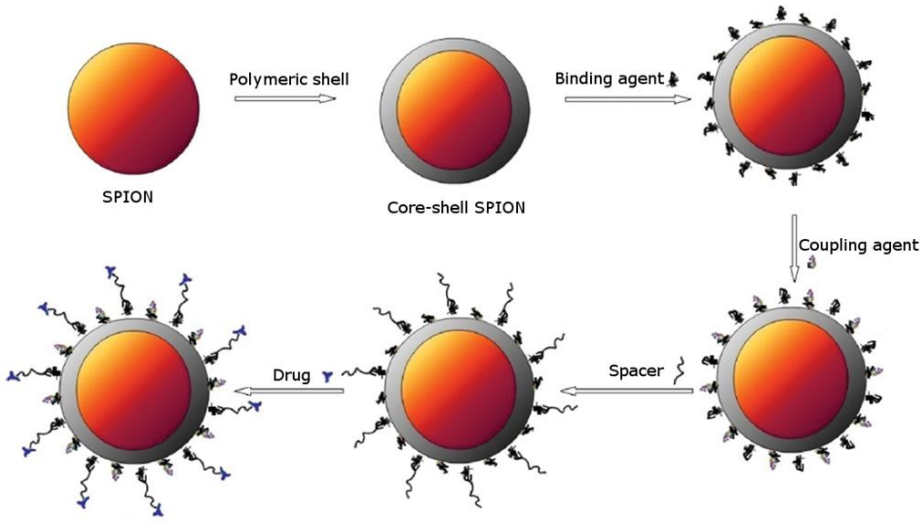

Figure 6.9 Schematic representation of core-shell SPION and drug conjugation

SPIONs are known to be cleared from the body *via* endogenous metabolic iron pathways. Histopathological evaluation revealed no iron-positive pigments in macrophages from major organs like liver, lungs, spleen, brain, kidney, and heart [51]. Gupta et al reported that SPIONs coated with polyethylene glycol are nontoxic to human [52].

However, iron overload at the target site is considered one of the main causes of SPION-associated toxicity: after the coating, the breaking up of the biopolymer can cause the release of high levels of bare Fe_2O_3 nanoparticles, thus producing an imbalance in homeostasis. This phenomenon can alter cellular responses, leading to DNA damage, inflammatory response, oxidative stress, genetic changes, disruption of cytoskeletal organization of cells and cytotoxicity.

6.1.4 *Nanomagnetosols: Inhalable SPIONs*

The inhalation of medical aerosols is widely used for the treatment of lung disorders such as asthma [53], chronic obstructive pulmonary diseases [54], cystic fibrosis [55], respiratory infections [56] and lung cancer [57]. Targeted aerosol delivery to the affected lung tissue may improve therapeutic efficiency.

Dames et al. proposed the use of an aerosol formulation containing SPIONs (*Nanomagnetosol*) in order to improve the targeting of the aerosol toward a specific region of lungs by using an external magnetic field [58] (**Figure 6.10**).

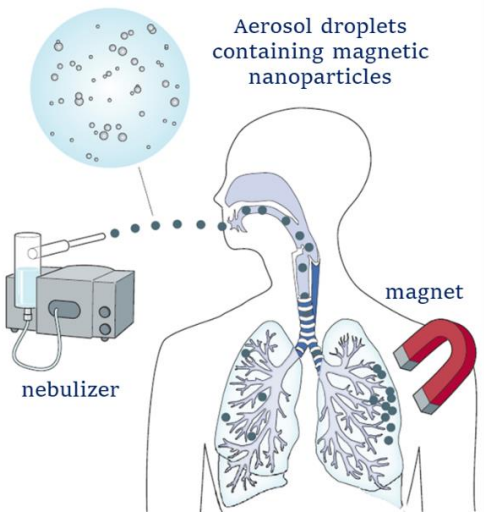

Figure 6.10 Schematic representation of *nanomagnetosol* targeting principle

This novel approach is very intriguing since it allows the deposition in the specific targeting of diseased lung areas. Being *nanomagnetosols* SPION-based drugs, they are characterized by a plethora of possible drug formulations and properties; moreover, they can be combined with other nanocarriers, such as liposomes and micelles, commonly used in aerosol formulations. Drug delivery to the lungs can be also achieved by using dry powder inhalers, characterized by higher stability of the pharmaceutical. In this case, nanoparticles can be loaded on the so-called Trojan microparticles, made of biocompatible polymers [59].

Another noticeable advantage of *nanomagnetosols* is that the actual drug carrier is the aerosol droplet as a whole, which is characterized by a dimension in the μm scale, thus containing hundreds of SPIONs. Hence, this microscopic carrier in the first airways acts as one extremely large SPION, when subjected to the magnetic field. Since the magnetic force acting on a magnetic particle is proportional to the third power of its radius, packaging a multitude of magnetic nanoparticles in a larger carrier, such as an aerosol droplet, highly improves magnetic guidability.

Many challenges affect aerosol drug development: i) scaled-up magnetic field-generating equipment used by Dames, in order to provide sufficient magnetic flux density and field gradient at the target site; ii) the optimization of the magnetic field application; iii) the assessment of the safety of the aerosolized material.

6.1.5 *Quorum Sensing and Quorum Quenching*

Cell-to-cell bacterial communication, known as *quorum sensing* (QS), relies on the production, secretion and detection of diffusible small signaling molecules called *autoinducers* (AIs). More precisely, bacteria produce AI, which are then secreted in the environment, thus they can be perceived, by specific receptors, by other bacterial cells of the same species that occupy the same niche.

Therefore, trough QS bacteria can modulate their gene expression patterns in a growth- and cell-density dependent manner, in response to the concentration of chemical signals in the local environment, thus allowing a coordinated and synchronized response of the overall population. One of the main interesting aspect of QS is that the signaling molecules also trigger their own biosynthesis, thus they have been termed *autoinducers*.

QS regulates several bacteria vital functions requiring the coordinative action of numerous cells to be effective, such as bioluminescence, production of secondary metabolites, biofilm formation, sporulation and motility. Many bacterial pathogens, such as *Pseudomonas aeruginosa*, control the expression of virulence factors *via* QS networks (**Figure 6.11**).

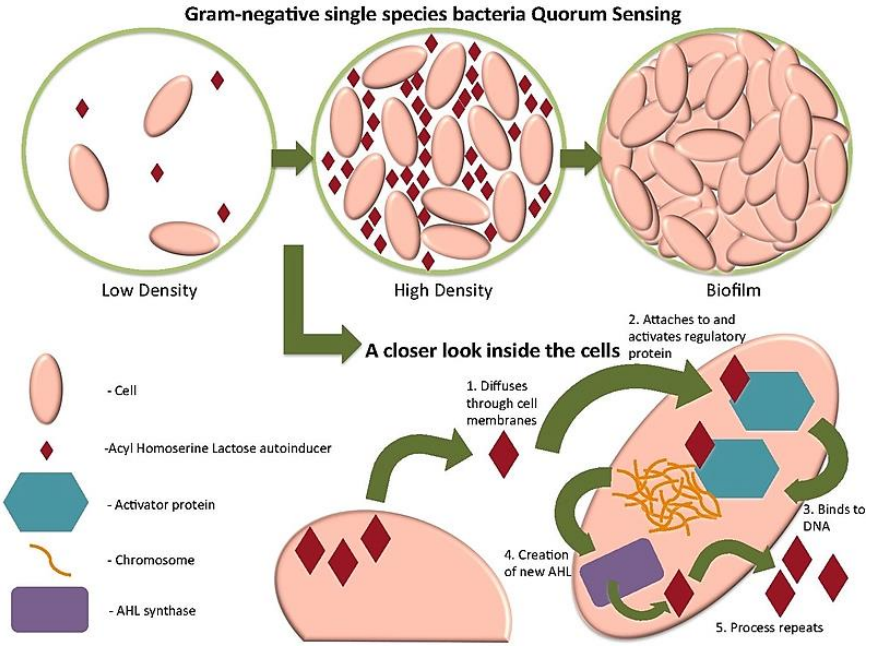

Figure 6.11 Quorum sensing schematic representation

Several classes of compounds have been identified as *quorum sensing molecules* (QSM) [60] (**Figure 6.12**):

1. The majority of Gram-positive bacteria use **peptide-pheromones**, which are specific to species and strains. These QSMs are small cyclic or linear peptides, that can be detected either by a membrane-bound sensors that are able to transduce the signal by cascade process, or can be internalized into the cell, in order to directly interact with regulators modulating gene expressions.
2. **Autoinducers-1**, N-acyl-homoserine lactones (AHLs), are mostly produced from Gram-negative bacteria. Their structure is characterized by a common lactone ring and an aliphatic chain, whose length and substituent depend on both the secreting bacterium and the specific *quorum systems*.

3. The signaling molecule **autoinducer-2** (AI-2), is a complex mixture of several interconvertible furanones derived from 4,5-dihydroxy-2,3-pentanedione (DPD), and it is considered to be a universal signal involved in both intra- and interspecies communication, since it is secreted by a wide range of both Gram-negative and Gram-positive bacteria.
4. Hormones **autoinducer-3**, or AI-3 (epinephrine and norepinephrine) are common in human opportunistic pathogens.
5. **Fatty acids** such as *cis*-11-methyl-2-dodecenoic acid, the so-called diffusible signal factor, and esters, such as 3-Hydroxypalmitic acid methyl ester (3-OH-PAME), have proposed as QSM
6. **Quinolones** are reported as QSM, for example, in *Pseudomonas Aeruginosa*.

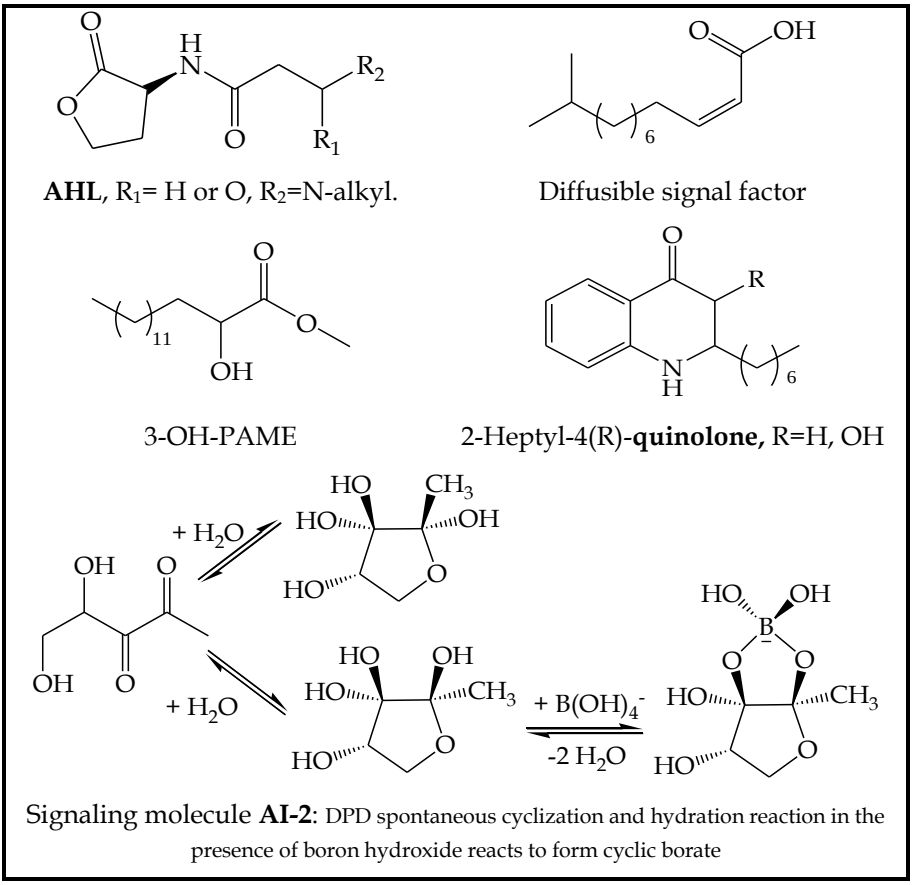

Figure 6.12 *Quorum sensing molecules*

Different Gram-negative bacteria use more than one QS system and can combine these systems in additive [61], hierarchical (one induces a second one in a cascade system) [62], or overlapping models [63].

Bacterial pathogens represent a noticeable risk to human health due to the rapid dissemination of antibiotic-resistant strains, thus resulting in increasing infectivity, lethality and drug overdosing. Bacteria such as *Pseudomonas aeruginosa* have develop an efficient multidrug resistance, thus resulting in high mortality rates. Other species have noticeable economic impact such as plant bacterial pathogens [64] or fish and crustacean bacterial pathogens [65] and can be dangerous for human consumption.

The variety of QSM and the complexity of signaling networks makes *quorum sensing* a very sophisticated communication system, used by bacteria to coordinate their activities based on the local population density. Increasing research interest is devoted to the development of agents able to interfere with the QS system of pathogenic bacteria, in order to decrease bacterial virulence and to develop new antibacterial therapies. Disrupting the signaling process is called *quorum sensing inhibition* or *quorum quenching* (QQ).

Nowadays, different QQ approaches are possible:

1. inhibition of the biosynthesis of the QSMs
2. inhibition of the QSMs detection by blocking the signal receptor
3. enzyme-catalyzed degradation or modification of the signal molecules

When compared to bactericidal or bacteriostatic strategies, QQ allows to develop therapies characterized by lower side-effects or to overcome the antibiotic resistance of pathologic bacteria.

Nature has developed different tools to interfere with QS: *quorum quenching* allows bacteria to modulate the behavior of the microbial community or interfere with other bacteria' *quorum sensing* systems, by the production and secretion of molecules structurally similar to QSMs, acting as *quorum sensing inhibitors* [66,67].

6.1.6 *Pseudomonas Aeruginosa*

Lung infections are responsible for most of the morbidity and mortality in patients with cystic fibrosis (CF). The bacterial pathogens are increasing their antibiotic resistance and virulence, thus resulting in complex therapies and shortening patient's life expectancy. In recent years, the bacteria community in CF lungs has changed considerably due to the intensive antibiotic usage, thus resulting in the emerging of bacteria characterized by antibiotic resistance or new pathogens. One of the most important issues for clinical research is to develop therapies for multidrug-resistant bacteria [68].

Among this class, *Pseudomonas aeruginosa* is one of the most studied microorganism (**Figure 6.13**). It is an aerobic and motile Gram-negative bacterium, causing several health disorders in both animals and humans. It is responsible of several acute and chronic infections, i.e. pneumonia, septic shock, urinary tract infections, gastrointestinal infections, skin and soft tissues infections in patients with cystic fibrosis, neutropenic, premature infants, burn victims and immunosuppressed patients [69].

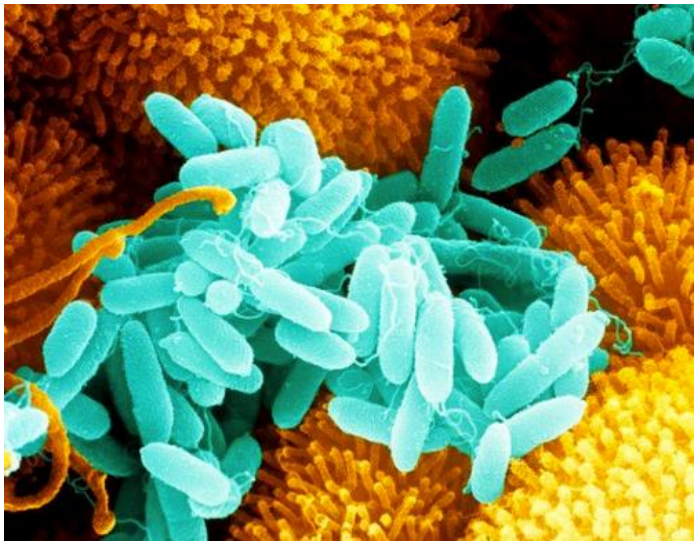

Figure 6.13 Colored scanning electron micrograph of *Pseudomonas aeruginosa* bacteria on ciliated human nasal epithelium [70].

Pseudomonas infections have been reported to be present in various stages, thus including attachment and colonization, local invasion and disseminated systemic infections [67]. They are invasive, toxicogenic and multidrug resistant, leading to several hospital infections in immunocompromised

patients, often resulting in high mortality rate. The major clinical issue for patients affected by CF is a progressive loss of pulmonary functions caused by chronic lung infection by *Pseudomonas aeruginosa*, thus resulting in the premature death of more than 80% of patients [71]. The fight against this bacterium is challenging, since repeated bouts of inflammation progressively lead to lung damage. Although antibiotics can decrease the frequency and duration of acute events, *Pseudomonas* is able to establish permanent residence in host lungs by biofilm formation and through use of oxoreductive metabolites.

Previous studies demonstrated that this bacterium uses *quorum sensing* to coordinate several biological functions, thus including formation of biofilms, modulation of immune responses, motility and production of virulence agents [72]. This is one of the most interesting aspect of QS: the bacterium is able to grow inside host tissues without harming them, until the population reaches a threshold concentration. After that limit, it forms biofilms, starts the secretion of secondary cytotoxic metabolites, becoming very aggressive, and finally overcomes the host's immune system, leading to the infection [70].

The QS network of *Pseudomonas Aeruginosa* consists of three systems termed *las*, *rhl*, and *pqs* that are organized hierarchically (**Figure 6.14**).

The detailed *quorum sensing* system is reported in several published articles [73] and can be summarized as follows:

1. The *las* system (blue) is responsible for the biosynthesis of N–3–oxododecanoyl–homoserine lactone (AI–1) and initiates both other QS systems.
2. The *rhl* system (green) contains a positive feedback loop that leads to a rapid increase of autoinducer concentration involving the second autoinducer *N*–butyryl–homoserine lactone (AI–2).
3. The *pqs* system (red) uses the *Pseudomonas* quinolone signal (PQS) using several QSMs, the most important of which is the 2-heptyl-3-hydroxy-4-quinolone, able to regulate many genes, thus including those devoted to the production and secretion of both cytotoxic secondary metabolites, such as pyocyanin, elastase, exotoxin A and exotoxin S, and the molecules used in biofilm formation (rhamnolipids).

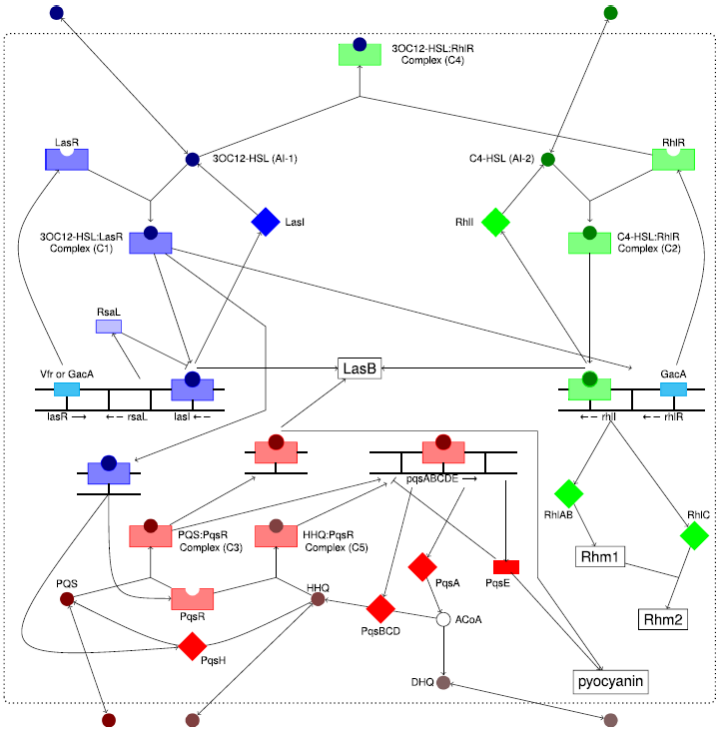

Figure 6.14 Schematic representation of QS system of *Pseudomonas Aeruginosa* [73]

Among the virulence factors, the most important in lung infections is pyocyanin (5-methyl-1-hydroxyphenzine), a blue, redox-active phenazine (**Figure 6.15**).

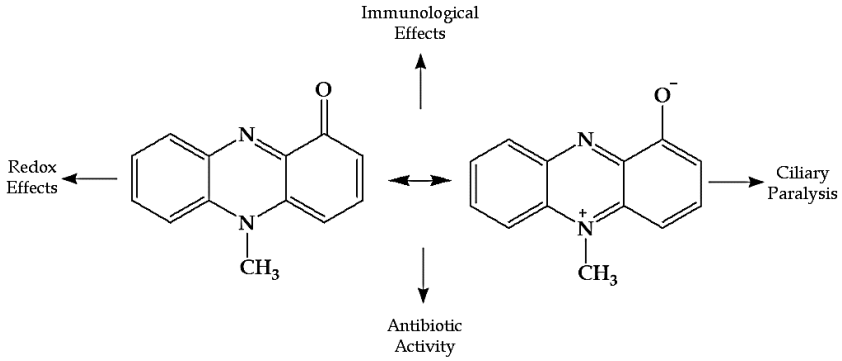

Figure 6.15 Pyocyanin chemical structure and biological major effects

Pyocyanin is a zwitterion presenting both hydrophobic and hydrophilic regions, thus it can easily interact with cytoplasmic membranes. Redox

activity involve the host cell NADH, thus producing reactive radical oxygen species, such as oxygen superoxide O_2^-, and hydrogen peroxide (H_2O_2), leading to significant oxidative stress [74]. In addition, pyocyanin interferes with cellular respiration by using the electrons removed during the oxidation steps of the Krebs cycle to increase the production of reactive oxygen species. Through redox cycling, pyocyanin can also inactivate a1-protease inhibitor, used by the host to protect lung tissue from protease-mediated injury, and reduce nitric oxide, thus exerting major influences over blood flow, pressure and immune functions.
Ciliary clearance of inhaled particles is the first line of defense against infection of the lungs. Both pyocyanin and its degradation products can affect ciliary function leading to a decrease of the cilia beat frequency until their complete paralysis [75].

Moreover, pyocyanin is able to interfere with the immune system of the host, leading to decrease the leukocytes concentration in the site of inflammation and increasing their apoptosis. These features allow to overcome the host immune system and establish chronic infections [76,77]. Pyocyanin has antibiotic activity against other bacteria and fungi, thus allowing *Pseudomonas aeruginosa* to compete with other microorganisms.

Due to the antibiotic resistance, *Pseudomonas* is one of the most challenging bacteria in clinical therapy, thus new therapies have to be proposed. The use of QQ to interfere with the QS system of the bacteria (thus reducing the virulence and the antibiotic resistance) could be an interesting approach.

6.1.7 *Odorant Binding Proteins*

Odorant Binding Proteins (OBPs) are monomeric or, rarely dimeric, proteins with a molecular mass of 19 kDa (or 38 kDa in the case of the dimers) classified among the Lipocalins. These proteins are expressed in animals, plants and bacteria, and despite the low sequence homology (usually less than 20%), present a common structural frame, the *lipocalin folding*, characterized by two domains: a nine-strand β-barrel connected by a short linker (hinge sequence) to a C-terminal α-helix. The β-barrel consists of 70–80% of the total number of amino acid residues and represents the ligand-binding site (**Figure 6.16**) [78]. A large variety of protein forms presenting different binding specificities have been developed during the evolutionary pathway.

Lipocains can be used for the production of artificial affinity receptors, thus proving to be a noticeable alternative to antibodies as recognition elements in biosensors [79]. Protein scaffolds are characterized by stable frames that do not modify their overall 3D structure in response to multiple substitutions in the amino acid sequence.

OBPs are multifunctional scavengers for small hydrophobic molecules dissolved in the mucus lining the nasal epithelia of mammals. They are able to bind a large number of natural and synthetic structurally unrelated organic compounds belonging to different chemical classes, characterized by hydrophobicity and molecular masses ranging between 150 and 300 Da. In the OBP-ligand complex, the guest molecule maximizes the number of hydrophobic interactions with the non-polar amino acid residues covering the surface of the cavity. Bovine OBP is a dimer in which the C-terminal domain (residues 125–159) is swapped between the two monomers, a peculiar feature specific for the bovine species (**Figure 6.16** bottom).

Porcine OBP is a monomer characterized by with an empty cavity able to complex ligands with a high degree of hydrophobicity having molecular mass ranging from 160 to 200 Da (**Figure 6.16** top).

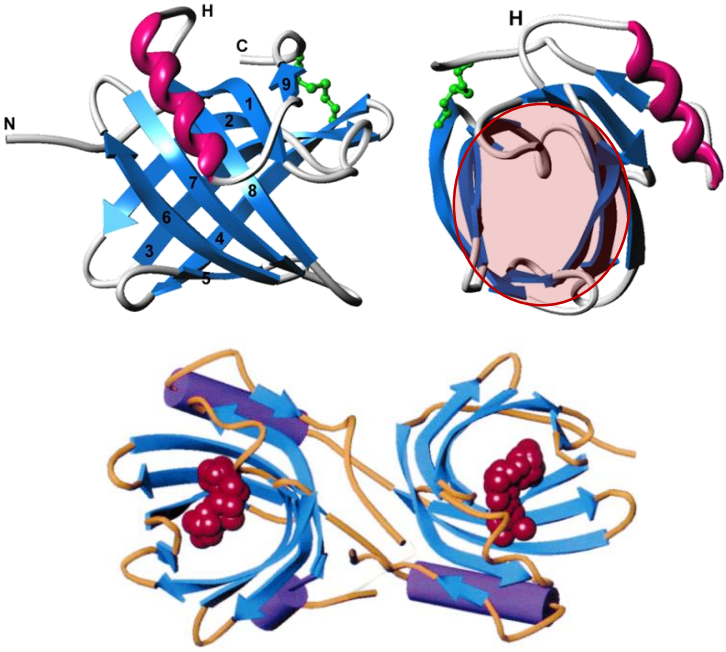

Figure 6.16 porcine Odorant Binding Protein (top), ligand binding site is highlighted in red, and bovine Odorant Binding Protein (bottom)

The complexation occurs independently from the guest odorous properties, chemical class, and molecular structure. The values of the dissociation constants of the different OBP–ligand binding complexes range between 120 nM and 0.46 mM [80].

Recombinant forms of OBPs have been developed and produced with high yields by heterologous bacterial systems, mainly using *Escherichia coli*. Mutant Proteins tagging with six histidine residues at the amino terminal allow their purification in a single step by affinity chromatography with a nickel-nitrilotriacetic acid (Ni-NTA) agarose resin [81].

Recombinant bovine OBP was utilized by Bianchi et al. for developing a bovine odorant binding protein-based filtering cartridge for the removal herbicides from water [80].

The aim of this research study is the development of OBP-functionalized SPIONs to be used as nanomagnetosols for lung infection. This innovative approach of *quorum quenching* is devoted to the complexation of *quorum sensing* molecules and virulence factors of *Pseudomonas aeruginosa*, thus allowing to overcome the antibiotic resistance and especially the redox activity of pyocyanin. Moreover, the use of functionalized superparamagnetic nanoparticles could allow to target the drug in the specific diseased area, thus increasing the concentration of the protein in the inflammation zone and effectively interfere with the *quorum sensing* of the bacterial colony. This new hybrid bionanosystem is design to be used to decrease the virulence of aggressive antibiotic resistant bacteria in cooperation with typical antibiotic therapies.

6.2 Materials and Methods

6.2.1 Chemicals and materials

Benzyl alcohol anhydrous (99.8%), iron (III) acetylacetonate ($Fe(acac)_3$), dichloromethane anhydrous (≥ 99.8%), ethanol anhydrous (> 99.8%), hexane anhydrous (95%), 2-propanol anhydrous (99.5%), potassium phosphate dibasic trihydrate (≥ 99.0%), potassium dihydrogen phosphate (> 99%) and pyocyanin from *Pseudomonas aeruginosa* (≥ 98%) were purchased from Merk (Milan, Italy).

11-Phosphonoundecanoic acid (> 98%), 3-phosphonopropionic acid (> 94%) and 1-(3-dimethyl-aminopropyl)-3-ethylcarbodiimide (EDC) (97%) were from abcr (76187 Karlsruhe, Germany). HisPur™ Ni-NTA Resin was purchased from ThermoFischer (Waltham, MA USA).

Infrared spectra were recorded using a FT-IR Nicolet 5700 spectrometer (Thermo Fisher Scientific, Inc., Waltham, MA, USA), equipped with an ATR Smart Orbit TM, operating between 400 and 4000 cm^{-1}.

Nanoparticles' magnetization was measured by using a vibrating sample magnetometer (VSM) from Princeton Applied Research equipped with a 12-inch electromagnet from LakeShore (Westerville, USA), a recirculating chiller 73029 LakeShore e gaussmeter 450 LakeShore. The maximum applied field was 2 T. All the magnetization measurements were performed by Dr. F. Casoli from CNR-IMEM, Parma.

X-ray powder diffraction (XRD) data were collected on a Thermo ARL X'TRA X-ray diffractometer $Cu_{K\alpha}$ X-radiation at 40 kV and 30 mA.
The nanoparticles were also analyzed by X-ray photoelectron spectroscopy (XPS) by using a high intensity twin anode source, XR 50 (SPECS GmbH, Berlin, Germany) and a hemispherical energy analyzer with wide-angle lens - Phoibos 150 Wal (SPECS GmbH, Berlin, Germany). The measurements were performed by using the Kα emission of Al (1486.6 eV).

Conventional and high-resolution transmission electron microscopy (TEM) and energy dispersive X-ray spectroscopy (EDX) in scanning mode (STEM) were carried out on the solution of the nanoparticles using a JEOL2200FS microscope working at 200 keV. Samples were prepared by depositing a drop of a suspension of the particles in hexane on carbon-coated copper grids. TEM analyses were performed by Dr. L. Nasi from CNR-IMEM of Parma.

UV-vis analyses were performed by using a Thermo Evolution 260 Bio + SPE 8w Peltier Water Cooled Cell-Changer, ThermoFischer (Waltham, MA USA).

6.2.2 *OBP biosynthesis*

The biosynthesis was performed by the Veterinary Science Department of the University of Parma.

The recombinant form of bOBP and pOBP, with six histidine residues at the amino terminal, were obtained from a BL21-DE3 *E. coli* strain transformed with the expression vector pT7-7 containing the appropriate OBP cDNA, as previously reported [81].

Purification of the protein was carried out by affinity chromatography using Ni-NTA agarose according to the manufacturer's instructions, followed by dialysis in 50 mM sodium phosphate pH=7.8. Protein purity was assessed by SDS–PAGE and its concentration was determined by measuring the absorbance value at 280 nm.

Functionality of the protein in solution was determined by direct titrations using the fluorescent ligand 1-aminoanthracene (AMA), as previously reported [80]. Briefly, samples of 0.5 µM 6XHisbOBP in 20 mM Tris–HCl buffer pH=7.8 were incubated overnight at 4 °C with increasing concentrations of AMA (0.15–20 µM). Fluorescence emission spectra were recorded between 450 and 550 nm with a PerkinElmer LS 50 luminescence spectrometer (PerkinElmer, Waltham, MA, USA) (excitation and emission slits at 5 nm) at a fixed excitation wavelength of 380 nm. The formation of the binding complex between 6XHis-bOBP and AMA was monitored as an increase in the fluorescence emission intensity at 480 nm.

6.2.3 *OBP Ni-NTA Agarose Resin Filter*

In order to assess the OBPs affinity toward QSMs preliminary experiments were performed by filtering solutions of pyocyanin at two concentration levels, i.e. 500 and 2100 µg/l in phosphonate buffer (pH=7.8), on a Ni-NTA resin functionalized with 8 mg/ml of the respective OBP.

The filters were obtained according to the procedure previously reported [80].

Briefly, a liquid-liquid extraction was performed on 8.0 mg/mL purified protein solution (in 50 mM sodium phosphate pH 7.8) with dichloromethane (phosphonate solution:dichloromethane =2:1), in order to remove any low

molecular weight metabolites from *E. coli* cultures occupying the ligand binding sites of 6XHis-bOBP.

For the subsequent coupling step, the aqueous phase was collected and immediately loaded onto a column containing 250 µL of Ni-NTA agarose. The resin was washed with 5 mL of the same phosphate buffer and the effective amount of 6XHis-bOBP bound to the solid matrix was determined by measuring the absorbance of the washed solution at 280 nm.

6.2.4 *UV-Vis Analysis*

The pyocyanin solutions were analyzed by UV-Vis analysis under the following conditions:

- Virtual dual beam optics
- Software: Thermo Insight
- 100% baseline correction
- Range λ: 300-750 nm
- Band width: 1 nm
- Integration time: 0.25 s

Method validation was performed by using phosphonate buffer 50 mM, pH=7.8.

Detection (y_D) and quantitation (y_Q) responses were expressed as signals based on the mean blank (x_b) and the standard deviation of blank responses (s_b) as follows:

$y_D = x_b + 2t\ s_b$

$y_Q = x_b + 10t\ s_b$

where *t* is the constant of the *t*-Student one-tailed distribution at 95% confidence level. The values x_b and s_b were calculated by performing ten measurements of blank solution.

The respective LODs and LOQs were obtained as a projection of the corresponding signals y_D and y_Q through the calibration plot of the corresponding analytes.

Calibration curves (six concentration levels, three replicated measurements for each level) were evaluated by analyzing standard solutions of pyocyanin in phosphonate buffer. Linearity was evaluated on six concentration levels in 50-2500 µg/l range.

Homoscedasticity was verified by applying the Bartlett test. Mandel's fitting test was also performed to check the goodness of fit and linearity. The significance of the intercept (significance level 5%) was established by running a Student's t-test.

Repeatability and intermediate precision were calculated in terms of RSD % on two concentration levels i.e. 100 and 250 µg/l by performing six replicated measurements for each level. Intermediate precision was estimated over three days verifying homoscedasticity of the data and performing the analysis of variance (ANOVA) at the confidence level of 95%.

Trueness was calculated in terms of relative recovery rate (RR%) as follows:

$R.R.\% = c_1/c_2\ 100$

where c_1 is the measured concentration and c_2 is the concentration calculated from the quantity spiked into the sample. Two concentration levels i.e. 200 and 2100 µg/l for each analyte with 10 replicated measurements were analyzed.

Finally, the analysis of filtered solutions, with an initial concentration of 1000 and 2100 µg/l was performed.

6.2.5 *SPION synthesis*

The SPION were obtained by thermal decomposition and reduction of iron (III) acetylacetone under nitrogen atmosphere. 1.00 g of $Fe(acac)_3$ and 20 ml of benzyl alcohol were added in a three-neck round-bottom flask. The solution was vigorously stirred at ambient temperature under nitrogen flow for 1h, then it was heated at 175°C for 48 h. Then the mixture was cooled at ambient temperature by keeping the magnetic stirring and the inert atmosphere.

The black precipitate was sonicated, centrifuged and magnetically decanted; finally, the precipitate was washed with absolute ethanol (3 times) and dichloromethane (1 time). The obtained nanoparticles were stored in hexane and were stable up to 1 month.

The nanoparticles were characterized by VSM, TEM, XRD, XPS and FT-IR analyses.

6.2.6 SPION functionalization with carboxyalkylphosphonic acids

A solution of 11-phosphonoundecanoic acid or 3-phosphonopropionic acid in 2-propanol anhydrous (1 mM) was prepared under nitrogen. Then the dried SPIONs were added to the solution under vigorous stirring and sonicated for 1h. A molar ratio carboxyalkylphosphonic acid/SPIONs 2:1 was the optimum. The nanoparticles were stirred at ambient temperature under nitrogen for 16 h, then the nanoparticles were magnetically decanted and washed with water. Again, the nanoparticles were characterized by VSM, TEM, EDX, XPS and FT-IR analyses.

6.2.7 SPION-bOBP functionalization

The nanoparticles functionalized with the carboxyalkylphosphonic acids were finally conjugated with the bOBP by using EDC as coupling agent. The w/w ratio between the SPIONs and the protein is 8.9:0.15, whereas the molar ratio SPIONs:EDC is 1:2, as reported by Wang and Lee [82]. The reaction was performed in phosphonate buffer (pH=7.3) at 4°C for 24 h under mechanical agitation. The nanoparticles were magnetically decanted, washed with phosphonate buffer and stored at 4°C. The supernatant solutions were stored at -20°C and were analyzed by BCA protein assay kit in order to obtain, by difference, the concentration of nanoparticles loaded on the SPIONs. The analysis was performed by UV-Vis spectroscopy, at 562 nm.

Calibration curves (eight concentration levels, three replicated measurements for each level) were evaluated by analyzing standard solutions of bOBP in phosphonate buffer in a concentration range blank-0.64 μg/l, corresponding to a 0-45.40 (μg OBP/ g SPION).

Homoscedasticity was verified by applying the Bartlett test. Mandel's fitting test was also performed to check the goodness of fit and linearity. The significance of the intercept (significance level 5%) was established by running a Student's *t*-test. Repeatability was calculated in terms of RSD % on two concentration levels i.e. 2.84 and 11.35 μg/l by performing six replicated measurements for each level.

The concentration of bOBP grafted on the nanoparticle was considered by three different samples from two protein batches.

Finally, the magnetization of the functionalized bOBP-SPIONs was evaluated by VSM analysis.

6.3 Results and discussion

This research study, performed in collaboration with both the Veterinary Science Department of the University of Parma and IMEM-CNR, Parma, had the aim to develop an odorant binding protein functionalized superparamagnetic nanoparticles system to be used in synergy with the common therapies for the treatment of antibiotic-resistant bacterial infections. The hybrid drug should allow to drive the active principle directly to the infected area of the lungs by exploiting SPIONs magnetic delivery, thus increasing the concentration of the drug in a local area. OBP is proposed as *quorum quenching* agent toward *quorum sensing molecules*, i.e. acyl-homoserine lactones and pyocyanin, the major virulence factor of *Pseudomonas aeruginosa*.

Despite several isoforms of OBPs have been purified and characterized from the nasal mucosa of several mammalian species, in this study, we considered only porcine OBP (pOBP), a monomeric lipocalin, and bovine OBP (bOBP), a dimer with domain swapping.

The choice of the mentioned OBPs as experimental models was based on the following background:

1. bOBP and pOBP are well characterized lipocalins [83]
2. Bovine and porcine OBP can bind a large number of structurally unrelated ligands
3. The recombinant His-tagged form and mutants of OBP are purified at high yields from *Escherichia coli* soluble extracts (30 mg/l of medium) [84]

A previous study [85] proved that bOBP was able to complex acyl-homoserine lactones i.e. n-butyryl -homoserine lactone, n-hexanoyl-L-homoserine lactone and n-heptanoyl-L-homoserine lactone, present in several Gram-negative bacteria *quorum sensing* systems and in the *rhl* system of *Pseudomonas aeruginosa*; in addition, unpublished data proved that both bOBP and pOBP can bind n-3-oxo-dodecanoyl-L-homoserine lactone, the *quorum sensing molecule* of the *las* QS system of *Pseudomonas*.

6.3.1 OBPs complexation capabilities toward pyocyanin

The binding capabilities of the two different odorant binding proteins were tested toward pyocyanin, the major virulence factor of *Pseudomonas aeruginosa*. The complexation of this molecule is of pivotal importance in order to develop a new drug to be used in cooperation with common antibiotic, in order to remove the redox activity of the pyocyanin *via* protein binding.

All the tests were performed by using OBP filters according to the study of Bianchi et al. [80] for the removal of common herbicides from water: the 6XHis tagged proteins were linked to a Ni-NTA agarose resin as shown in **Figure 6.17**.

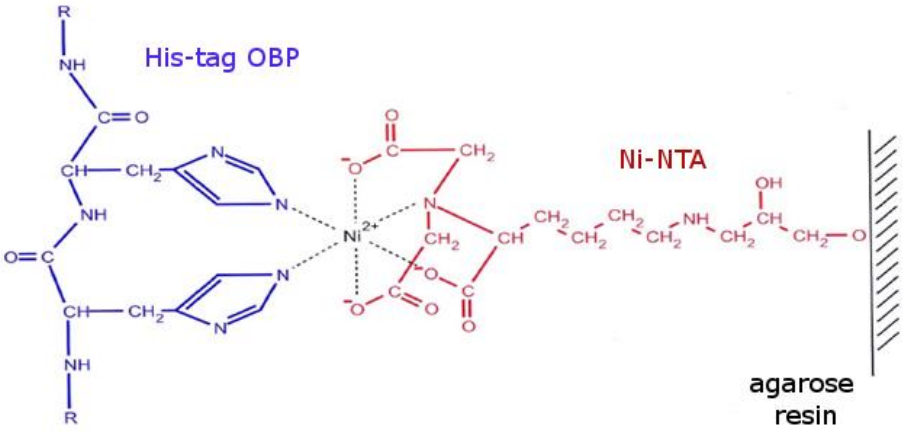

Figure 6.17 schematic representation of 6XHis-tagged protein - resin functionalization

As previously reported, the binding capability of Ni-NTA agarose was 8 mg of protein loaded per 1 mL of resin, thus obtaining a system characterized by no protein leaking even after prolonged buffered washing.

The filter was obtained by packing a 1 ml syringe with filtering paper, glass wool and 250 µl of functionalized resin and washed with 1 ml of phosphonate buffer (50 mM, pH=7.8) (**Figure 6.18**).

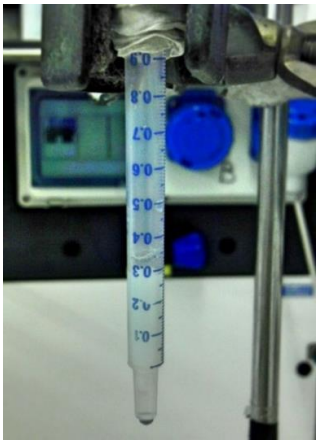

Figure 6.18 OBP-filter

The pyocyanin solutions were eluted through the filter and then 6 washing cycles with phosphonate buffer were performed, in order to remove the unbounded pyocyanin. The analysis of filtered solutions was performed in order to determine which protein among bOBP and pOBP had the highest binding capability toward pyocyanin.

The binding tests on the 6XHis-bOBP- and 6XHis-pOBP-functionalized resin were based on the UV-vis spectrophotometric evaluation of the concentration of the eluted pyocyanin. Two absorbance peaks were considered, i.e. 380 and 310 nm.

The method was validated by following the EURACHEM guidelines [86]. The first step was the analysis of a batch of standard solutions of pyocyanin in phosphonate buffer (50mM, pH=7.8), thus obtaining LODs and LOQs values, of 17 and 50 µg/l respectively. Linearity was assessed by considering six concentration levels in the LOQ-2500 µg/l range, thus obtaining a linear fitting, as confirmed by Mandel's fitting test. The model was characterized by no significant intercept (Student's *t*-test, significance level 5%) and a slope coefficient=7.4 10^{-5} (±0.1 10^{-5}).

Repeatability was evaluated in terms of RSD% on two concentration levels i.e. 100 and 250 µg/l, thus obtaining RDS% of 6.0 and 3.9 respectively, whereas intermediate precision was characterized by RSD% in the 5.6-12.5% range (n=6).

The calculated recovery rate for the pyocyanin were 92.62(±0.03) and 93.75 (±0.05) respectively (n=10).

Two filtered solutions, characterized by a loading concentration of 1000 and 2100 µg/l respectively, were finally analyzed, obtained the results reported in **Figure 6.19**.

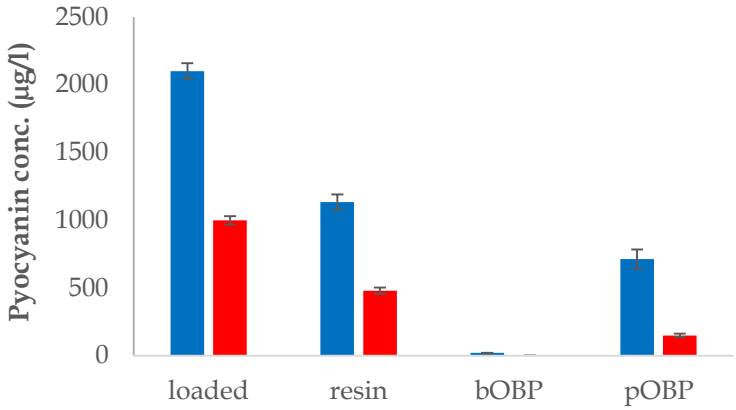

Figure 6.19 complexation capabilities of the filtering system: loaded solution, Ni-NTA resin, bOBP-functionalized resin and p-OBP functionalized

As can be clearly seen in **Figure 6.19** the bare resin was able to retain about 50% (44±8% and 52±5.2% for the highest and the lowest concentration levels, respectively) of pyocyanin. The functionalization with pOBP improved the retention capabilities to 66±13% and 85±15% for the two considered levels, whereas the linkage of bOBP allowed an almost complete binding of pyocyanin. On the basis of these findings, the bOBP was characterized by the highest binding capabilities with respect to pOBP. The results were in agreement with HPLC-MS measurements (unpublished study), demonstrating that the bOBP was characterized by excellent complexation capabilities toward 3-oxo-dodecanoyl-L-homoserine lactone, leading to its complete complexation at 100 µg/l.

6.3.2 *Design of the bOBP-SPION functionalization*

Due to the higher binding capabilities of bOBP toward both QSM molecules and pyocyanin respect to pOBP, the bovine odorant binding protein was chosen as functionalizing protein for the development of a new magnetic drug. A 3D representation of the protein is depicted in **Figure 6.20**. The overall dimension of the dimeric protein is 40 x 40 x 70 Å [87], very close to that of a single nanoparticle.

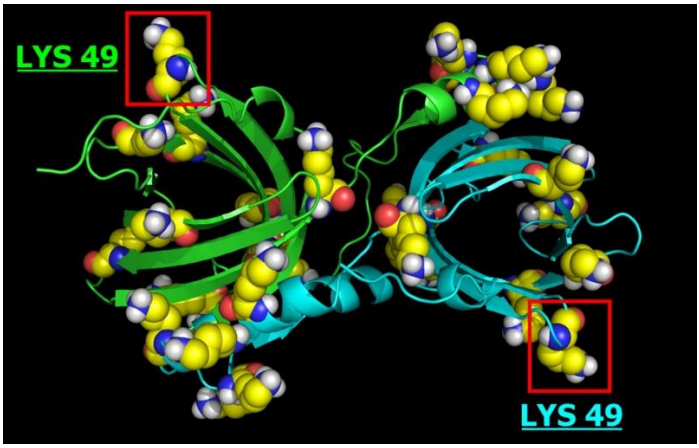

Figure 6.20 3D structure of the bOBP. The lysine amino acids are highlighted

As depicted in the figure, the protein is characterized by several lysine amino acids on the surface, thus increasing the solubility in water and phosphonate buffer. In particular, the two Lys 49 groups (one for each monomeric part of the protein), which are freely exposed to the solvent, can be suitable for substitution or functionalization. The SPIONs' functionalization could be achieved *via* amide bond between the OBP amino terminal groups and a carboxylic acid function belonging to a proper spacer. This has to be characterized by the presence of both a carboxylic acid substituent suitable for protein conjugation and a functional group able to form strong bonds with the NPs.

Phosphonate groups have proven to be suitable for binding iron oxide nanoparticles [88-90], thus carboxyalkylphosphonic acids were selected as SPION-bOBP linkers.

6.3.3 *SPION Core*

The iron oxide core was synthetized by thermal decomposition and reduction of iron III acetylacetone in benzyl alcohol (**Scheme 6.1**). This reaction is known to produce nanoparticles characterized by a size distribution in the 3-20 nm. The reaction conditions for the present synthesis were those optimized in a previous study [91]:

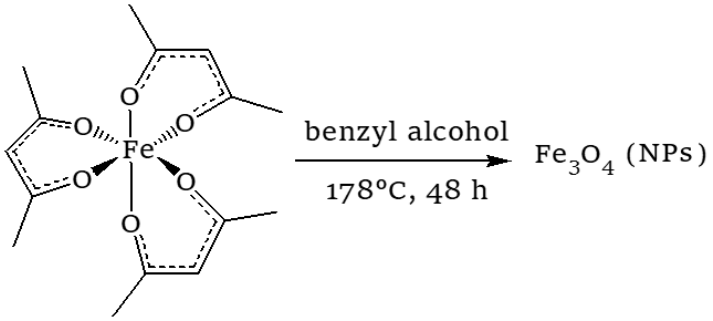

Scheme 6.1

The obtained nanoparticles were characterized by a quick and strong response when submitted to an external magnetic field, thus allowing their easy separation from the solution and their magnetic driving through a determined area (**Figure 6.21**).

Figure 6.21 behavior of the obtained SPIONs in absence and in presence of an external magnetic field

The TEM image of the obtained bare nanoparticles is shown in **Figure 6.22.** The beads were characterized by an average diameter of 6.5± 1.1 nm and a spherical shape: the dimensions and geometry are suitable for their use as drug nanocarriers. In order to obtain reliable and statistically significant results hundreds of particles were counted and analyzed.

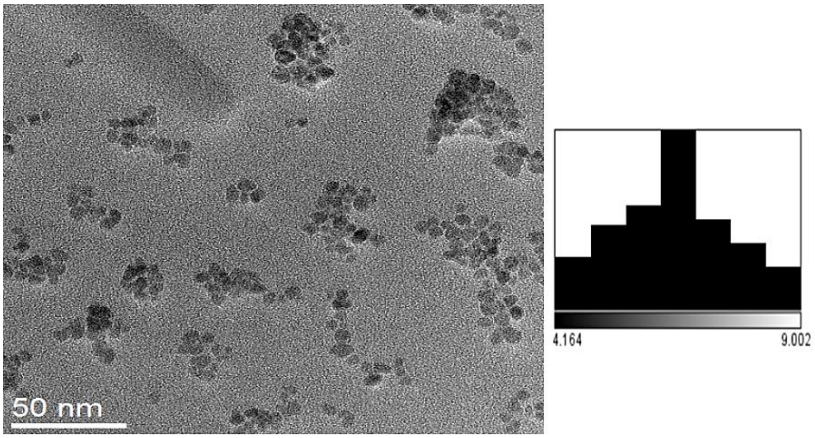

Figure 6.22 TEM image of the necked magnetic nanoparticles

Diffraction pattern of the magnetite nanoparticles was obtained by TEM analysis by Selected Area (Electron) Diffraction (SAED) in order to obtain the diffraction of the sample's crystal structure (**Figure 6.23**).

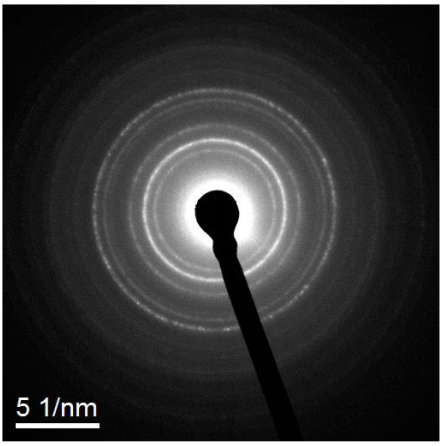

Figure 6.23 SAED image of the bare SPIONs

The synthesis of Fe_3O_4 was assessed both by means of XRD and XPS spectra (**Figure 6.24**): as for the XRD the observed peaks corresponding to the (2 2 0), (3 1 1), (3 3 3), (4 0 0) and (4 4 0) reflections of Fe_3O_4 (JCPDS 82-1533), whereas the XPS spectrum of Fe 2p, showed two peaks attributable of magnetite nanoparticles at 711 and 725 eV, related to Fe 2p 3/2 and Fe 2p 1/2, respectively.

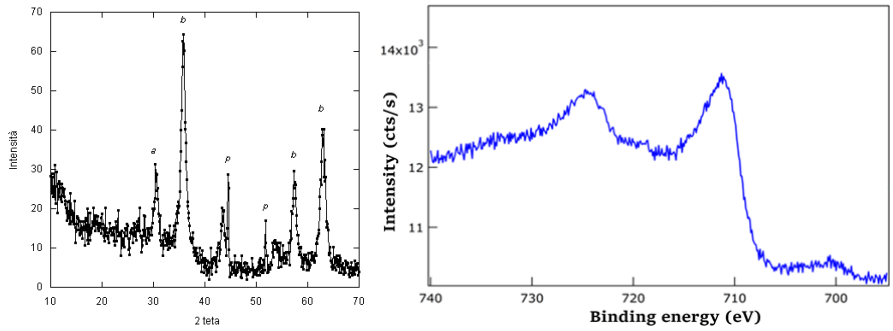

Figure 6.24 XRD (left) and XPS (right) analyses of the bare nanoparticles

The nanoparticles were also charcaterized by ATR/FT-IR analysis, showing a band at υ = 555 cm^{-1} related to the streching of Fe–O groups.

Finally, the magnetization curve of the obtained nanoparticles (**Figure 6.25**) was achieved by VSM analysis and the saturation magnetization value, 57 emu/g, was typical of superparamagnetic nanoparticles.

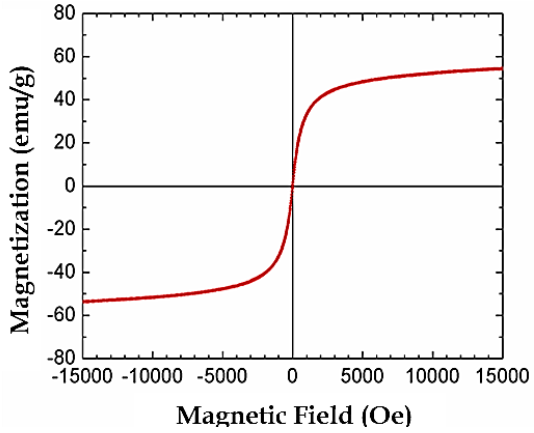

Figure 6.25 Magnetization curve of the bare nanoparticles

6.3.4 *SPION-Carboxyalkylphosphonic Acids Functionalization*

The functionalization by using carboxyalkylphosphonic acids was devoted to: i) protect the core of the nanoparticle from oxidation and aggregation phenomena; ii) increase their solubility in water and phosphonate buffer solutions (pH=7.8); iii) provide free carboxylic groups for further protein conjugation.

The phosphonate group has been already used in literature to bind iron oxide nanoparticles, thus producing a strong coordination bond between the spacer and the core of the material. In order to study the effect of the length of the alkyl chain, two different carboxyalkylphosphonic acids were used for functionalization, namely 11-phosphonoundecanoic acid and 3-phosphonopropionic acid (**Scheme 6.2**). The reaction conditions has to be compatible with the potential pharmaceutical application of the drug, thus the use of water and easy-to-remove and/or non-toxic solvents was proposed.

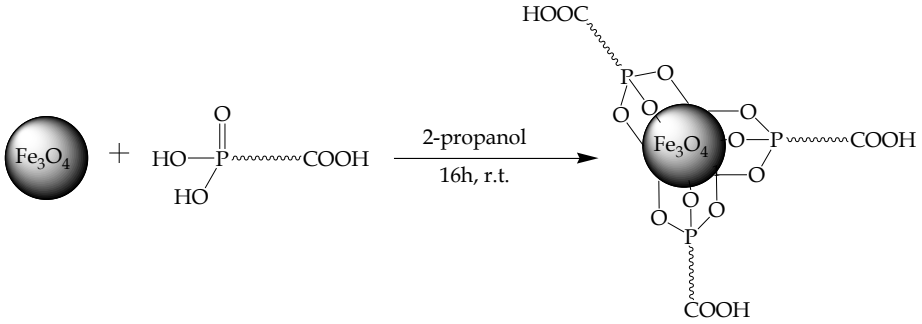

Scheme 6.2

Two different reactions were performed:

1. The first reaction was performed in a biphasic system (water and hexane) [92]. Since the presence of an emultsion was observed, the nanoparticles could not be separated between the two different phases.

   Another problem was related to the 11-phosphonoundecanoic poor solublity in distilled water, thus requiring to increase of the pH of the solution at 7.8.

   The ATR/FT-IR analysis on the obtained nanoparticles did not show any peak related to the Fe-O-P bond, whereas the band associated to the P-O-H bond was present (υ = 976 cm^{-1}): this procedure was discarded, since the carboxyalkylphosphonic acids were not able to bind effectively the iron oxide core.
2. The second reaction was performed in 2-propanol using a concentration of carboxyalkylphosphonic acids of 1 mM [93]. The reaction was performed at room temperature. Different carboxyalkylphosphonic acids/SPIONs ratios were tested and the best results were achieved using a 1:2 acid/SPION ratio.

The ATR/FT-IR analysis of the obtained nanoparticles showed the presence of IR bands at υ = 1030-1040 cm^{-1}, attributable to Fe-O-P bond stretching, whereas the bands related to the unbounded phosphonic group i.e. υ = 970-980 cm^{-1} (P-O-H stretching) and υ = 1260-1670 cm^{-1} (P=O stretching) were not present. Stretching bands at υ = 1400-1410 cm^{-1} and at υ = 1580-1590 cm^{-1} were associated to the asymmetric ν_{as} (COO^-) and the symmetric ν_s (COO^-) stretching of the free carboxylic acid [93].

The functionalized nanoparticles were then investigated by TEM-EDX. The obtained elemental spectrum (**Figure 6.26**), showed the presence of the phosphorous peak at 2.00 eV.

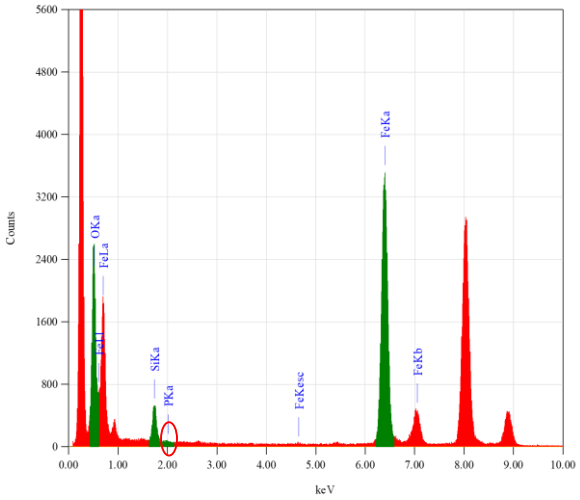

Figure 6.26 EDX spectrum

An element mapping was also performed, thus allowing to locate the presence of selected elements, i.e. Fe, O and P, within the sample (**Figure 6.27**).

As depicted in **Figure 6.27** the mapping of the phosphorous showed that its concentration is related to the presence of iron and oxygen, thus the phosphorous is present on the nanoparticles.

Considering the results achieved by FT-IR and TEM-EDX analyses, it can be stated that the phosphonic groups bounded the iron oxide core, whereas the carboxylic acid was free for further conjugation.

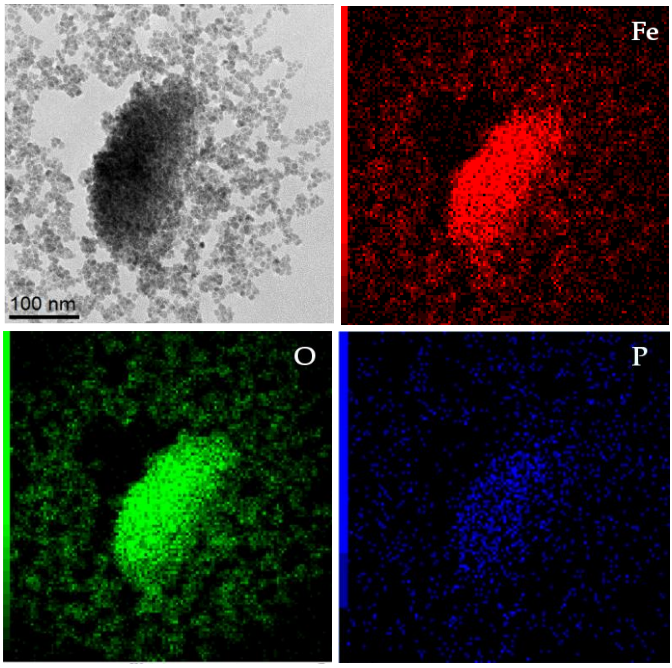

Figure 6.27 TEM image and EDX mapping from top-left to bottom-right: TEM image, iron, oxygen and phosphorus

Finally, the magnetization curves for both 11-phosphonoundecanoic- and 3-phosphonopropionic-functionalized nanoparticles were obtained: as expected, due to the increase of the nanoparticle volume, a reduction of the saturation magnetizations was observed with values of 47 and 50 emu/g, for the long- and short-chain acids respectively.

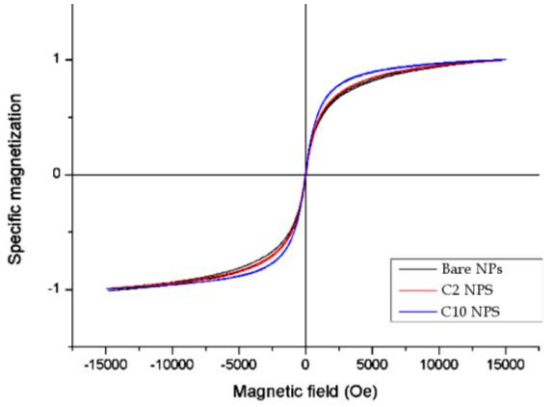

Figure 6.28 Magnetization curves of the bare (black), 11-phosphonoundecanoic- (C10, blue) and 3-phosphonopropionic-functionalized (C2, red) nanoparticles

6.3.5 SPION-bOBP Conjugation

The carboxyalkylphosphonic-functionalized nanoparticles were then conjugated with the bovine odorant binding protein. The reaction was achieved by amide bond formation between the free carboxylic group of the spacer and the amino groups on the bOBP surface. The conjugation was mediated by using EDC as coupling agent, as reported in several studies [82, 94-96]. This reagent allowed to obtain the protein click with high yield in very mild condition, thus maintaining the protein in its natural folding.

The protein conjugation was obtained by following the reaction conditions proposed by Wang et al. [82] (**Scheme 6.3**).

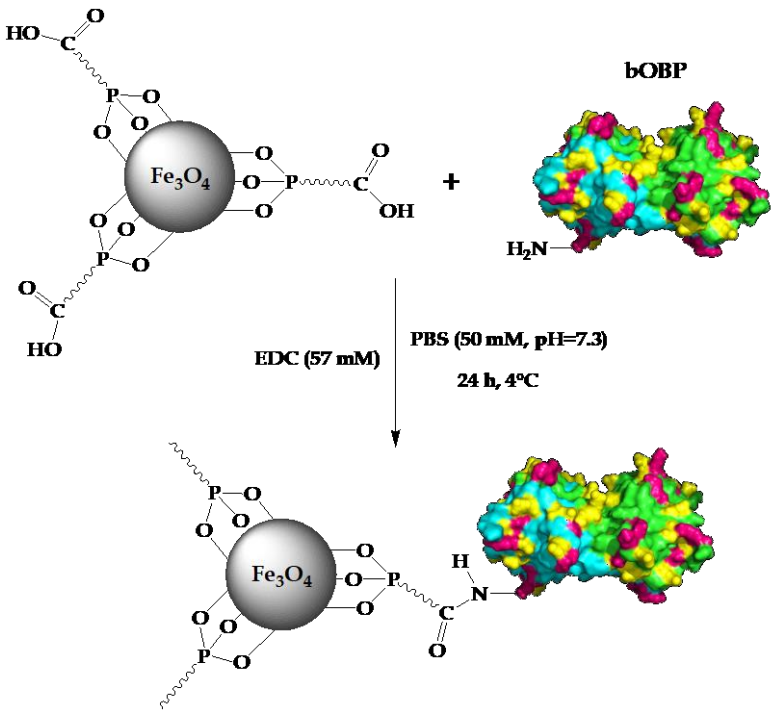

Scheme 6.3

The bOBP-functionalized nanoparticles were magnetically decanted and repeatedly washed with phosphonate buffer (50 mM pH=7.8, 3 wash x 5 ml). It has to be noticed that, due to both their small dimensions and the reduced length of the spacer, the phosphonopropionic-functionalized SPIONs could not be separated easily from the solution. The washing solutions were also characterized by a brown color and high turbidity, whereas nanoparticles

functionalized by the long-chain spacer were better separated from both the reaction and the washing solutions (**Figure 6.29**).

Figure 6.29 phosphonopropionic (left) and phosphonoundecanoic functionalized (right) bOBP-SPIONs

The observed behavior could be explained by taking into account the different hydrophilicity of the functionalized nanoparticles: the long-chain nanoparticles can be separated from the phosphonate buffer solution due to the enhanced hydrophobicity.

Due to the difficulties occurred in the separation of the propyl-functionalized nanoparticles, only the phosphonoundecanoic functionalized SPIONs were characterized.

The amount of the loaded protein was obtained by using the bicinchoninic acid (BCA) protein assay kit. This is largely applied in order to evaluate the concentration of proteins in water solution and phosphonate buffers. The method is based on the reduction of Cu^{2+} to Cu^{1+} by proteins in an alkaline medium (Biuret reaction) followed by the reaction of the cuprous cation with a reagent of the assay kit containing bicinchoninic acid. The complex, obtained by the chelation of Cu^{+} by two molecules of BCA, is characterized by an excellent water solubility and a strong absorbance at 562 nm, allowing to perform a highly sensitive colorimetric detection of proteins in solution.

Since it was not possible to evaluate directly the amount of bOBP on the functionalized SPIONs, the concentration of the not-conjugated protein in both the reaction and washing solutions was determined.

As a first step, the analysis of a batch of blank and standard solutions of bOBP in the 0.02 to 0.64 µg/l range was performed, thus obtaining calibration curve

(y=0.00238(±0.00007)x+0.0764(±0.0015)). A very good repeatability in standard solution analysis was obtained, with RSD% <5% (n=3).

The analysis of reagent solutions before and after the SPIONs functionalization were performed (**Figure 6.30**). The protein concentration loaded on the nanoparticles was obtained by difference.

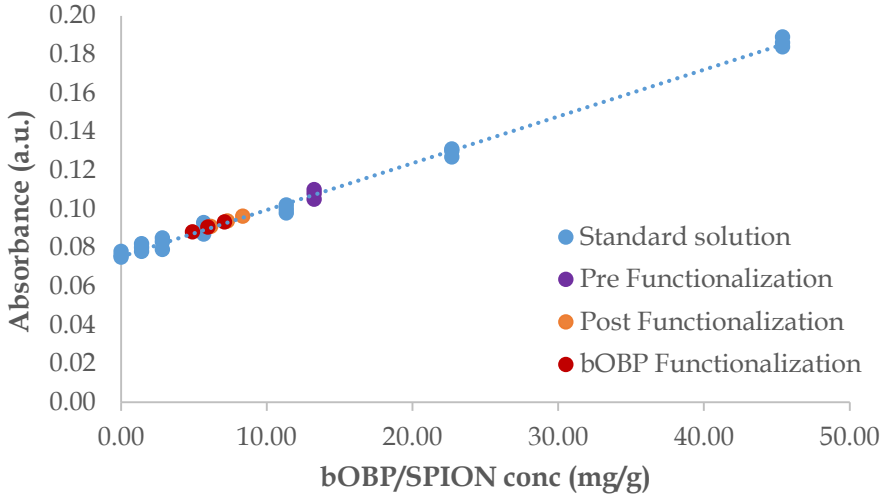

Figure 6.30 Example of calibration curve obtained by using BCA protein assay kit

Data proved that the bOBP was loaded on the developed nanoparticles with a concentration of 6.0±1.2 mg bOBP/g SPIONs, which is in line with the results published in literature for similar proteins.

Finally, the magnetization measurements performed on the bOBP-functionalized nanoparticles showed a saturation magnetization of 44 emu/g: the decrease of this value can be explained taking into account the increased volume of the developed hybrid nanosystem and considering that the weight include both magnetic (the core) and non-magnetic (the linker and the bOBP) components.

6.4 Conclusions

A new hybrid system composed by a superparamagnetic iron oxide core, a shell of phosphonoundecanoic acid and bovine odorant binding protein as active component was developed.

The main features of the hybrid system are reported below:

1. By the use of an external magnetic field it is possible to drive the system to a localized area of lungs, where inflammation is present, thus allowing both to increase the local concentration of the active principle and reduce the side-effects due to the diffusion of the drug in the body.
2. The bOBP is a protein characterized by enhanced complexation capabilities toward the *quorum sensing molecules*, thus being suitable for *quorum quenching* applications.
3. bOBP is capable of binding pyocyanin. This molecule is one of the most dangerous virulence factors and, due to its redox activity, is the main responsible for the antibiotic resistance of *Pseudomonas aeruginosa*.

The development of bOBP-functionalized SPIONs can be considered as a first step in order to obtain a hybrid system able to bind different inducers or metabolites produced by antibiotic resistant bacteria.

The study allowed to perform the synthesis of superparamagnetic nanoparticles characterized by a superparamagnetic iron-oxide core, with an average diameter of 6.5 ± 1.1 nm, able to reach alveolar region of lungs.

The nanoparticles were functionalized by a long-chain phosphonic acid, which allowed the conjugation with the bOBP, thus obtaining a concentration of 6.0±1.2 mg bOBP/g SPIONs.

6.5 Acknowledgement

Thanks to Prof. R. Ramoni, Prof. S. Grolli and Dr. V. Conti from the Veterinary Department of University of Parma for the collaboration during all the research study. Thanks also to Dr. L. Nasi and Dr. F. Casoli from IMEM-CNR of Parma for the nanoparticle characterization.

6.6 References

[1] R. Liang, M. Wei, D.G. Evans, X. Duan, *Inorganic nanomaterials for bioimaging, targeted drug delivery and therapeutics*, Chem. Commun., 50 (2014) 14071–14081.

[2] L. Tang, J. Cheng, *Nonporous silica nanoparticles for nanomedicine application*, Nano Today, 8 (2013) 290–312.

[3] F. Novio, J. Simmchen, N. Vázquez-Mera, L. Amorín-Ferré, D. Ruiz-Molina, *Coordination polymer nanoparticles in medicine*, Coordin. Chem. Rev., 257 (2013) 2839-2847.

[4] X. Huang, P.K. Jain, I.H. El-Sayed, M.A. El-Sayed, *Gold nanoparticles: interesting optical properties and recent applications in cancer diagnostics and therapy*, Nanomed., 2 (2007) 681–693.

[5] A. Gharatape, R. Salehi, *Recent progress in theranostic applications of hybrid gold nanoparticles*, Eur. J. Med. Chem., 138 (2017) 221-233.

[6] B.B. Manshian, J. Jiménez, U. Himmelreich, S.J. Soenen, *Personalized medicine and follow-up of therapeutic delivery through exploitation of quantum dot toxicity*, Biomaterials, 127 (2017) 1-12.

[7] C. Janko, J. Zaloga, M. Pöttler, S. Dürr, D. Eberbeck, R. Tietze, S. Lyer, C. Alexiou, *Strategies to optimize the biocompatibility of iron oxide nanoparticles – "SPIONs safe by design"*, J. Magn. Magn. Mater., 431 (2017) 281-284.

[8] N. Sounderya, Y. Zhang, *Use of core/shell structured nanoparticles for biomedical applications*, Recent Pat. Biomed. Eng., 1 (2008) 34–42.

[9] A. Mahmud, X.B. Xiong, H.M. Aliabadi, A. Lavasanifar, *Polymeric micelles for drug targeting*, J. Drug Target., 15 (2007) 553–584.

[10] J.J. Panda, A. Mishra, A. Basu, V.S. Chauhan, *Stimuli responsive self-assembled hydrogel of a low molecular weight free dipeptide with potential for tunable drug delivery*, Biomacromolecules, 9 (2008) 2244–2250.

[11] L.E. Scheeren, D.R. Nogueira, L.B. Macedo, M.P. Vinardell, M. Mitjans, M.R. Infante, C.M. Rolim, *PEGylated and poloxamer-modified chitosan nanoparticles incorporating a lysine-based surfactant for pH-triggered doxorubicin release*, Colloids Surf. B Biointerfaces, 138 (2016) 117-127.

[12] L.E. LaConte, N. Nitin, O. Zurkiya, D. Caruntu, C.J. O'Connor, X. Hu, G. Bao, *Coating thickness of magnetic iron oxide nanoparticles affects R2 relaxivity*, J. Magn. Reson. Imaging, 26 (2007) 1634-1641.

[13] V. P. Torchilin, *Recent advances with liposomes as pharmaceutical carriers*, Nat. Rev. Drug Discov., 4 (2005) 145–160.

[14] M. Selin, L. Peltonen, J. Hirvonen, L.M. Bimbo, *Dendrimers and their supramolecular nanostructures for biomedical applications*, J. Drug Deliv. Sci. Tec., 34 (2016) 10-20.

[15] D. Shcharbin, N. Shcharbin, V. Dzmitruk, E. Pedziwiatr-Werbick, M.S. Mignani, J. de la Mata, R. Gómez, M.A. Muñoz-Fernández, J.P. Majoral, M. Bryszewska, *Dendrimer-protein interactions versus dendrimer-based nanomedicine,* Colloid. Surface. B, 152 (2017) 414-422.

[16] P.A. Tran, L. Zhang, T.J. Webster, *Carbon nanofibers and carbon nanotubes in regenerative medicine*, Adv. Drug Deliver. Rev., 61 (2009) 1097-1114.

[17] S. Peretz, O. Regev, *Carbon nanotubes as nanocarriers in medicine*, Curr. Opin. Colloid In., 17 (2012) 360-368.

[18] A. Fabbro, M. Prato, L. Ballerini, *Carbon nanotubes in neuroregeneration and repair*, Adv. Drug Deliver. Rev., 65 (2013) 2034-2044.

[19] P. Sharma, S. Brown, G. Walter, S. Santra, B. Moudgil, *Nanoparticles for bioimaging*, Adv. Colloid Interfac., 123–126 (2006) 471–485.

[20] P. Padmanabhan, A. Kumar, S. Kumar, R. Kumar Chaudhary, B. Gulyás, *Nanoparticles in practice for molecular-imaging applications: An overview*, Acta Biomater., 41 (2016) 1–16.

[21] Q. Liu, B. Guo, Z. Rao, B. Zhang, J.R. Gong, Strong Two-Photon-Induced Fluorescence from Photostable, *Biocompatible Nitrogen-Doped Graphene Quantum Dots for Cellular and Deep-Tissue Imaging*, Nano Lett., 13 (2013) 2436–2441.

[22] K. Stockhofe, J.M. Postema, H. Schieferstein, T.L. Ross, *Radiolabeling of Nanoparticles and Polymers for PET Imaging*, Pharmaceuticals, 7 (2014) 392–418.

[23] J. Garcia, T. Tang, A.Y. Louie, *Nanoparticle-based multimodal PET/MRI probes*, Nanomedicine, 10 (2015) 1343-1359.

[24] S. Santra, R. P. Bagwe, D. Dutta, J. T. Stanley, G. A. Walter, W. Tan, B. M. Moudgil, R. A. Mericle, *Synthesis and Characterization of Fluorescent, Radio-Opaque, and Paramagnetic Silica Nanoparticles for Multimodal Bioimaging Applications*, Adv. Mater., 17 (2005) 2165-2169

[25] A. Z. Wilczewska, K. Niemirowicz, K.H. Markiewicz, H. Car, *Nanoparticles as drug delivery systems*, Pharmacol. Rep., 64 (2012) 1020-1037.

[26] P.M. Deckert, *Current constructs and targets in clinical development for antibody-based cancer therapy*, Curr. Drug Targets, 10 (2009) 158–175.

[27] M. Hong, S. Zhu, Y. Jiang, G. Tang, Y. Pei, *Efficient tumor targeting of hydroxycamptothecin loaded PEGylated niosomes modified with transferrin*, J. Control. Release, 133 (2009) 96–102.

[28] L. Karmani, D. Labar, V. Valembois, V. Bouchat, P.G. Nagaswaran, A. Bol, J. Gillart, P. Levêque, C. Bouzin, D. Bonifazi, C. Michiels, O. Feron, V. Grégoire, S. Lucas, T. Vander Borght, B. Gallez, *Antibody-functionalized nanoparticles for imaging cancer: influence of conjugation to gold nanoparticles on the biodistribution of 89Zr-labeled cetuximab in mice*, Contrast Media Mol. Imaging, 8 (2013) 402-408.

[29] K. Greish, *Enhanced permeability and retention (EPR) effect for anticancer nanomedicine drug targeting*, Methods Mol. Biol., 624 (2010) 25-37.

[30] C. M. Sorensen, *Nanoscale Materials in Chemistry* (Ed.: K. J. Klabunde), Wiley, New York, NY, USA, 2001.

[31] M.W. Freeman, A. Arrott, J.H.L. Watson, *Magnetism in medicine*, J. Appl. Phys., 31 (1960) 404S.

[32] S.K. Yen, P. Padmanabhan, S.T. Selvan, *Multifunctional Iron Oxide Nanoparticles for Diagnostics, Therapy and Macromolecule Delivery*, Theranostics, 3 (2013) 986-1003.

[33] K. Niemirowicz, K.H. Markiewicz, A.Z. Wilczewska, H. Car, *Magnetic nanoparticles as new diagnostic tools in medicine,* Adv. Med. Sci., 57 (2012) 196-207

[34] P. Pradhan, R. Banerjee, D. Bahadur, C. Koch, O. Mykhaylyk, C. Plank, *Targeted magnetic liposomes loaded with doxorubicin*, Methods Mol. Biol., 605 (2010) 279-293.

[35] W. Shi, J. Wang, X. Fan, H. Gao, *Size and shape effects on diffusion and absorption of colloidal particles near a partially absorbing sphere: Implications for uptake of nanoparticles in animal cells*, Phys. Rev. E - Stat. Nonlinear, Soft Matter Phys., 78 (2008) 061914-1-061914-11.

[36] R. Toy, P.M. Peiris, K.B. Ghaghada, E. Karathanasis, *Shaping cancer nanomedicine: The effect of particle shape on the in vivo journey of nanoparticles*, Nanomedicine, 9 (2014) 121–134.

[37] J.A. Champion, S. Mitragotri, *Role of target geometry in phagocytosis*, Proc. Natl. Acad. Sci. USA, 103 (2006) 4930–4934.

[38] A. Ganguly, R. Kundu, K.V. Ramanujachary, S.E. Lofland, D. Das, N.Y. Vasanthacharya, T. Ahmad, A.K. Ganguli, *Role of carboxylate ion and metal oxidation state on the morphology and magnetic properties of nanostructured metal carboxylates and their decomposition products*, J. Chem. Sci., 120 (2008) 521–528.

[39] T. Sugimoto, E. Matijevic, *Formation of uniform spherical magnetite particles by crystallization from ferrous hydroxide gels*, J. Colloid. Interface Sci., 74 (1980) 227–243.

[40] R. Massart, *Preparation of aqueous magnetic liquids in alkaline and acidic media*, IEEE Trans Magn. 17 (1981) 1247–1248.

[41] G.C. Hadjipanayis, R.W. Siegel, *Nanophase materials: synthesis, properties and applications*, NATO ASI Series, Applied Sciences, vol. E260, Kluwer Academic, Dordrecht, Netherland, 1994.

[42] P. Tartaj, M.P. Morales, S. Veintemillas-Verdaguer, T. González-Carreno, C.J. Serna, *The preparation of magnetic nanoparticles for applications in biomedicine*, J. Phys. D Appl. Phys., 36 (2003) R182.

[43] A.K. Gupta, S. Wells, *Surface modified superparamagnetic nanoparticles for drug delivery: preparation, characterization and cytotoxicity studies*, IEEE Trans Nanobiosci., 3 (2004) 66–73.

[44] S. Sun, H. *Zeng, Size-controlled synthesis of magnetite nanoparticles*, J. Am. Chem. Soc., 124 (2002) 8204–8205.

[45] N. Pinna, M. Niederberger, *Surfactant-Free Nonaqueous Synthesis of Metal Oxide Nanostructures*, Angew. Chem. Int., 47 (2008) 5292 – 5304.

[46] A.K. Gupta, M. Gupta, *Cytotoxicity suppression and cellular uptake enhancement of surface modified magnetic nanoparticles*, Biomaterials, 26 (2005) 1565–1573.

[47] O. Veiseh, J.W. Gunn, M. Zhang, *Design and fabrication of magnetic nanoparticles for targeted drug delivery and imaging*, Adv Drug Deliv Rev. 62 (2010) 284–304.

[48] J.M. Harris, R.B. Chess, *Effect of pegylation on pharmaceuticals*, Nat. Rev. Drug Discov., 3 (2003) 214–221.

[49] A. Petri-Fink, M. Chastellain, L. Juillerat-Jeanneret, A. Ferrari, H. Hofmann, *Development of functionalized superparamagnetic iron oxide nanoparticles for interaction with human cancer cells*, Biomaterials, 26 (2005) 2685–2694.

[50] E. Amstad, S. Zurcher, A. Mashaghi, J.Y. Wong, M. Textor, E. Reimhult, *Surface functionalization of single superparamagnetic iron oxide nanoparticles for targeted magnetic resonance imaging*, Small, 5 (2009) 1334–1342.

[51] S. Y Liu, Y. Han, L.P. Yin, L. Long, R. Liu, *Toxicology studies of a superparamagnetic iron oxide nanoparticle in vivo*, Adv. Mater. Res., 47 (2008) 1097–1100.

[52] A.K. Gupta, S. Wells, *Surface-modified superparamagnetic nanoparticles for drug delivery: preparation, characterization, and cytotoxicity studies*, IEEE Trans. Nanobioscience, 3 (2004) 66–73.

[53] M. Kondo, J. Tamaoki, *Therapeutic approaches of asthma and COPD overlap*, Allergol. Int., (2017) 1-4.

[54] T.G. O'Riordan, *Aerosol delivery devices and obstructive airway disease*, Expert. Rev. Med. Devices., 2 (2005) 197–203.

[55] R. Dinwiddie, *Anti-inflammatory therapy in cystic fibrosis*, J. Cyst. Fibros., 4 Suppl. 2 (2005) 45–48.

[56] J.K. Hagerman, K.E. Hancock, M.E. Klepser, *Aerosolised antibiotics: a critical appraisal of their use*, Expert Opin. Drug Deliv., 3 (2006) 71–86.

[57] R.D. Rao, S.N. Markovic, P.M. Anderson, *Aerosol therapy for malignancy involving the lungs*, Curr. Cancer Drug Targets, 3 (2003) 239–250.

[58] P. Dames, B. Gleich, A. Flemmer, K. Hajek, N. Seidl, F. Wiekhorst, D. Eberbeck, I. Bittmann, C. Bergemann, T. Weyh, L. Trahms, J. Rosenecker, C. Rudolph, *Targeted delivery of magnetic aerosol droplets to the lung*, Nat. Nano., 2 (2007) 495–499.

[59] F. Tewes, C. Ehrhardt, A.M. Healy, *Superparamagnetic iron oxide nanoparticles (SPIONs)-loaded Trojan microparticles for targeted aerosol delivery to the lung*, Eur. J. Pharm. Biopharm., 86 (2014) 98–104.

[60] S. Fetzner, *Quorum quenching enzymes*, J. Biotechnol., 201 (2015) 2–14.

[61] L. Plener, N. Lorenz, M. Reiger, T. Ramalho, U. Gerland, K. Jung, *The phosphorylation flow of the vibrio harveyi quorum-sensing cascade determines levels of phenotypic heterogeneity in the population*, J. Bacteriol., 197 (2015) 1747-1756.

[62] J. Lee, L. Zhang, *The hierarchy quorum sensing network in Pseudomonas aeruginosa*, Protein. Cell, 6 (2015) 26-41.

[63] N. Schmid, G. Pessi, Y. Deng, C. Aguilar, A.L. Carlier, A. Grunau, U. Omasits, L.H. Zhang, C.H. Ahrens, L. Eberl, *The AHL and BDSF-dependent*

quorum sensing systems control specific and overlapping sets of genes in Burkholderia cenocepacia H111, PLoS One, 7 (2012) e49966

[64] J. Mansfield, S. Genin, S. Magori, V. Citovsky, M. Sriariyanum, P. Ronald, M. Dow, V. Verdier, S.V. Beer, M.A. Machado, I. Toth, G. Salmond, G.D. Foster, *Top 10 plant pathogenic bacteria in molecular plant pathology*, Mol. Plant Pathol., 13 (2012) 614-629.

[65] D.T. Gauthier, *Bacterial zoonoses of fishes: a review and appraisal of evidence for linkages between fish and human infections*, Vet. J. Lond. Engl., 203 (2015) 27-35.

[66] M. Givskov, R. de Nys, M. Manefield, L. Gram, R. Maximilien, L. Eberl, S. Molin, P.D. Steinberg, S. Kjelleberg, *Eukaryotic interference with homoserinelactone-mediated prokaryotic signaling*, J. Bacteriol., 178 (1996) 6618–6622.

[67] B. LaSarre, M.J. Federle, *Exploiting quorum sensing to confuse bacterialpathogens*, Microbiol. Mol. Biol. Rev., 77 (2013) 73–111.

[68] F. Bittar, H. Richet, J.C. Dubus, M. Reynaud-Gaubert, N. Stremler, J. Sarles, D. Raoult, J.M. Rolain, *Molecular detection of multiple emerging pathogens in sputa from cystic fibrosis patients*, PLoS One, 3 (2008) e2908.

[69] S.L. Gellatly, R.E. Hancock, *Pseudomonas aeruginosa: new insights into pathogenesis and host defenses*, Pathog. Dis., 67 (2013) 159–173.

[70] http://www.sciencephoto.com/media/11601/view.

[71] J.B. Goldberg, G.B. Pier, *The role of the CFTR in susceptibility to Pseudomonas aeruginosa infections in cystic fibrosis*, Trends Microbiol., 8 (2000) 514–520.

[72] T. Rasamiravaka, M. El Jaziri, *Quorum-sensing mechanisms and bacterial response to antibiotics in P. aeruginosa*, Curr. Microbiol., 73 (2016) 747–753.

[73] N. S Schaadt, A. Steinbach, R.W. Hartmann, V. Helms, *Rule–based regulatory and metabolic model for Quorum sensing in P. aeruginosa*, BMC Syst. Biol., 7 (2013) 81-95

[74] G.W. Lau, B.C. Goumnerov, C.L. Walendziewicz, J. Hewitson, W. Xiao, S. Mahajan-Miklos, R.G. Tompkins, L.A. Perkins, L.G. Rahme, *The Drosophila melanogaster toll pathway participates in resistance to infection by the gram-negative human pathogen Pseudomonas aeruginosa*, Infect Immun., 71 (2003) 4059–4066.

[75] J.T. Jackowski, Z. Szepfalusi, D.A. Wanner, Z. Seybold, M.W. Sielczak, I.T. Lauredo, T. Adams, W.M. Abraham, A. Wanner, *Effects of P. aeruginosa-*

derived bacterial products on tracheal ciliary function: role of O2 radicals, Am. J. Physiol., 260 (1991) L61–L67.

[76] I.T. Lauredo, J.R. Sabater, A. Ahmed, Y. Botvinnikova, W.M. Abraham, *Mechanism of pyocyanin- and 1-hydroxyphenazine-induced lung neutrophilia in sheep airways*, J. Appl. Physiol., 85 (1998) 2298–2304.

[77] L. Allen, D.H. Dockrell, T. Pattery, D.G. Lee, P. Cornelis, P.G. Hellewell, M.K. Whyte, *Pyocyanin production by Pseudomonas aeruginosa induces neutrophil apoptosis and impairs neutrophil-mediated host defenses in vivo*, J. Immunol., 174 (2005) 3643–3649.

[78] F. Vincent, R. Ramoni, S. Spinelli, S. Grolli, M. Tegoni, C. Cambillau, *Crystal structures of bovine odorant-binding protein in complex with odorant molecules*, Eur. J. Biochem., 271 (2004) 3832–3842.

[79] R.Ramoni, S. Bellucci, I. Grycznyski, Z. Grycznyski, S. Grolli, M. Staiano, G. De Bellis, F. Micciulla, R. Pastore, A. Tiberia, V. Conti, E. Merli, A. Varriale, M. Rossi, S. D'Auria, *The protein scaffold of the lipocalin odorant-binding protein is suitable for the design of new biosensors for the detection of explosive components*, J. Phys.: Condens. Matter, 19 (2007) 395012.

[80] F. Bianchi, G. Basini, S. Grolli, V. Conti, F. Bianchi, F. Grasselli, M. Careri, R. Ramoni, *An innovative bovine odorant binding protein-based filtering cartridge for the removal of triazine herbicides from water*, Anal. Bioanal. Chem., 405 (2013) 1067–1075.

[81] S. Grolli, E. Merli, V. Conti, E. Scaltriti, R. Ramoni, *Odorant binding protein has the biochemical properties of a scavenger for 4-hydroxy-2-nonenal in mammalian nasal mucosa*, FEBS J., 273 (2006) 5131–5142.

[82] T.H. Wang, W.C. Lee, *Immobilization of Proteins on Magnetic Nanoparticles*, Biotechnol. Bioprocess Eng., 8 (2003) 263-267.

[83] M. Tegoni, R. Ramoni, E. Bignetti, S. Spinelli, C. Cambillau, *Domain swapping creates a third putative combining site in bovine odorant binding protein dimer*, Nat. Struct. Biol., 3 (1996) 863–867.

[84] R. Ramoni, F. Vincent, A.E. Ashcroft, P. Accornero, S. Grolli, C. Valencia, M. Tegoni, C. Cambillau, *Control of domain swapping in bovine odorant-binding protein*, Biochem. J., 365 (2002) 739–748.

[85] T. Apostoli, *Interaction between bovine Odorant Binding Protein (OBP) and bioactive molecules of biotechnological interest*, Corso di laurea in Chimica, Università degli Studi di Parma, a.a. 2013-2014.

[86] *The Fitness for Purpose of Analytical Methods: A Laboratory Guide to Method Validation and Related Topics*, EURACHEM Guide, 1st English ed., LGC Ltd., Teddington, U.K., 2014, http://www.eurachem.ul.pt.

[87] M. Tegoni, R. Ramoni, E. Bignetti, S. Spinelli, C. Cambillau, *Domain swapping creates a third putative combining site in bovine odorant binding protein dimer*, Nat. Struct. Biol., 3 (1996) 863-867.

[88] C. Tudisco, V. Olivieri, M. Cantarella, G. Vecchio, G.G. Condorelli, *Cyclodextrin anchoring on magnetic Fe_3O_4 Nanoparticles Modified with Phosphonic Linkers*, Eur. J. Inorg. Chem, 2012 (2012) 5323-5331.

[89] B. Zhang, T. Kong, W. Xu, R. Su, Y. Gao, G. Cheng, *Surface Functionalization of Zinc Oxide by Carboxyalkylphosphonic Acid Self-assabled monolayers*, Langmuir, 26 (2010) 4514-4522.

[90] C. Tudisco, M. T. Cambria, F. Sinatra, F. Bertani, A. Alba, A. E. Giuffrida, S. Saccone, E. Fantechi, C. Innocenti, C. Sangregorio, E. Dalcanale, G.G. Condorelli, *Multifunctional magnetic nanoparticles for enhanced intracellular drug transport*, J. Mater. Chem. B, 3 (2015) 4134-4145.

[91] F. Bianchi, V. Chiesi, F. Casoli, P. Luches, L. Nasi, M. Careri, A. Mangia, *Magnetic solid-phase extraction based on diphenyl functionalization of Fe_3O_4 magnetic nanoparticles for the determination of polycyclic aromatic hydrocarbons in urine samples*, J. Chromatogr. A, 1231 (2012) 8–15.

[92] J.C. Si, Y. Xing, M.L. Peng, C. Zhang, N. Buske, C. Chen, Y.L. Cui, *Solvothermal synthesis of tunable iron oxide nanorods and their transfer from organic phase to water phase*, Cryst. Eng. Comm., 16 (2014) 512–516.

[93] E. Smecca, A. Motta, M.E. Fragalà, Y. Aleeva, G.G. Condorelli, *Spectroscopic and Theoretical Study of the Grafting Modes of Phosphonic Acids on ZnO Nanorods*, J. Phys. Chem. C, 117 (2013) 5364−5372.

[94] U. Dembereldorj, E.O. Ganbold, J.H. Seo, S.Y. Lee, S.I. Yang, S.W. Joo, *Conformational changes of proteins adsorbed onto ZnO nanoparticle surfaces investigated by concentration-dependent infrared spectroscopy*, Vib. Spectrosc., 59 (2012) 23–28.

[95] B. Teste, J. Vial, S. Descroix, T. Georgelin, J.M. Siaugue, J. Petr, A. Varenne, M.C. Hennion, *A chemometric approach for optimizing protein covalent immobilization on magnetic core-shell nanoparticles in view of an alternative immunoassay*, Talanta, 81 (2010) 1703-1710.

[96] Y. Sui, Y. Cui, Y. Nie, G.M. Xia, G.X. Sun, J.T. Han, *Surface modification of magnetite nanoparticles using gluconic acid and their application in immobilized lipase*, Colloid Surface. B, 93 (2012) 24– 28.

Future Perspectives

This PhD thesis has the aim of developing new materials for MS-based methods, sample pretreatment and clinical applications. Future studies would be performed in order to optimize the proposed methods, develop and investigate new materials and test wider ranges of analytes.

The development of four new cavitands, namely MeQxBox, EtQxBox, MonoTriptyQxCav and DiTriptyQxCav and their application for the selective detection of BTEX in contaminated air is discussed in **Chapter 1**. The materials were then applied to develop a new stand-alone device capable of detecting benzene and TEX without the need of chromatographic separation, boosting the speed of the analysis. In this case, an algorithm was applied to calculate the concentration of benzene, due to a partial coelution of TEX. Future studies would be devoted to optimize the device setup, in order to achieve a complete separation of benzene toward the other aromatic compounds. In addition, the design of new receptors will be devoted to increase the specificity toward benzene.

As for the detection of SVOCs, the main feature of the NGAC sorbent proposed in **Chapter 2** was related to the capability of operating in presence of high levels of relative humidity However, taking into account that the TD-GC-MS system used in the present work was characterized by several drawbacks, instrumental modifications like change of the secondary trap material and reduction of the transfer-line length will be devoted to overcome the reported limitations and to obtain better performances. In addition, a functionalization or the use of different geometries (wires, beads, denuder walls…) of the sorbent could be performed in order obtain higher enrichment capabilities.

Regarding the development of a MEPS-LC-MS method for the simultaneous determination of dexamethasone and dexamethasone disodium phosphate in human aqueous humor (**Chapter 3**), future perspectives rely on the development of new materials to be used as drug delivery systems for the administration of both DEX and DEX-SP.

In **Chapter 4** the development of an inorganic coating to boost the performances of Direct-EI LC-MS is demonstrated. The technique was applied for the detection of standard solutions of models compounds. Future studies will be devoted to both assess the performance of Direct-EI LC-MS using the

silica-based ion source in real-world matrices and to modify the instrumental configuration in order to achieve reproducible results.

The development of rapid and reliable screening techniques for high throughput analyses is one of the main research area of analytical chemistry. In **Chapter 5** the development of a DESI-HRMS method for the detection of NPS is discussed. The use of a homemade PLA substrate allowed to achieve the best analytical performances. Future studies will be focused on the development of additional substrates for DESI-MS: polymeric materials characterized by different hydrophobicity and morphology will be developed as bulk surface, whereas functionalization by using nanomaterials will be tested to improve method performances. Finally, the detection of other drugs and analytes of environmental concern, will be performed.

Finally, as for the matter discussed in **Chapter 6**, i.e. the development of a OBP-functionalized SPION, future studies will be carried out to increase the amount of OBP immobilized on the SPION, as well as to demonstrate the activity of the nanoparticles both as *quorum quenching agents* and antibiotic drugs in vitro experiments.

Publications:

1 F. Bianchi, A. Bedini, N. Riboni, R. Pinalli, A. Gregori, L. Sidisky, E. Dalcanale, M. Careri, *Cavitand-based solid-phase microextraction coatings for the selective detection of nitroaromatic explosives in air and soil*, Anal. Chem., 86, (2014) 10646-52.

2 N. Riboni, F. Bianchi, J.W. Trzcinski, C. Massera, R. Pinalli, L. Sidisky, E. Dalcanale, M. Careri *Conformationally blocked quinoxaline cavitand as solid-phase microextraction coating for the selective detection of BTEX in air*, Anal. Chim. Acta, 905 (2016) 79-84.

3 F. Bertani, N. Riboni, F. Bianchi, G. Brancatelli, E. Sterner, R. Pinalli, T. M. Swager, E. Dalcanale *Triptycene-roofed quinoxaline cavitands for the supramolecular detection of BTEX in air*, Chem. Eur. J., 22 (2016) 3312-3319.

4 J. Trzcinski, R. Pinalli, N. Riboni, A. Pedrini, F. Bianchi, S. Zampolli, I. Elmi, C. Massera, F. Ugozzoli, E. Dalcanale, *In search of the ultimate benzene sensor: the EtQxBox solution*, ACS Sensors, 2 (2017) 590-598.

5 N. Riboni, L. Magrini, F. Bianchi, M. Careri, A. Cappiello, *Sol-gel coated ion sources for liquid chromatography-direct electron ionization mass spectrometry*, Anal. Chim. Acta, 978 (2017) 35-41.

6 F. Bianchi, M. Mattarozzi, N. Riboni, P. Mora, S.A. Gandolfi, M. Careri, *A rapid microextraction by packed sorbent − liquid chromatography tandem mass spectrometry method for the determination of dexamethasone disodium phosphate and dexamethasone in aqueous humor of patients with uveitis*, J. Pharm. Biomed. Anal., 142 (2017) 343–347.

7 F. Bianchi, N. Riboni, V. Trolla, G. Furlan, G. Avantaggiato, G. Iacobellis, M. Careri, *Differentiation of aged fibers by Raman spectroscopy and multivariate data analysis*, Talanta, 154 (2016) 467-473.

8 F. Bianchi, N. Riboni, P. Carbognani, L. Gnetti, E. Dalcanale, L. Ampollini, M. Careri, *Solid-phase microextraction coupled to gas chromatography followed by multivariate data analysis for the identification of volatile organic compounds as possible biomarkers in lung cancer tissues*, J. Pharm. Biomed. Anal., 146 (2017) 329-323.